takece.com
Continuing Education Simplified!

Vascular Ultrasound: Clinical Applications

Topic List:-

Chapter 4

Ultrasound-Guided Vascular Access during Cardiopulmonary Resuscitation

Anton Kasatkin, Aleksandr Urakov and Anna Nigmatullina

Additional information is available at the end of the chapter

http://dx.doi.org/10.5772/intechopen.79400

Abstract

The chapter considers the possibilities for using ultrasound to increase the efficiency and safety of the intravascular access in patients during cardiac arrest, cardiopulmonary resuscitation, and advanced life support. It provides the grounds for the real-time use of ultrasound for ensuring satisfactory central vascular access; the main principles of this methodology and current recommendations are described as well. In addition, the article presents special aspects of visualization of ultrasound vessels in cardiopulmonary resuscitation, as well as puncture and catheterization techniques. It is crucial that resuscitators, who are often at the forefront of patient resuscitation, understand how to properly use this potentially life-saving procedure.

Keywords: cardiopulmonary resuscitation, advanced life support, ultrasound, vascular access, vascular visualization

1. Introduction

Providing satisfactory vascular access is still a critical part of resuscitation. Timely administration of drugs through intravenous access can improve the survival rate of patients after circulatory arrest. The time passed from the arrest to drug administration is an independent predictor of return to the spontaneous circulation [1]. In this regard, it is difficult to overestimate the importance of providing satisfactory vascular access for the patient with circulatory arrest. It is important to remember that the benefits of early vascular access must be considered together with the importance of uninterrupted cardiopulmonary resuscitation (CPR) [2]. When choosing vascular access, it is a common practice firstly to focus on visualization and palpation of the

subcutaneous veins in the accessible parts of the body, as well as on the anatomical landmark (landmark technique). Subcutaneous veins in the extremities and the external jugular veins completely satisfy these requirements. The insertion of the catheter into visualized subcutaneous vein is considered to be quick and safe. It should be remembered that visualization and palpation of the subcutaneous veins can be difficult in patients in critical condition (bleeding, hypovolemic shock, burns of limbs, or hypothermia). In this case, infrared thermography [3] and near-infrared vein visualization [4] can be applied. If the catheterization of the subcutaneous veins is difficult or impossible, then intraosseous access (IO) is recommended by current clinical guidelines [5]. Nowadays, IO route is proved to be quite effective in adults and children with out-of-hospital cardiac arrest [6]. It is assumed that insertion of a central venous catheter requires the interruption of CPR and can be technically challenging and associated with complications. However, the introduction of real-time ultrasound-guided central venous catheter (CVC) insertion into clinical practice significantly increased its safety, accuracy, and effectiveness compared to the conventional landmark technique [7, 8]. It is known that central venous access is required for administering drug solutions, monitoring venous pressure, and for performing extracorporeal oxygenation and detoxification, which cannot be achieved by other types of access. In addition, ultrasound-guided catheterization of the internal jugular (IJV) and femoral veins (FV) may not require the cessation of chest compression and placing a patient in a forced position (head-down tilt positions) during CPR. It is critical that resuscitators, who are often at the forefront of patient resuscitation, understand how to properly use this potentially life-saving procedure.

2. History

The use of ultrasound imaging support for IJV location was first described in 1978 [9]. The use of ultrasound for real-time CVC insertion was reported in 1984. Legler and Nugent [10] showed that Doppler localization of the IJV facilitates central venous cannulation. Later, the results of studies showing the advantage of using ultrasound for catheterization of subclavian (SV) and FV were published [11]. The first results of studies on the use of ultrasound for catheterization of the central vein during CPR were published in 1997. Hilty et al. [12] showed that real-time ultrasound-guided FV catheterization was faster and produced a lower rate of inadvertent arterial catheterization and a higher rate of success during CPR than the standard landmark-oriented approach. Benassi et al. [13] showed the benefits of the real-time ultrasound cannulation of the femoral vessels for establishing venoarterial extracorporeal membrane oxygenation in acute cardiopulmonary failure.

3. Principles of vessel visualization using ultrasound

Two-dimensional (2D) gray-scale imaging (**Figure 1**), color (**Figure 2**), and spectral Doppler (**Figure 3**) ultrasonography are used for ultrasonic visualization of vascular structures, surrounding tissues, and anatomical formations [14]. The best resolution of surface structures in the immediate vicinity of the skin surface is provided by high-frequency (>7 MHz) linear ultrasonic sensors. The operator must have an idea of the probe orientation, the image on

http://dx.doi.org/10.5772/intechopen.79400

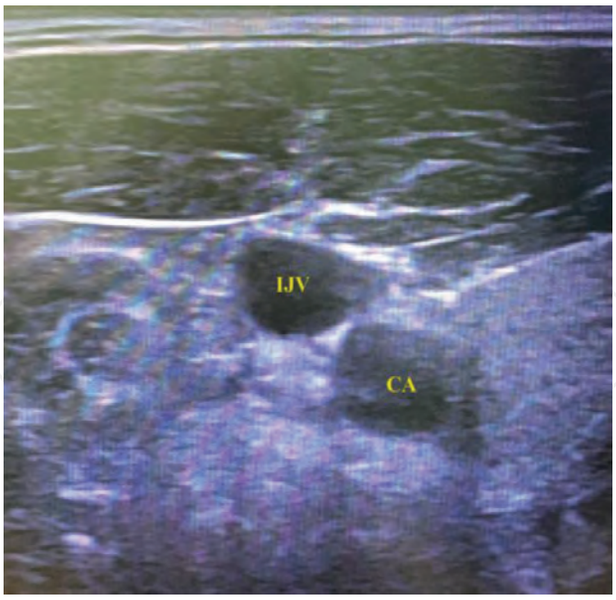

Figure 1. Ultrasound 2D image of the right internal jugular vein (IJV) and carotid artery (CA).

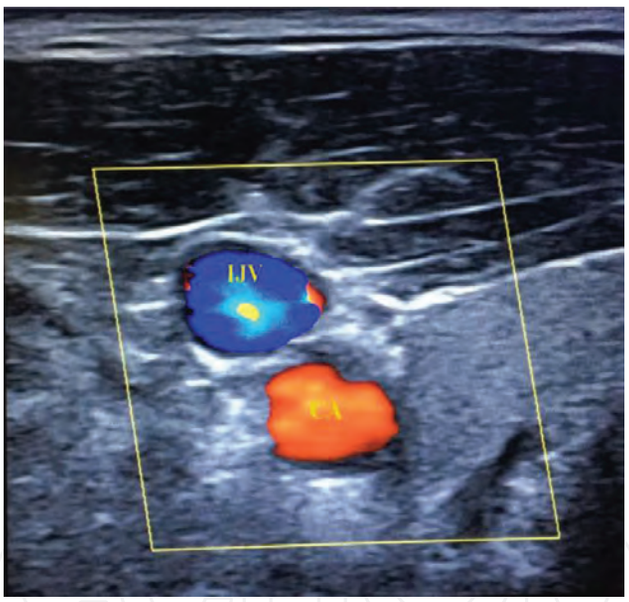

Figure 2. Ultrasound color Doppler imaging of the right internal jugular vein (IJV) and carotid artery (CA).

the display, the physics of ultrasound, the mechanism of image generation, and the artifacts, and be able to interpret 2D images of the vessel lumen and surrounding structures. A two-dimensional image of a blood vessel is usually displayed either along the long axis (**Figure 4**), the short axis (**Figure 5**) or the oblique short axis (**Figure 6**).

3.1. Ultrasonic visualization of blood vessels in people with spontaneous circulation

The basic differences between a vein and an artery in an ultrasound 2D image are the irregular form of the vein (the artery is generally round) and the wall thickness (the arterial walls are

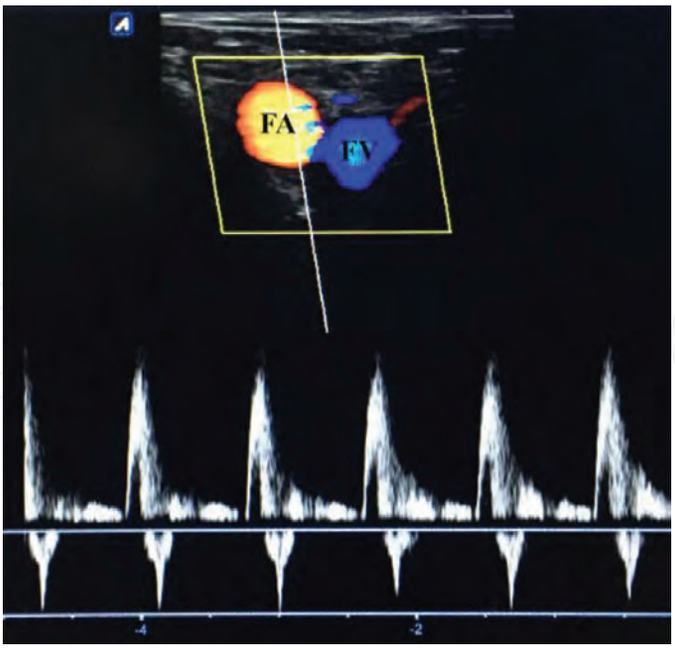

Figure 3. Ultrasound color Doppler and spectral Doppler imaging of the right femoral artery (FA) and femoral vein (FV).

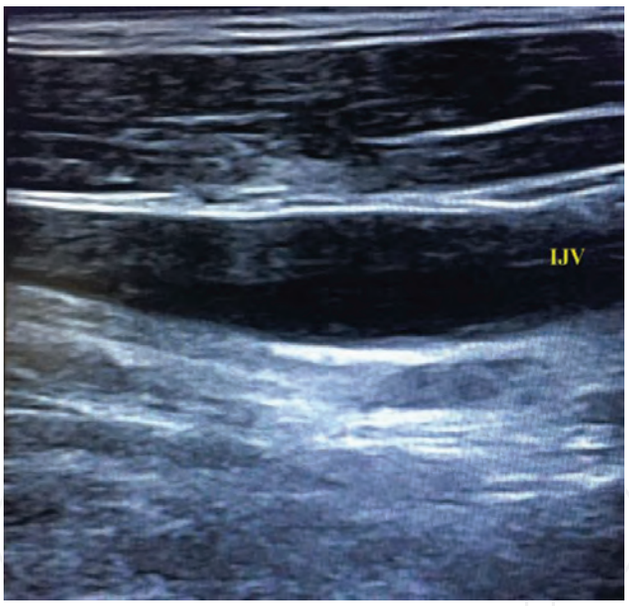

Figure 4. A two-dimensional image of the right internal jugular vein (IJV) along the long axis view.

thicker), but the major difference is vein compressibility under a slight external surface pressure (**Figures 7** and **8**). The lack of vein compressibility may indicate the presence of a thrombus. Using Doppler also helps to distinguish a vein from an artery. Respiratory-based vein excursion may also allow us to distinguish it from the artery [15]. Respiratory-based vein excursion is a change in its diameter based on the respiration phase. It is known that, in contrast to the arteries, the IJV, SV, and FV diameter decreases during inhalation and increases during exhalation [16]. In patients with hypovolemia, the IJV may completely collapse during inhalation

http://dx.doi.org/10.5772/intechopen.79400

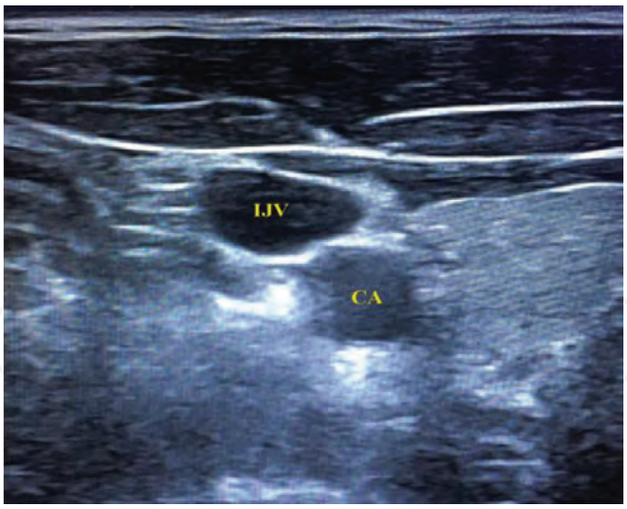

Figure 5. A two-dimensional image of the right internal jugular vein (IJV) and carotid artery (CA) along the short axis view.

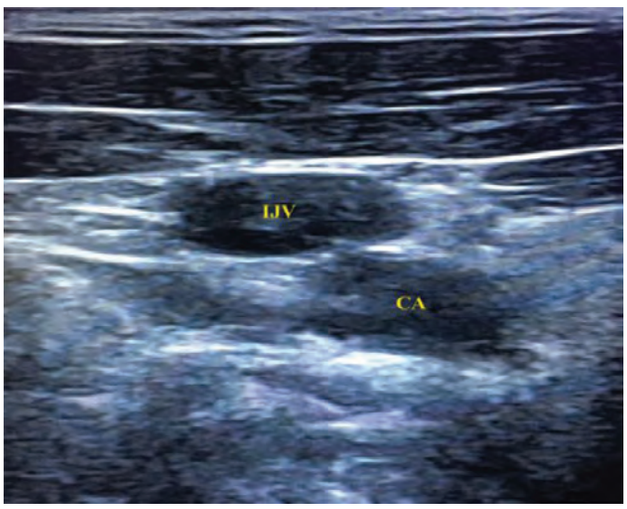

Figure 6. A two-dimensional image of the right internal jugular vein (IJV) and carotid artery (CA) along the oblique short view.

(**Figure 9**). It must be remembered that the color does not determine the nature of the blood flow (venous or arterial), but depends on the flow direction (from the probe or to the probe). By default, the device marks the blood flow directed toward the probe as red, and the blood flowing away from the probe is marked as blue. The change in the inclination of the probe can lead to the change in the vessel color on the screen of the ultrasonic device.

3.2. Special aspects of ultrasound imaging of vessels during cardiac arrest and CPR

During circulatory arrest, the blood pressure on the walls of arteries decreases; they lose elasticity and are compressed together with veins when external surface pressure is applied by the ultrasonic probe. In this regard, compressibility during cardiac arrest is characteristic of both the vein and the artery. When performing chest compression, the blood pressure on the

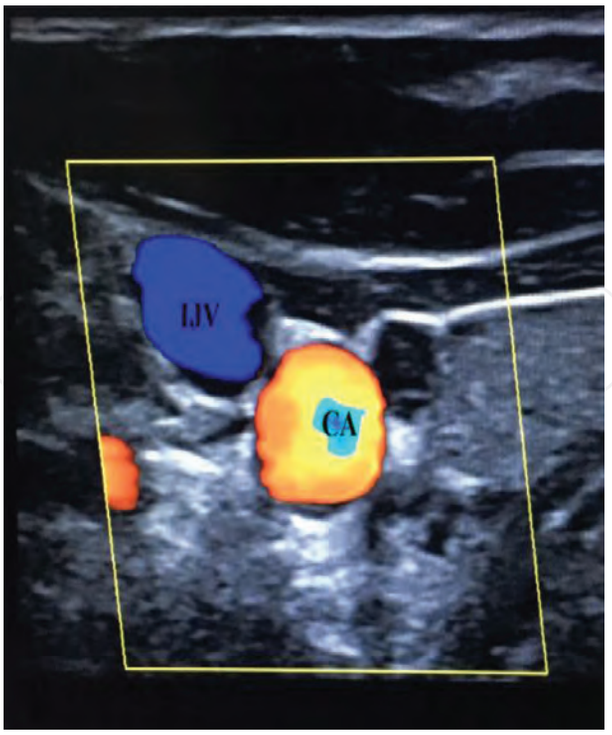

Figure 7. Ultrasound color Doppler imaging of the right internal jugular vein (IJV) and carotid artery (CA) before external surface pressure.

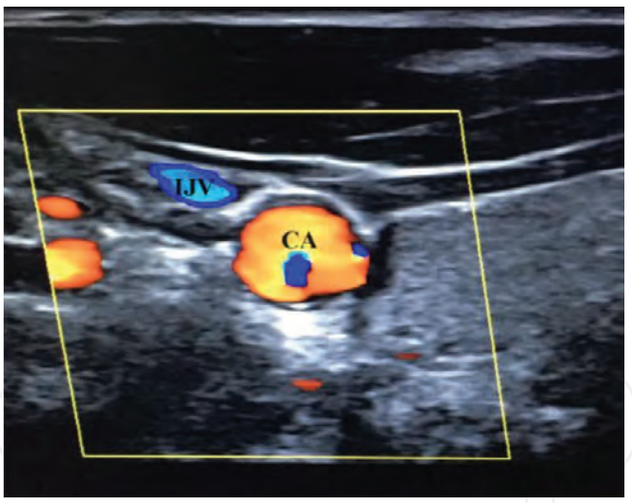

Figure 8. Ultrasound color Doppler imaging of the right internal jugular vein (IJV) and carotid artery (CA) after external surface pressure.

walls in the arteries increases. An increase in blood pressure (more than 60 mmHg) leads to an increase in the elasticity of the arteries walls, which again makes them noncompressible when pressed [17]. During CPR rhythmic change in diameter is typical for both veins and arteries due to compression and decompression of the chest with a frequency of 100–120 per minute (diameter of the CA may change by 30–40% and IJV by 50–60%). Using a Doppler is a reliable way to distinguish the artery from the vein by the flow direction.

http://dx.doi.org/10.5772/intechopen.79400

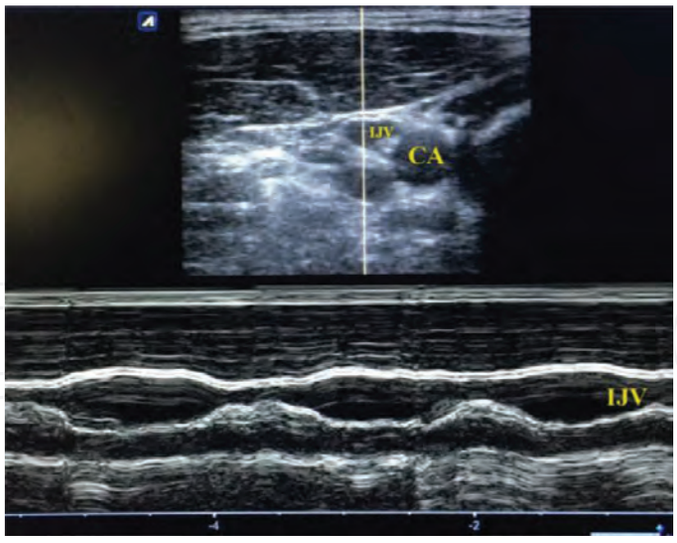

Figure 9. Measuring right internal jugular vein (IJV) diameter in healthy volunteer using M-mode ultrasonography.

The ratio of the sizes (diameters) of IJV, SV, and FV veins in patients with cardiac arrest may vary. If the cause of cardiac arrest is hypovolemia (blood loss), then the ratio of the veins diameter will be as follows: IJV < SV > FV. If the cause of cardiac arrest was thromboembolism, acute myocardial infarction or tamponade, the ratio of the veins diameter will be different: FV < SV > IJV.

4. IJV anatomy, access, and catheterization technique

IJV emerges from the outer jugular opening at the base of the skull posterior to the internal carotid artery (CA), then proceeds caudally, and shifts, taking anterolateral position in regards to CA. Denys and Uretsky [18] showed that the IJ was located anterolateral in regards to CA in 92% (**Figure 7**), >1 cm lateral to the carotid in 1%, medial to the carotid in 2%, and outside of the path predicted by landmarks in 5.5% of patients. Preliminary ultrasound evaluation of the vein patency, size, location, and possible anomalies is mandatory, it ensures avoiding futile attempts as in patients whose IJV is absent or thrombosed or who have congenital anomalies. Surrounding structures (subcutaneous tissue, carotid artery, thyroid, and lymph nodes) must also be analyzed. The properly trained clinicians use real-time ultrasound during IJV cannulation whenever possible to improve cannulation success and reduce the incidence of complications associated with the insertion of large bore catheters. Before the procedure, a patient should be placed in position on his back. The head can be turned to the contralateral side from 0 to 40°. The head-down tilt position should be used, when possible, for increasing the vein size, eliminating the vein respiratory excursion, reducing the risk of air embolism during IJV cannulation, and consequently improving the success of CVC insertion. For more than 65% of patients requiring CVC, the 10° head-down tilt position is sufficient to increase the size of IJV. In certain clinical situations, the head-down tilt position may not be applied.

4.1. Approach to vein puncture

Currently, three types of approach for real-time ultrasound-guided IJV catheterization are described: central (classical), lateral, and lateral oblique.

For classical IJV approach, one can use short or long axis vein visualization and in-plane (when included in the plane of the ultrasound beam) or out-of-plane (only a very limited part of the needle can be visualized by the ultrasound beam) needle visualization [14]. The long axis view of the IJV can be obtained by positioning the ultrasound probe in longitudinal orientation on the patient's neck. This view shows the course of the IJV, and with this probe positioning, the needle is inserted in-plane at the level of the cranial edge of the ultrasound probe; this allows the operator to visualize the entire length of the needle through the soft tissue and into the IJV [19]. With this type of technique, the information of the carotid artery, lymph nodes, and thyroid may be lost. In addition, the IJV access will be at least 3 cm cranial from the upper margin of the clavicle, for the limitation imposed by the ultrasound probe length. This fact makes it difficult to apply this kind of approach in patients with a short neck. The short axis view of the vein can be obtained by positioning the ultrasound probe in a transverse orientation (90° rotation from the long axis) on the patient's neck (the ultrasound probe is perpendicular to the course of the IJV). This view allows the visualization of the carotid artery, lymph nodes, and thyroid. With this position of the ultrasound probe, the needle is usually inserted vertically (vertical out-of-plane technique) above the middle part of the ultrasound probe in a position 1–1.5 cm cranial from the upper margin of the clavicle. This allows the operator to simultaneously visualize the IJV and all surrounding structures and ensures a caudal vein access [20]. With this type of technique, the operator has a very limited view of the needle (**Figure 10**).

The lateral short axis in-plane technique is a combination of the advantages of both previously mentioned conventional techniques, but without their limitations [21]. The ultrasound probe is positioned in a transverse orientation (short axis), with a good view of the IJV and its surrounding structures. The needle is inserted at the level of the lateral edge of the ultrasound probe [22]. This guarantees the visualization of the entire length of the needle during vein access (**Figure 11**).

This allows the operator to avoid iatrogenic puncture complications, such as arterial puncture and pneumothorax. The ultrasound-guided lateral short axis in-plane technique for percutaneous IJV cannulation can be successfully applied in patients without hypovolemia. Using this method for patients with hypovolemia and veins with a small diameter (less than 7 mm) may result in vein perforation [23].

The real-time ultrasound-guided lateral oblique short axis in-plane technique may be successfully applied in patients with hypovolemia and a small IJV size. The lateral oblique short axis view of the vein can be obtained by positioning the ultrasound probe rotated in 10–50° from the short axis. This method can be applied as follows: set the sensor so that the vein image in the transverse axis is located in the middle of the screen of the ultrasound scanner and measure the maximum distance between the lateral and medial walls at the time of inspiration of the patient. If this distance is less than 7 mm, the sensor is rotated by moving

http://dx.doi.org/10.5772/intechopen.79400

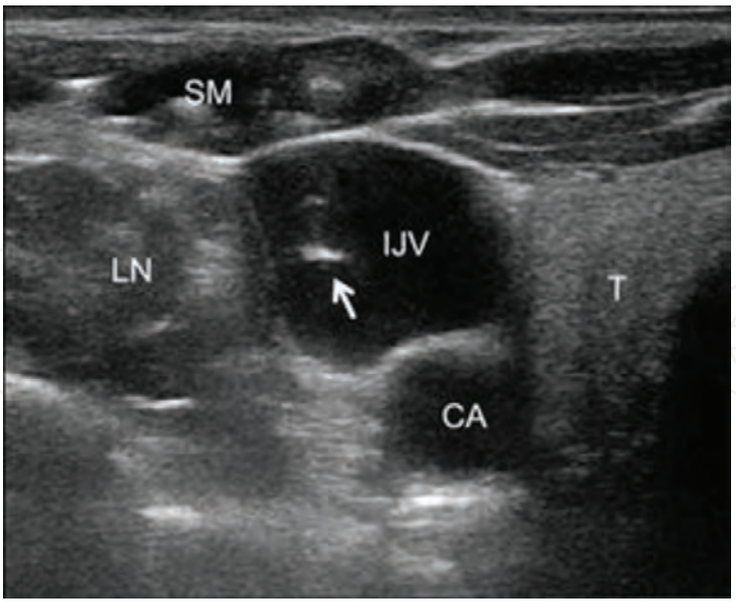

Figure 10. Short axis vertical out-of-plane technique ultrasound image of the right neck area showing the internal jugular vein (IJV), carotid artery (CA), lymph nodes (LN), sternocleidomastoid muscle (SM), and the thyroid (T). The needle is visible in a limited fashion into the internal jugular vein as a bright dot (arrow). From J Vasc Access [22].

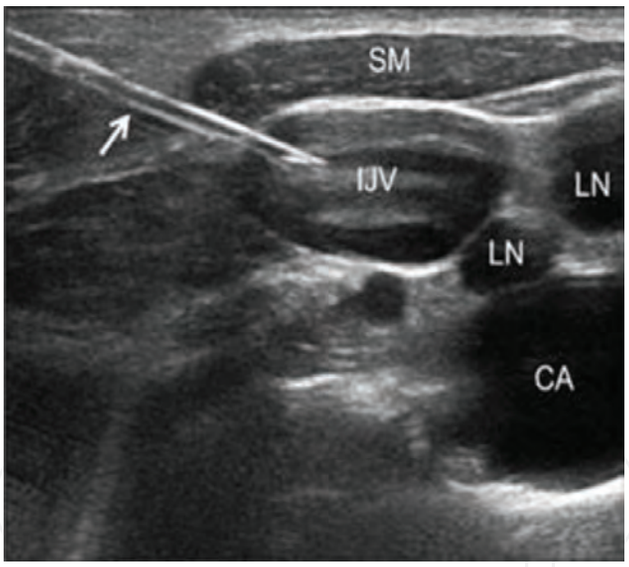

Figure 11. Short axis, lateral in-plane technique ultrasound image of the right neck area showing the internal jugular vein (IJV), carotid artery (CA), lymph nodes (LN), and the sternocleidomastoid muscle (SM). The needle is visible in its entire length with the full tip into the internal jugular vein (arrow). From J Vasc Access [22].

its lateral part upwards and the medial part downwards, and the rotation of the sensor is stopped when the distance between the walls of the vein is more than 7 mm. Fix the sensor in this position. Puncture needle is then inserted, and the vein is punctured in the sensor plane. [24]. This maneuver allows us to increase the size of the vein compared to the size in short axis (**Figure 12**).

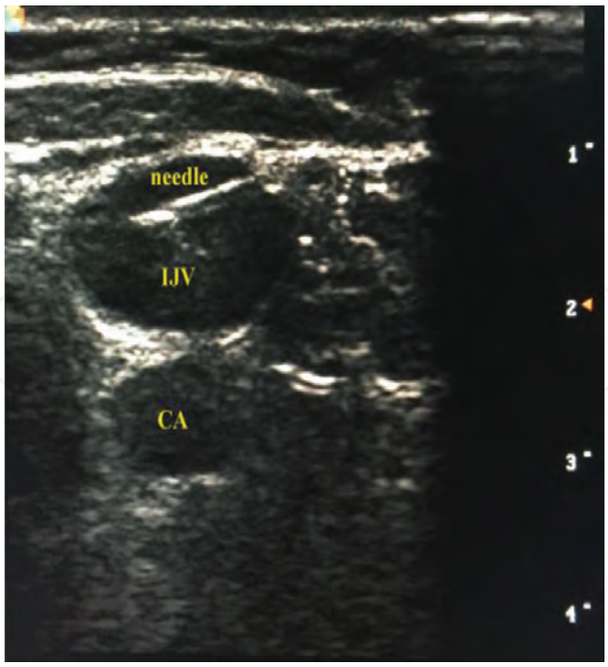

Figure 12. Lateral oblique short axis in-plane technique ultrasound image of the internal jugular vein (IJV), carotid artery (CA), and needle is visible in its entire length with the full tip into the internal jugular vein.

5. FV and FA anatomy, access, and catheterization techniques

Common femoral vein and common femoral artery (FA) lie within the femoral triangle formed by the inguinal ligament, the long adductor muscle, and the sartorius muscle. An important landmark for determining the location of the femoral vein in patients with spontaneous circulation is the femoral artery pulsation, since the vein is usually located medial to the artery in the vascular lacuna of the femoral triangle. This vascular interposition is constant only under the inguinal ligament (**Figure 13**). Change in the relative location of the vessels occurs in the caudal direction. In particular, the FA may overlap the femoral vein at a level of 1 cm below the inguinal ligament. In this regard, ultrasound imaging will accurately localize the FV and differentiate it from the femoral artery (**Figure 14**).

During CPR, it is possible to reliably distinguish the artery from the vein during the chest compression in the direction of the flow with the help of the Doppler. The advantages of choosing a femoral vein are the possibility to perform its catheterization without disrupting the CPR, lack of control devices in this area, and the ability for the resuscitator to access the patient's chest and airways. In addition, this access prevents pneumo- and hemothorax. Well-known complications of catheterization are vascular damage, bleeding, and arteriovenous fistulas.

Before the catheterization, the patient should be placed on his back, with his thigh slightly retracted, and rotated outwards. This technique allows us to increase the accessibility of the common femoral vein in 70–80% of adults [25]. It is possible to increase the cross-sectional

http://dx.doi.org/10.5772/intechopen.79400

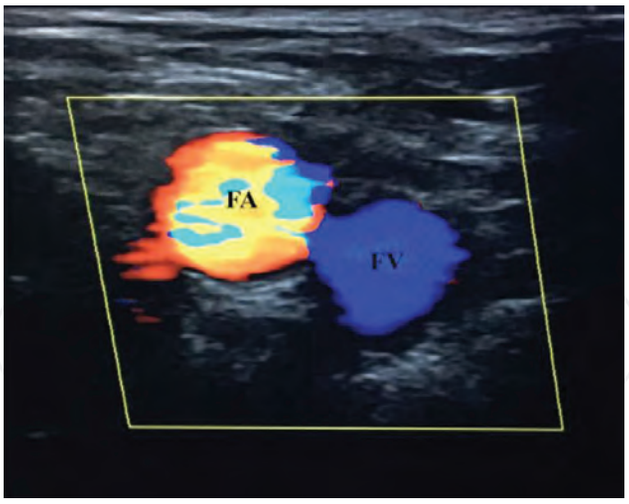

Figure 13. Ultrasound color Doppler imaging of the right femoral artery (FA) and femoral vein (FV). The US probe is installed under the inguinal ligament.

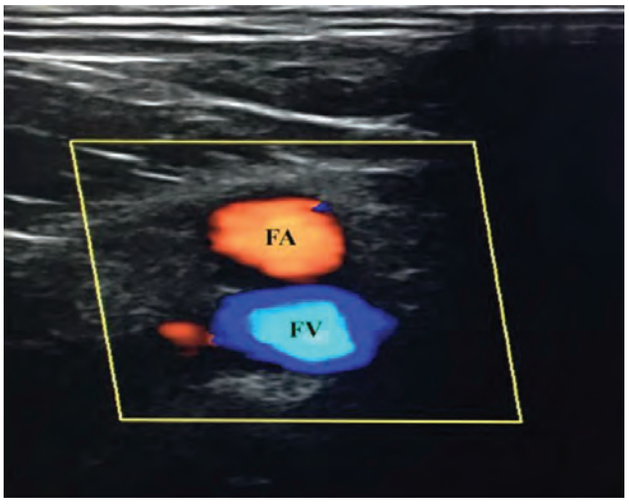

Figure 14. Ultrasound color Doppler imaging of the right femoral artery (FA) and femoral vein (FV). The US probe is installed at a level of 1 cm below the inguinal ligament.

area of the common femoral vein by more than 50% by using head-elevation tilt positions [26]. However, no data on the safety of this maneuver in patients with cardiac arrest and CPR are currently available. First, the femoral vessels in the transverse plane are visualized using a real-time 2D ultrasound, placing an ultrasonic probe under the inguinal ligament. The differentiation between the vein and artery during CPR is performed with a Doppler. The short axis out-of-plane technique is often used for the catheterization of the FV and FA. The long axis in-plane technique is preferable when longitudinal scanning of the femoral vessels is possible. The real-time ultrasound-guided lateral oblique short axis in-plane technique can also be applied. At the same time, no evidence of its preference is available.

Nowadays, femoral vessels are chosen for inserting venoarterial extracorporeal membrane oxygenator devices for extracorporeal CPR and extracorporeal life support [27]. The research results reveal promising outlook of this area of research aimed at saving human life.

6. SV catheterization techniques

The use of a subclavian vein for central venous access during CPR surgery cannot be recommended due to certain limitations. Providing access to the vein may require CPR interruption, and in particular, thorax compression. Besides, a defibrillation electrode may be located in the subclavian area. During CPR, there is a risk of post-puncture pneumo- and hemothorax during SV catheterization. Compared to IJV and FV, the SV anatomical location and its course under the clavicle bone may challenge ultrasound imaging and are accompanied by various artifacts (**Figure 15**).

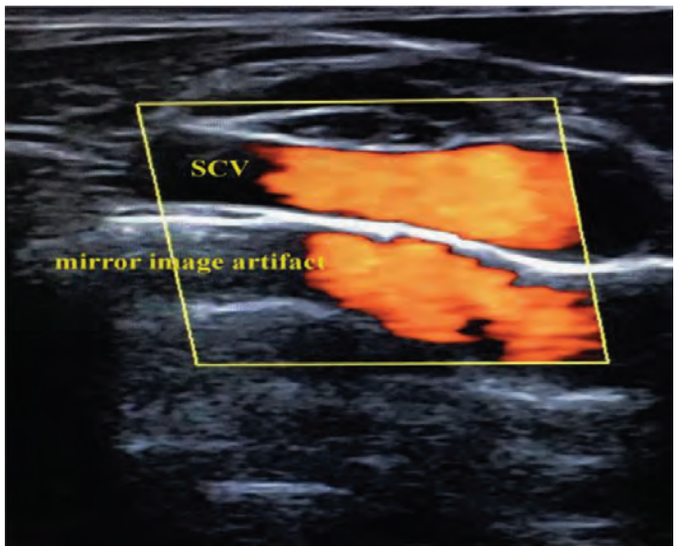

Figure 15. Ultrasound color Doppler imaging of the right subclavian vein (SV) with mirror image artifact.

7. Advantages of ultrasound-guided vascular access during CPR

It can be argued that the use of ultrasound facilitates the identification of the insertion site anatomy, localization of the vessels and their sizes, and differentiating between veins and arteries. Real-time US guidance for puncture allows us to confirm patency of the vessel, as well as needle, wire, and catheter position in the vessel. In addition, ultrasound can be used to determine the change in the filling, and thus, the cross-sectional lumen of the patient, depending on the change in the patient's position (head-down or head-elevation tilt position). In the clinical setting, these advantages allow us to choose the most secure access for puncture and the catheterization of the targeted vessel without interrupting the CPR, reduce the time of intravascular access, minimize the number of unsuccessful catheterization attempts, and reduce the risk of post-puncture complications.

8. Limitations of ultrasound-guided vascular access during CPR

The operator performing ultrasound-guided vascular access is certainly required to have special knowledge and practical skills in visualization of anatomical structures, in particular, blood vessels, during CPR. We assume that anesthesiologists, intensivists, and emergency physicians must be educated about it. To ensure this, special training of operators involved in CVC insertion should be organized. In addition, an intensive care unit must be equipped with US machines to exclude procedural delays. Ultrasound-guided vascular cannulation proved to be effective for cardiopulmonary resuscitation during in-hospital cardiac arrest. This method, however, is not to be recommended during out-of-hospital cardiac arrest, since nowadays there are no data proving its safety and efficiency.

9. Conclusions

Providing satisfactory intravascular access remains an important component of the CPR. Taking into account the advantages of ultrasound-guided central vascular access, it should be consid-ered along with other types of access (peripheral and intraosseous) in patients with in-hospital cardiac arrest.

Conflict of interest

None declared.

Author details

References

[1] Kudenchuk PJ, Cobb LA, Copass MK, Cummins RO, Doherty AM, Fahrenbruch CE, Hallstrom AP, Murray WA, Olsufka M, Walsh T. Amiodarone for resuscitation after out-of-hospital cardiac arrest due to ventricular fibrillation. The New England Journal of Medicine. 1999;**341**:871-878

[2] Rittenberger JC, Menegazzi JJ, Callaway CW. Association of delay to first intervention with return of spontaneous circulation in a swine model of cardiac arrest. Resuscitation. 2007;**73**:154-160

[3] Urakov AL, Kasatkin AA, Urakova NA. Change in local temperature of venous blood and venous vessel walls as a basis for imaging superficial veins during infrared phlebography using temperature-induced tissue contrasting. In: Ng EYK, Etehadtavakol M, editors. Application of Infrared to Biomedical Sciences, Series in BioEngineering. Singapore: Springer Nature Singapore Pte Ltd; 2017. pp. 429-436. DOI: 10.1007/978-981-10-3147-2_24

[4] Ficke BW, Ransom EF, Oakes JE. Near-infrared vein visualization in index finger pollicization. The Journal of Hand Surgery. 2017;**42**(6):481.e1-481.e2. DOI: 10.1016/j.jhsa.2017.03.039

[5] Santos D, Carron PN, Yersin B, Pasquier M. EZ-IO((R)) intraosseous device implementation in a pre-hospital emergency service: A prospective study and review of the literature. Resuscitation. 2013;**84**:440-445

[6] Anson J. A review of intraosseous access in resuscitation. Anesthesiology. 2014;**120**:1015-1031

[7] Brass P, Hellmich M, Kolodziej L, Schick G, Smith AF. Ultrasound guidance versus anatomical landmarks for internal jugular vein catheterization. Cochrane Database of Systematic Reviews. 2015;**9**(1):CD006962. DOI: 10.1002/14651858.CD006962.pub2

[8] Brass P, Hellmich M, Kolodziej L, Schick G, Smith AF. Ultrasound guidance versus anatomical landmarks for subclavian or femoral vein catheterization. Cochrane Database of Systematic Reviews. 2015;**9**(1):CD011447. DOI: 10.1002/14651858.CD011447

[9] Ullman JI, Stoelting RK. Internal jugular vein location with the US Doppler blood flow detector. Anesthesia and Analgesia. 1978;**57**:118. DOI: 10.1213/00000539-197801000-00024

[10] Legler D, Nugent M. Doppler localization of the internal jugular vein facilitates central venous cannulation. Anesthesiology. 1984;**60**(5):481-482

[11] Kawamura R, Okabe M, Namikawa K. Subclavian vein puncture under ultrasonic guidance. Journal of Parenteral and Enteral Nutrition. 1987;**11**(5):505-506

[12] Hilty WM, Hudson PA, Levitt MA, Hall JB. Real-time ultrasound-guided femoral vein catheterization during cardiopulmonary resuscitation. Annals of Emergency Medicine. 1997;**29**(3):331-336

[13] Benassi F, Vezzani A, Vignali L, Gherli T. Ultrasound guided femoral cannulation and percutaneous perfusion of the distal limb for VA ECMO. Journal of Cardiac Surgery. 2014;**29**(3):427-429. DOI: 10.1111/jocs.12319

[14] Troianos CA, Hartman GS, Glas KE, Skubas NJ, Eberhardt RT, Walker JD, Reeves ST. Special articles: Guidelines for performing ultrasound guided vascular cannulation: Recommendations of the American Society of Echocardiography and the Society of Cardiovascular Anesthesiologists. Anesthesia and Analgesia. 2012;**114**:46-72. DOI: 10.1213/ANE.0b013e3182407cd8

[15] Kasatkin AA, Urakov AL, Nigmatullina AR. Using ultrasonography to determine optimal head-down tilt position angle in patients before catheterization of the internal jugular vein. Indian Journal of Critical Care Medicine. 2017;**21**:160-162

[16] Kent A, Patil P, Davila V, Bailey J, Jones C, Evans D, Boulger C, Adkins E, Balakrishnan J, Valiyaveedan S, Galwankar S, Bahner D, Stawicki S. Sonographic evaluation of intravascular volume status: Can internal jugular or femoral vein collapsibility be used in the absence of IVC visualization? Annals of Thoracic Medicine. 2015;**10**(1):44-49. DOI: 10.4103/1817-1737.146872

[17] Dietrich CF, Horn R, Morf S, Chiorean L, Dong Y, Cui XW, Atkinson NS, Jenssen C. Ultrasound-guided central vascular interventions, comments on the European Federation of Societies for Ultrasound in Medicine and Biology guidelines on interventional ultrasound. Journal of Thoracic Disease. 2016;**8**:E851-E868. DOI: 10.21037/jtd.2016.08.49

[18] Denys BG, Uretsky BF. Anatomical variations of internal jugular vein location: Impact on central venous access. Critical Care Medicine. 1991;**19**:1516-1519

[19] Denys BG, Uretsky BF, Reddy PS. Ultrasound-assisted cannulation of the internal jugular vein. A prospective comparison to the external landmark-guided technique. Circulation. 1993;**87**:1557-1562

[20] Gallieni M, Martina V, Rizzo MA. Central venous catheters: Legal issues. The Journal of Vascular Access. 2011;**12**:273-279

[21] Rossi UG, Dahmane M, Petrocelli F, Patrone L, Gola G, Ferro C. Comparison between vertical and lateral ultrasound-guided technique for percutaneous internal jugular venous cannulation in permanent central venous access. Cardiovascular and Interventional Radiology. 2012;**35**:S211

[22] Rossi U, Rigamonti P, Tichà V, Zoffoli E, Giordano A, Gallieni M, Cariati M. Percutaneous ultrasound-guided central venous catheters: The lateral in-plane technique for internal jugular vein access. The Journal of Vascular Access. 2014;**15**(1):56-60. DOI: 10.5301/jva.5000177

[23] Mey U, Glasmacher A, Hahn C, et al. Evaluation of an ultrasound-guided technique for central venous access via the internal jugular vein in 493 patients. Support Care Cancer. 2003;**11**(3):148-155

[24] Kasatkin A, Nigmatullina A, Urakov A, Shchegolev A. Method for internal jugular catheterisation by lateral access. RU Patent 2,655,449. 2018

[25] Werner SL, Jones RA, Emerman CL. Effect of hip abduction and external rotation on femoral vein exposure for possible cannulation. The Journal of Emergency Medicine. 2008;**35**:73-75

[26] Hopkins JW, Warkentine F, Gracely E, Kim IK. The anatomic relationship between the femoral artery and common femoral vein in frog leg position versus straight leg position in pediatric patients. Academic Emergency Medicine. 2009;**16**:579-584

[27] Mosier J, Kelsey M, Raz Y, Gunnerson K, Meyer R, Hypes C, Malo J, Whitmore S, Spaite D. Extracorporeal membrane oxygenation (ECMO) for critically ill adults in the emergency department: History, current applications, and future directions. Critical Care. 2015;**19**:431. DOI: 10.1186/s13054-015-1155-7

IntechOpen

9

Ultrasound Guided Vascular Access

Hamid Shokoohi, Ali Pourmand and Keith Boniface
George Washington University Medical Center,
Washington DC,
USA

1. Introduction

Vascular access is an important procedure for clinicians to master. Chronic medical conditions, intravenous drug use, and obesity can all make placements of vascular catheters in central and peripheral veins challenging and time-consuming. External landmarks have traditionally guided the placement of the needle for the performance of central venous catheterization. The proximity of such structures as the large arteries of the chest and neck as well as the apex of the lung results in a 6.2-11.3% rate of immediate mechanical complications when performing subclavian or internal jugular catheterization.[1] In recent years there have been significant improvements in portable ultrasound technology including the development of relatively inexpensive ultrasound machines with sufficient resolution to guide needle placement through tissues. These machines are now found throughout the house of medicine by the bedside of patients. Multiple studies have been performed demonstrating the benefits of ultrasound guidance of central venous catheter placement by multiple specialties, and the same technique has been extended to the placement of peripheral intravenous catheters.[2,3,4,5,6] In this chapter, we describe the use of ultrasound for guidance of vascular access.

2. Use of ultrasound for vascular access

2.1 Transducer selection

Transducer characteristics, such as frequency and shape, determine ultrasound image quality. For the purpose of vascular access, it is ideal to use high frequency and small footprint transducers. The high-frequency linear array transducer provides higher resolution of the superficial areas of soft tissue including artery and veins. The flat and small footprint shape of the linear array transducer is less prone to slip off of the vessel of interest. Modern transducers are designed to generate a range of frequencies. For example, linear 5-12 MHz transducer can be used to adequately scan deeper targets if it used in lower range of frequencies. In general, transducers in the range of 5-12 MHz are preferred as the depths of target vessels for accesses are often limited to 2-4 cm below the skin surface.[7]

2.2 Modes

B-Mode and color Doppler are the main ultrasound modes used for the purpose of venous access. B-mode ultrasound produces recognizable two dimensional (2D) gray scale images.

Color Doppler is an application to characterize blood flow. The doppler effect occurs when blood flow of red blood cells move toward or away the ultrasound transducer. If the flow in a vessel is moving towards the transducer, the color displayed in the vessel is RED and when the flow is moving away from the transducer, the perceived frequency display is BLUE (BART – Blue Away and Red Toward). (Figure 1A, B) To clearly display the presence of a flow in an artery or vein, it is necessary to create an angle between the transducer and the direction of the flow. The color Doppler detection of flow is optimal when the transducer is parallel (0 degrees) to the flow and it is worst when the transducer is perpendicular (90 degrees) to the vessel, so in clinical practice, some angulations of the transducer are necessary to optimize color Doppler signal.

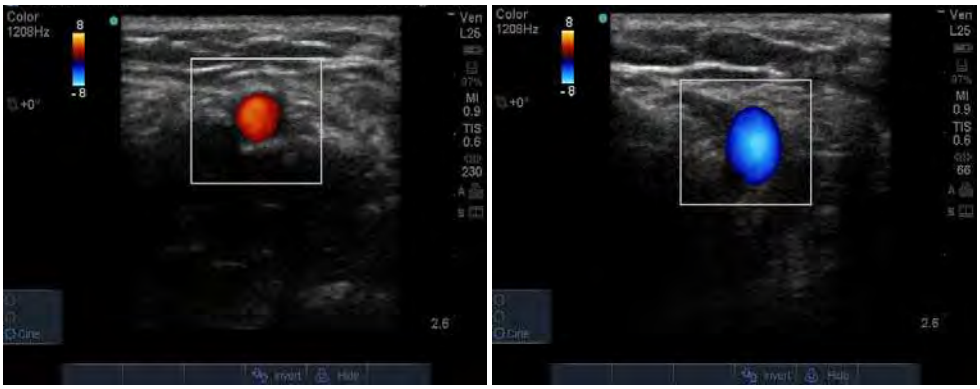

Fig. 1. (A) Transverse view, the brachial artery without compression with color flow TOWARD the transducer, (B) Transverse view, the brachial artery without compression with color flow AWAY from the transducer

2.3 Optimizing image quality

Best visualization of target vessels with ultrasound requires an optimal machine setting. In general, proper transducer selection and the selection of pre-programmed vascular ultrasound settings provide acceptable quality images. Additional controls that can further improve the image quality include gain, depth, focus and frequency.

Depth: Proper depth adjustment provides better target vessel imaging and facilitates tracking the needle through the tissues. By increasing the depth setting, the target vessel gets smaller and smaller. With too shallow a depth setting, important structures in the vicinity of the target vessel (such as a neighboring artery) may be lost off the far edge of the screen. It is therefore important to select the appropriate depth setting according to the target vessel location.

Gain: The brightness of the image on the screen is controlled by the gain setting of the ultrasound machine, and the quality of images displayed on monitor also depends on the selected gain. Increasing the gain makes the image brighter, while decreasing the gain makes the image darker. In addition to the overall gain, selected regions of the screen can be adjusted by selecting gain controls for the near field or far field. Inappropriately increased gain will add "noise" artifact to the image that adversely impact the quality of images.

Focus: The highest resolution of the displayed image is at the focal zone. Some machines automatically adjust the focal zone to the center of the screen, however, in systems with a manually adjustable focus, it is important to place the 'focus' at the level of the target vessel of interest.

3. Image orientation

Proper transducer orientation is an important step to accomplish a successful procedure. Most transducers have an indicator of some sort on one side of the probe that corresponds to a mark displayed on one side of the displayed image on the screen. (Figure 2A and 2B)

Fig. 2. (A) A high frequency linear transducer for vascular procedure, with orientation indicator (B) Localization and matching orientation indicator with ultrasound indicator on screen (green dot)

The aim is to keep the indicator on the side of the probe oriented in the same direction as the orientation mark side of the monitor. By default, the orientation mark is usually displayed at the left side of the image and keeping the indicator toward the left side of provider will largely prevent further confusion about the orientation. If there is any confusion about the orientation of the probe, a finger can be rubbed on one side of the transducer surface after gel application to produce an image on the screen and confirm the orientation.

3.1 Preparing a sterile transducer

Central venous access is a sterile procedure. In order to use ultrasound, the probe needs to become part of the sterile field. When preparing for the procedure a sterile ultrasound sheath should be placed on the sterile field. Ask your assistant to apply ample sterile or non-sterile gel into the sterile sheath. Place the ultrasound transducer inside the sterile sheath and ensure that gel is applied generously between the transducer and inside of the sheath covering. Smooth the sheath covering over the transducer surface to avoid any wrinkles or trapped air that could impede full contact. Wrap the sterile rubber band supplied with most commercially available probe covers around the transducer to avoid transducer movement inside the sheath during ultrasound scanning.[8,9]

Alternatively, if a sterile probe cover is not available, a sterile glove can be used to cover the transducer surface, although this does not cover the cable of the ultrasound probe and care

must be taken during the procedure to prevent contamination of the sterile field by the cable. Applying generous amount of gel into the sterile glove and sliding the transducer into the glove's thumb may prevent air trapping or wrinkle on the contact surface. (Figure 3)

1.	Sterilize the skin surface thoroughly with an antiseptic solution
2.	Surround the CVC placement location with full body sterile fenestrated drape
3.	Using sterile technique, open the probe cover packet onto the sterile work field
4.	The gowned and gloved provider places ½ of the contents of the sterile gel inside the sheath
5.	Place the transducer inside the sheath, taking care to displace any air bubbles between the probe face and the probe cover
6.	Extend the sterile sheath to cover the cord completely
7.	Hold the sheath in place with a rubber band around the transducer head
8.	Place the transducer on the sterile field
9.	Use a package of sterile acoustic gel
10.	Apply sufficient amount of sterile gel over the site of scanning
11.	Place the transducer over the procedure site, identify target vessel, and proceed with cannulation

Table 1. Preparing the ultrasound transducer for central venous catheterization

Fig. 3. Probe position and needle insertion to approach internal jugular Central line access by using a sterile glove as an alternative to sterile probe cover

4. Planes and views

Transverse and longitudinal views are two main planes used for the purpose of vascular access. In transverse view, the transducer plane is in cross section of the target vessel and the vessel is displayed on the screen as a circle. In longitudinal view, transducer plane and vessel plane are parallel and the vessel is displayed on the screen as a long tube running across the screen. A longitudinal view allows visualization of entire vessel of interest, but it

requires that transducer beam, needle and target vessel be held parallel, which can be challenging for the novice user.[10,11]

In general, we recommend starting with transverse view as it allows visualizing adjacent structures including artery and nerve in the area and is easier to visualize the tip of needle and its insertion. The provider can switch between the two views during the procedure as needed to track the progress of the needle moving toward the target vessel.

4.1 Differentiating artery and vein

Differentiating between artery and vein is essential to safely perform ultrasound guided vascular access. Compressibility of veins is the simplest way to distinguish artery from vein. Veins typically compress with minimal pressure applied from the probe, while arteries retain much of their original shape and appearance. When performing internal jugular vein placement one may visualize the influence of respiratory variation on the vein diameter. Valsalva maneuvers and trendelenberg positioning make the vein larger but have minimal affect on the carotid artery. The application of color Doppler is also very useful in differentiating artery from vein. Arteries have pulsatile flow visualized on color Doppler, while the vein has minimal flow. (Figure 4A and 4B)

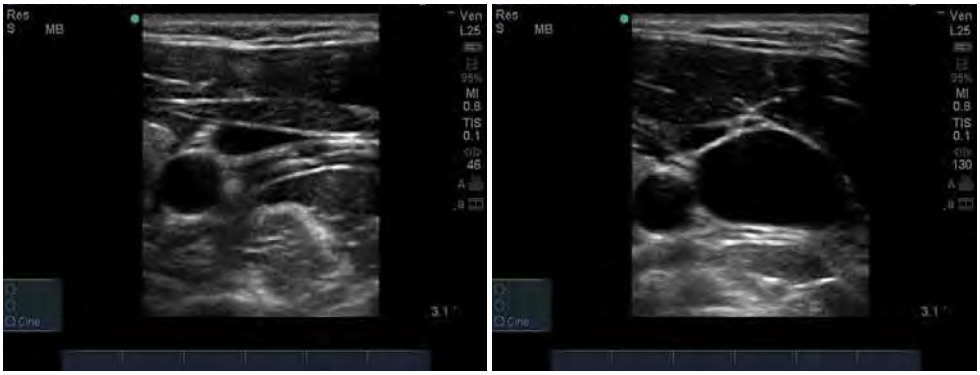

Fig. 4. (A) Transverse view of right internal jugular vein (with mild compression) and adjacent carotid artery (B) Transverse view of a distended right internal jugular vein during Valsalva maneuver and adjacent carotid artery

4.2 Scanning techniques

Static vs. Dynamic: The guidance of vascular access using ultrasound can be categorized as static or dynamic. In the static use of ultrasound, the provider would apply ultrasound to localize the vein and mark the site of needle insertion on the skin; after that the procedure will be performed much like a traditional landmark-based approach.

In dynamic guidance, the provider uses the ultrasound in "real time," with continuous visualization of the needle insertion throughout the procedure. The authors highly recommend the dynamic approach on performing central venous access considering the possibility of changes due to patient movement in the time interval between marking and needle insertion in the static approach. The success rates for dynamic guidance as compared

with the static technique is significantly higher. Direct ultrasound guidance gives the opportunity of visualizing the needle in real time to puncture the vein and avoid puncturing adjacent artery and nerves but it is more technically demanding because it requires significant eye–hand coordination and it requires a sterile probe cover throughout the procedure.

One-provider vs. Two-provider: The dynamic use of ultrasound can be conducted by a provider operating alone, or by two providers. In the one-provider method, the provider holds the ultrasound transducer with the non-dominant hand and the needle with the dominant hand. In the two-provider method, a sterile assistant will hold and control the probe while the provider performs the needle insertion under real-time ultrasound guidance. We recommend the one-provider method, as it not only allows for more flexibility and the ability to perform the procedure independently, but also enables the provider to make very small movements of the ultrasound probe in conjunction with the needle to enhance localization of the needle tip. In a small study among 44 cases focusing on the specific question of whether single- vs. two-provider technique was advantageous revealed no significant differences.[12,13]

Out-of-Plane vs. In-Plane Approach: Needle insertion can be performed in either in- plane (longitudinal) or out-of- plane (transverse) in relation to the ultrasound transducer. During the in-plane insertion, the needle is placed parallel to the transducer and the full length of the needle shaft and tip are visualized. In the out-of plane approach, the needle is placed perpendicular to the transducer and either the needle shaft or the tip is visualized as a hyperechoic dot on monitor. In this method, needle, vein, adjacent artery or vein and tissue movements are observed. The choice of these two methods depends on the location of the vessel, provider experience, and anatomic relationships. In a study by Blaivas et al. they reported that the technique utilizing a transverse, short-axis view of the needle in vascular access was easier for novices to learn than a technique using longitudinal scan.[11]

5. Ultrasound - guided catheter insertion techniques

5.1 Internal jugular vein

Anatomy and ultrasound technique: The internal jugular vein (IJ) is typically located anterior and lateral to the carotid artery; however, there is a significant anatomic variation where the vein can overly the artery and even be medial to the artery. As described above, the IJ vein and carotid artery can be differentiated by the fact that the vein is compressible, non-pulsatile, and distensible by the Trendelenberg position or the Valsalva maneuver.[14] (Figure 4A and 4B)

Contralateral rotation of the head significantly affects the relative anatomy of the IJ vein and carotid artery. Extreme contralateral head rotation can decrease IJ vein diameter and increase overlap on the carotid artery.[8,14]

In longitudinal view, the IJ vein can be followed inferiorly, down to the level of the sternoclavicular joint where it joins the subclavian vein on each side and drains into the superior vena cava.[8]

Positioning and preparation: Proper positioning of the patient significantly affects the likelihood of a successful procedure. For the IJ cannulation, patient's head should be rotated

slightly contralaterally, with the neck extended. Extreme rotation of the neck may increase the amount of overlap of the carotid artery and IJ vein. The patient should be placed in Trendelenburg position in order to maximally distend the IJ vein. The ultrasound machine should be placed by the same side of the bed and directly in front of the provider to provide a direct line of vision that is ergonomic and efficient.

An initial examination of the surrounding areas and the target vessels should be performed to confirm the patency of the IJ vein and absence of thrombosis prior to applying the sterile probe cover and prepping the patient. Following this important step, the procedural areas of the neck and upper chest should then be prepared in the usual manner, and full barrier precautions should be used to maintain sterility of the procedure.[2,8,9] A sterile probe cover should be applied as discussed in Table 1. The CVC catheter should be set up per normal routine. The catheter ports should be flushed to remove air and to check for their patency. The equipment needed for catheter insertion, including the CVC kit should be set and place within an easy reach. Local anesthetic should be applied at the site of puncture.

Catheter Insertion: Provider should use the dominant hand to handle the needle and the non-dominant hand to hold and handle the transducer. If prefer to start with transverse view, the needle is placed perpendicular to the transducer directly underneath the middle of the transducer while jugular vein placed in the center of the screen. The needle insertion site should be 0.5-1 cm proximal to the transducer. In this approach, the needle tip and the shaft are visualized as a hyperechoic dot on monitor. If the needle tip cannot be visualized, indenting the tissue overlying the vein or moving the transducer along the axis of the vein while "agitating" the needle may enhance the image of the needle and tip. If consider longitudinal plane, the needle is placed inline with and parallel to the transducer in which the entire length of the needle and the tip are visualized as puncture the vein. Once the vessel has been successfully punctured, the transducer can be set aside and the procedure can proceed normally with wire and catheter placement. The wire should be advanced slowly with no pressure at the length of the needle plus 5-6 cm. considering the short distance of the puncture site and superior vena cava to the right jugular vein extreme precaution should be used not to advance the catheter too far to prevent right atrial or ventricular wire insertion. After wire placement, the needle is removed and a small incision is made around the wire insertion to facilitate dilator insertion. After removal of the dilator, the catheter is then advanced to the desired distance that is 4-5 cm shorter in the right jugular vein compare to the left IJ vein.[8,9] Once the line is in place, it should be properly flushed in all ports, secured, and dressed. Post procedure chest X ray is required to confirm proper catheter placement and the lack of complications including pneumothorax to start using the central catheter.

5.2 Subclavian vein

Anatomy and ultrasound technique: Subclavian vein is a continuation of the axillary vein at the lateral border of the first rib that crosses over the first rib and passes in front of the anterior scalene muscle that separates the vein from subclavian artery. The subclavian vein (SC) continues in main length behind the medial third of clavicle which makes it less available for ultrasound scanning. At the junction of Sternoclavicular joint in each side SC veins join to the IJ veins and form the innominate vein to the left and brachiocephalic vein to the right side.[15]

To visualize the Subclavian vein, the ultrasound transducer is placed at the supraclavicular space posterior to the long axis of clavicle to obtain a longitudinal view of the SC vein. At this level it is critical to differentiate SC vein from the SC artery as they pass in parallel along side of each other. The SC vein can be distinguished from the artery by the fact that the SC vein is in a more medial and superficial than artery and by following its path medially it can be traced to IJ vein. The SC vein is not pulsating and affected by Valsalva maneuver similar to IJ vein.

SC vein can be visualized at the infraclavicular region by placing transducer at the mid third of clavicle while the half of the footprint covering the cross section of the clavicle and the lower half investigating the infraclavicular region.

Catheter insertion: The SC vein access with ultrasound guidance can be performed through either supraclavicular or infraclavicular approach. In supraclavicular approach while the vein is visualized the probe will be adjusted toward the medial end of the vein near the junction of IJ vein to provide sufficient space for the needle placement under real time ultrasound guidance. Following the puncture site identification, the area is prepped and draped sterilely and the ultrasound transducer sterile cover should applied as described previously. Furthermore, the ipsilateral IJV area should be prepped in case of possible catheter misplacement required proper ultrasound guided repositioning. While the needle gains access to the SC vein the guide wire would advance and the transducer can be set aside and proceed with a normal procedural steps according to the Seldinger's technique.

Typically, the subclavian vein is more difficult to visualize by ultrasound due to its position under the clavicle, which requires significant angulations and manipulation of the transducer to acquire and maintain sufficient imaging during real time procedure. Therefore, it is less ideal procedure compare to ultrasound guided IJ CVC access.

5.3 Femoral vein

The proximal femoral vein is medial to the femoral artery, deep to the fascia iliaca and superficial to the iliopsoas muscle. At the lower level the vein gradually descend posterior to the femoral artery that would be deeper in ultrasound scanning. For the purpose of CVC placement provider should consider more proximal (cephalad) puncture site where the vein is medial to the artery. Minimal pressure on the vein can totally compress the vein confirming the lack of thrombosis. Often, inguinal lymph nodes also appear as hyperechoic structure in the region that need to be distinguished by scanning proximally and distally in this region. The femoral vein should be distinguished from the artery by the fact that the vein is in a more medial and deeper than artery and by examining its compressibility and lack of pulsatile doppler.

Catheter insertion: Before applying sterile procedures, we recommend to perform a systematic anatomical survey from medial to lateral and superficial to deep, distinguishing vein from artery and investigating the presence of thrombi. The groin area should be exposed while patient is in supine and the leg is in natural position. After area and transducer preparation in a sterile manner (table 1), transducer should be placed along the inguinal crease. If the femoral artery and nerve are deep, the machine imaging capability should be adjusted appropriately by increasing the depth and adjusting the gain. Starting with a short axis view will provide a sufficient image of adjacent structure and facilitate a

proper needle insertion. However, transducer can be rotated 90 degree while the femoral vein image keep in the center of screen and it provide a longitudinal view of the vein. While the venous puncture confirmed, the procedure should be proceed identical to the SC and IJ vein access considering the Seldinger's technique.

6. Ultrasound - guided peripheral venous access

Intravenous (IV) access is a basic and critical procedure, which routinely performs, in medical community. IV access usually uses to administer medication, IV fluid, obtaining blood sample and it is one of the necessary actions for patients who need to be admitted in hospital. This procedure usually performs by medical technician or nurses, but sometimes they are unable to obtain access and this could delay patients' care. This section will discuss important key features regarding peripheral IV access and pitfalls to enhance success rate to insert IV access without any invasive procedure.

Fig. 5. Transverse probe position to approach peripheral IV access with orientation indicator toward to right side of patient

6.1 Anatomy

The upper extremity consists of two types of veins, superficial and deep. These 2 sets of veins have several communications, known as anastomose. The deep veins accompany the arteries. They are connected to the superficial system by perforating veins. The depth of vein is measured by distance from skin. The superficial veins start on the back of the hand as a dorsal arch. Cephalic and Basilic veins are example of superficial veins. Dorsal veins of the hand empty into the cephalic vein on the lateral aspect and into the basilic vein on the medial aspect of the forearm. The cephalic vein ascends in the radial (lateral) aspect of wrist and courses laterally upward around the anterior surface of the forearm. Under the front of the elbow it divides to some branches, which receives a communicating branch from the deep veins of the forearm and passes across to join the basilic vein. In the upper arm, the cephalic vein terminates in the infraclavicular fossa, and empty into the axillary vein. The

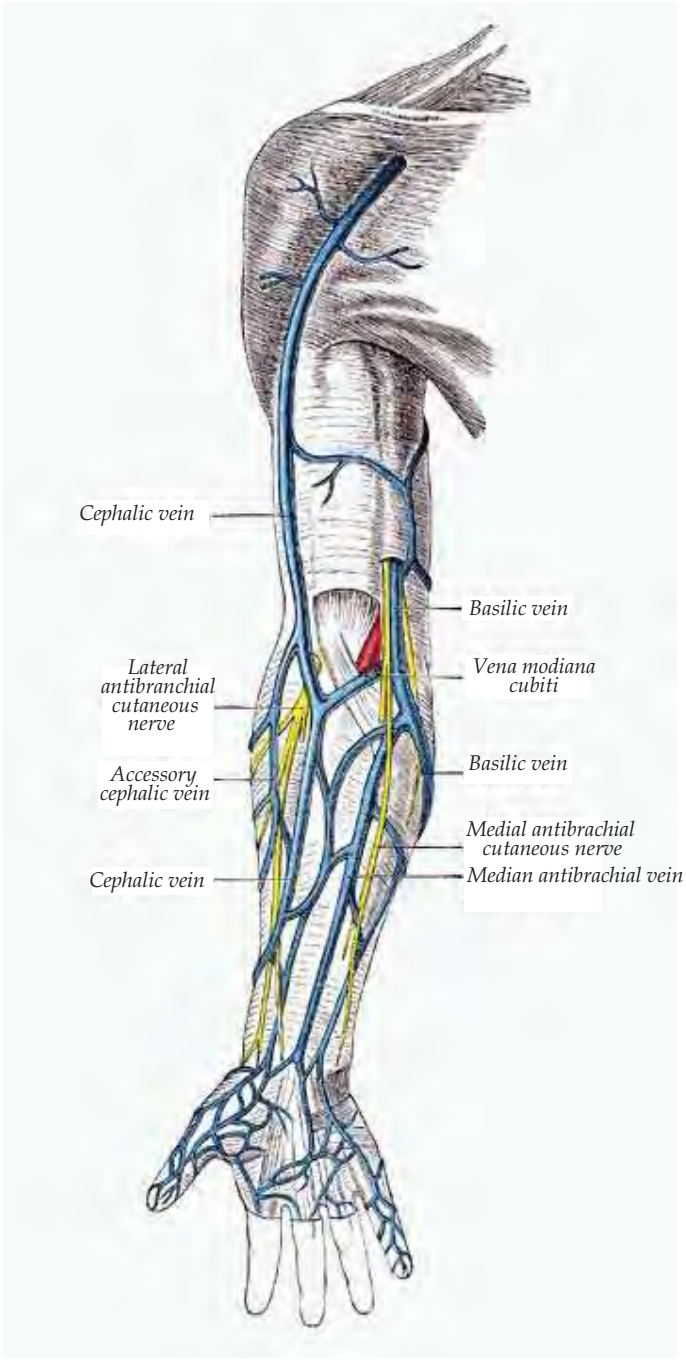
Cephalic vein
Basilic vein
Lateral antibranchial cutaneous nerve
Vena modiana cubiti
Accessory cephalic vein
Basilic vein
Medial antibrachial cutaneous nerve
Cephalic vein
Median antibrachial vein

Fig. 6.

basilic vein runs medially along the ulnar part of the forearm and penetrates the deep fascia as it courses past the elbow in the upper arm. It then joins with the deep brachial veins to become the axillary vein. The median cubital vein joins the cephalic and the basilic veins on the ventral surface of the elbow. The axillary vein becomes the subclavian vein at the lateral border of the first rib. At the medial border of the scalenus anterior muscle, the subclavian vein joins with the internal jugular vein to become the brachiocephalic vein, with the subclavian vein coursing anterior to the scalenus anterior muscle. The left and right brachiocephalic veins join to become the superior vena cava, which empties into the right atrium.[16,17]

6.2 Preparation

The ability to obtain US guided IV access is a skill that combines knowledge of peripheral IV access and US. Provider should collect necessary equipment prior to start the procedure at the bedside. Provider should consider contraindication to start IV access in upper extremities such as burn, cellulitis, end stage renal disease access, scar from previous trauma or surgery, and breast cancer on dependent arm. Provider should explain the procedure to patient and request permission to start IV access. Basic equipment at bedside should consist of appropriate angiocatheter size, tourniquet, skin cleaning instrument (alcohol or betadine swab), 2x2 gauze, tape, band-aid, sterile transparent dressing, blood tube, iv tubing and extensor, vaccutainer, normal saline flush, sharp container, biohazard bag, gloves, sterile lubricant and of course ultrasound machine.

6.3 Procedure

This procedure can be done as one or two person procedure. Usually one-person procedure is a routine and acceptable procedure. In this procedure provider can have a control of probe and can change angle, depth or approach instead of asking the second person to manage probe. The high frequency, linear probe is appropriate for peripheral IV access. Using high frequency probe will show superficial structure. The vascular structure consists of vein and artery. Veins will be anechoic structures and easily compressible with probe pressure. Arteries are anechoic structures, which they could be compressible but they have a pulse and will pulsate under probe pressure. There is another way to distinguish between veins and arteries using color Doppler flow. In this scenario, arteries will have central red color flow pulsating compare with veins that there is a blue non-pulsating color.

After having equipment ready for IV access and explain procedure to patient, skin needs to be clean with cleansing agents, and then tourniquet should be applied to upper arm. Ultrasound probe with orientation marker should be facing to right side of patient this will correlate with an indicator on the left side of US monitor and left side of probe. The next step is to use sterile gel to locate vascular structure. As mentioned above, veins are easily compressible with transducer pressure and should be located in the middle of screen. The depth key should be adjusted to make sure veins are in an approachable depth. Vascular structure on short axis should be circular versus long axis. Using short axis approach, the vein should be in the middle of screen. In this situation, middle of transducer is compatible with middle of US screen. Appropriate angiocatheter size

should be use and clean 3cm above the antecubital area, then introduce angiocath with 45 degree and cannulate skin. You should see the tip of needle as a hyperechoic structure and you should approach the vein. You will stop advancing your needle as soon as you get blood flush back. Now remove introducer and advance plastic angiocatheter all the way in. You need to attach extensor and apply sterile dressing to accomplish your procedure. (Figure 5)

6.4 Complication

There are several complication related to peripheral IV access. These complications are divided to vascular, infectious, and neurological. Vascular complication include arterial puncture and formation of hematoma, local infiltration or extravasations of fluid, superficial or deep vein thrombosis. The most common infectious complications with US guided IV access are phlebitis and cellulitis. Soft tissue swelling and superficial vein thrombosis can mimic the infection at IV site. Paresthesia due to nerve irritation and local infiltration is the most common complication. There is no long-term nerve damage was reported.

7. US guided arterial line

The radial artery is the extension of the brachial artery. It is originating inferior to elbow along the lateral side of forearm along the radius bone. The main part of focus is radial artery in wrist.

Arterial line placement is an invasive procedure, which it requires skill and expertise to perform it. It is painful procedure and needs a lot of preparation. Preparation is already discussed in aforementioned section, but arterial line kit is additional equipment that we need for this procedure.

7.1 Indication

There are several indications for arterial line placement. Reliable and frequent blood pressure measurements in patients who are hemodynamically unstable, access to arterial blood for frequent acid-base, or blood gas sampling.[18]

7.2 Procedure

US guided arterial line requires fewer attempts and more success rate. After prep and drape in sterile fashion, and cover US probe with sterile cover, arterial line should be located. The characteristic of artery as mentioned above is pulsating in nature with special color Doppler and non compressible. US probe should be in radial side of wrist with orientation indicator facing to right side of patient. After anterior surface of the artery is punctured with the bevel of the angiocatheter facing up and pulsatile blood return, this indicates an intra-arterial position. The rest of procedure is the same as described in peripheral IV access.

The arterial line complications include arterial puncture and hematoma, thrombosis, and infection.

8. References

[1] McGee DC, Gould MK. Preventing complications of central venous catheterization. NEJM 2003;348(12):1123-33

[2] Hind DH, Calvert N, McWilliams R, et al. Ultrasonic locating devices for central venous cannulation: meta-analysis. BMJ 2003;327:361

[3] Denys BG, Uretsky BF, Reddy PS. Ultrasound-assisted cannulation of the internal jugular vein, A prospective comparison to the external landmark-guided technique; Circulation 1993;87 (5):1557-62

[4] Brannam L, Blaivas M, Lyon M, Flake M. Emergency nurses' utilization of ultrasound guidance for placement of peripheral intravenous lines in difficult-access patients. Academic Emergency Medicine 2004;11(12):1361-3

[5] Schoenfeld E, Boniface K, Shokoohi H. ED technicians can successfully place ultrasound-guided intravenous catheters in patients with poor vascular access. American Journal of Emergency Medicine 2011;29(5):496-501

[6] Constantino TG, Parikh AK, Satz WA, Fojtik JA. Ultrasonography-guided peripheral intravenous access versus traditional approaches in patients with difficult intravenous access. Ann Emerg Med 2005;46(5):456-461

[7] Resnick JR, Cydulka R, Jones R., Comparison of two transducers for ultrasound-guided vascular access in long axis. J Emerg Med. 2007 Oct;33(3):273-6

[8] Leung J, Duffy M, Finckh A. ,Real-time ultrasonographically-guided internal jugular vein catheterization in the emergency department increases success rates and reduces complications: a randomized, prospective study. Ann Emerg Med. 2006 Nov;48(5):540-7

[9] Khoo SW, Han DC., The use of ultrasound in vascular procedures. Surg Clin North Am. 2011 Feb;91(1):173-84

[10] Stone MB, Moon C, Sutijono D, Blaivas M , Needle tip visualization during ultrasound-guided vascular access: short-axis vs long-axis approach. Am J Emerg Med. 2010 Mar;28(3):343-7

[11] Blaivas M, Brannam L, Fernandez E: Short axis versus long-axis approaches for teaching ultrasound-guided vascular access on a new inanimate model. Acad Emerg Med 2003; 10:1307–13116

[12] Milling T, Holden C, Melniker L, et al: Randomized controlled trial of single-operator vs. two-operator ultrasound guidance for internal jugular central venous cannulation. Acad Emerg Med 2006; 13:245–247

[13] Rose JS, Norbutas CM. , A randomized controlled trial comparing one-operator versus two-operator technique in ultrasound-guided basilic vein cannulation. J Emerg Med. 2008 Nov;35(4):431-5

[14] Maecken T, Marcon C, Bomas S, Zenz M, Grau T., Relationship of the internal jugular vein to the common carotid artery: implications for ultrasound-guided vascular access. Eur J Anaesthesiol. 2011 May;28(5):351-5

[15] Mallin M, Louis H, Madsen T, A novel technique for ultrasound-guided supraclavicular subclavian cannulation. Am J Emerg Med. 2010 Oct;28(8):966

[16] Gregg SC, Murthi SB, Sisley AC, Stein DM, Scalea TM., Ultrasound-guided peripheral intravenous access in the intensive care unit. J Crit Care. 2010 Sep;25(3):514-9

[17] Costantino TG, Kirtz JF, Satz WA., Ultrasound-guided peripheral venous access vs. the external jugular vein as the initial approach to the patient with difficult vascular access. J Emerg Med. 2010 Oct;39(4):462-7

[18] Shiloh AL, Savel RH, Paulin LM, Eisen LA., Ultrasound-guided catheterization of the radial artery: a systematic review and meta-analysis of randomized controlled trials. Chest. 2011 Mar;139(3):524-9

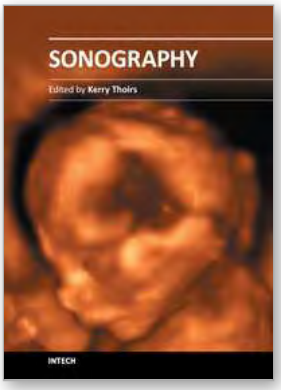

Sonography

Edited by Dr. Kerry Thoirs

ISBN 978-953-307-947-9
Hard cover, 346 pages
Publisher InTech
Published online 03, February, 2012
Published in print edition February, 2012

Medical sonography is a medical imaging modality used across many medical disciplines. Its use is growing, probably due to its relative low cost and easy accessibility. There are now many high quality ultrasound imaging systems available that are easily transportable, making it a diagnostic tool amenable for bedside and office scanning. This book includes applications of sonography that can be used across a number of medical disciplines including radiology, thoracic medicine, urology, rheumatology, obstetrics and fetal medicine and neurology. The book revisits established applications in medical sonography such as biliary, testicular and breast sonography and sonography in early pregnancy, and also outlines some interesting new and advanced applications of sonography.

How to reference

In order to correctly reference this scholarly work, feel free to copy and paste the following:

Hamid Shokoohi, Ali Pourmand and Keith Boniface (2012). Ultrasound Guided Vascular Access, Sonography, Dr. Kerry Thoirs (Ed.), ISBN: 978-953-307-947-9, InTech, Available from: http://www.intechopen.com/books/sonography/ultrasound-guided-vascular-access

INTECH
open science | open minds

InTech Europe
University Campus STeP Ri
Slavka Krautzeka 83/A
51000 Rijeka, Croatia
Phone: +385 (51) 770 447
Fax: +385 (51) 686 166
www.intechopen.com

InTech China
Unit 405, Office Block, Hotel Equatorial Shanghai
No.65, Yan An Road (West), Shanghai, 200040, China
中国上海市延安西路65号上海国际贵都大饭店办公楼405单元
Phone: +86-21-62489820
Fax: +86-21-62489821

1

Non-Coronary Vessel Exploration Under Intravascular Ultrasound: Principles and Applicability

Gaël Y. Rochefort
Inserm U658 Ipros Chro, Orleans
France

1. Introduction

Intravascular Ultrasound (IVUS) has become rapidly one of the gold technologies for the endovascular exploration. Next to angiography, which only gives information about the lumen of the investigated vessels, IVUS describes both the luminal and trans-mural anatomy of vascular structures. Actual devices offer several configurations and transducers mounted at the end of an intra-luminal catheter to produce real-time grayscale or color images of blood vessels and cardiac structures. The ultrasound probes miniaturization has permitted closer imaging and magnified details of the vessel wall and plaque. Recent IVUS catheters use phased array imaging where the micro-transducers are enveloped around a catheter tip. Typically, IVUS images show the vessel wall in histological detail: the intima reflects ultrasound brightly and is white, the media is echolucent and dark, and the surrounding adventitia is white.

IVUS has thus become a safe and valuable tool in exploring the disease severity and the treatment completeness during surgical endovascular procedures (Jinzaki et al., 1993; Nishanian et al., 1999), such as assessing the severity of an arterial disease before treatment (Scoccianti et al., 1994), determining the plaque morphology and localization or checking the completeness of stent deployment (Diethrich, 1993; Laskey et al., 1993). Very recently, color flow IVUS and three-dimensional (3D) reconstruction have both introduced significant advances in the understanding of IVUS images (Irshad et al., 2001; Reid et al., 1995; White et al., 1994). The very latest advance, called virtual histology IVUS, provides a color-coded map of the plaque components, thus providing a better understanding of the arterial plaque structure and morphology (Nair et al., 2001; Vince & Davies, 2004).

2. IVUS principle

IVUS gives series of tomographic images of the explored vessel wall. During acquisition, an IVUS catheter is entered into a vessel and then withdrawn through a given vessel segment during simultaneous and continuous imaging, resulting in series of cross section images. Current catheters have frequencies from 30 to 40 MHz, planar resolutions from 50 to 150 μm, and a typical sampling rate of 30 images per second (Di Mario et al., 1995).

2.1 Acquisition using pullback devices

The current methods used to quantify a volumetric IVUS analysis are usually achieved by a simple summation of a targeted subsample of the 2-D images into a volumetric dataset (Chandrasekaran et al., 1994; Rosenfield et al., 1992; Rosenfield et al., 1991). In that case, the accurate volume calculations need the precise localization of each 2-D cross-sectional image used in the longitudinal axis of the vessel segment (Di Mario et al., 1995; Roelandt et al., 1994). To do so, a manual pullback was firstly performed, with recording of the time and length of the acquisition, and the image location was estimated from the pullback start point and the average pullback velocity. Alternatively, displacement sensors were used to record the IVUS catheter translation during the manual pullback procedure (Hagenaars et al., 2000). Since it is obviously difficult to maintain a consistent speed during manual pullback, most current systems have introduced a motorized pullback device with a constant speed (usually around 0.5 mm/s) (Cavaye et al., 1992; Liu et al., 1999; Matar et al., 1994).

2.2 Cardiac synchronization and frame selection

Since images are recorded at 30 frames per second, with a pullback speed of 0.5 mm/s, 60 frames are recorded for each 1-mm vessel segment. Since, a coronary segment of 3 to 10 cm is typically explored, 1800 to 6000 individual frames are usually recorded. Therefore, these large datasets are often sub-sampled using constant intervals (0.5 - 1.0 mm) or using an electrocardiogram gating: the 1-mm interval without respect to the cardiac cycle is often used for manual analysis, whereas computerized algorithms require different sampling intervals (Klingensmith et al., 2000a; von Birgelen et al., 1996a). Therefore, consecutive frames sub-sampled with a 1-mm interval are corresponding to changes in the lumen and vessel areas during the different phases of the cardiac cycle.

A typical "sawtooth" artifact can be seen on longitudinal 2-D pullback displays when the sub-sampling is performed without synchronization to the cardiac cycle. This sawtooth artifact is less marked when the explored vessel exhibit a reduced compliance (such as stented vessels or stenotic vessels). Nevertheless, it is recommended to get the cardiac cycle synchronization since it allows the cyclic cycle artifacts to be eliminated (von Birgelen et al., 1996b; von Birgelen et al., 1997b). In fact, different physiologic, cyclic signals are commonly used to synchronize the IVUS images to the cardiac cycle, including the arterial blood pressure and the electrocardiogram signals (Allan et al., 1998; Sonka et al., 1998).

When operating a retrospective gating, IVUS images and electrocardiogram signals are acquired continuously, since the electrocardiogram signals are required to sort the images and to perform the analysis of the volumetric dataset (Klingensmith et al., 2000a; Kovalski et al., 2000). On the other hand, when operating a prospective gating, the IVUS images are only acquired at a given times of the cardiac cycle and the catheter is then moved to acquire the next gated image (Bruining et al., 1998; von Birgelen et al., 1997a; von Birgelen et al., 1995). This last gating method presents the advantage to not requiring additional steps to perform the analysis of the dataset, and a volumetric dataset is available immediately after the acquisition pullback.

2.3 Transferring the IVUS dataset to an analysis system

The whole raw IVUS data, composed of the reflected acoustic signals, are displayed on IVUS consoles. This dataset could also be stored on S-VHS videotape, on CD-ROM or magneto-optical disks. Recent IVUS consoles have digital output capabilities that allow direct data

transfer in digital format, and may provide radiofrequency outputs composed of raw IVUS acoustic signals. This signal processing approach is particularly adapted for a computerized image analysis, since it allows traditional measurements but also radiofrequency-based tissue characterization (Nair et al., 2001; Nair et al., 2002).

3. Devices, recording methods and techniques

3.1 Devices

Typical mechanical IVUS transducers produce cross-sectional images by rotating at the tip of the catheter using a flexible, high-torque cable. These transducers are creating a cone-shaped ultrasound beam that allows the vessel to be imaged slightly forward or in front of the transducer assembly.

An optimized visualization is obtained when using IVUS catheter having appropriate size and frequency. Thus, the clinician has to make a compromise between the highest frequency *vs.* depth of penetration *vs.* catheter size. He also has to consider the wire guide diameter and the guide-wire exchanges utility. IVUS catheters used for most aortic and iliac procedures can be advanced over a 0.035-inch guide wire and range in size and frequency from 6 to 8 Fr and 8 to 20 MHz, respectively. An IVUS probe, ranging between 8 to 15 MHz is commonly used for aortic procedures, allowing an adequate circumferential imaging. The following Table 1 is presenting the current available catheters applicable for peripheral vascular and coronary interventions.

Intravascular Ultrasound Catheters	Size (Fr)	Guide Wire (in)	Frequency (MHz)	Target vessel
Volcano Corporation catheters (phase array)				
Eagle Eye Gold IVUS Imaging (color-flow and virtual histology)	3.5	0.014	20	Carotid renal iliac Femoral
Visions PV 0.018 F/X IVUS Imaging (color-flow)	3.5	0.018	20	Femoral popliteal tibial
Visions PV 8.2F IVUS Imaging	8.2	0.038	8.3	Aorta iliac
Boston Scientific catheters (rotating crystal)				
Atlantis SR Pro	3.2	0.014	40	Femoral popliteal tibial
Atlantis SR Plus	3	0.014	40	Femoral popliteal tibial
Atlantis SR	3.2	0.014	40	Femoral popliteal tibial
Atlantis PV Peripheral Imaging	8	0.035	15	Aorta iliac
Sonicath Ultra Ultrasound	9	0.035	9	Aorta iliac
Sonicath Ultra Ultrasound	3.2	0.018	20	Femoral popliteal tibial
Sonicath Ultra Ultrasound	6	0.035	12.5	Iliac femoral
Sonicath Ultra Ultrasound	6	0.035	20	Femoral popliteal tibial

Table 1. Specifications of commonly used intravascular ultrasound (IVUS) catheters in peripheral occlusive interventions.

3.2 Access to vessels

Depending on the size of the considered vessel (see Table 1), IVUS catheters can be introduced percutaneously through a standard vascular access sheath (5 to 9 Fr). The 8.2 Fr, 10-MHz catheter is one of the most commonly used catheter for aorta-iliac intervention, since it requires a 0.035-inch guide wire and thus can be quickly prepared, introduced, and/or exchanged with other catheters. However, this specific catheter requires a 9 Fr sheath that can be disproportionate for lower extremity interventions.

Most current percutaneous trans-luminal angioplasty balloons and stents targeted for infra-inguinal regions require only 6 Fr sheaths. The 3.4 Fr, 3.2 Fr, or 2.9 Fr catheters, using 0.018-inch and 0.014-inch guide wires, are more suitable for the typical retrograde common femoral artery puncture and access to the contra-lateral femoral-popliteal segments (Hiro et al., 1998; Saketkhoo et al., 2004). In some case, especially with tortuous vessels and when antegrade puncture of the common femoral vessel is required, the 3 Fr catheters are also useful.

Lengths of IVUS catheters are vary from 90 to 150 cm, thus allowing imaging of small tibial vessels from a contra-lateral up-and-over approach. The smaller catheters require 0.018-inch or 0.014-inch guide wires and are commonly used for infra-inguinal interventions, whereas the larger IVUS catheters need 0.035-inch guide wires and used for larger vessel interventions (Hiro et al., 1998).

3.3 Image acquisition and quality

An optimal visualization requires a careful positioning of the catheter tip within the vessel and an appropriate size matching of the device to the artery caliber, meaning that an IVUS intervention necessitates a pre-procedural estimation the target vessel diameters (Figure 1). The best image quality is obtained when the IVUS catheter is parallel to the vessel wall and when the ultrasound beam is perpendicular to the luminal surface. Some artificial differences in the wall thickness measurement may be obtained when the IVUS catheter has an eccentric position, leading to the vessel wall to appear more hyperechoic than the distant wall. Angulations may promote an elliptical image of the vessel lumen, especially when

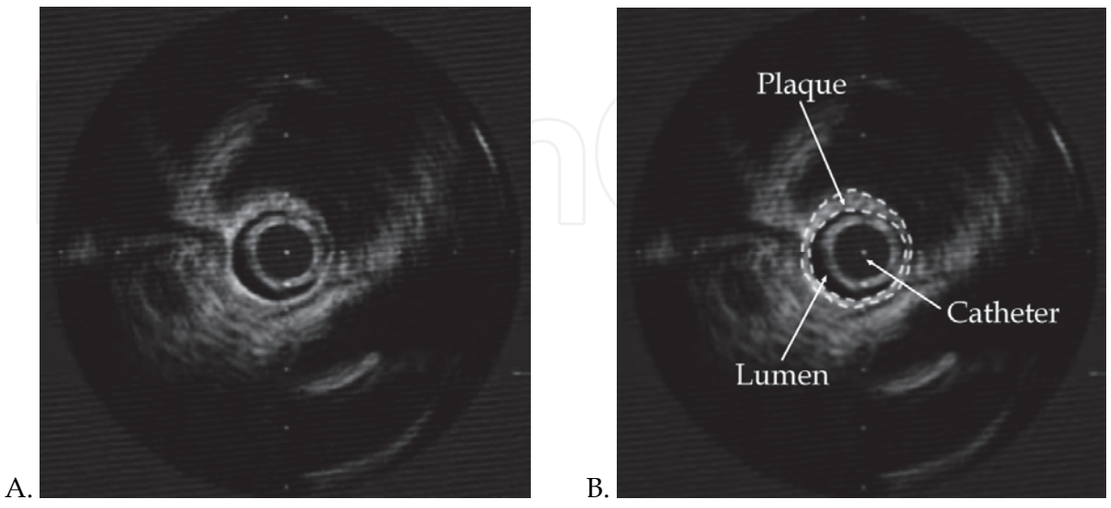

Fig. 1. Illustration of quantitative measurements with IVUS. Examples show an *in vivo* IVUS image digitized from video (A) and the detected borders overlaid (B).

considering tortuous aortas and the thoracic arch. In such cases, the minimal diameter (minor axis) is the best accurate measurement to measure the vessel diameter in angled images and/or tortuous vessels (Roelandt et al., 1994). At last, withdrawing the catheter through the lumen, rather than advancing it, promotes the acquisition of the best-quality images (Danilouchkine et al., 2009).

During the procedure, real-time images of the investigated vessel are displayed on a monitor and are usually recorded digitally. The IVUS devices also allow the on-line and/or off-line measurements of vessel dimensions, luminal diameters, and cross-sectional areas. Recent IVUS units, comprising a motorized and/or automated withdrawing the catheter through the vessel at a controlled rate, may display a longitudinal gray-scale image of the investigated vessel with accurate reconstructed views (Hagenaars et al., 2000). These two-dimensional longitudinal reconstructions allow distances to be measured from one point to another (Liu et al., 1999) and cross-sectional trans-mural wall morphology to be visualized (Di Mario et al., 1995). In fact, the discrimination of plaque, normal tissue, thrombus, dissections, and flaps is often much better appreciated on the two-dimensional longitudinal IVUS reconstructions than on traditional angiographic images (Reid et al., 1995).

4. Data processing and analysis

The dataset for volumetric analysis is represented by image series composed of two-dimensional sections from the investigated vessels. Typically, images are selected at 1-mm inter-slice spacing. Then, to perform a quantitative 3-D reconstruction, the first and most critical step is to precisely identify and trace the anatomical structures of the studied vessel. In fact, identifying the luminal border is essential to discriminate the blood-intima interface, whereas recognizing the external elastic membrane border is important to precisely distinguish the boundary between the media and the adventitia (Kovalski et al., 2000). The space between these 2 borders is the plaque-media complex and is classically used as the measurement for plaque cross-sectional area (Prati et al., 2002).

In stented vessel segments, the lumen/intimal interface and the stent borders are both measured, and the area between these borders is representing the neointimal tissue. In these stented vessel segments, the external elastic membrane border is frequently not distinguished because of signal drop-out behind the stent. In current atherosclerosis research trials, the assessment of stent, luminal and external elastic membrane borders is often performed with manual planimetry using commercially or freely available computer programs. This provides the accurate discrimination of image artifacts and true border locations but this analysis requires the border detection in hundreds of images. Therefore, the use of automated image-processing techniques allows fast online analysis (Sanz-Requena et al., 2007).

4.1 Automated 2-D/3-D border-detection methods

Different approaches have been described to detect the luminal and external elastic membrane borders from 2-D IVUS images, including texture-based methods (Papadogiorgaki et al., 2007), knowledge-based graph searching (Bovenkamp et al., 2009), region growing (Sanz-Requena et al., 2007), radial gradient searching (Luo et al., 2003), and active contours (Sanz-Requena et al., 2007; Takagi et al., 2000). These 2-D border-detection techniques are now used online in newer IVUS imaging consoles, allowing the quantitative evaluation of lumen and plaque measurements. Because the user provides his expertise to augment the algorithm or correct results, the semi-automated techniques typically require

more time but are have a better accuracy. These 2-D border-detection methods are particularly used when the analysis of only a small number of images is required, e.g. during the guidance of interventional procedures (Sarno et al., 2011).
When a fast analysis of many images is required, highly automated techniques for border detection are used and do not require significant user intervention. For example, 3-D border-detection methods using the inter-slice information can provide fast border detection from a large number of images (Cardinal et al., 2010). A graph-searching approach researching the globally optimal contour path through the image data has been developed on the basis of associated cost values (Zhang et al., 1998). Furthermore, this 2-D frame analysis method allows the results to be propagated down the sequence by using the identified 2-D contours in order to limit the search region. Another 2-D border-detection method uses cost values to find longitudinal contours along the volumetric data. Then, these contours guide the cost function minimization in the transverse 2-D images (Koning et al., 2002). Alternatively, several useful approaches use deformable models to perform an active contour detection (Klingensmith et al., 2000a; Kovalski et al., 2000) (Shekhar et al., 1999). One of them uses a balloon force to inflate a model from the catheter outward toward the luminal and medial-adventitial borders (Kovalski et al., 2000). Another deformable model uses a cylindrical model to manually or automatically approximate the structure of the luminal or medial-adventitial surface, and a deformable model algorithm is then used in a 3-D process to attach the defined structure to the surface of interest (Klingensmith et al., 2000a; Shekhar et al., 1999). All these methods allowing the 3-D border-detection have clearly established their overall usefulness for fast border identification in a large sequence of images (Klingensmith et al., 2000a; Kovalski et al., 2000; Shekhar et al., 1999; von Birgelen et al., 1996a; Zhang et al., 1998).
A major limitation of all these 3-D border-detection methods is the lack of a true gold standard for comparison. Histology sections might represent the more powerful gold standard, but they are only available at autopsy, and the required fixation always induces the tissue to shrink (Siegel et al., 1985). Some researchers have tried to evaluate the accuracy of their methods using cylindrical phantoms, but they did not test accuracy in clinical IVUS images (von Birgelen et al., 1996a). Other studies have compared the detected borders with borders traced manually by a single expert, but the obtained inter-observer variability in manual identification of the luminal and medial-adventitial borders might greatly limit the value of these comparisons in IVUS images (Haas et al., 2000; Zhang et al., 1998). At last, some studies have used multiple expert observers for validation, but the number of analyzed images is seriously limited and not sufficient to assess the ability and accuracy of these algorithms (Klingensmith et al., 2000a; Kovalski et al., 2000; Shekhar et al., 1999). Therefore, there is a need of validation of these techniques in large datasets.

4.2 3-D reconstructions of vessel segments

All measurements and evaluations made in 2-D tomographic slices are useful for stent sizing or comparisons of lesions to a reference site, but fail to provide a volumetric perspective. To do such volumetric calculations, the border measurements obtained in consecutive 2-D slices of a vessel segment are integrated, the area enclosed by the luminal border and external elastic membrane border is considered for each slice, and the atheroma area is calculated. The 3-D measurement of lumen, plaque, and vessel volumes are usually calculated with Simpson's rule or trapezoidal integration by the multiplying 2-D area and slice thickness (Finet et al., 2003; von Birgelen et al., 1997a). This last method is suitable for

short and straight vessel segments, such as coronary stented lesions, but it does not allow the precise measurement of a longer and curved segment.
The volumetric approach using 3-D border-detection techniques is currently applied in serial IVUS studies examining atherosclerotic disease progression or regression, allowing the assessment of plaque burden in an entire vessel segment through fast analysis of large image sequences. New interventional approaches also use a volumetric IVUS imaging approach to provide new mechanistic insights, such as innovative techniques aimed at the prevention and treatment of in-stent restenosis correlated with histomorphometry measurements (Mehran et al., 1998; Murata et al., 2002); approaches in understanding the effects of radiation therapy and the arterial remodeling on a stented segment (brachytherapy) (Lekston et al., 2008; Weichert et al., 2003; Zimarino et al., 2002; Zimmermann et al., 2005); or using drug-eluting stents on the neointimal hyperplasia development (Jensen et al., 2008; Min et al., 2007; Sano et al., 2006).

4.3 Geometrically correct 3-D IVUS and advanced data processing

Since the curvature of vessels is not taken into account with these straight 3-D IVUS methods, this limitation can be overcome by fusing the curvature information provided by biplane angiography or other techniques with the IVUS border information (Schuurbiers et al., 2009; Sherknies et al., 2005; Tu et al., 2010; Wahle et al., 2006). To do so, one common method is to acquire two separate angiographic images from different angles at the beginning of the ultrasound scanning imaging procedure and to use the catheter outline reconstructed from these images as a template for placement of the IVUS-derived contours (Bourantas et al., 2005; Klingensmith et al., 2000b; Sherknies et al., 2005; von Birgelen et al., 1995; Weichert et al., 2003). Another method consists in following the IVUS transducer in time and space throughout the IVUS pullback using biplane angiography, thus the precise locations of IVUS image acquisitions are recorded in sequence and are used as a reconstruction template (Klingensmith et al., 2000b; Miyazaki et al., 2010; Wallace et al., 2005). However, this method might be difficult because of the cardiac and respiratory motion and the higher radiation exposure during the whole procedure.
Next to the precise location in 3-D space, other geometric considerations of the IVUS probe during image acquisition are important to be taken in account for an accurate 3-D reconstruction (Roelandt et al., 1994; Thrush et al., 1997). For example, the geometry of the reconstructed vessel can be distorted by a rotation of the catheter during pullback. These changes in the angular orientation of the catheter can be corrected by using analytical calculation based on the Frenet-Serret rules and optimizing the fit after projecting the reconstructed lumen from different rotational angles onto the angiogram images (Briguori et al., 2001; Wahle et al., 1999). Axial movements of the catheter due to the cardiac contraction are another cause for 3-D reconstruction inaccuracies. This geometric artifact can be reduced using a cardiac-gating and spatiotemporal location of the IVUS transducer throughout the pullback (Arbab-Zadeh et al., 1999). However, even if some errors in generating 3-D images can potentially surround withy these geometric assumptions, these corrections help improve the interpretability, usefulness and accuracy of the 3-D reconstructions. Repeatability is also a really important consideration in the accuracy and usefulness of 3-D reconstruction techniques. This aspect is however closely related to the reproducibility of the 3-D border-detection process (von Birgelen et al., 1996a).
Offline digitization of IVUS images and retrieval of biplane angiographic images, but also digitization and intense computer processing are both required to obtain a correct

geometrically 3-D reconstruction (Prati et al., 1998). Therefore, all these factors, in addition to the artifacts induced by the respiratory and cardiac motions, limit the *in vivo* applicability of the techniques. Other developments of real-time transducer tracking and online radiofrequency IVUS data acquisition can be integrated into the IVUS console to provide accurate 3-D models of investigated vessels within a few minutes after the acquisition (Nair et al., 2002). These add-ons seem really powerful since they could provide an interactive tool for assessing the diagnostic of the pathology, giving an assessment of luminal dimensions, but also vessel and plaque size from any viewing angle and position. Furthermore, these interactive models could allow rotation and manipulation of these virtual 3-D models on the console computer, authorizing the placement of a virtual stent inside the reconstructed artery, thus permitting a stent with the length and size to be appropriately chosen (Atary et al., 2009; Hong et al., 2010).
Other addendum could be integrated into the geometrically correct 3-D models, including analysis of hemodynamic forces, radiofrequency-derived histology, and 3-D stress maps. Therefore, a more precise morphologic plaque classification is possible with the analysis of radiofrequency data. In fact, the back-scattered radiofrequency IVUS data seems to permit the precise characterization of plaque composition, distinguishing the regions of calcified plaque *vs.* calcified necrosis *vs.* collagen (Nair et al., 2001). Another complement might consist on adding the mechanical properties of the investigated tissue. In fact, elastography represents the way a given tissue is responding to an applied force, as a function of its mechanical properties. Thus, the local mechanical properties of the tissue can be determined by comparing the images of a vessel acquired at 2 different levels of static compression (*e.g.* during systole and diastole steps of the cardiac cycle). This strain image (elastogram) may allow a better understanding of the relation between the progression of a disease and the *in vivo* mechanical properties of the vessel (Baldewsing et al., 2007; Cespedes et al., 1997; de Korte & van der Steen, 2002; Liang et al., 2008).

4.4 Comparison of IVUS with other imaging modalities

Even if IVUS might represent the most clinically established technique, other methodologies for vessel investigation are also available, such as angiography or tomographic imaging with magnetic resonance imaging (MRI) and computed tomography (CT). The current IVUS imaging plane resolution achieved in vessel cross sections is of 50 to 150 μm, whereas current frame rates (typically 30 frames/s), pullback speeds (usually 0.5 mm/s), and an ECG-gating or sub-sampling yield images at approximately 0.5- to 1.0-mm intervals (Gatta et al., 2009). On the other hand, the in-plane resolution of magnetic resonance imaging is around 1 mm and the through-plane resolution is between 3 to 5 mm with 2-D techniques (Escolar et al., 2006; Schaar et al., 2007), but the magnetic resonance imaging may allow, under several limitation in spatial resolution and signal-to-noise ratios, the atherosclerotic plaque components to be distinguished (Karmonik et al., 2006). At last, the in-plane resolution of computed tomography is less than 1 mm and the minimum through-plane resolution is approximately 1.25 to 1.50 mm. Some contrast-enhanced protocols are sometimes used to differentiate calcified and non-calcified plaque using contrast agents during computed tomography imaging of vessels (Nasir et al., 2010; Pundziute et al., 2008).
Another important difference between IVUS and the other imaging modalities concerns the orientation of the imaging plane. In fact, since the IVUS probe is inside the vessel during the acquisition, the IVUS imaging plane is oriented perpendicular to the vessel axis, which is optimal for assessing cross-sectional dimensions. On the other hand, magnetic resonance

images can be acquired along some body axes (e.g. axial, sagittal, or coronal planes or in a plane oblique to these orthogonal planes) and computed tomography images are typically only acquired in the axial plane, but these images can be reformatted to another orthogonal plane or an oblique plane with image processing techniques (McPherson et al., 2005). Therefore, these plane or oblique images allow only the measurement of relatively short portions of a vessel (only for images that are perpendicular to the vessel axis) and the curvature of the vessel introduces angulation errors in parameter measurement such as the wall thickness (Sherknies et al., 2005).

4.5 Color IVUS and virtual histology IVUS

Color flow IVUS is produced by computer software that detects a difference between the movements of echogenic blood particles from two sequential adjacent frames. Then the blood flow is colored by the software in a red or bleu and is displayed as axial and 3D longitudinal renderings with a very high image resolution (McLeod et al., 2004; Nair et al., 2002). The rendering color of the flow may change from red to orange when there is very fast blood flow (e.g., a tight stenosis). However, the flow velocities cannot be calculated with this technique, image resolution is very high. The color flow IVUS is available on Eagle Eye Gold and the Visions PV 018 catheters (Volcano Corporation, Rancho Cordova, CA) (see Table 1 for specifications). During a color flow IVUS pull-back, the blood flow is displayed in the vessel lumen, pulsing with each cardiac cycle. Unfortunately, the color flow is not gated with the heart rate and cannot be performed when virtual histology images are being acquired. These color flow IVUS are the helpful in distinguishing echolucent disease from luminal blood flow and can also be used to perform peripheral interventions in patients with renal failure or allergy, avoiding the use of contrast media (Goderie et al., 2010; Irshad et al., 2001).

Whereas conventional grayscale ultrasound images are generated from the intensity of the reflected signals that are collected by the probe, virtual histology IVUS images are obtained from the frequency and intensity of the returning signals and frequency varies depending on the tissues (Vince & Davies, 2004). An histological classification has then be realized by comparing the reflected virtual histology data with true histological sections of diseased vessels, and a color-coded map of the different components of the arterial disease has been established (dark green, fibrous; yellow/green, fibro-fatty; white, calcified; red, necrotic lipid core plaque) (McLeod et al., 2004; Nair et al., 2002). This color-coded map is of major importance since it allows the operator to have detailed information about the constituents and the nature of the plaque (Sarno et al., 2011). The virtual histology IVUS is available on Eagle Eye Gold catheter (Volcano Corporation, Rancho Cordova, CA) (see Table 1 for specifications) and is gated with the heartbeat. During the procedure using the "Volcano" setting, the segment length of the vessel to be examined is determined and the luminal border and the external elastic lamina border of the artery are automatically detected by the edge-tracking computer software but might require some manual adjustments. Then, virtual histology images of the delineated plaque can then be processed online with a few minutes, thus allowing clinical decisions to be made promptly, whereas some additional processing can be done offline (Vince & Davies, 2004).

5. Therapeutic interventions

5.1 Percutaneous trans-luminal angioplasty

The accurate measurement of the true luminal diameter, the assessment of the calcific nature of the plaque, the precise delineation of wall morphology, and the ability to carefully

visualize the post-balloon result are both required for a successful percutaneous trans-luminal angioplasty of peripheral arterial lesions. In that purpose, IVUS images can delineate the luminal and adventitial surfaces of vessel segments, can discriminate between normal and diseased components, can accurately localization and measurement of the thickness of plaque, and can also differentiate calcified and non-calcified vascular lesions (Pundziute et al., 2008; Rodriguez-Granillo et al., 2006). In fact, since the ultrasound energy is strongly reflected by calcified plaque, it appears as a very bright image with dense acoustic shadowing behind it. Not only luminal dimensions and wall thickness determined by IVUS are accurate to within 0.05 mm (Rodriguez-Granillo et al., 2006), the luminal cross-sectional areas measured from IVUS correlate well with calculated from biplanar angiograms (Cooper et al., 2001; Irshad et al., 2001). Therefore, IVUS allows the sized balloon or stent to be appropriately chosen can whereas conventional angiography is somewhat limited in its ability to provide sensitive data regarding the effects of percutaneous trans-luminal angioplasty. The IVUS advantage is also to provide a precise evaluation of the lesion morphology, such as the luminal dimensions, the trans-mural lesion characteristics and the area of blood flow. Furthermore, the IVUS determination of plaque volume before and after the procedure offers a real quantitative method to estimate the amount of lesion debulking or displacement and a reference point from which to assess the lesion recurrence/restenosis (Kim et al., 2004; Takeda et al., 2003).

The adjunctive use of IVUS during percutaneous trans-luminal angioplasty has been reported on several studies. For example, in patients with lesions of the superficial femoral artery treated with percutaneous trans-luminal angioplasty, IVUS has been reported to accurately detect the presence of dissections, plaque fractures, internal elastic lamina ruptures, and thinning of the media that occurred during the balloon angioplasty (Oshima et al., 1998; Tang et al., 2010). IVUS has also showed that, after a percutaneous trans-luminal angioplasty, the luminal enlargement is mainly produced by stretching of the arterial wall while the volume of the lesion remains relatively constant (Tang et al., 2010).

After a percutaneous trans-luminal angioplasty the restenosis risk has also been correlated to IVUS findings during the initial procedure, providing important information regarding the post-procedural follow-up and surveillance (Montorsi et al., 2004; Xu et al., 1995). The percutaneous trans-luminal angioplasty of a calcific plaque leads to a higher incidence of dissection than a fibrous lesion, whereas fibrous plaques or concentric lesions without signs of fracture or dissection are prone to have late restenosis after a percutaneous trans-luminal angioplasty (Garcia-Garcia et al., 2009; Su et al., 2009). In the same way, IVUS is also able to readily identify that early restenosis following interventions is associated with luminal thrombus, extensive dissection, and oversized balloon dilatation, while late restenosis correlates with residual stenosis, lower residual lumen surface, undersized balloon use, concentric fibrous plaque, absence of dissection, and absence of calcification (Irshad et al., 2001). IVUS is thus able to enhance percutaneous trans-luminal angioplasty procedures by allowing peri-procedural decisions to be made regarding the need for additional interventions.

5.2 Intravascular stents

Dissections, elastic recoil, residual stenosis, a significant residual pressure gradient across the lesion, or plaque ulceration with local thrombus accumulation are common indications for an intravascular stent placement after percutaneous trans-luminal angioplasty. Primary stenting is also commonly used in the treatment of certain lesions, especially common iliac or renal disease (Moise et al., 2009). These intravascular stents are used to increase the

patency of arterial occlusive lesions that have undergone angioplasty by reducing technical failure and restenosis rates. However, placing stents is not without risk since ineffective stent expansion can lead to early thrombosis or a stent migration, whereas overexpansion can result in vessel perforation or excessive intimal hyperplasia (Adlakha et al., 2010).
Establishing the need for stenting as well as the guiding of a stent deployment has been clearly helped by IVUS. Furthermore, defining the appropriate angioplasty diameter endpoint and confirming adequacy of stent deployment have been reported to clearly improve the long-term patency of a vessel undergoing balloon angioplasty and stenting (Waksman et al., 2009).

5.3 Venous interventions

The requirement of IVUS in endovascular interventions of venous disease is not as well described as for arterial lesions, while there are many useful indications for IVUS use in venous obstructive lesions (Raju et al., 2010; Raju & Neglen, 2006). In fact, traditional venography for iliac vein obstruction has numerous limitations, and IVUS imaging yields findings not obvious on venography . In fact, intra-luminal webs or external compression and subsequent deformity represent abnormalities that might disturb the diagnostic. Thus, IVUS can provide an accurate assessment of the degree of vein stenosis whereas the venography can sometimes underestimates this stenosis degree by 30% (Nair et al., 2002). In the same way, IVUS allows more appropriately sized venous stents to be placed after venoplasty. Since more and more venous interventions are being performed for acute deep venous thromboses, effort thromboses, or congenital stenosis, the requirement IVUS might represent a powerful adjunct to delineate the often unclear anatomy related to the venous system (Raju et al., 2010).

6. Conclusion

IVUS requirement has moved rapidly from a purely diagnostic imaging modality to a useful adjunct for vessel endografting to playing an ever-increasing role in peripheral occlusive interventions. This shift has been mainly supported by the miniaturization of the elements, allowing the device and catheter to be as small-profile as the latest stents or balloons, and by the powerful helped that can give IVUS for the most optimal outcomes. While vascular interventions are becoming more and more complex and venture into smaller target vessels, success will be related to the degree of accuracy of the guidance system employed during the procedure. Thus, IVUS is representing an important component of current and future endovascular interventions and should be integrated into the routine practice of the advanced endovascular surgeon and training programs.

7. References

Adlakha, S., Sheikh, M., Wu, J., Burket, M.W., Pandya, U., Colyer, W., Eltahawy, E., & Cooper, C.J. (2010). Stent fracture in the coronary and peripheral arteries. *J Interv Cardiol*, Vol. 23, No. 4, (Publication date: 2010/09/02), pp. 411-419, I.S.S.N.: 1540-8183

Allan, J.J., Smith, R.S., DeJong, S.C., McKay, C.R., & Kerber, R.E. (1998). Intracardiac echocardiographic imaging of the left ventricle from the right ventricle: quantitative experimental evaluation. *J Am Soc Echocardiogr*, Vol. 11, No. 10, (Publication date: 1998/11/06), pp. 921-928, I.S.S.N.: 0894-7317

Arbab-Zadeh, A., DeMaria, A.N., Penny, W.F., Russo, R.J., Kimura, B.J., & Bhargava, V. (1999). Axial movement of the intravascular ultrasound probe during the cardiac cycle: implications for three-dimensional reconstruction and measurements of coronary dimensions. *Am Heart J*, Vol. 138, No. 5 Pt 1, (Publication date: 1999/10/28), pp. 865-872, I.S.S.N.: 0002-8703

Atary, J.Z., Bergheanu, S.C., van der Hoeven, B.L., Atsma, D.E., Bootsma, M., van der Kley, F., Zeppenfeld, K., Jukema, J.W., & Schalij, M.J. (2009). Impact of sirolimus-eluting stent implantation compared to bare-metal stent implantation for acute myocardial infarction on coronary plaque composition at nine months follow-up: a Virtual Histology intravascular ultrasound analysis. Results from the Leiden MISSION! intervention study. *EuroIntervention*, Vol. 5, No. 5, (Publication date: 2010/02/10), pp. 565-572, I.S.S.N.: 1969-6213

Baldewsing, R.A., Schaar, J.A., Mastik, F., & van der Steen, A.F. (2007). Local elasticity imaging of vulnerable atherosclerotic coronary plaques. *Adv Cardiol*, Vol. 44, No. (Publication date: 2006/11/01), pp. 35-61, I.S.S.N.: 0065-2326

Bourantas, C.V., Kourtis, I.C., Plissiti, M.E., Fotiadis, D.I., Katsouras, C.S., Papafaklis, M.I., & Michalis, L.K. (2005). A method for 3D reconstruction of coronary arteries using biplane angiography and intravascular ultrasound images. *Comput Med Imaging Graph*, Vol. 29, No. 8, (Publication date: 2005/11/10), pp. 597-606, I.S.S.N.: 0895-6111

Bovenkamp, E.G., Dijkstra, J., Bosch, J.G., & Reiber, J.H. (2009). User-agent cooperation in multiagent IVUS image segmentation. *IEEE Trans Med Imaging*, Vol. 28, No. 1, (Publication date: 2009/01/01), pp. 94-105, I.S.S.N.: 1558-0062

Briguori, C., Anzuini, A., Airoldi, F., Gimelli, G., Nishida, T., Adamian, M., Corvaja, N., Di Mario, C., & Colombo, A. (2001). Intravascular ultrasound criteria for the assessment of the functional significance of intermediate coronary artery stenoses and comparison with fractional flow reserve. *Am J Cardiol*, Vol. 87, No. 2, (Publication date: 2001/01/12), pp. 136-141, I.S.S.N.: 0002-9149

Bruining, N., von Birgelen, C., de Feyter, P.J., Ligthart, J., Li, W., Serruys, P.W., & Roelandt, J.R. (1998). ECG-gated versus nongated three-dimensional intracoronary ultrasound analysis: implications for volumetric measurements. *Cathet Cardiovasc Diagn*, Vol. 43, No. 3, (Publication date: 1998/04/16), pp. 254-260, I.S.S.N.: 0098-6569

Cardinal, M.H., Soulez, G., Tardif, J.C., Meunier, J., & Cloutier, G. (2010). Fast-marching segmentation of three-dimensional intravascular ultrasound images: a pre- and post-intervention study. *Med Phys*, Vol. 37, No. 7, (Publication date: 2010/09/14), pp. 3633-3647, I.S.S.N.: 0094-2405

Cavaye, D.M., White, R.A., Kopchok, G.E., Mueller, M.P., Maselly, M.J., & Tabbara, M.R. (1992). Three-dimensional intravascular ultrasound imaging of normal and diseased canine and human arteries. *J Vasc Surg*, Vol. 16, No. 4, (Publication date: 1992/10/01), pp. 509-517; discussion 518-509, I.S.S.N.: 0741-5214

Cespedes, E.I., de Korte, C.L., van der Steen, A.F., von Birgelen, C., & Lancee, C.T. (1997). Intravascular elastography: principles and potentials. *Semin Interv Cardiol*, Vol. 2, No. 1, (Publication date: 1997/03/01), pp. 55-62, I.S.S.N.: 1084-2764

Chandrasekaran, K., Sehgal, C.M., Hsu, T.L., Young, N.A., D'Adamo, A.J., Robb, R.A., & Pandian, N.G. (1994). Three-dimensional volumetric ultrasound imaging of arterial pathology from two-dimensional intravascular ultrasound: an in vitro study.

Angiology, Vol. 45, No. 4, (Publication date: 1994/04/01), pp. 253-264, I.S.S.N.: 0003-3197

Cooper, B.Z., Kirwin, J.D., Panetta, T.F., Weinreb, F.M., Ramirez, J.A., Najjar, J.G., Blattman, S.B., Rodino, W., & Song, M. (2001). Accuracy of intravascular ultrasound for diameter measurement of phantom arteries. *J Surg Res*, Vol. 100, No. 1, (Publication date: 2001/08/23), pp. 99-105, I.S.S.N.: 0022-4804

Danilouchkine, M.G., Mastik, F., & van der Steen, A.F. (2009). Reconstructive compounding for IVUS palpography. *IEEE Trans Ultrason Ferroelectr Freq Control*, Vol. 56, No. 12, (Publication date: 2009/12/31), pp. 2630-2642, I.S.S.N.: 1525-8955

de Korte, C.L., & van der Steen, A.F. (2002). Intravascular ultrasound elastography: an overview. *Ultrasonics*, Vol. 40, No. 1-8, (Publication date: 2002/08/06), pp. 859-865, I.S.S.N.: 0041-624X

Di Mario, C., von Birgelen, C., Prati, F., Soni, B., Li, W., Bruining, N., de Jaegere, P.P., de Feyter, P.J., Serruys, P.W., & Roelandt, J.R. (1995). Three dimensional reconstruction of cross sectional intracoronary ultrasound: clinical or research tool? *Br Heart J*, Vol. 73, No. 5 Suppl 2, (Publication date: 1995/05/01), pp. 26-32, I.S.S.N.: 0007-0769

Diethrich, E.B. (1993). Endovascular treatment of abdominal aortic occlusive disease: the impact of stents and intravascular ultrasound imaging. *Eur J Vasc Surg*, Vol. 7, No. 3, (Publication date: 1993/05/01), pp. 228-236, I.S.S.N.: 0950-821X

Escolar, E., Weigold, G., Fuisz, A., & Weissman, N.J. (2006). New imaging techniques for diagnosing coronary artery disease. *CMAJ*, Vol. 174, No. 4, (Publication date: 2006/02/16), pp. 487-495, I.S.S.N.: 1488-2329

Finet, G., Weissman, N.J., Mintz, G.S., Satler, L.F., Kent, K.M., Laird, J.R., Adelmann, G.A., Ajani, A.E., Castagna, M.T., Rioufol, G., & Pichard, A.D. (2003). Mechanism of lumen enlargement with direct stenting versus predilatation stenting: influence of remodelling and plaque characteristics assessed by volumetric intracoronary ultrasound. *Heart*, Vol. 89, No. 1, (Publication date: 2002/12/17), pp. 84-90, I.S.S.N.: 1468-201X

Garcia-Garcia, H.M., Shen, Z., & Piazza, N. (2009). Study of restenosis in drug eluting stents: new insights from greyscale intravascular ultrasound and virtual histology. *EuroIntervention*, Vol. 5 Suppl D, No. (Publication date: 2009/09/17), pp. D84-92, I.S.S.N.: 1774-024X

Gatta, C., Pujol, O., Rodriguez Leor, O., Mauri Ferre, J., & Radeva, P. (2009). Fast rigid registration of vascular structures in IVUS sequences. *IEEE Trans Inf Technol Biomed*, Vol. 13, No. 6, (Publication date: 2009/08/01), pp. 1006-1011, I.S.S.N.: 1558-0032

Goderie, T.P., van Soest, G., Garcia-Garcia, H.M., Gonzalo, N., Koljenovic, S., van Leenders, G.J., Mastik, F., Regar, E., Oosterhuis, J.W., Serruys, P.W., & van der Steen, A.F. (2010). Combined optical coherence tomography and intravascular ultrasound radio frequency data analysis for plaque characterization. Classification accuracy of human coronary plaques in vitro. *Int J Cardiovasc Imaging*, Vol. 26, No. 8, (Publication date: 2010/04/17), pp. 843-850, I.S.S.N.: 1875-8312

Haas, C., Ermert, H., Holt, S., Grewe, P., Machraoui, A., & Barmeyer, J. (2000). Segmentation of 3D intravascular ultrasonic images based on a random field model. *Ultrasound Med Biol*, Vol. 26, No. 2, (Publication date: 2000/03/21), pp. 297-306, I.S.S.N.: 0301-5629

Hagenaars, T., Gussenhoven, E.J., van Essen, J.A., Seelen, J., Honkoop, J., & van der Lugt, A. (2000). Reproducibility of volumetric quantification in intravascular ultrasound

images. *Ultrasound Med Biol*, Vol. 26, No. 3, (Publication date: 2000/04/25), pp. 367-374, I.S.S.N.: 0301-5629

Hiro, T., Hall, P., Maiello, L., Itoh, A., Colombo, A., Jang, Y.T., Salmon, S.M., & Tobis, J.M. (1998). Clinical feasibility of 0.018-inch intravascular ultrasound imaging device. *Am Heart J*, Vol. 136, No. 6, (Publication date: 1998/12/08), pp. 1017-1020, I.S.S.N.: 0002-8703

Hong, Y.J., Jeong, M.H., Kim, S.W., Choi, Y.H., Ma, E.H., Ko, J.S., Lee, M.G., Park, K.H., Sim, D.S., Yoon, N.S., Yoon, H.J., Kim, K.H., Park, H.W., Kim, J.H., Ahn, Y., Cho, J.G., Park, J.C., & Kang, J.C. (2010). Relation between plaque components and plaque prolapse after drug-eluting stent implantation--virtual histology-intravascular ultrasound. *Circ J*, Vol. 74, No. 6, (Publication date: 2010/05/11), pp. 1142-1151, I.S.S.N.: 1347-4820

Irshad, K., Reid, D.B., Miller, P.H., Velu, R., Kopchok, G.E., & White, R.A. (2001). Early clinical experience with color three-dimensional intravascular ultrasound in peripheral interventions. *J Endovasc Ther*, Vol. 8, No. 4, (Publication date: 2001/09/13), pp. 329-338, I.S.S.N.: 1526-6028

Jensen, L.O., Maeng, M., Thayssen, P., Christiansen, E.H., Hansen, K.N., Galloe, A., Kelbaek, H., Lassen, J.F., & Thuesen, L. (2008). Neointimal hyperplasia after sirolimus-eluting and paclitaxel-eluting stent implantation in diabetic patients: the Randomized Diabetes and Drug-Eluting Stent (DiabeDES) Intravascular Ultrasound Trial. *Eur Heart J*, Vol. 29, No. 22, (Publication date: 2008/10/04), pp. 2733-2741, I.S.S.N.: 1522-9645

Jinzaki, M., Ido, K., Shinmoto, H., Nakatsuka, S., & Hiramatsu, K. (1993). [Advantages of intravascular ultrasound--preliminary experience in patients with peripheral and renal vascular disease]. *Nippon Igaku Hoshasen Gakkai Zasshi*, Vol. 53, No. 4, (Publication date: 1993/04/25), pp. 478-480, I.S.S.N.: 0048-0428

Karmonik, C., Basto, P., & Morrisett, J.D. (2006). Quantification of carotid atherosclerotic plaque components using feature space analysis and magnetic resonance imaging. *Conf Proc IEEE Eng Med Biol Soc*, Vol. 1, No. (Publication date: 2007/10/20), pp. 3102-3105, I.S.S.N.: 1557-170X

Kim, Y.H., Hong, M.K., Lee, S.W., Lee, C.W., Han, K.H., Kim, J.J., Park, S.W., Mintz, G.S., & Park, S.J. (2004). Randomized comparison of debulking followed by stenting versus stenting alone for ostial left anterior descending artery stenosis: intravascular ultrasound guidance. *Am Heart J*, Vol. 148, No. 4, (Publication date: 2004/10/02), pp. 663-669, I.S.S.N.: 1097-6744

Klingensmith, J.D., Shekhar, R., & Vince, D.G. (2000a). Evaluation of three-dimensional segmentation algorithms for the identification of luminal and medial-adventitial borders in intravascular ultrasound images. *IEEE Trans Med Imaging*, Vol. 19, No. 10, (Publication date: 2000/12/29), pp. 996-1011, I.S.S.N.: 0278-0062

Klingensmith, J.D., Vince, D.G., Kuban, B.D., Shekhar, R., Tuzcu, E.M., Nissen, S.E., & Cornhill, J.F. (2000b). Assessment of coronary compensatory enlargement by three-dimensional intravascular ultrasound. *Int J Card Imaging*, Vol. 16, No. 2, (Publication date: 2000/08/06), pp. 87-98, I.S.S.N.: 0167-9899

Koning, G., Dijkstra, J., von Birgelen, C., Tuinenburg, J.C., Brunette, J., Tardif, J.C., Oemrawsingh, P.W., Sieling, C., Melsa, S., & Reiber, J.H. (2002). Advanced contour detection for three-dimensional intracoronary ultrasound: a validation--in vitro and

in vivo. *Int J Cardiovasc Imaging*, Vol. 18, No. 4, (Publication date: 2002/07/19), pp. 235-248, I.S.S.N.: 1569-5794

Kovalski, G., Beyar, R., Shofti, R., & Azhari, H. (2000). Three-dimensional automatic quantitative analysis of intravascular ultrasound images. *Ultrasound Med Biol*, Vol. 26, No. 4, (Publication date: 2000/06/17), pp. 527-537, I.S.S.N.: 0301-5629

Laskey, W.K., Brady, S.T., Kussmaul, W.G., Waxler, A.R., Krol, J., Herrmann, H.C., Hirshfeld, J.W., Jr., & Sehgal, C. (1993). Intravascular ultrasonographic assessment of the results of coronary artery stenting. *Am Heart J*, Vol. 125, No. 6, (Publication date: 1993/06/01), pp. 1576-1583, I.S.S.N.: 0002-8703

Lekston, A., Chudek, J., Gasior, M., Wilczek, K., Wiecek, A., Kokot, F., Gierlotka, M., Niklewski, T., Fijalkowski, M., Szygula-Jurkiewicz, B., Wojnicz, R., Bialas, B., Osuch, M., Maciejewski, B., & Polonski, L. (2008). Angiographic and intravascular ultrasound assessment of immediate and 9-month efficacy of percutaneous transluminal renal artery balloon angioplasty with subsequent brachytherapy in patients with renovascular hypertension. *Kidney Blood Press Res*, Vol. 31, No. 5, (Publication date: 2008/09/06), pp. 291-298, I.S.S.N.: 1423-0143

Liang, Y., Zhu, H., & Friedman, M.H. (2008). Estimation of the transverse strain tensor in the arterial wall using IVUS image registration. *Ultrasound Med Biol*, Vol. 34, No. 11, (Publication date: 2008/07/16), pp. 1832-1845, I.S.S.N.: 1879-291X

Liu, J.B., Bonn, J., Needleman, L., Chiou, H.J., Gardiner, G.A., Jr., & Goldberg, B.B. (1999). Feasibility of three-dimensional intravascular ultrasonography: preliminary clinical studies. *J Ultrasound Med*, Vol. 18, No. 7, (Publication date: 1999/07/10), pp. 489-495, I.S.S.N.: 0278-4297

Luo, Z., Wang, Y., & Wang, W. (2003). Estimating coronary artery lumen area with optimization-based contour detection. *IEEE Trans Med Imaging*, Vol. 22, No. 4, (Publication date: 2003/05/31), pp. 564-566, I.S.S.N.: 0278-0062

Matar, F.A., Mintz, G.S., Douek, P., Farb, A., Virmani, R., Javier, S.P., Popma, J.J., Pichard, A.D., Kent, K.M., Satler, L.F., & et al. (1994). Coronary artery lumen volume measurement using three-dimensional intravascular ultrasound: validation of a new technique. *Cathet Cardiovasc Diagn*, Vol. 33, No. 3, (Publication date: 1994/11/01), pp. 214-220, I.S.S.N.: 0098-6569

McLeod, A.L., Watson, R.J., Anderson, T., Inglis, S., Newby, D.E., Northridge, D.B., Uren, N.G., & McDicken, W.N. (2004). Classification of arterial plaque by spectral analysis in remodelled human atherosclerotic coronary arteries. *Ultrasound Med Biol*, Vol. 30, No. 2, (Publication date: 2004/03/05), pp. 155-159, I.S.S.N.: 0301-5629

McPherson, A., Karrholm, J., Pinskerova, V., Sosna, A., & Martelli, S. (2005). Imaging knee position using MRI, RSA/CT and 3D digitisation. *J Biomech*, Vol. 38, No. 2, (Publication date: 2004/12/16), pp. 263-268, I.S.S.N.: 0021-9290

Mehran, R., Mintz, G.S., Hong, M.K., Tio, F.O., Bramwell, O., Brahimi, A., Kent, K.M., Pichard, A.D., Satler, L.F., Popma, J.J., & Leon, M.B. (1998). Validation of the in vivo intravascular ultrasound measurement of in-stent neointimal hyperplasia volumes. *J Am Coll Cardiol*, Vol. 32, No. 3, (Publication date: 1998/09/19), pp. 794-799, I.S.S.N.: 0735-1097

Min, P.K., Jung, J.H., Ko, Y.G., Choi, D., Jang, Y., & Shim, W.H. (2007). Effect of cilostazol on in-stent neointimal hyperplasia after coronary artery stenting: a quantative

coronary angiography and volumetric intravascular ultrasound study. *Circ J*, Vol. 71, No. 11, (Publication date: 2007/10/30), pp. 1685-1690, I.S.S.N.: 1346-9843

Miyazaki, S., Hiasa, Y., & Kishi, K. (2010). Very late thrombosis after subintimal sirolimus-eluting stent implantation during percutaneous coronary intervention for chronic total occlusion. *J Invasive Cardiol*, Vol. 22, No. 8, (Publication date: 2010/08/04), pp. E162-165, I.S.S.N.: 1557-2501

Moise, M.A., Alvarez-Tostado, J.A., Clair, D.G., Greenberg, R.K., Lyden, S.P., Srivastava, S.D., Eagleton, M., Sarac, T.S., & Kashyap, V.S. (2009). Endovascular management of chronic infrarenal aortic occlusion. *J Endovasc Ther*, Vol. 16, No. 1, (Publication date: 2009/03/14), pp. 84-92, I.S.S.N.: 1526-6028

Montorsi, P., Galli, S., Fabbiocchi, F., Trabattoni, D., Ravagnani, P.M., & Bartorelli, A.L. (2004). Randomized trial of conventional balloon angioplasty versus cutting balloon for in-stent restenosis. Acute and 24-hour angiographic and intravascular ultrasound changes and long-term follow-up. *Ital Heart J*, Vol. 5, No. 4, (Publication date: 2004/06/10), pp. 271-279, I.S.S.N.: 1129-471X

Murata, T., Hiro, T., Fujii, T., Yasumoto, K., Murashige, A., Kohno, M., Yamada, J., Miura, T., & Matsuzaki, M. (2002). Impact of the cross-sectional geometry of the post-deployment coronary stent on in-stent neointimal hyperplasia: an intravascular ultrasound study. *Circ J*, Vol. 66, No. 5, (Publication date: 2002/05/28), pp. 489-493, I.S.S.N.: 1346-9843

Nair, A., Kuban, B.D., Obuchowski, N., & Vince, D.G. (2001). Assessing spectral algorithms to predict atherosclerotic plaque composition with normalized and raw intravascular ultrasound data. *Ultrasound Med Biol*, Vol. 27, No. 10, (Publication date: 2001/12/04), pp. 1319-1331, I.S.S.N.: 0301-5629

Nair, A., Kuban, B.D., Tuzcu, E.M., Schoenhagen, P., Nissen, S.E., & Vince, D.G. (2002). Coronary plaque classification with intravascular ultrasound radiofrequency data analysis. *Circulation*, Vol. 106, No. 17, (Publication date: 2002/10/23), pp. 2200-2206, I.S.S.N.: 1524-4539

Nasir, K., Rivera, J.J., Yoon, Y.E., Chang, S.A., Choi, S.I., Chun, E.J., Choi, D.J., Budoff, M.J., Blumenthal, R.S., & Chang, H.J. (2010). Variation in atherosclerotic plaque composition according to increasing coronary artery calcium scores on computed tomography angiography. *Int J Cardiovasc Imaging*, Vol. 26, No. 8, (Publication date: 2010/04/30), pp. 923-932, I.S.S.N.: 1875-8312

Nishanian, G., Kopchok, G.E., Donayre, C.E., & White, R.A. (1999). The impact of intravascular ultrasound (IVUS) on endovascular interventions. *Semin Vasc Surg*, Vol. 12, No. 4, (Publication date: 2000/01/29), pp. 285-299, I.S.S.N.: 0895-7967

Oshima, A., Itchhaporia, D., & Fitzgerald, P. (1998). New developments in intravascular ultrasound. *Vasc Med*, Vol. 3, No. 4, (Publication date: 1999/04/02), pp. 281-290, I.S.S.N.: 1358-863X

Papadogiorgaki, M., Mezaris, V., Chatzizisis, Y.S., Giannoglou, G.D., & Kompatsiaris, I. (2007). Texture Analysis and Radial Basis Function Approximation for IVUS Image Segmentation. *Open Biomed Eng J*, Vol. 1, No. (Publication date: 2007/01/01), pp. 53-59, I.S.S.N.: 1874-1207

Prati, F., Crea, F., Labellarte, A., Sommariva, L., Marino, P., Caradonna, E., Manzoli, A., Pappalardo, A., & Boccanelli, A. (2002). Normal distribution of an intravascular ultrasound index of vessel remodeling. *Ital Heart J*, Vol. 3, No. 12, (Publication date: 2003/03/04), pp. 710-714, I.S.S.N.: 1129-471X

Prati, F., Mallus, M.T., & Lioy, E. (1998). Three-dimensional reconstruction techniques applied to intracoronary images. *G Ital Cardiol*, Vol. 28, No. 4, (Publication date: 1998/06/09), pp. 460-467, I.S.S.N.: 0046-5968

Pundziute, G., Schuijf, J.D., Jukema, J.W., Decramer, I., Sarno, G., Vanhoenacker, P.K., Boersma, E., Reiber, J.H., Schalij, M.J., Wijns, W., & Bax, J.J. (2008). Evaluation of plaque characteristics in acute coronary syndromes: non-invasive assessment with multi-slice computed tomography and invasive evaluation with intravascular ultrasound radiofrequency data analysis. *Eur Heart J*, Vol. 29, No. 19, (Publication date: 2008/08/07), pp. 2373-2381, I.S.S.N.: 1522-9645

Raju, S., Darcey, R., & Neglen, P. (2010). Unexpected major role for venous stenting in deep reflux disease. *J Vasc Surg*, Vol. 51, No. 2, (Publication date: 2009/12/17), pp. 401-408; discussion 408, I.S.S.N.: 1097-6809

Raju, S., & Neglen, P. (2006). High prevalence of nonthrombotic iliac vein lesions in chronic venous disease: a permissive role in pathogenicity. *J Vasc Surg*, Vol. 44, No. 1, (Publication date: 2006/07/11), pp. 136-143; discussion 144, I.S.S.N.: 0741-5214

Reid, D.B., Douglas, M., & Diethrich, E.B. (1995). The clinical value of three-dimensional intravascular ultrasound imaging. *J Endovasc Surg*, Vol. 2, No. 4, (Publication date: 1995/11/01), pp. 356-364, I.S.S.N.: 1074-6218

Rodriguez-Granillo, G.A., McFadden, E.P., Aoki, J., van Mieghem, C.A., Regar, E., Bruining, N., & Serruys, P.W. (2006). In vivo variability in quantitative coronary ultrasound and tissue characterization measurements with mechanical and phased-array catheters. *Int J Cardiovasc Imaging*, Vol. 22, No. 1, (Publication date: 2005/12/20), pp. 47-53, I.S.S.N.: 1569-5794

Roelandt, J.R., di Mario, C., Pandian, N.G., Wenguang, L., Keane, D., Slager, C.J., de Feyter, P.J., & Serruys, P.W. (1994). Three-dimensional reconstruction of intracoronary ultrasound images. Rationale, approaches, problems, and directions. *Circulation*, Vol. 90, No. 2, (Publication date: 1994/08/01), pp. 1044-1055, I.S.S.N.: 0009-7322

Rosenfield, K., Kaufman, J., Pieczek, A.M., Langevin, R.E., Jr., Palefski, P.E., Razvi, S.A., & Isner, J.M. (1992). Human coronary and peripheral arteries: on-line three-dimensional reconstruction from two-dimensional intravascular US scans. Work in progress. *Radiology*, Vol. 184, No. 3, (Publication date: 1992/09/11), pp. 823-832, I.S.S.N.: 0033-8419

Rosenfield, K., Losordo, D.W., Ramaswamy, K., Pastore, J.O., Langevin, R.E., Razvi, S., Kosowsky, B.D., & Isner, J.M. (1991). Three-dimensional reconstruction of human coronary and peripheral arteries from images recorded during two-dimensional intravascular ultrasound examination. *Circulation*, Vol. 84, No. 5, (Publication date: 1991/11/01), pp. 1938-1956, I.S.S.N.: 0009-7322

Saketkhoo, R.R., Razavi, M.K., Padidar, A., Kee, S.T., Sze, D.Y., & Dake, M.D. (2004). Percutaneous bypass: subintimal recanalization of peripheral occlusive disease with IVUS guided luminal re-entry. *Tech Vasc Interv Radiol*, Vol. 7, No. 1, (Publication date: 2004/04/09), pp. 23-27, I.S.S.N.: 1089-2516

Sano, K., Mintz, G.S., Carlier, S.G., Fujii, K., Takebayashi, H., Kimura, M., Costa, J.R., Jr., Tanaka, K., Costa, R.A., Lui, J., Weisz, G., Moussa, I., Dangas, G.D., Mehran, R., Lansky, A.J., Kreps, E.M., Collins, M., Stone, G.W., Moses, J.W., & Leon, M.B. (2006). Volumetric intravascular ultrasound assessment of neointimal hyperplasia and nonuniform stent strut distribution in sirolimus-eluting stent restenosis. *Am J Cardiol*, Vol. 98, No. 12, (Publication date: 2006/12/06), pp. 1559-1562, I.S.S.N.: 0002-9149

Sanz-Requena, R., Moratal, D., Garcia-Sanchez, D.R., Bodi, V., Rieta, J.J., & Sanchis, J.M. (2007). Automatic segmentation and 3D reconstruction of intravascular ultrasound images for a fast preliminar evaluation of vessel pathologies. *Comput Med Imaging Graph*, Vol. 31, No. 2, (Publication date: 2007/01/12), pp. 71-80, I.S.S.N.: 0895-6111

Sarno, G., Garg, S., Gomez-Lara, J., Garcia Garcia, H.M., Ligthart, J., Bruining, N., Onuma, Y., Witberg, K., van Geuns, R.J., de Boer, S., Wykrzykowska, J., Schultz, C., Duckers, H.J., Regar, E., de Jaegere, P., de Feyter, P., van Es, G.A., Boersma, E., van der Giessen, W., & Serruys, P.W. (2011). Intravascular ultrasound radiofrequency analysis after optimal coronary stenting with initial quantitative coronary angiography guidance: an ATHEROREMO sub-study. *EuroIntervention*, Vol. 6, No. 8, (Publication date: 2011/02/19), pp. 977-984, I.S.S.N.: 1969-6213

Schaar, J.A., Mastik, F., Regar, E., den Uil, C.A., Gijsen, F.J., Wentzel, J.J., Serruys, P.W., & van der Stehen, A.F. (2007). Current diagnostic modalities for vulnerable plaque detection. *Curr Pharm Des*, Vol. 13, No. 10, (Publication date: 2007/04/14), pp. 995-1001, I.S.S.N.: 1873-4286

Schuurbiers, J.C., Lopez, N.G., Ligthart, J., Gijsen, F.J., Dijkstra, J., Serruys, P.W., Van der Steen, A.F., & Wentzel, J.J. (2009). In vivo validation of CAAS QCA-3D coronary reconstruction using fusion of angiography and intravascular ultrasound (ANGUS). *Catheter Cardiovasc Interv*, Vol. 73, No. 5, (Publication date: 2009/03/25), pp. 620-626, I.S.S.N.: 1522-726X

Scoccianti, M., Verbin, C.S., Kopchok, G.E., Back, M.R., Donayre, C.E., Sinow, R.M., & White, R.A. (1994). Intravascular ultrasound guidance for peripheral vascular interventions. *J Endovasc Surg*, Vol. 1, No. (Publication date: 1994/09/01), pp. 71-80, I.S.S.N.: 1074-6218

Shekhar, R., Cothren, R.M., Vince, D.G., Chandra, S., Thomas, J.D., & Cornhill, J.F. (1999). Three-dimensional segmentation of luminal and adventitial borders in serial intravascular ultrasound images. *Comput Med Imaging Graph*, Vol. 23, No. 6, (Publication date: 2000/01/14), pp. 299-309, I.S.S.N.: 0895-6111

Sherknies, D., Meunier, J., Mongrain, R., & Tardif, J.C. (2005). Three-dimensional trajectory assessment of an IVUS transducer from single-plane cineangiograms: a phantom study. *IEEE Trans Biomed Eng*, Vol. 52, No. 3, (Publication date: 2005/03/12), pp. 543-549, I.S.S.N.: 0018-9294

Siegel, R.J., Swan, K., Edwalds, G., & Fishbein, M.C. (1985). Limitations of postmortem assessment of human coronary artery size and luminal narrowing: differential effects of tissue fixation and processing on vessels with different degrees of atherosclerosis. *J Am Coll Cardiol*, Vol. 5, No. 2 Pt 1, (Publication date: 1985/02/01), pp. 342-346, I.S.S.N.: 0735-1097

Sonka, M., Liang, W., Kanani, P., Allan, J., DeJong, S., Kerber, R., & McKay, C. (1998). Intracardiac echocardiography: computerized detection of left ventricular borders. *Int J Card Imaging*, Vol. 14, No. 6, (Publication date: 1999/08/24), pp. 397-411, I.S.S.N.: 0167-9899

Su, J.L., Wang, B., & Emelianov, S.Y. (2009). Photoacoustic imaging of coronary artery stents. *Opt Express*, Vol. 17, No. 22, (Publication date: 2009/12/10), pp. 19894-19901, I.S.S.N.: 1094-4087

Takagi, A., Hibi, K., Zhang, X., Teo, T.J., Bonneau, H.N., Yock, P.G., & Fitzgerald, P.J. (2000). Automated contour detection for high-frequency intravascular ultrasound imaging:

a technique with blood noise reduction for edge enhancement. *Ultrasound Med Biol*, Vol. 26, No. 6, (Publication date: 2000/09/21), pp. 1033-1041, I.S.S.N.: 0301-5629

Takeda, Y., Tsuchikane, E., Kobayashi, T., Terai, K., Kobayashi, Y., Nakagawa, T., Sakurai, M., & Awata, N. (2003). Effect of plaque debulking before stent implantation on in-stent neointimal proliferation: a serial 3-dimensional intravascular ultrasound study. *Am Heart J*, Vol. 146, No. 1, (Publication date: 2003/07/10), pp. 175-182, I.S.S.N.: 1097-6744

Tang, G.L., Chin, J., & Kibbe, M.R. (2010). Advances in diagnostic imaging for peripheral arterial disease. *Expert Rev Cardiovasc Ther*, Vol. 8, No. 10, (Publication date: 2010/10/13), pp. 1447-1455, I.S.S.N.: 1744-8344

Thrush, A.J., Bonnett, D.E., Elliott, M.R., Kutob, S.S., & Evans, D.H. (1997). An evaluation of the potential and limitations of three-dimensional reconstructions from intravascular ultrasound images. *Ultrasound Med Biol*, Vol. 23, No. 3, (Publication date: 1997/01/01), pp. 437-445, I.S.S.N.: 0301-5629

Tu, S., Huang, Z., Koning, G., Cui, K., & Reiber, J.H. (2010). A novel three-dimensional quantitative coronary angiography system: In-vivo comparison with intravascular ultrasound for assessing arterial segment length. *Catheter Cardiovasc Interv*, Vol. 76, No. 2, (Publication date: 2010/07/29), pp. 291-298, I.S.S.N.: 1522-726X

Vince, D.G., & Davies, S.C. (2004). Peripheral application of intravascular ultrasound virtual histology. *Semin Vasc Surg*, Vol. 17, No. 2, (Publication date: 2004/06/09), pp. 119-125, I.S.S.N.: 0895-7967

von Birgelen, C., de Feyter, P.J., de Vrey, E.A., Li, W., Bruining, N., Nicosia, A., Roelandt, J.R., & Serruys, P.W. (1997a). Simpson's rule for the volumetric ultrasound assessment of atherosclerotic coronary arteries: a study with ECG-gated three-dimensional intravascular ultrasound. *Coron Artery Dis*, Vol. 8, No. 6, (Publication date: 1997/06/01), pp. 363-369, I.S.S.N.: 0954-6928

von Birgelen, C., Di Mario, C., Li, W., Schuurbiers, J.C., Slager, C.J., de Feyter, P.J., Roelandt, J.R., & Serruys, P.W. (1996a). Morphometric analysis in three-dimensional intracoronary ultrasound: an in vitro and in vivo study performed with a novel system for the contour detection of lumen and plaque. *Am Heart J*, Vol. 132, No. 3, (Publication date: 1996/09/01), pp. 516-527, I.S.S.N.: 0002-8703

von Birgelen, C., Di Mario, C., Reimers, B., Prati, F., Bruining, N., Gil, R., Serruys, P.W., & Roelandt, J.R. (1996b). Three-dimensional intracoronary ultrasound imaging. Methodology and clinical relevance for the assessment of coronary arteries and bypass grafts. *J Cardiovasc Surg (Torino)*, Vol. 37, No. 2, (Publication date: 1996/04/01), pp. 129-139, I.S.S.N.: 0021-9509

von Birgelen, C., Erbel, R., Di Mario, C., Li, W., Prati, F., Ge, J., Bruining, N., Gorge, G., Slager, C.J., Serruys, P.W., & et al. (1995). Three-dimensional reconstruction of coronary arteries with intravascular ultrasound. *Herz*, Vol. 20, No. 4, (Publication date: 1995/08/01), pp. 277-289, I.S.S.N.: 0340-9937

von Birgelen, C., Li, W., Bom, N., & Serruys, P.W. (1997b). Quantitative three-dimensional intravascular ultrasound. *Semin Interv Cardiol*, Vol. 2, No. 1, (Publication date: 1997/03/01), pp. 25-32, I.S.S.N.: 1084-2764

Wahle, A., Lopez, J.J., Olszewski, M.E., Vigmostad, S.C., Chandran, K.B., Rossen, J.D., & Sonka, M. (2006). Plaque development, vessel curvature, and wall shear stress in coronary arteries assessed by X-ray angiography and intravascular ultrasound. *Med*

Image Anal, Vol. 10, No. 4, (Publication date: 2006/04/29), pp. 615-631, I.S.S.N.: 1361-8415

Wahle, A., Prause, P.M., DeJong, S.C., & Sonka, M. (1999). Geometrically correct 3-D reconstruction of intravascular ultrasound images by fusion with biplane angiography--methods and validation. *IEEE Trans Med Imaging*, Vol. 18, No. 8, (Publication date: 1999/10/26), pp. 686-699, I.S.S.N.: 0278-0062

Waksman, R., Erbel, R., Di Mario, C., Bartunek, J., de Bruyne, B., Eberli, F.R., Erne, P., Haude, M., Horrigan, M., Ilsley, C., Bose, D., Bonnier, H., Koolen, J., Luscher, T.F., & Weissman, N.J. (2009). Early- and long-term intravascular ultrasound and angiographic findings after bioabsorbable magnesium stent implantation in human coronary arteries. *JACC Cardiovasc Interv*, Vol. 2, No. 4, (Publication date: 2009/05/26), pp. 312-320, I.S.S.N.: 1876-7605

Wallace, M.J., Ahrar, K., Tinkey, P., & Wright, K.C. (2005). Transvenous extrahepatic portacaval shunt with use of a modified prototype stent-graft: experimental study in animals. *J Vasc Interv Radiol*, Vol. 16, No. 2 Pt 1, (Publication date: 2005/02/17), pp. 261-267, I.S.S.N.: 1051-0443

Weichert, F., Muller, H., Quast, U., Kraushaar, A., Spilles, P., Heintz, M., Wilke, C., von Birgelen, C., Erbel, R., & Wegener, D. (2003). Virtual 3D IVUS vessel model for intravascular brachytherapy planning. I. 3D segmentation, reconstruction, and visualization of coronary artery architecture and orientation. *Med Phys*, Vol. 30, No. 9, (Publication date: 2003/10/08), pp. 2530-2536, I.S.S.N.: 0094-2405

White, R.A., Scoccianti, M., Back, M., Kopchok, G., & Donayre, C. (1994). Innovations in vascular imaging: arteriography, three-dimensional CT scans, and two- and three-dimensional intravascular ultrasound evaluation of an abdominal aortic aneurysm. *Ann Vasc Surg*, Vol. 8, No. 3, (Publication date: 1994/05/01), pp. 285-289, I.S.S.N.: 0890-5096

Xu, S., Nomura, M., Kurokawa, H., Ando, T., Kimura, M., Ishii, J., Hasegawa, H., Kondo, T., Tadiki, S., & Qi, P. (1995). Relationship between coronary angioscopic and intravascular ultrasound imaging and restenosis. *Chin Med J (Engl)*, Vol. 108, No. 10, (Publication date: 1995/10/01), pp. 743-749, I.S.S.N.: 0366-6999

Zhang, X., McKay, C.R., & Sonka, M. (1998). Tissue characterization in intravascular ultrasound images. *IEEE Trans Med Imaging*, Vol. 17, No. 6, (Publication date: 1999/02/27), pp. 889-899, I.S.S.N.: 0278-0062

Zimarino, M., Weissman, N.J., Waksman, R., De Caterina, R., Ahmed, J.M., Pichard, A.D., & Mintz, G.S. (2002). Analysis of stent edge restenosis with different forms of brachytherapy. *Am J Cardiol*, Vol. 89, No. 3, (Publication date: 2002/01/26), pp. 322-325, I.S.S.N.: 0002-9149

Zimmermann, A., Pollinger, B., Rieber, J., Konig, A., Erhard, I., Krotz, F., Sohn, H.Y., Kantlehner, R., Haimerl, W., Duhmke, E., Leibig, M., Theisen, K., Klauss, V., & Schiele, T.M. (2005). Early time course of neointima formation and vascular remodelling following percutaneous coronary intervention and vascular brachytherapy of in-stent restenotic lesions as assessed by intravascular ultrasound analysis. *Z Kardiol*, Vol. 94, No. 4, (Publication date: 2005/04/02), pp. 239-246, I.S.S.N.: 0300-5860

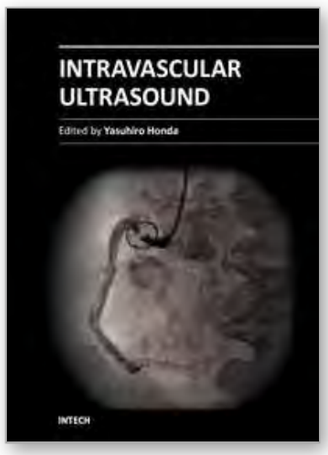

Intravascular Ultrasound
Edited by Dr. Yasuhiro Honda

ISBN 978-953-307-900-4
Hard cover, 207 pages
Publisher InTech
Published online 01, February, 2012
Published in print edition February, 2012

Intravascular ultrasound (IVUS) is a cardiovascular imaging technology using a specially designed catheter with a miniaturized ultrasound probe for the assessment of vascular anatomy with detailed visualization of arterial layers. Over the past two decades, this technology has developed into an indispensable tool for research and clinical practice in cardiovascular medicine, offering the opportunity to gather diagnostic information about the process of atherosclerosis in vivo, and to directly observe the effects of various interventions on the plaque and arterial wall. This book aims to give a comprehensive overview of this rapidly evolving technique from basic principles and instrumentation to research and clinical applications with future perspectives.

InTech Europe
University Campus STeP Ri
Slavka Krautzeka 83/A
51000 Rijeka, Croatia
Phone: +385 (51) 770 447
Fax: +385 (51) 686 166
www.intechopen.com

InTech China
Unit 405, Office Block, Hotel Equatorial Shanghai
No.65, Yan An Road (West), Shanghai, 200040, China
中国上海市延安西路65号上海国际贵都大饭店办公楼405单元
Phone: +86-21-62489820
Fax: +86-21-62489821

IntechOpen

3

Integrated Backscatter Intravascular Ultrasound

Masanori Kawasaki
Department of Cardiology,
Gifu University Graduate School of Medicine
Japan

1. Introduction

About 30 years ago, a pathological study by Horie et al. demonstrated that plaque rupture into the lumen of a coronary artery may precede and cause thrombus formation leading to acute myocardial infarction (Horie et al., 1978). In an angioscopic study, Mizuno et al. demonstrated that disruption or erosion of vulnerable plaques and subsequent thromboses are the most frequent cause of acute coronary syndrome (Mizuno et al., 1992). The stability of atherosclerotic plaques is related to the histological composition of plaques and the thickness of fibrous caps. Therefore, recognition of the tissue characteristics of coronary plaques is important to understand and prevent acute coronary syndrome. Accurate identification of the tissue characteristics of coronary plaques *in vivo* may allow the identification of vulnerable plaques before the development of acute coronary syndrome.
In the 1990's, a new technique was developed that could characterize myocardial tissues by integrated backscatter (IB) analysis of ultrasound images. This technique is capable of providing both conventional two-dimensional echocardiographic images and IB images. Ultrasound backscatter power is proportional to the difference of acoustic characteristic impedance that is determined by the density of tissue multiplied by the speed of sound. In studies of the myocardium, calibrated myocardial IB values were significantly correlated with the relative volume of interstitial fibrosis (Picano, 1990 et al.; Naito et al., 1996). In preliminary studies *in vitro*, IB values reflected the structural and biochemical composition of atherosclerotic lesion and could differentiate fibrofatty, fatty and calcification of arterial walls (Barziliai et al., 1987; Urbani et al., 1993; Picano et al., 1988). It was also reported that anisotropy of the direction and backscatter power is related to plaque type (De Kroon et al., 1991). Takiuchi et al. found that quantitative tissue characterization using IB ultrasound could identify lipid pool and fibrosis in human carotid and/or femoral arteries (Takiuchi et al., 2000). However, these studies were done *ex vivo* and different plaque types were measured in only a few local lesions. In the early 2000s, it was reported that IB values measured *in vivo* in human carotid arteries correlated well with postmortem histological classification (Kawasaki et al., 2001). This new non-invasive technique using IB values could characterize the two-dimensional structures of arterial plaques *in vivo*. With this technique, plaque tissues were classified based on histopathology into 6 types, *i.e*. intraplaque hemorrhage, lipid pool, intimal hyperplasia, fibrosis, dense fibrosis, and calcification. This technique was applied in the clinical setting to predict cerebral ischemic lesions after carotid artery stenting. From the analysis of receiver operating characteristic (ROC) curves, a relative intraplaque hemorrhage + lipid pool area of 50% measured by IB ultrasound imaging was the most reliable cutoff value

for predicting cerebral ischemic lesions evaluated by diffusion-weighted magnetic resonance imaging after carotid artery stenting (Yamada et al., 2010).
Since it was difficult to differentiate lipid pool from intimal hyperplasia using IB values, the anatomical features of the lesion were used for this purpose. Because lipid pool is generally located under a fibrous cap, a region of interest (ROI) that was either lipid pool or intimal hyperplasia was classified as lipid pool only when that region was located underneath a ROI with fibrosis. Intimal hyperplasia was identified when a ROI that was either lipid pool or intimal hyperplasia was not covered by a fibrous cap. Most of these two lesion types could be differentiated using this method.

2. IB-IVUS equipment and data acquisition

In the next generation, this ultrasound IB technique was applied to coronary arteries by use of intravascular ultrasound (IVUS) (Kawasaki et al., 2002). A personal computer (Windows XP Professional, CPU: 3.4 GHz) equipped with newly developed custom software was connected to an IVUS imaging system (VISIWAVE, Terumo, Japan) to obtain the radio frequency signal, signal trigger and video image outputs. An analog-to-digital converter digitized the signals at 400 MHz with 8-bit resolution, and the digitized data were stored on the hard drive of the PC for later analysis. In the IVUS analysis, 512 vector lines of ultrasound signal around the circumference were analyzed to calculate the IB values. The IB values for each tissue component were calculated using a fast Fourier transform, and expressed as the average power, measured in decibels (dB), of the frequency component of the backscattered signal from a small volume of tissue. Ultrasound backscattered signals were acquired using a 38 or 43 MHz mechanically-rotating IVUS catheter (ViewIT, Terumo, Tokyo, Japan), digitized and subjected to spectral analysis. The tissue IB values were calibrated by subtracting the IB values from the IB value of a stainless steel needle placed at a distance of 1.5 mm from the catheter. IB-IVUS color-coded maps were constructed based on the IB values by use of custom software written by our group. Conventional IVUS images and IB-IVUS color-coded maps were immediately displayed side-by-side on a monitor. Color-coded maps of the coronary arteries were finally constructed after excluding the vessel lumen and area outside of the external elastic membrane by manually tracing the vessel lumen and external elastic membrane on the conventional IVUS images. With a transducer frequency of 38 or 43 MHz, the wavelength was calculated as 36 or 41 μm, respectively, assuming a tissue sound speed of approximately 1,560 m/sec.

3. Correlation between IB-IVUS and histological images

To compare IB-IVUS images with histological images, coronary cross-sections obtained at autopsy were stained with hematoxylin-eosin, elastic van Gieson and Masson's trichrome. In the training study, three pathologic subsets were identified in each ROI: lipid pool (extracellular lipid, macrophages, microcalcification and/or foam cells), fibrosis and calcification. Necrotic core that consisted of lipid pool, microcalcification and remnants of foam cells and/or dead lymphocytes were classified as lipid pool in the IB-IVUS analysis. In the validation study, coronary arterial cross-sections were classified into three categories: fibrocalcific, fibrous and lipid-rich.
To evaluate overall ultrasound signal attenuation, IB values of the same lesions (n = 10) were measured after moving the lesions 2.5 - 4.0 mm from the IVUS catheter. Including the

attenuation by flowing blood, an overall attenuation of 4.0 dB/mm was determined to be the most appropriate, and this value was used to correct for ultrasound signal attenuation. Therefore, when color-coded maps were constructed, each IB value was corrected by adding 4.0 dB/mm when the ROI was located 1.5 mm further away from the catheter and subtracting 4.0 dB/mm when the ROI was located 1.5 mm closer to the catheter. Color-coded maps consisted of four major components: fibrous (green), dense fibrosis (yellow), lipid pool (blue), calcification (red).

The histological analysis of each ROI showed the presence of typical tissue components including calcification (n = 41), fibrosis (n = 102) and lipid pool (n = 99). With the 38 MHz ultrasound mode, the average IB values in each ROI of these tissue components were -7.3 ± 6.5, -27.0 ± 5.3 and -51.2 ± 3.3 dB, respectively; however, with the 43 MHz ultrasound mode, the average IB values were -10.6 ± 6.1, -30.4 ± 4.9 and -54.0 ± 3.9 dB, respectively. The differences among IB values of lipid pool, fibrosis or calcification were significant ($p<0.001$). IB values were highest in calcification and lowest in lipid pool. There was no overlap between the IB values of lipid pool and calcification. According to the analysis of ROC curves, an IB value of ≤ -39 dB (area under curve = 0.98) was the most reliable cutoff point for discriminating lipid pool (90% sensitivity, 92% specificity) and fibrosis (94% sensitivity, 93% specificity), and an IB value of > -17 dB (area under curve = 0.99) was the most reliable cutoff point for discriminating calcification and fibrosis with the 38 MHz mode. An IB value of ≤ -42 dB (area under curve = 0.98) was the most reliable cutoff point for discriminating lipid pool and fibrosis and an IB value of > -20 dB (area under curve = 0.99) was the most reliable cutoff point for discriminating calcification and fibrosis with the 43 MHz mode.

Based on the above cutoff points, two-dimensional color-coded maps of tissue characteristics were constructed. A total of 95 cross-sections were diagnosed as fibrocalcific, fibrous or lipid-rich by the IB-IVUS reader, who was blinded to the histological diagnoses. There was no difference in the diagnosis of the images obtained using either the 38 MHz or 43 MHz ultrasound signal. The overall agreement between the classifications made by IB-IVUS and histology (lipid-rich: n = 35, fibrous: n = 33 and fibrocalcific: n = 27) was excellent (Cohen's $\kappa = 0.83$, 95% CI: 0.73 - 0.92).

4. Comparison between IB-IVUS and virtual hostology IVUS

Virtual histology IVUS (Virtual Histology Version 1.4, Volcano Corp., CA, USA) images were acquired by a VH-IVUS console with a 20 MHz phased-array catheter and stored on CD-ROM for offline analysis. To clarify the rotational and cross-sectional position of the included segment, multiple surgical needles were carefully inserted into the coronary arteries before IB-IVUS and VH-IVUS imaging to serve as reference points to compare the two imaging modalities.

In qualitative comparison, small (0.3mm x 0.3mm) region-of-interest (ROI)s were set on the same sites of histological and IVUS images. In quantitative comparison, histological images from cross-sections that were stained with Masson's trichrome were digitized, and the areas that were stained blue were automatically selected by a multipurpose image processor (LUZEX F, Nireco Co., Tokyo, Japan). Then the relative fibrous area (fibrous area / plaque area) was automatically calculated by the LUZEX F system.

In the direct qualitative comparison, the overall agreement between the histological and IB-IVUS diagnoses was higher (Cohen's $\kappa = 0.81$, 95% CI: 0.74-0.90) than between the

histological and VH-IVUS diagnoses (Cohen's κ = 0.30, 95% CI: 0.14-0.41) (Okubo et al., 2008 (a); Okubo et al., 2008 (b)).
In the direct quantitative comparison, the % fibrosis area determined by IB-IVUS was significantly correlated with the relative area of fibrosis based on histology (r=0.67, p<0.001), whereas the % fibrous area and % fibrous area + % fibro-fatty area determined by VH-IVUS were not correlated with the relative area of fibrosis based on histology (Figure 1) (Okubo et al., 2008).

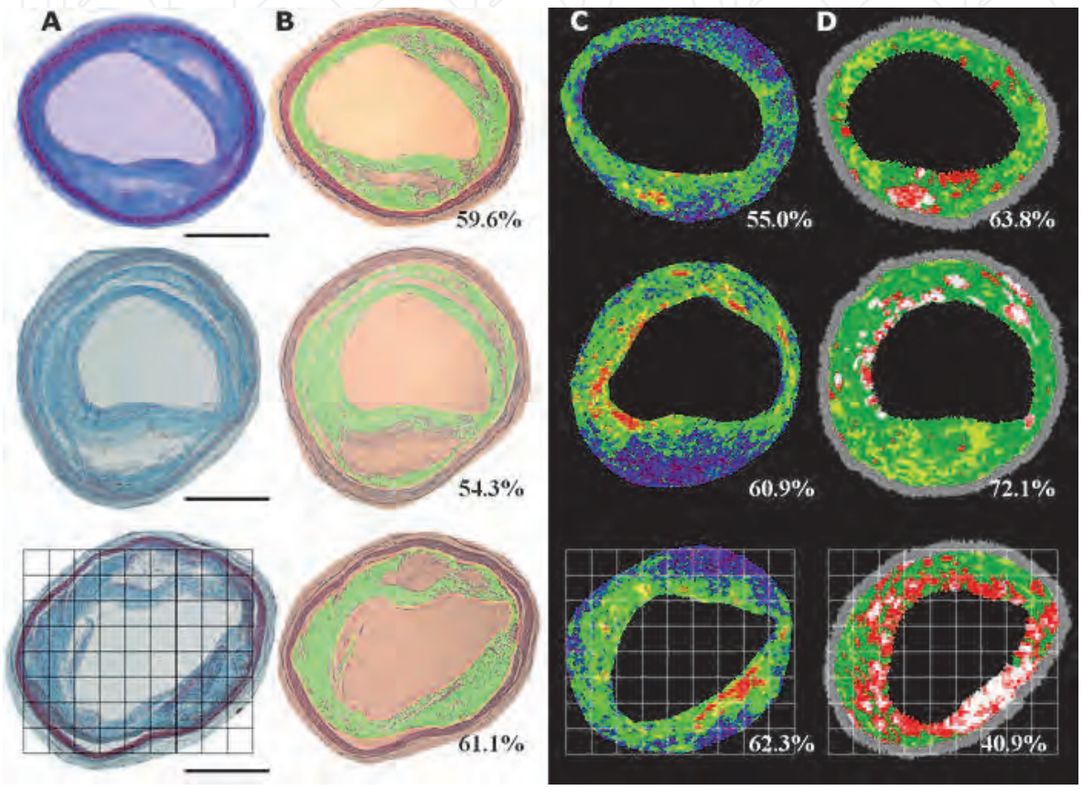

Fig. 1. Representative lesion used in the direct comparison study. A: histological images stained with Masson's trichrome. Bar = 1 mm. B: Images after quantification by the image processor. Areas that were stained blue by Masson's trichrome were automatically selected (green area) by the multipurpose image processor (LUZEX F) and the relative fibrous area (fibrous area / plaque area) was automatically calculated by the system. C: IB-IVUS images corresponding to sections analyzed by histology. D: IVUS-VH images corresponding to sections analyzed by histology. Percentages indicate the relative fibrous areas determined by each method.

5. Comparison of the thickness of the fibrous cap measured by IB-IVUS and optical coherence tomography in vivo

During routine selective percutaneous coronary intervention in 42 consecutive patients, a total of 28 cross-sections that consisted of lipid overlaid by a fibrous cap were imaged by both IVUS and optical coherence tomography in 24 patients with stable angina pectoris. A 0.016-inch optical coherence tomography catheter (Imagewire, LightLab Imaging, Inc.,

Westford, MA) was advanced into the coronary arteries. IB-IVUS and optical coherence tomography (M2 OCT Imaging system, LightLab Imaging, Inc., Westford, MA) were performed in each patient at the same site without significant stenosis as described below.
IB-IVUS images were obtained every one second using an automatic pullback device at a rate of 0.5 mm/sec. optical coherence tomography images were obtained using an automatic pullback system at a rate of 0.5 mm/sec. IB-IVUS images were obtained at 0.5 mm intervals, whereas optical coherence tomography images were obtained at 0.03 mm intervals. Therefore, the segments of coronary artery to compare between the two methods were selected based on the IB-IVUS images. Then, these same coronary segments were identified in optical coherence tomography using the distance from easily-definable side branches and calcification as reference markers to ensure that IB-IVUS and optical coherence tomography were compared at the same site. The cross-sections that did not have sufficient imaging quality to analyze tissue characteristics were excluded from the comparison. In the IB-IVUS analysis, images were processed by a smoothing method that averaged nine IB values in nine pixels located in a square field of the color-coded maps to reduce uneven surfaces of tissue components produced by signal noise.

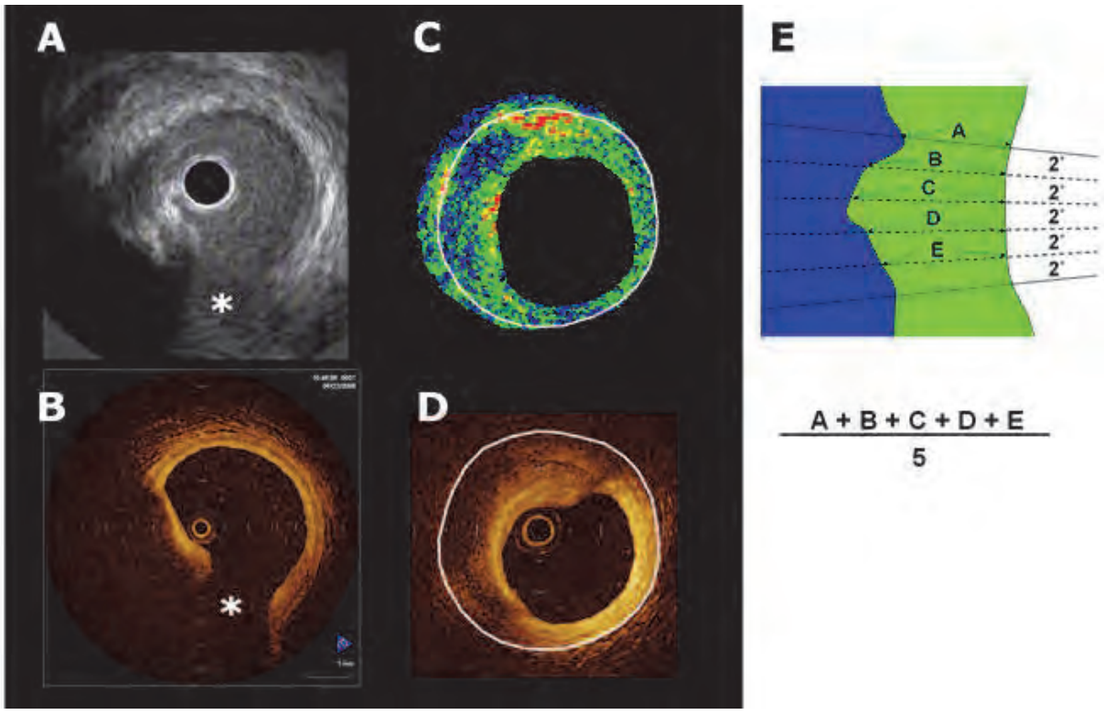

Fig. 2. The same coronary segments were selected for imaging using the distance from easily-identifiable side branches and calcification as reference markers to ensure that integrated backscatter intravascular ultrasound (IB-IVUS) and optical coherence tomography (OCT) were compared at the same site. (A) Conventional IVUS image. (B) Corresponding OCT image. (C) IB-IVUS image. (D) Corresponding OCT image. (E) Fibrous caps that overlaid lipid pool were divided into regions-of-interest (ROIs) (every 10˚ from the center of the vessel) and the thickness of fibrous caps was measured as an average. The average thickness of fibrous cap was measured by averaging the thickness of fibrous cap every 2˚ within ROIs. *: septal branch.

Fibrous caps that overlaid lipid pool were divided into ROI (every 10˚ rotation from the center of the vessel lumen) and the average thickness was determined. The average thickness of fibrous cap was determined by averaging the thickness of fibrous cap every 2˚ within the ROIs (Figure 2). The areas where the radial axis from the center of the vessel lumen crossed the tangential line of the vessel surface with an angle less than a 80˚ were excluded from the comparison.

The thickness of fibrous cap measured by IB-IVUS was significantly correlated with that measured by optical coherence tomography ($y = 0.99x - 0.19$, $r = 0.74$, $p<0.001$) (Figure 3) (Kawasaki et al., 2010).

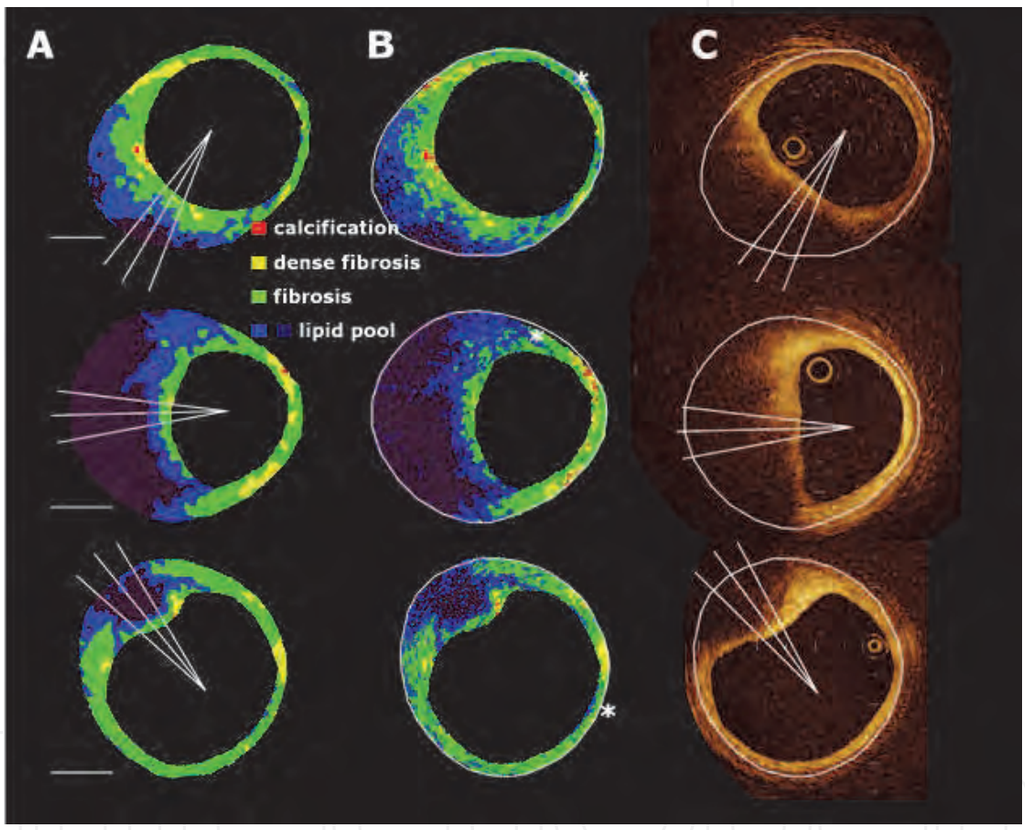

Fig. 3. (A) Representative integrated backscatter intravascular ultrasound (IB-IVUS) images processed by a smoothing method. (B) Original IB-IVUS images (C) Corresponding optical coherence tomography. *: attenuation by guide wire. Bar = 1mm.

A Bland-Altman plot showed that the mean difference between the thickness of fibrous cap measured by IB-IVUS and optical coherence tomography (IB-IVUS - optical coherence tomography) was -2 ± 147 μm (Figure 4). The difference between the two methods appeared to increase as the thickness of the fibrous cap increased. Optical coherence tomography has a better potential for characterizing tissue components located on the near side of the vessel lumen, whereas IB-IVUS has a better potential for characterizing tissue components of entire plaques (Kawasaki et al., 2006).

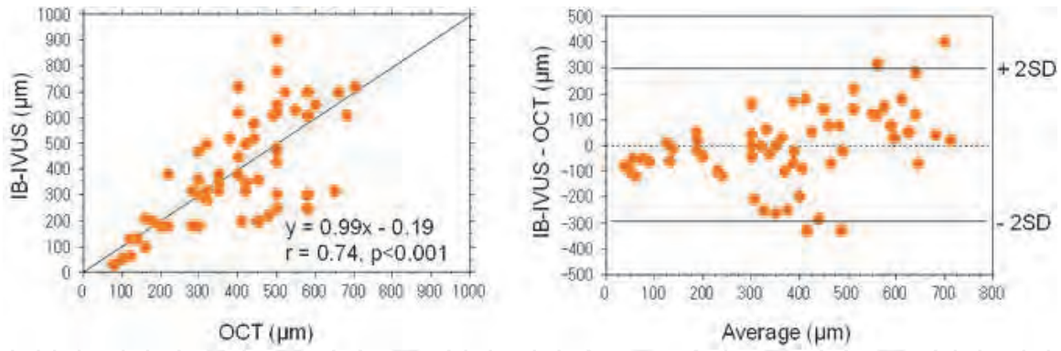

Fig. 4. Left: Correlation between the thickness of fibrous cap measured by integrated backscatter intravascular ultrasound and optical coherence tomography. Right: Bland-Altman plot.

6. Clinical studies conducted by use of IB-IVUS

There have been many clinical studies performed using IB-IVUS. In a prospective study, IB-IVUS was performed in 140 patients with stable angina pectoris in one or two arterial segments without significant stenosis (Sano et al., 2006). The % lipid area was greater in plaques that caused acute coronary syndrome than in plaques that did not cause acute coronary syndrome (72 ± 10 versus 50 ± 16%, $p<0.001$). The % fibrous area was smaller in plaques that caused acute coronary syndrome than in plaques that did not cause acute coronary syndrome (23 ± 6 versus 47 ± 14%, $p<0.001$) (Figure 5).

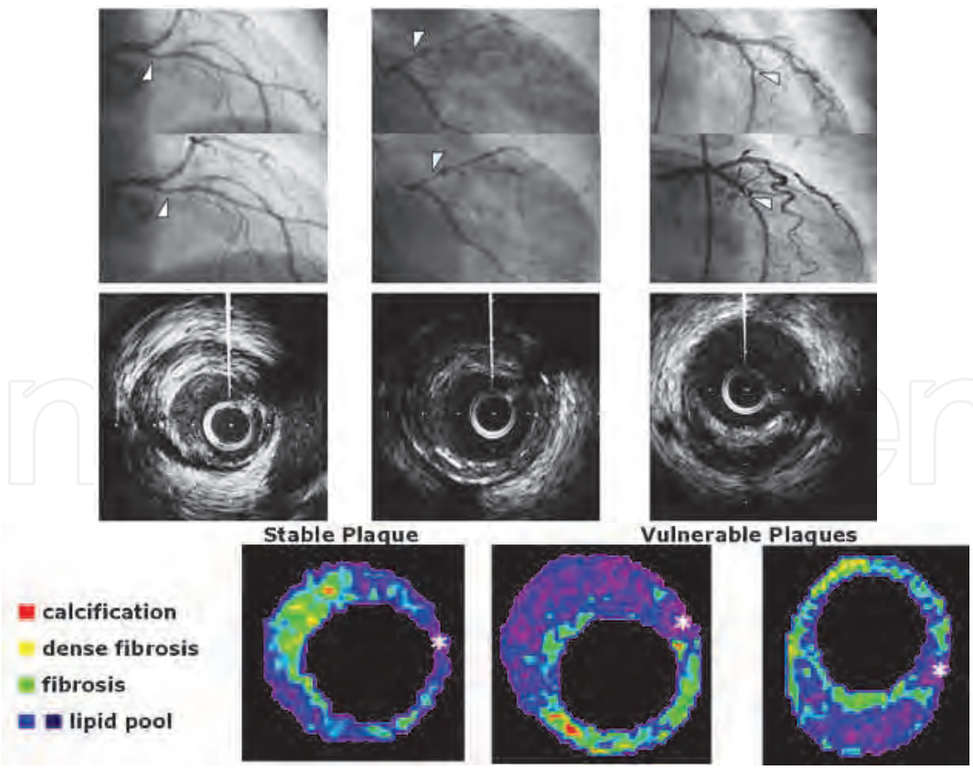

Fig. 5. Images of lesion in patients with (right) and without (left) acute coronary syndrome. (*) indicates the guidewire artifact.

The optimum cutoffs for the calculation of diagnostic accuracy to classify plaques that caused acute coronary syndrome were obtained from the ROC curve. The optimal cutoffs of % fibrous area and % lipid area were 25% and 65% respectively. Regarding remodeling index, Takeuchi et al. reported that % lipid volume in the positive remodeling plaques was greater than the non-positive remodeling plaques (40.5 ± 14.8 versus 26.4 ± 15.9%, $p<0.001$) and they concluded that positive remodeling lesions contain more lipid-rich components compared with non-positive remodeling lesions, which may account for the higher incidence of acute coronary syndrome and plaque vulnerability (Takeuchi et al., 2009).

During percutaneous coronary intervention, 107 non-culprit intermediate plaques in left anterior descending coronary arteries were analyzed by IB-IVUS (Komura et al., 2010). Plaques in the proximal segment had a higher % lipid content than did plaques in the distal segment (36.1 ± 12.3 versus 18.6 ± 13.1%, $p<0.01$). A total of 155 consecutive patients who underwent percutaneous coronary intervention were investigated by IB-IVUS. Lipid-rich plaques measured by IB-IVUS proved to be an independent morphologic predictor of non-target ischemic events after percutaneous coronary intervention, and the risk was particularly increased in patients with elevated serum C-reactive protein levels (Amano et at., 2011). Amano et al. reported that patients with metabolic syndrome showed a significant increase in % lipid area (38 ± 19% versus 30 ± 19%, $p=0.02$) and metabolic syndrome was associated with lipid-rich plaques, contributing to an increase of plaque vulnerability (Amano et al., 2007). Kimura et al. demonstrated that the ratio of LDL to HDL cholesterol was an independent predictor of lipid area / non- lipid area (Kimura et al., 2010).

A substantial reduction of acute cardiac events has been shown in most lipid-lowering trials, despite only a minimal geometric regression of plaque (Brown BG et al., 1993; Fernández-Ortiz A et al., 1994). These findings suggest that plaque stability was increased by the removal of lipids from lipid-rich plaques. Three-dimensional IB-IVUS demonstrated that statin therapy for 6 months reduced the lipid volume in patients with stable angina (pravastatin: 25.5 ± 5.7 to 21.9 ± 5.3%, $p<0.05$; atorvastatin: 26.5 ± 5.2 to 19.9 ± 5.5%, $p<0.01$) without reducing the degree of stenosis. To improve the accuracy of the volumetric analysis, polar coordinates in the two-dimensional color-coded maps were transformed into Cartesian coordinates (64 x 64 pixels) using computer software, because the size of each ROI was different in the polar coordinates. Three-dimensional IB-IVUS offers the potential for quantitative volumetric tissue characterization of coronary atherosclerosis (Kawasaki et al., 2005) (Figure 6).

Otagiri et al. investigated the effectiveness of rosuvastatin in patients with acute coronary syndrome using IB-IVUS. They demonstrated that reduction rate of % lipid volume after 6 months of rosuvastatin therapy was significantly correlated with the baseline values ($r = -0.498$, $p=0.024$) (Otagiri et al., 2011). Early intervention with rosuvastatin in acute coronary syndrome patients caused significant reduction of the non-culprit plaque during 6 months. This regression was mainly due to the decrease in the lipid component measured by IB-IVUS.

7. Technical consideration

The fixation and processing of arterial samples for histopathology decreases the total vessel and luminal cross-sectional area, but the absolute wall area (total vessel cross-sectional area minus luminal cross-sectional area) does not change in vessels with minimal atherosclerotic narrowing (Lockwood et al., 1991; Siegel et al., 1985). Several studies have documented that formalin fixation does not significantly affect the morphology and quantitative echo characteristic of plaque tissue from human aortic walls (Kawasaki et al., 2001; Picano et al., 1983).

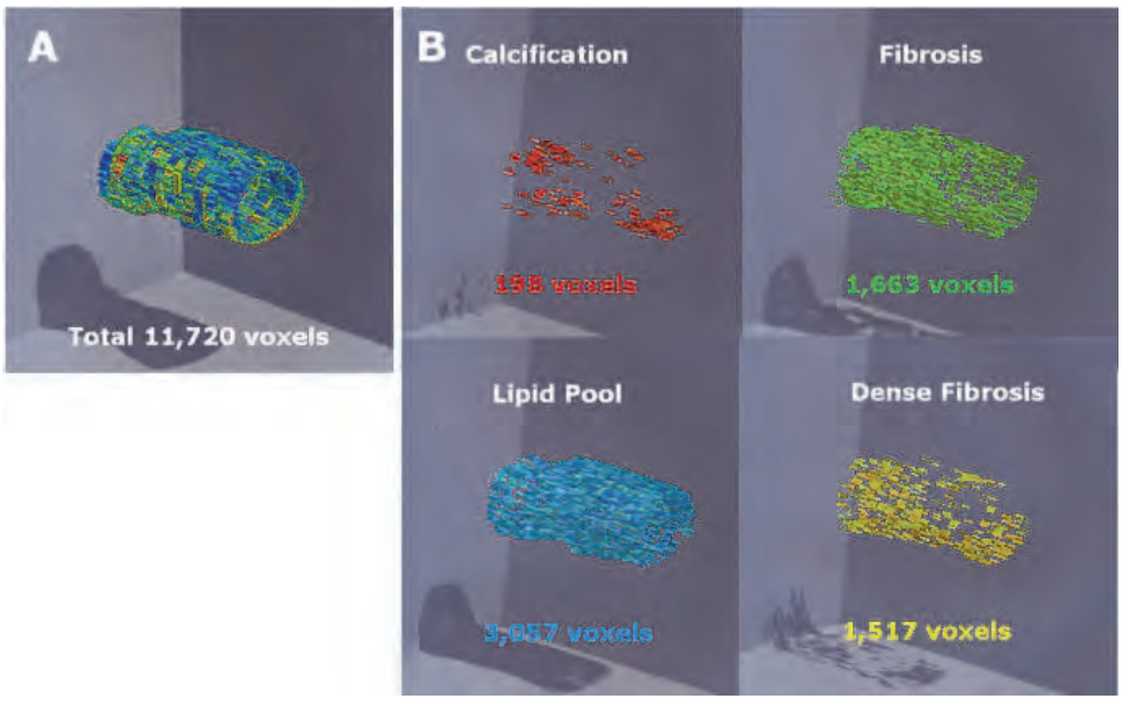

Fig. 6. A: Three-dimensional color-coded maps of coronary arterial plaques constructed by three-dimensional IB-IVUS. B: Three-dimensional color-coded maps of each characteristic. The number of voxels of each tissue characteristic was automatically calculated.

IB-IVUS occasionally underestimates calcified lesions and overestimates lipid pool behind calcification due to the acoustic shadow derived from calcification. Acoustic shadow caused by calcification hinders the precise determination of the tissue characteristics of coronary plaques. However, there were many cases in which lesions that were classified as lipid pool by IB-IVUS due to the acoustic shadow behind calcification actually included lipid core in the same lesion analyzed by histology (n = 16/21, 76%). Our results are consistent with previous results that showed that necrotic core and fibrofatty components were located behind calcification (83 - 89%) (Kume et al., 2007). Since calcification usually originates in lesions with lipid accumulation, the diagnosis of lipid pool by IB-IVUS in lesions behind calcification was usually accurate.

8. Limitations

There were a few limitations of the ultrasound method. First, the angle-dependence of the ultrasound signal makes tissue characterization unstable when lesions are not perpendicular to the ultrasound axis. Picano et al. reported that angular scattering behavior is large in calcified and fibrous tissues, whereas it is slight to nonexistent in normal and fatty plaques (Picano et al., 1985). According to that report, although there was no crossover of IB values between fibrous and fibrofatty within an angle span of 10°, or between fibrous and fatty within an angle span of 14°, this angle-dependence of the ultrasound signal might be partially responsible for the variation of IB values obtained from each tissue component. There was also a report that demonstrated the degree of angle-dependence of 30 MHz ultrasound in detail (Courtney et al., 2002). In that report, the angle-dependence of 30 MHz ultrasound in the

arterial intima and media was 1.11dB/10°. When the 40 MHz catheter was used, the angle dependence increased in arterial tissue. This angle-dependence of the ultrasound signal may decrease the diagnostic accuracy for differentiating tissue components.

Second, the guidewire was not used in the process of imaging because the present studies were performed *ex vivo*. Imaging artifacts *in vivo* due to the guidewire may decrease the diagnostic accuracy. However, removal of the guidewire during imaging after completing the intervention procedure and/or excluding the area behind calcification from the analysis may be necessary in the clinical setting to eliminate this problem. Finally, detecting thrombus from a single IVUS cross-section was not possible because we usually look at multiple IVUS images over time for speckling, scintillation, motion and blood flow in the "microchannel" (Mintz et al., 2001). The analysis of IB values in multiple cross-sections over time is required for the detection of thrombus.

9. References

Amano T, Matsubara T, Uetani T, Nanki M, Marui N, Kato M, Arai K, Yokoi K, Ando H, Ishii H, Izawa H, Murohara T. (2007). Impact of metabolic syndrome on tissue characteristics of angiographically mild to moderate coronary lesions integrated backscatter intravascular ultrasound study. *J Am Coll Cardiol* Vol 49:1149-56.

Amano T, Matsubara T, Uetani T, Kato M, Kato B, Yoshida T, Harada K, Kumagai S, Kunimura A, Shinbo Y, Ishii H, Murohara T. (2011). Lipid-rich plaques predict non-target-lesion ischemic events in patients undergoing percutaneous coronary intervention. *Circ J* Vol 75;157-66.

Barziliai B, Shffitz JE, Miller JG, Sobel BE. (1987). Quantitative ultrasonic characterization of the nature of atherosclerotic plaques in human aorta. *Circ Res.*Vol 60: 459-63.

Brown BG, Zhao XQ, Sacco DE, Albers JJ. (1993). Lipid lowering and plaque regression. New insights into prevention of plaque disruption and clinical events in coronary disease. *Circulation*. Vol 87:1781-91.

Courtney BK, Robertson AL, Maehara A, Luna J, Kitamura K, Morino Y, et al. (2002). Effect of transducer position on backscattered intensity in coronary arteries. *Ultrasound in Med & Biol*. Vol 28:81-91.

De Kroon MGM, van der Wal LF, Gussenhoven WJ, Rijsterborgh H, Bom N. (1991). Backscatter directivity and integrated backscatter power of arterial tissue. *Int J Card Imaging*.Vol 6:265-75.

Fernández-Ortiz A, Badimon JJ, Falk E, Fuster V, Meyer B, Mailhac A, Weng D, Shah PK, Badimon L. (1994). Characterization of the relative thrombogenecity of atherosclerotic plaque components: implications for consequences of plaque rapture. *J Am Coll Cardiol* Vol 23:1562-9.

Horie, T., Sekiguchi, M., Hirosawa, K. (1978). Coronary thrombosis in pathogenesis of acute myocardial infarction. Histopathological study of coronary arteries in 108 necropsied cases using serial section. *Br Heart J* Vol. 40:153-61.

Kawasaki M, Takatsu H, Noda T, Ito Y, Kunishima A, Arai M, Nishigaki K, Takemura G, Morita N, Minatoguchi S, Fujiwara H. (2001). Non-invasive tissue characterization of human atherosclerotic lesions in carotid and femoral arteries by ultrasound integrated backscatter. -Comparison between histology and integrated backscatter images before and after death- *J Am Coll Cardiol.* Vol 38:486-92

Kawasaki M, Takatsu H, Noda T, et al. (2002) In vivo quantitative tissue characterization of human coronary arterial plaques using integrated backscatter intravascular ultrasound and comparison with angioscopic findings. Circulation Vol 105:2487-92.

Kawasaki M, Sano K, Okubo M, Yokoyama H, Ito Y, Murata I, Tsuchiya K, Minatoguchi S, Zhou X, Fujita H, Fujiwara H. (2005). Volumetric quantitative analysis of tissue characteristics of coronary plaques after statin therapy using three dimensional integrated backscatter intravascular ultrasound. *J Am Coll Cardiol* Vol 45:1946-1953.

Kawasaki M, Bouma BE, Bressner J, Houser SL, Nadkarni SK, MacNeill BD, Jang IK, Fujiwara H, Tearney GJ. (2006). Diagnostic accuracy of optical coherence tomography and integrated backscatter intravascular ultrasound images for tissue characterization of human coronary plaques. *J Am Coll Cardiol* Vol 48:81-8.

Kawasaki M, Hattori A, Ishihara Y, Okubo M, Nishigaki K, Takemura G, Saio M, Takami T, Minatoguchi S. (2010). Tissue characterization of coronary plaques and assessment of thickness of fibrous cap using integrated backscatter intravascular ultrasound. Comparison with histology and optical coherence tomography. *Circ J* Vol 74:2641-48.

Kimura T, Itoh T, Fusazaki T, Matsui H, Sugawara S, Ogino Y, Endo H, Kobayashi K, Nakamura M. (2010). Low-density lipoprotein-cholesterol/high-density lipoprotein-cholesterol ratio predicts lipid-rich coronary plaque in patients with coronary artery disease--integrated-backscatter intravascular ultrasound study. *Circ J* Vol 74:1392-8.

Komura N, Hibi K, Kusama I, Otsuka F, Mitsuhashi T, Endo M, Iwahashi N, Okuda J, Tsukahara K, Kosuge M, Ebina T, Umemura S, Kimura K. (2010). Plaque location in the left anterior descending coronary artery and tissue characteristics in angina pectoris: an integrated backscatter intravascular ultrasound study. *Circ J* Vol 74: 142-7.

Kume T, Okura H, Kawamoto T, Akasaka T, Toyota E, Neishi Y, et al. (2007). Assessment of the histological characteristics of coronary arterial plaque with severe calcification. *Circ J*. Vol 71:643-7.

Lockwood GR, Ryan LK, Hunt JW, Foster FS. (1991). Measurement of the ultrasound properties of vascular tissue and blood from 35-65Mhz. *Ultrasound Med Biol*. Vol 17:653-66.

Mintz GS, Nissen SE, Anderson WD, Bailey SR, Erbel R, Fitzgerald PJ, et al. (2001). American College of Cardiology clinical expert consensus document on standards for acquisition, measurement and reporting of intravascular ultrasound studies (IVUS). A report of the American College of Cardiology task force on clinical expert consensus documents developed in collaboration with the European society of cardiology endorsed by the society of cardiac angiography and interventions. *J Am Coll Cardiol*. Vol 37:1478-92.

Mizuno K, Satomura K, Miyamoto A, Arakawa K, Shibuya T, Arai T, Kurita A, Nakamura H, Ambrose JA. (1992). Angioscopic evaluation of coronary artery thrombi in acute coronary syndromes. *N Engl J Med* Vol 326:287-91.

Naito J, Masuyama T, Mano T, Kondo H, Yamamoto K, Nagano R, Doi Y, Hori M, Kamada T. (1996). Ultrasound myocardial tissue characterization in the patients with dilated cardiomyopathy: Value in noninvasive assessment of myocardial fibrosis. *Am Heart J*. Vol 131:115-21.

Okubo M, Kawasaki M, Ishihara Y, Takeyama U, Kubota T, Yamaki T, Ojio S, Nishigaki K, Takemura G, Saio M, Takami T, Minatoguchi S, Fujiwara H. (2008). Development of

integrated backscatter intravascular ultrasound for tissue characterization of coronary plaques. *Ultrasound Med Biol*. Vol 34:655-63. (a)

Okubo M, Kawasaki M, Ishihara Y, Takeyama U, Yasuda S, Kubota T, Tanaka S, Yamaki T, Ojio S, Nishigaki K, Takemura G, Saio M, Takami T, Fujiwara H, Minatoguchi S. (2008). Tissue characterization of coronary plaques: comparison of integrated backscatter intravascular ultrasound with virtual histology intravascular ultrasound. *Circ J* Vol 72:1631-9. (b)

Otagiri K, Tsutsui H, Kumazaki S, Miyashita Y, Aizawa K, Koshikawa M, Kasai H, Izawa A, Tomita T, Koyama J, Ikeda U. (2011). Early intervention with rosuvastatin decreases the lipid components of the plaque in acute coronary syndrome: analysis using integrated backscatter IVUS (ELAN study). *Circ J* Vol 75:633-41.

Picano E, Landini L, Distante A, Sarnelli R, Benassi A, L'Abbate A. (1983). Different degreed of atherosclerosis detected by backscattered ultrasound: An in vitro study on fixed human aortic walls. *J Clin ultrasound.* Vol 11:375-379.

Picano E, Landini L, Distante A, Salvadori M, Lattanzi F, Masini M, et al. (1985). Angle dependence of ultrasonic backscatter in arterial tissues: a study in vitro. *Circulation*.Vol 72:572-6.

Picano E, Landini L, Lattanzi F, Salvadori M, Benassi A, L'Abbate A. (1988). Time domain echo pattern evaluation from normal and atherosclerotic arterial walls: a study in vitro. *Circulation*. Vol 77:654-9.

Picano E, Pelosi G, Marzilli M, Lattanzi F, Benassi A, Landini L, L'Abbate A. (1990). In vivo quantitative ultrasonic evaluation of myocardial fibrosis in humans. *Circulation.* Vol 81:58-64.

Sano K, Kawasaki M, Ishihara Y, Okubo M, Tsuchiya K, Nishigaki K, Zhou X, Minatoguchi S, Fujita H, Fujiwara H. (2006). Assessment of vulnerable plaques causing acute coronary syndrome using integrated backscatter intravascular ultrasound. *J Am Coll Cardiol* Vol 47:734-41.

Siegel RJ, Swan K, Edwalds G, Fishbein MC. (1985). Limitations of postmorterm assessment of human coronary artery size and luminal narrowing: differential effects of tissue fixation and processing on vessel with different degrees of atherosclerosis. *J Am Coll Cardiol.* Vol 5:342-346

Takeuchi H, Morino Y, Matsukage T, Masuda N, Kawamura Y, Kasai S, Hashida T, Fujibayashi D, Tanabe T, Ikari Y. (2009). Impact of vascular remodeling on the coronary plaque compositions: an investigation with in vivo tissue characterization using integrated backscatter-intravascular ultrasound *Atherosclerosis*. Vol 202:476-8

Takiuchi S, Rakugi H, Honda K, Masuyama T, Hirata N, Ito H, Sugimoto K, Yanagitani Y, Moriguchi K, Okamura A, Higaki J, Ogihara T. (2000). Quantitative ultrasonic tissue characterization can identify high-risk atherosclerotic alteration in human carotid arteries. *Circulation* Vol 102:766-70.

Urbani MP, Picano E, Parenti G, Mazzarisi A, Fiori L, Paterni M, Pelosi G, Landini L. (1993). In vivo radiofrequency-based ultrasonic tissue characterization of the atherosclerotic plaque. *Stroke.* Vol 24:1507-12.

Yamada K, Kawasaki M, Yoshimura S, Enomoto Y, Asano T, Minatoguchi S, Iwama T. (2010). Prediction of silent ischemic lesions after carotid artery stenting using integrated backscatter ultrasound and magnetic resonance imaging. *Atherosclerosis* Vol 208:161-6

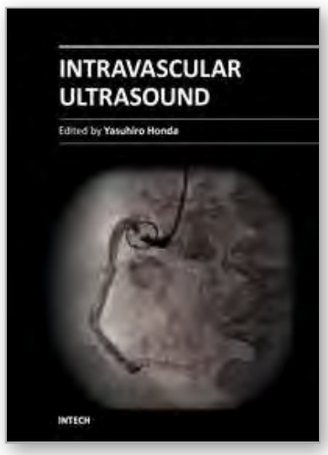

Intravascular Ultrasound
Edited by Dr. Yasuhiro Honda

ISBN 978-953-307-900-4
Hard cover, 207 pages
Publisher InTech
Published online 01, February, 2012
Published in print edition February, 2012

Intravascular ultrasound (IVUS) is a cardiovascular imaging technology using a specially designed catheter with a miniaturized ultrasound probe for the assessment of vascular anatomy with detailed visualization of arterial layers. Over the past two decades, this technology has developed into an indispensable tool for research and clinical practice in cardiovascular medicine, offering the opportunity to gather diagnostic information about the process of atherosclerosis in vivo, and to directly observe the effects of various interventions on the plaque and arterial wall. This book aims to give a comprehensive overview of this rapidly evolving technique from basic principles and instrumentation to research and clinical applications with future perspectives.

INTECH
open science | open minds

InTech Europe
University Campus STeP Ri
Slavka Krautzeka 83/A
51000 Rijeka, Croatia
Phone: +385 (51) 770 447
Fax: +385 (51) 686 166
www.intechopen.com

InTech China
Unit 405, Office Block, Hotel Equatorial Shanghai
No.65, Yan An Road (West), Shanghai, 200040, China
中国上海市延安西路65号上海国际贵都大饭店办公楼405单元
Phone: +86-21-62489820
Fax: +86-21-62489821

IntechOpen

7

Clinical Applications of Intravascular Ultrasound

Dermot Phelan, Sajjad Matiullah and Faisal Sharif
University College Hospital Galway
Ireland

1. Introduction

Intravascular Ultrasound (IVUS) is an invasive grey scale tomographic imaging modality providing cross-sectional images of the vessel wall. The reflected or scattered ultrasound signal received at the transducer is converted to a voltage. This voltage is known as radiofrequency data or backscattered signal. The time delay and amplitude of these emitting pulses provides 256 such backscattered signals or A-scans to produce one image. For IVUS imaging, high ultrasound frequencies typically centred between 25-50 MHz are used. The size of conventional IVUS catheter is 2.9 and 3.5 Fr and has a typical pullback speed of 0.5 mm/s and a frame rate of 30 images per second. At 30 MHz the wavelength is 50 μm, which yields a spatial resolution of >150μm allowing detail evaluation of the blood vessel wall.
IVUS imaging is complementary to coronary angiography and allows the simultaneous assessment of lumen and components of the vessel wall. In the IVUS image the catheter is in the centre of the image surrounded by vessel lumen, the three layers of the vessel and surrounding structures (Figure 1). It can assess plaque geometry including plaque burden and size, luminal area, longitudinal extent of the disease, circumferential extent of the

Fig. 1. IVUS of normal coronary artery

plaque, arterial remodelling and plaque vulnerability. Therefore IVUS provides detailed insight to the anatomy of plaque burden and allows the interventional cardiologist to adapt an optimal strategy for percutaneous coronary intervention (PCI) and subsequently assess the success of this strategy. In this chapter we will describe the potential applications of IVUS for every day use in the catheterization laboratory.

2. Clinical applications of IVUS

2.1 Assessment of vessel size for stent selection and ischemia evaluation

Standard coronary angiography is intrinsically limited to evaluate three-dimensional anatomical coronary cross sectional area due to planar silhoutte imaging. In addition, the plaque burden, its delineation and constituents cannot be assessed by coronary angiography. With angiography, the severity of stenosis is assessed by minimal lumen diameter at the lesion site, in comparison with an adjacent normal appearing reference. However, it is well documented that atherosclerosis is diffuse in nature and may appear normal in a small calibre coronary artery with concentric plaque (Figure 2)(Grondin, Dyrda et al. 1974; Roberts and Jones 1979). IVUS provides a complete 360 degrees tomographic view that allows accurate lumen measurements. In fact direct comparison of atherosclerotic disease by angiography and IVUS are frequently discrepant often as a result of eccentric plaque.(Figure 2) IVUS studies have clearly demonstrated that there is no correlation between the size of the atheroma and the size of the lumen(Topol and Nissen 1995) . This difference can be explained by positive (expansive) remodelling where lumen size is maintained due to plaque accumulation within in the vessel wall and resulting vessel wall expansion. It is claimed that these positive plaques are more unstable and vulnerable to rupture than negative (constrictive) plaques and also responsible for in-stent restenosis (ISR) following coronary intervention.(Schoenhagen, Ziada et al. 2000).

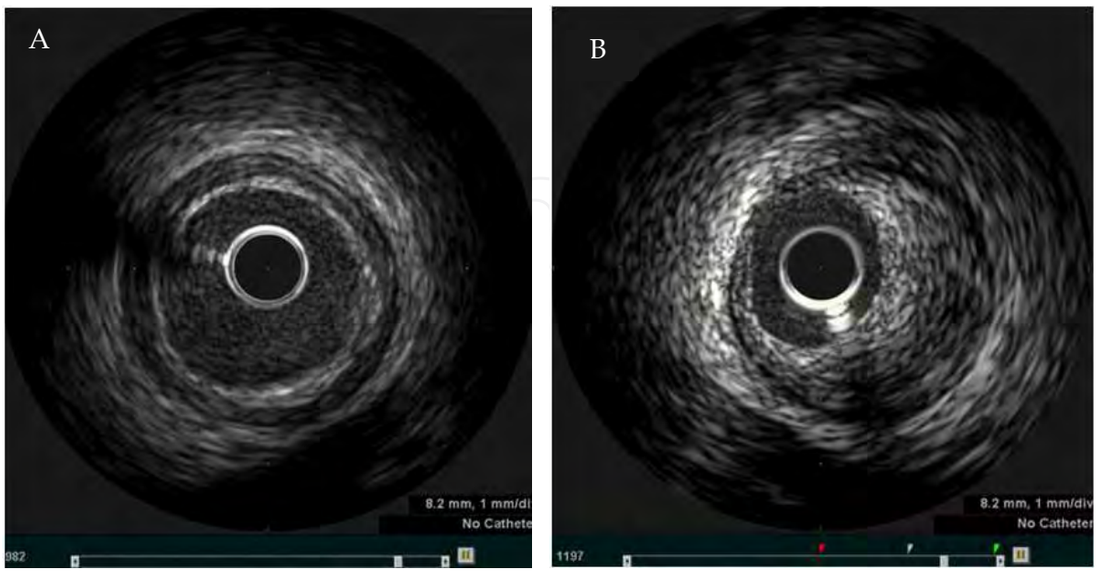

Fig. 2. IVUS images of A) concentric plaque and B) eccentric plaque

In addition to accurate stent sizing, IVUS can be used to evaluate lesion lumen area to predict the presence or absence of myocardial ischemia and/or significant coronary stenosis. There was strong correlation between lesion lumen area of < 4.0 mm2 on IVUS and positive stress myocardial perfusion SPECT in seventy native coronary lesions (Nishioka, Amanullah et al. 1999). In another study, IVUS guided deferral of coronary intervention of 248 lesions with luminal area of >4 mm^2 resulted in clinical rates of 4.4% and target lesion revascularisation (TLR) of 2.8% at 12 month follow up. (Abizaid, Mintz et al. 1998).

2.2 Assessment of restenosis

Following coronary intervention, the formation of neointimal hyperplasia is mainly responsible for ISR (Figure 3). There is strong correlation with between late lumen loss and the degree of in-stent neointimal growth (r=0.98) (de Jaegere, Mudra et al. 1998; Hoffmann, Mintz et al. 1998). Although drug eluting stents (DES) has significantly reduced the incidence of neointimal proliferation, the rate of ISR still remains around 10-15%.

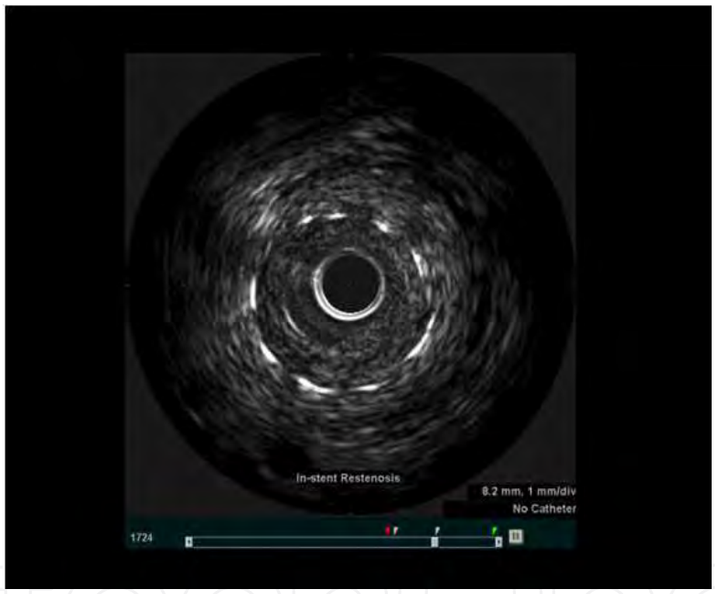

Fig. 3. IVUS image of in-stent restenosis

One of the main factors for ISR is stent **underexpansion** (Figure 4). IVUS can detect vessel stent subtleties not apparent by coronary angiography. In addition to assessing plaque geometry, IVUS can be used to achieve complete stent apposition and adequate geometric expansion within the stented segment. IVUS studies have demonstrated that incomplete stent and vessel wall apposition, residual stenosis and irregular eccentric lumen in the stented segment was present in almost 88% of the patients despite achieving an optimal angiographic result (Nakamura, Colombo et al. 1994) . Clinical trials have shown that patients who have their coronary intervention guided by IVUS have larger post procedure stent areas and significant reductions in TLR as compared to angiography-guided PCI alone (de Jaegere, Mudra et al. 1998; Schiele, Meneveau et al. 1998; Fitzgerald, Oshima et al. 2000; Sonoda, Morino et al. 2004; Hong, Mintz et al. 2006) In addition to detecting stent

underexpansion, IVUS can also assist in achieving optimal stent expansion, exclude stent edge dissections and plaque protrusion (Hong, Jeong et al. 2008).

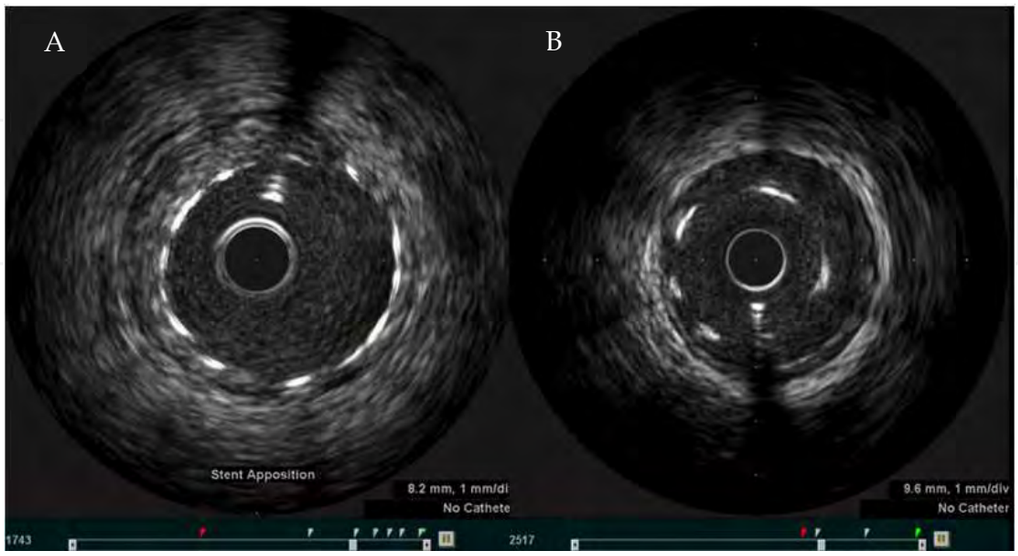

Fig. 4. IVUS demonstrating A) stent well apposed to vessel wall and B) stent mal-apposition

2.3 Guidance for left main stem intervention

Coronary interventions of unprotected left main coronary artery (UPLM) with bare metal stents in the 1990s were associated with high rates of revascularization (25% to 30%) due to restenosis (Black, Cortina et al. 2001; Park, Hong et al. 2001; Takagi, Stankovic et al. 2002). Although the use of DES for UPLM PCI have significantly reduced the rate of revascularization as compared with bare metal stents (BMS), the long term outcomes remain less favourable. Most of the poor outcomes following UPLM PCI relates to distal bifurcation intervention, which is a technically complex procedure. The current American College of Cardiology (ACC)/American Heart association (AHA) practice guidelines for PCI categorize UPLM stenting as a class IIb indication or IIa indication in selected patients without co-existing multivessel disease. At present there is a paucity of randomized control trial data comparing Coronary artery bypass grafting (CABG) to PCI in patients with UPLM. The best available evidence comes from the SYNTAX trial (SYNergy between Percutaneous Coronary Intervention with TAXus and Cardiac Surgery), which randomly assigned 1800 patients with either UPLM (n=705) or multivessel CAD not involving the left main stem (n=1095) (Ong, Serruys et al. 2006) . The major adverse cardiac or cerebrovascular events were not significantly different between the CABG and PCI groups (13.7 vs 15.8%). However, the rate of revascularization was significantly higher in those treated with PCI (11.8 vs 6.5 %). One of the main limitations of the SYNTAX trial was felt to be the lack of use of IVUS for UPLM in the PCI group.

While the European Society of Cardiology guidelines give IVUS-guided stenting of the UPLM a Class IIb recommendation we feel IVUS interrogation of the UPLM pre and post intervention should be used in all cases. Not least because IVUS interrogation has been demonstrated to, frequently prove angiographic assessment of the UPLM as inaccurate. This obviously may have significant impact on patient management resulting in either erroneous

treatment of a lesion which may appear severe angiographically but in fact has minimal plaque burden or failure to treat lesions which are mis-labelled as mild-to-moderate (Mintz and Maehara 2009).

Moreover, IVUS is an ideal method for confirming the presence of significant left main disease and also for guiding selection of stent size, assessing the presence and extent of calcification and especially evaluating the distal left main vessel and its branches. IVUS assessment pre and post left main intervention is very important to evaluate larger lumen area of the ostial and midshaft left main and adequate post dilatation post stenting. In comparison to native coronary vessels, a minimal luminal area of <6.0 mm2 is a commonly used threshold for significant left main disease (Sano, Mintz et al. 2007). While there are no randomized trials to inform practice in this area, registry data has shown a trend toward reduced mortality in IVUS guided UPLM PCI.(Park, Kim et al. 2009)

2.4 Guidance for Chronic Total Occlusion (CTO) intervention

CTOs are the most complex lesions that are considered for percutaneous coronary revascularization. PCI of CTO results in symptomatic improvement, improved left ventricle function and reduction in adverse remodelling. In addition recanalization of CTO leads to long-term survival benefit and avoidance of bypass surgery (Melchior, Doriot et al. 1987; Ivanhoe, Weintraub et al. 1992; Chung, Nakamura et al. 2003; Cheng, Selvanayagam et al. 2008). The number of CTO interventions has risen gradually due to better operator experience, technical improvements, and newer procedural techniques (these include contra-lateral coronary injection, "parallel" wire techniques, subintimal tracking and re-entry (STAR), retrograde approach with control antegrade retrograde tracking (CART), reverse CART). Despite these advances, the success rate of CTO interventions remains low (<60%)(Di Mario, Werner et al. 2007), largely due to difficulty crossing the occlusion with the guidewire and entering the true distal lumen beyond the occlusion (Safian, McCabe et al. 1988; Kinoshita, Katoh et al. 1995). In most instances of failed CTO intervention, the guidewire enters the false lumen (subintimal space) at the site of occlusion, often making it impossible to re-enter the true lumen (Figure 5). CTO interventions can be performed via an antegrade approach or retrograde approach using septal collaterals (Surmely, Tsuchikane et al. 2006).

IVUS studies provide insights into the anatomy of the CTO lesion. In one report IVUS demonstrated presence of calcium mostly across the side branch take-off, especially in abrupt-origin CTOs (Fujii, Mintz et al. 2006). This anatomical variance can explain the preferential entry of the guidewire into the side branch at the point of occlusion. The use of IVUS for CTO interventions can be extremely useful especially in ensuring that the guidewire is positioned within the coronary lumen (true or false), and also helps to identify the optimal entry point within the CTO cap(Ochiai, Ogata et al. 2006). IVUS can help to avoid subintimal stenting during CTO intervention as this has been reported to result in stent thrombosis and stent mal-apposition due to the formation of multiple aneurysms (Erlich, Strauss et al. 2006; Tsujita, Maehara et al. 2009). IVUS imaging for CTO can also detect vessel wall haematoma, dissection and small perforations that are not detected by routine coronary angiography. Further advances in IVUS technology especially the development of 'forward facing IVUS' will significantly improve our anatomical understanding of the chronically occluded lumen. Although IVUS guided intervention of chronic occlusions may enhance procedural outcome, the current use of this technology for CTO intervention is limited only to experienced operators.

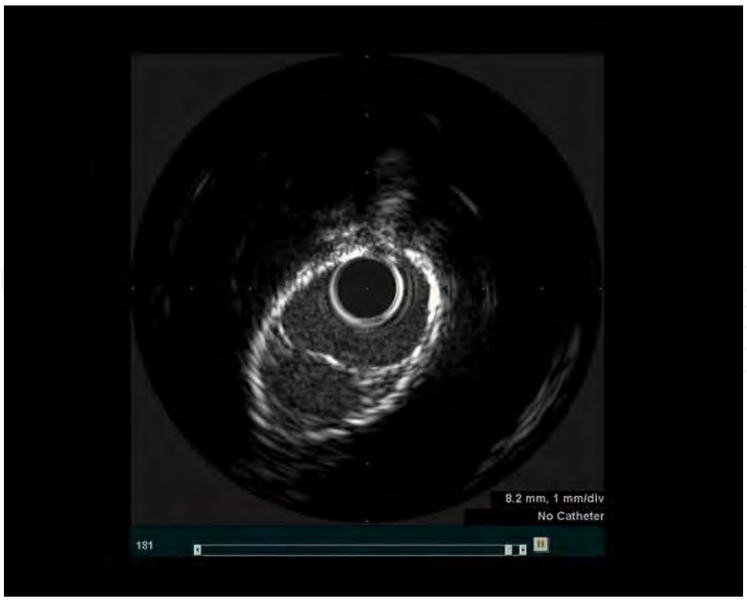

Fig. 5. IVUS image of false lumen

2.5 Guidance for bifurcation lesion intervention

PCI of bifurcation lesions have been associated with lower procedural success rate and worse clinical outcome than when used to treated non-bifurcation lesions. This is largely related to the complexity of the bifurcation lesions, significant anatomical variation of the bifurcation lesion, and lack of standard guidelines for the treatment of bifurcation lesions. The current therapeutic strategies for bifurcation lesions have mainly stemmed from personal clinical experience of the operators. (Suzuki, Angiolillo et al. 2007). In recent years there has been better understanding of bifurcation lesions especially with use of DES, acceptance of provisional stenting (acceptance of a suboptimal result in a small side branch SB), specific treatment of bifurcation lesions with a two-stent strategy and increasing use of final kissing balloon. The use of IVUS for bifurcation lesions can provide valuable information especially in anatomical evaluation of plaque burden, plaque location, angle assessment, lumen size of main branch [MB] and [SB]. In addition post PCI, IVUS can assist in evaluation of plaque shift, change in carina angle, dissection, and above all optimal stent deployment (Costa, Mintz et al. 2005). We feel that IVUS guided optimization of the bifurcation lesion post intervention, especially the ostium of a large side branch will enhance long term outcome of these technically challenging subset of lesions.

2.6 Vulnerable plaque assessment

The composition of atherosclerotic plaque is heterogeneous by nature and contains 1) fibrocellular components (extracellular matrix and smooth muscle cells), 2) lipid-cellular components (crystalline cholesterol and cholesterol esters mixed with macrophages), 3) thrombotic components (platelets and fibrin) and 4) calcium (Figure 6) (Fuster, Badimon et al. 1992; Fuster, Badimon et al. 1992; Stary 2000; Virmani, Kolodgie et al. 2000). Vulnerable plaques that result in rupture have been now well described as thin cap fibroatheroma (TCFA).

Fig. 6. IVUS image of atherosclerotic plaque

Ultrasound provides some information about the morphological features of atherosclerotic plaque. The American College of Cardiology Clinical Expert Consensus Document for IVUS imaging has described that a vulnerable plaque can appear as an 'echolucent' plaque (Mintz, Nissen et al. 2001). Frequently these echolucent plaques have a prominent echogenic border at the lumen-intima interface. This may correspond to the TCFA. However, it should be emphasized that the fibrous cap of TCFA is <65 μm and therefore could not be detected using this modality. Imaging IVUS provides limited insight into the chemical composition of the plaque and is dependent on simple interpretation of acoustic reflections. Lipid-laden echolucent plaques can be detected with a sensitivity of between 78% and 95% and specificity of 30% (Mallery, Tobis et al. 1990; Potkin, Bartorelli et al. 1990). Furthermore, reduced echogenicity may also be observed in large necrotic zones, intramural hemorrhage or a thrombus.

Echodense plaques have an intermediate echogenicity between echolucent and highly echogenic calcified plaques. The echodensity of plaques correlate well with plaque fibrosis in histological studies. The identification of echolucent plaques is subjective and no prospective clinical trials are available. In an IVUS based study, echolucent plaque was identified in 31 patients from a total of 144 patients. Of these 31 patients, 23 patients (74%) presented with unstable angina. Plaque rupture was confirmed by injecting contrast with subsequent filling of the plaque cavity on IVUS (Ge, Haude et al. 1995). In another study, IVUS images of 114 coronary lesions with <50% stenosis were recorded and followed up for two years.(Yamagishi, Terashima et al. 2000). The patients who developed Acute coronary syndrome during the follow up were identified and events correlated with large echolucent zones in the eccentric plaques at the time of their first IVUS study. These plaques had histological features similar to vulnerable plaques and were associated with increased risk of instability. In addition, IVUS can also identify vulnerable plaques at high risk of rupture in vessels with adaptive remodelling (von Birgelen, Klinkhart et al. 2001).

IVUS has excellent blood penetration and in the absence of calcium is able to visualize and calculate plaque area, volume and eccentricity. The use of IVUS to identify TCFA and lipid pool is at present limited. It suffers from signal attenuation and geometric effects that result in different backscatter signal properties from similar tissues due to differences in tissue

orientation and position relative to the imaging transducer. Ultra- high frequency catheters can be employed to achieve high resolution and visualize subluminal fibrous cap, while low-resolution components can be used for better penetration of the plaque to assess plaque components.

The conventional IVUS image undergoes considerable processing such as envelope detection, time-gain compensation, and logarithmic compression to create real time imaging. However, this processing significantly reduces the ability to characterize the imaged tissue, the echogenicity of the imaged tissue is difficult to repeat and interpret quantitatively. The reflected unprocessed ultrasound signal in the form of A-scan or individual backscattered signals (256 A scans for an image) is called the radiofrequency data and it is the analysis of these individual A-scans that holds potential for tissue characterization. This imaging modality is known as IVUS virtual histology (IVUS –VH) or IVUS radiofrequency (IVUS-RF).

Ex-vivo studies have demonstrated that raw backscattered ultrasound signal allows a more detailed analysis of the vessel components with scope to identify different tissue morphology (Moore, Spencer et al. 1998). IVUS-VH uses spectral analysis of radiofrequency data to construct tissue maps that classify plaque into four major components (fibrous [labeled green], fibrolipidic [labeled greenish-yellow], necrotic core [labeled red] and calcium [labeled white]) which were correlated with a specific spectrum of the radiofrequency signal and assigned color codes (Nair, Kuban et al. 2001). In a clinical study, IVUS-VH was used to investigate the presence of IVUS-derived thin cap fibroatheroma (IDTCFA) in non-culprit, non-obstructive (<50%) lesions in 55 patients who presented with acute coronary syndrome (Rodriguez-Granillo, Garcia-Garcia et al. 2005). The axial resolution of the IVUS-VH is between 100 to 150 μm and therefore in this study the authors assumed that the absence of visible atheroma tissue overlying a necrotic core would suggest a cap thickness of below 100 to 150 μm and used the absence of such tissue to define a thin fibrous cap. In this study, IDTCFA was defined and identified as a lesion with a necrotic core ≥10% without evident overlying fibrous tissue and percent atheroma volume (PAV) ≥40%. In this study significantly higher prevalence of IDTCFA was observed in patients with Acute coronary syndrome in comparison with controls [(3.0 IQR 0.0 to 5.0 vs. 1.0 IQR 1.0 to 2.8) p=0.018]. The large multicenter PROSPECT trial (700 patients with Acute coronary syndrome) looked at long-term outcomes of non-culprit lesions (based on IVUS-VH) at the time of Percutaneous coronary intervention of the culprit lesions. The investigators reported that only 11 percent of the patients had high event rate (i.e. 17%) in association with thin-capped fibroatheromas with minimal luminal area (MLA) ≤4 mm^2 and plaque burden ≥70%. Although high-risk focal sites can be detected with IVUS-VH, the predictive power (significantly higher numbers of vulnerable plaques than clinical events) of vulnerable plaque to cause a clinical event remains low.

IVUS-RF data acquisition and real time processing with three dimensional imaging and spectral analysis is a potential tool to assess vulnerable plaque *in vivo*. This imaging tool provides detailed volumetric assessment of the histological components of the plaque *in vivo* and therefore may represent a unique technique to identify the vulnerable plaque in future.

3. Conclusion

Over the past decade there has been a significant technological advance in cardiovascular imaging that has changed the way we assess coronary atherosclerosis and approach

coronary intervention. IVUS is a validated clinical tool that allows precise evaluation of angiographically stenotic lesions helping guide the cardiologist's approach to revascualisation and assess complications and sub-optimal results post-procedure. In addition it provides important information regarding non-critical but vulnerable plaque which is not appreciable by traditional coronary angiography. In an era of more complex and ambitious coronary intervention IVUS is a vitally important addition to the interventionalist's armamentarium. In this chapter we have briefly described the various potential uses of IVUS and their clinical application.

4. References

Abizaid, A., G. S. Mintz, et al. (1998). "Clinical, intravascular ultrasound, and quantitative angiographic determinants of the coronary flow reserve before and after percutaneous transluminal coronary angioplasty." *Am J Cardiol* 82(4): 423-8.

Black, A., R. Cortina, et al. (2001). "Unprotected left main coronary artery stenting: correlates of midterm survival and impact of patient selection." *J Am Coll Cardiol* 37(3): 832-8.

Cheng, A. S., J. B. Selvanayagam, et al. (2008). "Percutaneous treatment of chronic total coronary occlusions improves regional hyperemic myocardial blood flow and contractility: insights from quantitative cardiovascular magnetic resonance imaging." *JACC Cardiovasc Interv* 1(1): 44-53.

Chung, C. M., S. Nakamura, et al. (2003). "Effect of recanalization of chronic total occlusions on global and regional left ventricular function in patients with or without previous myocardial infarction." *Catheter Cardiovasc Interv* 60(3): 368-74.

Costa, R. A., G. S. Mintz, et al. (2005). "Bifurcation coronary lesions treated with the "crush" technique: an intravascular ultrasound analysis." *J Am Coll Cardiol* 46(4): 599-605.

de Jaegere, P., H. Mudra, et al. (1998). "Intravascular ultrasound-guided optimized stent deployment. Immediate and 6 months clinical and angiographic results from the Multicenter Ultrasound Stenting in Coronaries Study (MUSIC Study)." *Eur Heart J* 19(8): 1214-23.

Di Mario, C., G. S. Werner, et al. (2007). "European perspective in the recanalisation of Chronic Total Occlusions (CTO): consensus document from the EuroCTO Club." *EuroIntervention* 3(1): 30-43.

Erlich, I., B. H. Strauss, et al. (2006). "Stent thrombosis following the STAR technique in a complex RCA chronic total occlusion." *Catheter Cardiovasc Interv* 68(5): 708-12.

Fitzgerald, P. J., A. Oshima, et al. (2000). "Final results of the Can Routine Ultrasound Influence Stent Expansion (CRUISE) study." *Circulation* 102(5): 523-30.

Fujii, K., G. S. Mintz, et al. (2006). "Intravascular ultrasound profile analysis of ruptured coronary plaques." *Am J Cardiol* 98(4): 429-35.

Fuster, V., L. Badimon, et al. (1992). "The pathogenesis of coronary artery disease and the acute coronary syndromes (1)." *N Engl J Med* 326(4): 242-50.

Fuster, V., L. Badimon, et al. (1992). "The pathogenesis of coronary artery disease and the acute coronary syndromes (2)." *N Engl J Med* 326(5): 310-8.

Ge, J., M. Haude, et al. (1995). "Silent healing of spontaneous plaque disruption demonstrated by intracoronary ultrasound." *Eur Heart J* 16(8): 1149-51.

Grondin, C. M., I. Dyrda, et al. (1974). "Discrepancies between cineangiographic and postmortem findings in patients with coronary artery disease and recent myocardial revascularization." *Circulation* 49(4): 703-8.

Hoffmann, R., G. S. Mintz, et al. (1998). "Intimal hyperplasia thickness at follow-up is independent of stent size: a serial intravascular ultrasound study." *Am J Cardiol* 82(10): 1168-72.

Hong, M. K., G. S. Mintz, et al. (2006). "Intravascular ultrasound predictors of angiographic restenosis after sirolimus-eluting stent implantation." *Eur Heart J* 27(11): 1305-10.

Hong, Y. J., M. H. Jeong, et al. (2008). "Plaque prolapse after stent implantation in patients with acute myocardial infarction: an intravascular ultrasound analysis." *JACC Cardiovasc Imaging* 1(4): 489-97.

Ivanhoe, R. J., W. S. Weintraub, et al. (1992). "Percutaneous transluminal coronary angioplasty of chronic total occlusions. Primary success, restenosis, and long-term clinical follow-up." *Circulation* 85(1): 106-15.

Kinoshita, I., O. Katoh, et al. (1995). "Coronary angioplasty of chronic total occlusions with bridging collateral vessels: immediate and follow-up outcome from a large single-center experience." *J Am Coll Cardiol* 26(2): 409-15.

Mallery, J. A., J. M. Tobis, et al. (1990). "Assessment of normal and atherosclerotic arterial wall thickness with an intravascular ultrasound imaging catheter." *Am Heart J* 119(6): 1392-400.

Melchior, J. P., P. A. Doriot, et al. (1987). "Improvement of left ventricular contraction and relaxation synchronism after recanalization of chronic total coronary occlusion by angioplasty." *J Am Coll Cardiol* 9(4): 763-8.

Mintz, G. S. and A. Maehara (2009). "Serial intravascular ultrasound assessment of atherosclerosis progression and regression. State-of-the-art and limitations." *Circ J* 73(9): 1557-60.

Mintz, G. S., S. E. Nissen, et al. (2001). "American College of Cardiology Clinical Expert Consensus Document on Standards for Acquisition, Measurement and Reporting of Intravascular Ultrasound Studies (IVUS). A report of the American College of Cardiology Task Force on Clinical Expert Consensus Documents." *J Am Coll Cardiol* 37(5): 1478-92.

Moore, M. P., T. Spencer, et al. (1998). "Characterisation of coronary atherosclerotic morphology by spectral analysis of radiofrequency signal: in vitro intravascular ultrasound study with histological and radiological validation." *Heart* 79(5): 459-67.

Nair, A., B. D. Kuban, et al. (2001). "Assessing spectral algorithms to predict atherosclerotic plaque composition with normalized and raw intravascular ultrasound data." *Ultrasound Med Biol* 27(10): 1319-31.

Nakamura, S., A. Colombo, et al. (1994). "Intracoronary ultrasound observations during stent implantation." *Circulation* 89(5): 2026-34.

Nishioka, T., A. M. Amanullah, et al. (1999). "Clinical validation of intravascular ultrasound imaging for assessment of coronary stenosis severity: comparison with stress myocardial perfusion imaging." *J Am Coll Cardiol* 33(7): 1870-8.

Ochiai, M., N. Ogata, et al. (2006). "Intravascular ultrasound guided wiring for chronic total occlusions." *Indian Heart J* 58(1): 15-20.

Ong, A. T., P. W. Serruys, et al. (2006). "The SYNergy between percutaneous coronary intervention with TAXus and cardiac surgery (SYNTAX) study: design, rationale, and run-in phase." *Am Heart J* 151(6): 1194-204.

Park, S. J., M. K. Hong, et al. (2001). "Elective stenting of unprotected left main coronary artery stenosis: effect of debulking before stenting and intravascular ultrasound guidance." *J Am Coll Cardiol* 38(4): 1054-60.

Park, S. J., Y. H. Kim, et al. (2009). "Impact of intravascular ultrasound guidance on long-term mortality in stenting for unprotected left main coronary artery stenosis." *Circ Cardiovasc Interv* 2(3): 167-77.

Potkin, B. N., A. L. Bartorelli, et al. (1990). "Coronary artery imaging with intravascular high-frequency ultrasound." *Circulation* 81(5): 1575-85.

Roberts, W. C. and A. A. Jones (1979). "Quantitation of coronary arterial narrowing at necropsy in sudden coronary death: analysis of 31 patients and comparison with 25 control subjects." *Am J Cardiol* 44(1): 39-45.

Rodriguez-Granillo, G. A., H. M. Garcia-Garcia, et al. (2005). "In vivo intravascular ultrasound-derived thin-cap fibroatheroma detection using ultrasound radiofrequency data analysis." *J Am Coll Cardiol* 46(11): 2038-42.

Safian, R. D., C. H. McCabe, et al. (1988). "Initial success and long-term follow-up of percutaneous transluminal coronary angioplasty in chronic total occlusions versus conventional stenoses." *Am J Cardiol* 61(14): 23G-28G.

Sano, K., G. S. Mintz, et al. (2007). "Assessing intermediate left main coronary lesions using intravascular ultrasound." *Am Heart J* 154(5): 983-8.

Schiele, F., N. Meneveau, et al. (1998). "Impact of intravascular ultrasound guidance in stent deployment on 6-month restenosis rate: a multicenter, randomized study comparing two strategies--with and without intravascular ultrasound guidance. RESIST Study Group. REStenosis after Ivus guided STenting." *J Am Coll Cardiol* 32(2): 320-8.

Schoenhagen, P., K. M. Ziada, et al. (2000). "Extent and direction of arterial remodeling in stable versus unstable coronary syndromes : an intravascular ultrasound study." *Circulation* 101(6): 598-603.

Sonoda, S., Y. Morino, et al. (2004). "Impact of final stent dimensions on long-term results following sirolimus-eluting stent implantation: serial intravascular ultrasound analysis from the sirius trial." *J Am Coll Cardiol* 43(11): 1959-63.

Stary, H. C. (2000). "Natural history and histological classification of atherosclerotic lesions: an update." *Arterioscler Thromb Vasc Biol* 20(5): 1177-8.

Surmely, J. F., E. Tsuchikane, et al. (2006). "New concept for CTO recanalization using controlled antegrade and retrograde subintimal tracking: the CART technique." *J Invasive Cardiol* 18(7): 334-8.

Suzuki, N., D. J. Angiolillo, et al. (2007). "Percutaneous coronary intervention of bifurcation coronary disease." *Minerva Cardioangiol* 55(1): 57-71.

Takagi, T., G. Stankovic, et al. (2002). "Results and long-term predictors of adverse clinical events after elective percutaneous interventions on unprotected left main coronary artery." *Circulation* 106(6): 698-702.

Topol, E. J. and S. E. Nissen (1995). "Our preoccupation with coronary luminology. The dissociation between clinical and angiographic findings in ischemic heart disease." *Circulation* 92(8): 2333-42.

Tsujita, K., A. Maehara, et al. (2009). "Cross-sectional and longitudinal positive remodeling after subintimal drug-eluting stent implantation: multiple late coronary aneurysms,

stent fractures, and a newly formed stent gap between previously overlapped stents." *JACC Cardiovasc Interv* 2(2): 156-8.

Virmani, R., F. D. Kolodgie, et al. (2000). "Lessons from sudden coronary death: a comprehensive morphological classification scheme for atherosclerotic lesions." *Arterioscler Thromb Vasc Biol* 20(5): 1262-75.

Von Birgelen, C., W. Klinkhart, et al. (2001). "Plaque distribution and vascular remodeling of ruptured and nonruptured coronary plaques in the same vessel: an intravascular ultrasound study in vivo." *J Am Coll Cardiol* 37(7): 1864-70.

Yamagishi, M., M. Terashima, et al. (2000). "Morphology of vulnerable coronary plaque: insights from follow-up of patients examined by intravascular ultrasound before an acute coronary syndrome." *J Am Coll Cardiol* 35(1): 106-11.

Wu, X., Maehara A, et al. (2010). "Virtual histology intravascular ultrasound analysis of non-culprit attenuated plaques detected by grayscale intravascular ultrasound in patients with acute coronary syndromes." *J Am Coll Cardiol* 105(1):48-53.

Gregg W. Stone., Akiko Maehara, et al. (2011). " A Prospective Natural-History Study of Coronary Atherosclerosis". *N Engl J Med* 364:226-35.

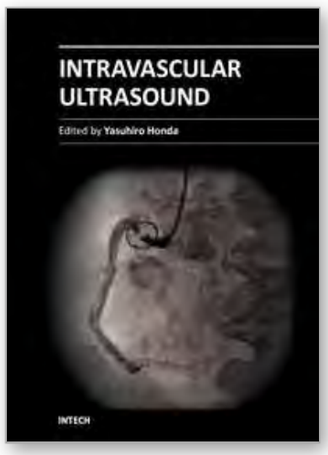

Intravascular Ultrasound
Edited by Dr. Yasuhiro Honda

ISBN 978-953-307-900-4
Hard cover, 207 pages
Publisher InTech
Published online 01, February, 2012
Published in print edition February, 2012

Intravascular ultrasound (IVUS) is a cardiovascular imaging technology using a specially designed catheter with a miniaturized ultrasound probe for the assessment of vascular anatomy with detailed visualization of arterial layers. Over the past two decades, this technology has developed into an indispensable tool for research and clinical practice in cardiovascular medicine, offering the opportunity to gather diagnostic information about the process of atherosclerosis in vivo, and to directly observe the effects of various interventions on the plaque and arterial wall. This book aims to give a comprehensive overview of this rapidly evolving technique from basic principles and instrumentation to research and clinical applications with future perspectives.

InTech Europe
University Campus STeP Ri
Slavka Krautzeka 83/A
51000 Rijeka, Croatia
Phone: +385 (51) 770 447
Fax: +385 (51) 686 166
www.intechopen.com

InTech China
Unit 405, Office Block, Hotel Equatorial Shanghai
No.65, Yan An Road (West), Shanghai, 200040, China
中国上海市延安西路65号上海国际贵都大饭店办公楼405单元
Phone: +86-21-62489820
Fax: +86-21-62489821

IntechOpen

Chapter 4

Diagnostic Use of Sonography in the Evaluation of Hypertension

Nikolaos Pagonas, Stergios Vlatsas and
Timm H. Westhoff

Additional information is available at the end of the chapter

http://dx.doi.org/10.5772/56171

1. Introduction

Hypertension is the most frequently treated disease in internal medicine. More than 1 billion people worldwide suffer from hypertension. Hypertension leads to cardiovascular end-organ damage increasing morbidity and mortality and is related with high costs to society, making this disease an important public health challenge. Sonography is a crucial diagnostic tool in the evaluation of a hypertensive patient. It is used both for the search of secondary forms of hypertension and for the identification of hypertensive end organ damage. There are several ultrasound examinations that may be warranted in hypertension. *Abdominal ultrasound* is recommended by several guidelines for the basic diagnostic workup in every newly diagnosed hypertensive patient. *Doppler sonography of the renal arteries* is reasonable only in a subset of hypertensives that are at increased risk of renal artery stenosis. *Echocardiography* is able to reveal cardiac end organ damage in terms of hypertensive heart disease. *Ultrasound of the carotid arteries* is frequently used to detect and evaluate in the case of hypertension-induced vascular end organ damage. The assessment of the *intima-media thickness* allows the detection of early stages of atherosclerotic wall changes. Prior to any structural vascular damage that may be visualized by ultrasound techniques, hypertension leads to functional changes of the endothelium, called endothelial dysfunction. Endothelial dysfunction encompasses a variety of changes in vascular function including a reduced endothelium-dependent vasodilation. This can be diagnosed by sonography measuring the diameter changes of the brachial artery in response to predefined endothelial stimuli. *Flow-mediated dilation* in response to hyperemia is regarded as the gold-standard in the non-invasive assessment of endothelial dysfunction. To date, it is rather used scientifically than in daily clinical practice. The present chapter provides

an overview on the practical performance of all of these ultrasound techniques in the approach to hypertension.

2. Abdominal ultrasound

The use of abdominal ultrasound in the evaluation of hypertension is twofold.

- In the detection of a secondary forms of hypertension.
- In the evaluation of subclinical organ damage induced by hypertension.

In the current European Society of Cardiology/European Society of Hypertension (ESC/ESH) guidelines for hypertension the use of abdominal ultrasound is recommended as a part of the evaluation of hypertensive individuals. The abdominal ultrasound supplies information about the etiology of hypertension as well as possible end organ damages.

The main interest is the morphology of the kidneys, the adrenal glands and of the aorta. Due to their retroperitoneal position, kidneys are completely and easily detectable. A 3.5-5 MHz probe is typically used to scan the kidney. The examination from dorsolateral allows the evasion of the intestinal loops and thus allows for a non-overlapping imaging in the supine position. The formerly widely spread examination in the lateral recumbent position is nowadays used only in exceptional cases. Renal ultrasound has now almost completely replaced intravenous urography in the anatomical exploration of the kidney. While the latter requires the injection of potentially nephrotoxic contrast medium, ultrasound is non-invasive and provides the necessary anatomic data about kidney size and shape, cortical thickness, urinary tract obstruction and renal masses [1]. Renal parenchymal disease is one of the most common causes of secondary hypertension which leads to a wide spectrum of morphologic alterations. The finding of bilateral upper abdominal masses at physical examination is consistent with polycystic kidney disease and should warrant an abdominal ultrasound examination. Acute parenchymal inflammatory processes like crescentic glomerulonephritis or acute interstitial nephritis sometimes predisposes individuals to measurable organ swelling. The cortical and medullary pyramids have in this case an anechoic profile. However, the morphological alterations seen via ultrasound in the acute kidney processes are less prominent than those seen in chronic kidney damage. Thus, the diagnostic performance in acute inflammatory renal disease is less effective. Chronic parenchymal diseases, such as chronic interstitial nephritis, glomerulonephritis or nephrosclerosis contribute to a progressive decrease in organ size. A kidney size below 90 mm should be interpreted as pathological. Over the course of the organ decrease, small scarring cortical retractions develop, which give the kidney surface a humped aspect. The renal parenchyma develops a hyperechoic pattern through progressive scarring. The border between parenchyma and pyelon becomes progressively nondescript. A variety of chronic parenchymal diseases can lead to the morphological end stage of a shrunken kidney. Sonographically, it is not possible to differentiate whether small kidneys are the cause or the result of hypertension. A unilateral small kidney as a possible indicator for a hemodynamic relevant renal artery stenosis should always lead to a further evaluation of the renal

http://dx.doi.org/10.5772/56171

arteries. Renal cell carcinomas as a rare cause of hypertension are depicted as a well delimitable structure from the surrounding tissue. Usually they can be depicted via ultrasound when they exceed 1 cm. With increasingly size there is an increase in their inhomogeneity, so that it is possible to detect areas of liquefied necrosis for example.

In the screening of secondary forms of hypertension abdominal ultrasound plays also a role in the depiction of the adrenal glands. For this purpose a detailed knowledge of the local anatomy is required. The adrenal glands are located within the retroperitoneum. The left adrenal gland, lacking the acoustic window of the liver and being obscured by air in the stomach, is inherently more difficult to scan than the right adrenal gland. On the right side, the right kidney and the inferior vena cava are landmarks for the examination of adrenal glands, whereas on the left side the aorta, the lower pole of the spleen and the upper pole of the kidney are points of orientation. The right adrenal gland is usually scanned with a right transcostal scan or a subcostal flank scan or oblique subcostal scan. On the left side it is better to use an intercostal flank scan through the spleen. The normal sized adrenal glands are only visible with trained examination techniques and by using high resolution technology, whereas enlarged adrenal glands are detectable in a high percentage of cases. Thirty percent of cases of primary aldosteronism are caused by adrenal adenomas. Seventy percent of cases are caused by adrenal hyperplasia. There are rare cases of adrenal carcinoma and the autosomal dominant condition of glucocorticoid remediable aldosteronism [2]. The micronodular hyperplasia is not possible to be detected via sonography. Adrenal adenomas have a round to oval shape and are uniformly hypoechoic with smooth margins, although some lesions have scalloped borders (polycyclic). Adenomas occasionally have an inhomogeneous appearance. Autopsy statistics indicate that they are quite common (10–20%), but most adenomas (90%) produce no endocrine symptoms, they are silent and too small to be detected by ultrasound. In one study the average size of adenomas was reported to be 1.5 cm, although they may exceed 5 cm in diameter. In a small percentage of patients adenomas are bilateral. Functioning and nonfunctioning adenomas are indistinguishable by their sonographic features [3]. Thus, ultrasound is not a sufficient test in the morphologic diagnosis of Conn syndrome. Upon the detection of a high aldosterone-to-renin ratio and after a confirmation test (e.g. suppression after administration of sodium chloride) the use of a CT or MRT scan is indicated. On the other hand, the detection of a unilateral adrenal mass seen in the ultrasound should be followed by a laboratory evaluation for the evaluation of Conn-Syndrome.

Phaeochromocytoma, a tumor of the adrenal medulla, is a rare secondary cause of hypertension (0.2 – 0.4% of all cases of elevated blood pressure) with an estimated annual incidence of 2 – 8 per million population.[4]. It can be inherited or acquired. Hypertension occurs in about 70% of all cases of phaeochromocytoma, being stable or paroxysmal in approximately equal proportions. The diagnosis is based on establishing an increase in plasma or urinary catecholamines or their metabolites (e.g. (nor-) metanephrines). Following the appearance of clinical symptoms (hypertension and tachycardia caused by increased catecholamine secretion), pheochromocytoma can be detected in 80-90% of cases via abdominal ultrasound. Most pheochromocytomas are already several centimeters in diameter when diagnosed. They have smooth margins, a round shape, and an inhomogeneous or complex echo structure. Hypoe-

choic liquid components may also be observed. A spectrum of appearances is possible. Pheochromocytomas are bilateral in approximately 10% of cases and extra-adrenal in 10–20%. The organ of Zuckerkandl should be looked for at the level of the origin of the inferior mesenteric artery, anterior to the aorta. Other extra-adrenal sites are the renal hilum, bladder wall, and thorax. Pheochromocytoma is occasionally seen posterior to the renal vein in transverse scans. Rarely, pheochromocytoma is diagnosed in the setting of multiple endocrine neoplasia (MEN). About 2% to 5% of pheochromocytomas are malignant. In recent years endosopic sonography is being used to obtain an adrenal gland biopsy [5-7].

Abdominal ultrasound is also being used in the evaluation of hypertension induced end-organ damage. Vascular end-organ damage may be visualized as atherosclerotic as well as aneurysmatic wall alterations, e.g. of the aorta. In the elderly (> 65 years) approximately 60% of the patients with hypertension have an isolated systolic hypertension. This is a result of the diminished elasticity of the large arterial vessels. Ultrasound can indicate a morphological correlate in form of a manifest aortosclerosis. Besides vascular end-organ damage abdominal ultrasound detects renal end organ damage. The correlate of hypertensive end-organ damage of the kidney is (benign) nephrosclerosis. The sonographic features include a reduced size, hyperechoic parenchyma, indefinite margin of parenchyma and pyelon, and scarring cortical retractions. As stated above, this unspecific sonographic appearance does unfortunately not allow a differentiation between cause and result of hypertension.

3. Echocardiography

Hypertension is one of the most important risk factors for heart failure with increasing risk in all age groups. The lifetime risk for developing heart failure is doubled for subjects with blood pressure > 160/100mm Hg compared to those with blood pressure < 140/90 mm Hg [8]. Systolic and diastolic heart failure are both associated with hypertension. There are several mechanisms, alone or in combination, leading to development of heart failure in the presence of hypertension: left ventricular hypertrophy (LVH), chamber remodeling, hemodynamic load and coronary microvascular disease with impaired coronary hemodynamics. To assess subclinical organ damage, such as ventricular hypertrophy, echocardiography is more sensitive than electrocardiography [9], which is a routine examination in all subjects with high blood pressure. However, the ESC/ESH guidelines suggest that in patients with low and intermediate cardiovascular risk an echocardiography should be performed for better global cardiovascular risk stratification which may implicate the appropriate pharmacological treatment [10]. The role of echocardiography is not limited to identification of (sub-) clinical organ damage in the pre-treatment phase. Since changes of the left ventricular hypertrophy in response to treatment are associated to cardiovascular fatal and non-fatal events [11], echocardiography can also be used to monitor treatment's success and re-assess overall risk.

Left ventricular hypertrophy is the first step toward the development of hypertensive heart disease. The echocardiographic evaluation of LVH includes measurements of the interventricular septum, left ventricular posterior wall thickness and end-diastolic diameter. Upon

http://dx.doi.org/10.5772/56171

these parameters obtained by M-Mode at the end of diastole (under two-dimensional control), the left ventricular mass is calculated according to the proposed formula [12]. Since LV mass is depended on gender and obesity, the thresholds for presence of LVH mass are indexed to body surface area and estimated for men (above 125g/m^2) and for women (above 110g/m^2) [10]. The adaptation of the left ventricle to hypertension is heterogenic and can be classified in three geometric patterns based on the LV mass and on the index of relative wall thickness (LV wall thickness / chamber radius). An increased ratio ≥ 0.42 combined with increased mass is referred to as concentric hypertrophy. The term eccentric hypertrophy refers to subjects with normal wall to radius ratio (< 0.42) but increased LV mass. The last pattern, the concentric remodeling, refers to subjects with normal ventricular mass but increased ratio (≥ 0.42). All three types of chamber remodeling in response to hypertension are related to increased cardiovascular risk. Interestingly, the incidence of cardiovascular events correlates with changes in geometric adaptation, independent of changes of the LV mass. The development or the persistence of a concentric geometry during treatment has been found to be associated with a greater incidence of cardiovascular events [13]. In the Losartan Intervention For Endpoint reduction in hypertension (LIFE) study [11] a regression of the left ventricular mass of about 25g/m^2 was associated with a 20% reduction in the incidence of the primary endpoint (cardiovascular mortality, myocardial infarction, stroke). Recent data have furthermore reinforced the predictive value of echocardiography in hypertensive patients. 35.000 normotensive and hypertensive participants with normal left ventricular ejection fraction were studied retrospectively. An abnormal left ventricular geometric pattern was found in 46% of the patients (35% with left ventricular concentric remodeling and 11% with LVH) and was associated with a double-risk of all-cause mortality compared to the patients with normal left ventricular geometry [14]. A prospective trial showed that hypertensive patients with echocardiographic LVH had significantly higher all-cause mortality and cardiovascular events [15]. Beyond the lower incidence of cardiovascular events, including sudden death, in patients with regression of echocardiographic left ventricular hypertrophy or a delayed increase in left ventricular mass [11], treatment-induced changes of left atrium dimension and ventricular geometry are also correlated with cardiovascular event rates [16, 17].

Even before evidence of left ventricular hypertrophy is present and before hypertension in young normotensive male offspring of hypertensive parents has developed, diastolic dysfunction may develop as an early end organ damage due to hypertension [18]. Patients with diastolic heart failure (also referred as heart failure with preserved ejection fraction) show similar long term impairments as patients with systolic heart failure [19]. The importance of an early recognition of diastolic dysfunction is imperative. Arterial hypertension with or without hypertrophy is the main cause of diastolic dysfunction, namely the inability of the heart to adequately fill with blood during diastole. There are several factors which lead to diastolic dysfunction in hypertension by impeding the active or passive phases of diastole. Of these, contractile alterations in myocytes, structural ventricular hypertrophy, extracellular and perivascular fibrosis, and myocardial ischemia are most often implicated. The European Society of Cardiology has recognized diastolic dysfunction diagnosed by echocardiography as criterion for the diagnosis of diastolic heart failure [20]. There are a number of specific echocardiographic indicators of diastolic dysfunction obtained during the examination. The

major four parameters include transmitral Doppler inflow velocity patterns, pulmonary venous Doppler flow patterns, tissue Doppler velocities and color M-mode flow propagation velocity (Vp). Transmitral Doppler flow is acquired by placing a pulsed wave (PW) sample volume at the level of the tips of the mitral leaflets in the apical four-chamber view. Normally, the ventricular inflow consists of an early (E) and a late filling peak (A). Respectively, the early filling peak velocity (E) and the late (atrial) peak velocity (A) should be recorded. In normal young individuals, more forward flow occurs during the early diastole largely due to the rapid decline in left ventricular pressure during the isovolumetric relaxation time (IVRT). Consequently, the E/A ratio is > 1 correlating with a normal relaxation. An E/A ratio < 1 together with prolonged IVRT and deceleration time (DT, rapid decline of the E) indicate an abnormal relaxation. By considering these three parameters two more patterns of impaired diastolic function are known: the "pseudonormal" pattern which turns to an impaired relaxation pattern when a Valsalva maneuver is performed and the restrictive pattern. The last one, occurring mostly in patients with restrictive cardiomyopathies (e.g., infiltrative sarcoidosis, endomyocardial fibrosis) and dilated cardiomyopathies with poor systolic function which is associated with increased mortality [21]. Unfortunately, mitral flow is influenced not only by the diastolic properties of the LV but also by other factors, including preload, afterload, heart rate and the presence of arrhythmias. Another indicator, the pulmonary venous flow can be used to assess diastolic function but it is also limited in case of mitral valve disease, heart block and tachycardia. A more precise assessment of the diastolic function can be made by using the tissue Doppler imaging (TDI). This enables the measurement of frequency Doppler shifts caused by myocardial motion as the mitral annulus recoils back toward the base in early (e') and late (a') diastole. The peak waves (e′ and a′) are obtained in analogy to those recorded by the mitral flow. TDI enables, depending of the placement of the sample volume, assessment of global or regional diastolic function. In patients with hypertension and hypertrophy, diastolic dysfunction is more evident at the basal septal segments [22]. The E/e' ratio (with e' assessed at a lateral segment) has been identified as the best parameter for diagnosis of diastolic heart failure [23]. An E/e' ratio below 8 is associated with normal filling pressures and a ratio > 12 to 15 is associated with elevated filling pressures. For values between 8 and 12 additional echocardiographic parameters (e.g., use of Valsalva with transmitral Doppler, pulmonary venous flow) are recommended to correctly classify diastolic function. By using the Doppler color M-mode another index of diastolic dysfunction, the propagation velocity of early diastolic flow (Vp) into the ventricle has been proposed. This index seems to be independent of the load conditions and can be useful to unmask diastolic dysfunction in hypertensive patients with pseudonormal mitral flow. However, in patients with normal left ventricular function the Vp may be normal despite an impaired left ventricular relaxation indicating a major limitation of the index. Beside diastolic dysfunction, an enlarged left atrium was found in patients with hypertension and preserved ejection fraction and is associated with elevated filling pressures of the left ventricle leading to clinical heart failure [24].

As described earlier, echocardiography assesses two main features of the hypertensive heart disease, left ventricular hypertrophy and diastolic dysfunction. Systolic dysfunction occurring in the presence or not of the aforementioned changes is assessed in the clinical practice by echocardiography. Assessment of the ejection fraction can be made visually, it requires

http://dx.doi.org/10.5772/56171

however a high level of expertise and is limited by subjectivity. Quantified, objective measurements of the LV systolic function have become standard practice in echocardiography. One parameters of the systolic function is fractional shortening obtained from M-Mode tracings in the parasternal long axis (method according to Teichmann). Though it is a simple and quick method, it is limited by the fact that it provides information about contractility along a single line. If regional wall motion abnormalities occur (e.g. in the presence of coronary artery disease) the severity of the dysfunction may be under - or overestimated, depending if the region of an abnormal wall motion is interrogated or not. As long as this method is only valid in symmetrically contracting hearts, it is inappropriate for the remodeled ventricles of patients with heart failure. The European and American guidelines recommended the biplane method of discs (modified Simpson's rule) as the echocardiographic method of choice for volume measurements and estimation of ejection fraction [25, 26]. The principle underlying this method is that the total LV volume is calculated from the summation of a stack of elliptical discs. The height of each disc is calculated as a fraction of the LV long axis based on the longer of the two lengths from the two and four-chamber views. The cross-sectional area of the disk is based on the two diameters obtained from the two- and four-chamber views. The method can also be used with one single plane, when two orthogonal views are not available. In this case, the presence of any extensive wall motion abnormalities may limit the results [25]. Practically, the endocardial borders in the apical 4- and 2-chamber views in end-diastole and end-systole are traced manually or automatically. The end-diastolic and end-systolic volumes (EDV, ESV) are calculated and the ejection fraction is estimated as follows: Ejection fraction = (EDV – ESV) / EDV. The reference values for the ejection fraction do not differ between men und women. An EF > 55% indicates a normal systolic function. An EF between 45-54% suggests a mildly abnormal function and an EF between 30-44% a moderately abnormal systolic function. A severely abnormal left ventricular function is indicated by an EF < 30%. This 2-D approach to assess EF is based on geometric assumptions, which are invalid in a nonsymmetrical contracting, remodeled ventricle. Over the last decade, several three-dimensional (3-D) echocardiographic techniques became available to measure LV volumes and mass. 3-D echocardiography does not rely on geometric assumptions for volume/mass calculations and is not subject to plane positioning errors, which can lead to chamber foreshortening. Compared to the gold-standard for assessment of left ventricular volumes and EF, the cardiac magnetic resonance, 3-D echocardiography showed significantly better agreement (smaller bias), lower scatter and lower intra- and inter-observer variability than 2-D echocardiography [27, 28]. Furthermore, 3-D echocardiography is also used in the assessment of diastolic function, as it is independent of load conditions.

In summary, echocardiography is a necessary diagnostic tool for risk stratification of patients with hypertension before treatment but also for follow-up assessment of end-organ damages during treatment. In 25-30% of hypertensive patients with low or moderate cardiovascular risk (based on risk factor evaluation and ECG), an increase of the LV mass may be identified by echocardiography leading to higher risk stratification and changes of therapeutic strategy [29, 30].

4. Doppler ultrasound of renal arteries

Renovascular hypertension is the second most common cause of secondary hypertension in approximately 2% of adult patients who present with blood pressure elevation when assessed in specialized centres [31]. This is caused by one or more stenoses of the extrarenal arteries, which in the elderly population have frequently an atherosclerotic nature. Fibromuscular dysplasia accounts for up to 25% of total cases and is the most common variety in young adults. Unfortunately there is not any optimal screening test available for the time. A screening test should have a high sensitivity in order to keep the false negative results in the lowest possible level. The Doppler ultrasound of renal arteries allows an analysis of the renal perfusion. According to various studies the sensitivity and specificity of Doppler ultrasound in the diagnosis of renal artery stenosis lies approximately at 90% [32, 33]. Due to the fact that renovascular hypertension in individuals with mild and medium hypertension has a prevalence below 1%, an unselective examination of all individuals with hypertension would lead to a high rate of false positive results. That would result to a high rate of unnecessary angiographies. On the other hand in a preselected population of hypertensives with clinical implications of increased probability of renal artery stenosis the Doppler ultrasound of the renal arteries is a very appropriate screening examination, due to the fact that the prevalence of renovascular hypertension in acute, severe and resistant hypertension is significantly higher (10-45%). In other words, the use of Doppler ultrasound as a diagnostic tool in a selected population, has a significantly higher positive predictive value with a still acceptable negative predictive value.

Clinical signs for a renovascular hypertension include the following:

- Hypertension in individuals younger than 30 years of age
- A unilateral small kidney or a difference in renal size more than 1.5cm
- Generalized atherosclerosis
- Abdominal bruit with lateralization,
- Resistant hypertension, defined as hypertension refractory to treatment with at least three antihypertensive drugs (including a diuretic agent)
- An elevation of the serum creatinine level > 30% under the treatment with an ACE inhibitor or an AT1-receptor antagonist

It should be mentioned, that a difference of more than 1.5 cm in length between the two kidneys, which is usually considered as being diagnostic for renal artery stenosis is only found in 60 – 70% of the patients with renovascular hypertension [34].

The examination itself can be limited by factors such as bowel gas, obesity, cooperation of the patient and from the fact that it is a highly operator dependent examination. The atherosclerotic induced renal artery stenosis is easily detectable, because it usually involves the ostium and the proximal 1/3 of the renal artery. On the other hand fibromuscular dysplasia involves the distal 2/3 of renal artery and their segmental branches and is thus difficult to depict. With

today's ultrasound technology it is possible to visualize approximately 88% of all main and accessory renal arteries [35]. In every renal artery angle corrected flow velocity measurements should be performed in at least 5 points. A velocity of 60-100cm/s is considered as normal, whereas a 70% stenosis leads to velocities of at least 180-200cm/s. Stenoses proximal to the ostium are easily obtainable with an epigastric transverse scan and distal stenoses or stenoses of segmental branches are better seen with a longitudinal flank scan (lateral position).

Additional intrarenal scanning permits the diagnosis of renal artery stenosis without direct imaging of the main renal artery. In 1994, Schwerk *et al*. introduced the Resistive Index (RI) obtained in the interlobar arteries as a reliable indirect parameter for detecting renal artery stenosis. The RI is a ratio of peak systolic and end diastolic velocity, derived from the Doppler spectrum of any vessel. The authors calculated the side-to-side difference of intrarenal RI > 5% with the lower RI in the post-stenotic kidney. Sensitivity and specificity were 100% and 94%, respectively, for moderate and severe RAS [36]. In the meantime, intrarenal RI has been frequently evaluated for different nephrological issues [37, 38]. In a single prospective study a high intrarenal RI was found to be negatively correlated with the outcome of intervention in patients with atherosclerotic renal artery stenosis [39]. A high RI (RI ≥ 80) was felt to reflect advanced renal damage, which would explain the interventional treatment failure. Radermacher et al. [39] investigated the efficacy of angioplasty of a renal artery stenosis in dependence of the RI. They concluded that an increased renal resistance index > 0.8 is associated with a poor prognosis despite correction of the stenosis. To date, the clinical impacts of these findings are discussed controversially.

5. Ultrasound of carotid arteries

The carotid wall thickening is an early marker of atherosclerosis and subclinical organ damage. It precedes the evolution of arteriosclerotic plaques. Ultrasound of the carotid arteries constitutes a very good opportunity to evaluate hypertension-induced vascular end organ damage. Several cardiovascular risk factors including male sex, ageing, elevated blood pressure, diabetes, smoking and obesity are positively associated with increased carotid intima-media thickness (IMT) in observational and epidemiological studies. Above these factors, high systolic blood pressures have the greatest effect on IMT [40]. An IMT > 0.9 mm in the common carotid artery is generally seen as abnormal; however there is a continuous relationship between IMT and cardiovascular events. An intima-media thickness (IMT) > 0.9 mm or the presence of a carotid plaque predict the occurrence of stroke and myocardial infarction [2, 41]. Particularly, in a meta-analysis of data from 8 studies in general populations, including about 37,000 subjects who were followed up for a mean of 5.5 years, the risk for a myocardial infarction increases by 10-15% and the stroke risk by 13-18% for every 0.1 mm increase of the IMT [42]. For the assessment of CVD risk, the carotid artery wall, rather than the degree of luminal narrowing, is examined to identify areas of increased thickness and non-occlusive atherosclerotic plaque, which represent early stages of arterial injury and atherosclerosis. Furthermore, the detection of early signs of vascular damage has to include ultrasound not only of the common carotid arteries, but of bifurcations and/or internal carotids

where atherosclerosis progresses more rapidly and plaques are more frequent [43]. Ultrasound imaging of the far wall of the carotid artery produces two echogenic lines, which correspond to the lumen-intima interface and the media-adventitia interface. The current ultrasound technology enables in the clinical practice the combined measurement of the thickness of the intimal and medial layers of the arterial wall which constitute the IMT. Carotid plaque is defined as the presence of focal wall thickening that is at least 50% greater than that of the surrounding vessel wall or as a focal region with IMT greater than 1.5 mm that protrudes into the lumen. Both near and far walls can be used for assessment of the IMT. However, IMT of the near wall is less accurate because the ultrasound beam is traveling from more to less echogenic layers at the adventitia-media and intima-lumen interfaces of the near wall [44]. Histological data suggest an underestimation of the IMT around 20% when the near wall is used [45]. A linear-array transducer operating at a frequency of at least 7 MHz [44]. Three methods most frequently used to measure the IMT by using B –Mode are the following: 1. Averaging the maximum IMT of the four far walls of the carotid bifurcations and of the distal common carotid arteries. 2. Assessing the mean maximum thickness (M max) of up to 12 different sites (right and left, near and far walls, distal common, bifurcation, and proximal internal carotid). 3. The maximum measured IMT of a single measurement is taken into account. The last method provides more reproducible results when IMT measurement is restricted to the far wall of the distal segment of the common carotid artery, providing only a 3% of relative difference between two successive measurements [46]. Analysis may be performed by manual cursor placement or by automated computerized edge detection. As we mentioned above, B-mode imaging is preferred over M-mode imaging. M-mode, in spite of a superior temporal resolution, provides measurement of one single point of thickness, rather than a segmental value as it is enabled by B-mode. However, carotid wall thickening is not uniform and a singe point measurement may not represent accurately the arterial status and is less reproducible for follow-up measurements. A novel noninvasive echo-tracking system measuring the IMT and other mechanical properties of the carotid wall has been proposed [47]. This method enables an additional evaluation of the carotid plaque stability and composition.

The normal IMT values are influenced by age and sex and IMT normal values may be defined in terms of statistical distribution within a healthy population. IMT values greater than the 75th percentile are considered high and indicate an increased cardiovascular risk. Values in the 25th to 75th percentile are considered average and indicative of unchanged CVD risk. Values less than or equal to 25th percentile are associated with a low CVD risk [44]. However, available data indicate that IMT > 0.9 mm represents a risk of myocardial infarction and/or cerebrovascular disease and in the clinical practice this cut-off value may better defined in terms of increased risk [48]. Recent data have further strengthened the relationship of carotid IMT and plaques with cardiovascular events. A new report from the European Lacidipine Study on Atherosclerosis (ELSA) trial suggests that baseline carotid IMT predicts cardiovascular events independent of blood pressure and this occurs both for the IMT value at the carotid bifurcations and for the IMT value at the level of the common carotid artery [49]. The adverse prognostic significance of carotid plaques has also been reported in patients with high normal blood pressure prospectively followed for about 13 years [50]. In the Risk Intervention Study (RIS) study patients with severe essential hypertension and high cardiovascular risk had a

http://dx.doi.org/10.5772/56171

significantly higher prevalence of atherosclerotic lesions compared to control subjects [51]. Assessment of IMT plays an important role in the risk stratification. Interestingly, about 30% of hypertensive subjects classified as at low or moderate added risk without ultrasound for carotid artery thickening or plaque were placed in the high added risk group after detecting of vascular damages [29].

The predictive value of the carotid ultrasound and its role in risk stratification has been demonstrated in a lot of trials as aforementioned. Whether a decrease of IMT progression is associated with a reduction of cardiovascular events and an improvement in prognosis remains at the time elusive. Therapeutic double blind trials have shown that antihypertensive drugs may have a more or less marked effect on carotid IMT progression. A recent meta-analysis of 22 randomized controlled trials has evaluated the effects of an antihypertensive drug versus placebo or another antihypertensive agent of a different class on carotid intima-media thickness. The results have shown that compared with no treatment, diuretics/± beta-blockers, ACE inhibitors and calcium antagonists attenuate the rate of progression of carotid intima-media thickening, in some trials even in the absence of any significant reduction of the blood pressure [52]. In patients with hypertension and hypercholesterolemia the administration of pravastatin prevents the progression of carotid intima-media thickness [53]. In the ELSA trial the treatment-induced changes of the IMT did not predict cardiovascular events as was the case by the baseline values. However, these results are not conclusive due to the smallness of the IMT changes and the large individual differences in baseline IMT [49].

Beyond the identification of subclinical organ damage of the carotid arteries, ultrasound is a useful tool for identification of carotid stenoses in progressive atherosclerosis. High blood pressure is a major risk factor for stroke with a correlation between elevated BP and occurrence of stroke. This correlation holds over a wide BP range, from systolic levels as low as 115 mm/Hg and diastolic levels as low as 70 mm/Hg [54], with systolic BP having a stronger association with higher stroke risk. Elevated BP is positively associated with both ischemic and hemorrhagic stroke, with a higher association appearing in hemorrhagic stroke and secondary prevention [56]. Large vessel disease of the extracranial arteries accounts for half of the ischemic strokes.

Doppler sonography is the most common imaging study performed for the diagnosis of carotid disease. It is part of the imaging tests taking place early after a transient ischemic attack (TIA) or stroke in order to identify patients with tight symptomatic arterial stenosis who could benefit from endarterectomy or angioplasty. Carotid Doppler-studies are fast, non-invasive and easily applicable however provide limited information, require skilled operators and are investigator-dependent. Doppler ultrasound has a similar specificity and sensitivity for carotid artery stenosis with computed tomography angiography (CTA) but both are inferior to contrast-magnetic resonance angiography (MRA) [57]. For asymptomatic patients with hypertension, assessment for carotid artery stenosis is also useful as part of risk stratification and is recommended for patients with two or more risk factors for atherosclerosis. Evidence of an internal carotid artery stenosis (ICA) supports recommendation of antiplatelet therapy and more strict control of risk factors to prevent stroke [58].

The first step of a carotid ultrasound test is to identify plaques via B-mode as referred above. Addition of color Doppler enables identification of origin and course of the internal carotid artery and a differentiation between severe stenosis and occlusion. Stenotic areas are identified in the presence of the "aliasing" phenomenon occurring due to high velocities in the center of the stenotic lumen and post-stenotic flow disturbances. Flow velocities in the spectral analysis are the main parameters used for evaluating the severity of carotid stenosis. Flow velocity must be sampled through the whole area of presumed stenosis until the distal end of the plaque is seen to ensure that the site of the highest velocity has been detected. Compared to angiographic data, a wide range of flow velocities was recorded for any given degree of angiographic stenosis so that the sensitivity and specificity of the method may vary [59]. A better correlation to angiographic determined stenoses is achieved by assessing the peak systolic velocity in the internal carotid artery and the ratio of the peak systolic velocity in the internal carotid artery to that in the ipsilateral common carotid artery as proposed by the current guidelines [60]. Based on Doppler sonography, carotid stenoses are classified into two grades: Grade 1- with the rate of stenosis measuring between 50% to 69% and Grade 2 measuring 70-99%, which also represents a severe non-occlusive disease. In equivocal cases, further imaging methods may be additionally used. In Table 1 the sonographic criteria for grading of carotid artery stenosis are summarized.

An ultrasound examination for detection of carotid stenoses and plaques and evaluation of the intima-media thickness should be performed in hypertensive patients with concomitant risk factors such as smoking, dyslipidemia, diabetes, obesity and family history of cardiovascular disease. The results can be useful for re-assessing CVD risk in some asymptomatic patients and consequently re-assessing therapeutic strategies. For accurate results, strict attention to quality control in image acquisition, measurement and interpretation are necessary.

Grade of Stenosis	Peak systolic velocity and visible criteria
no stenosis	< 125 cm/s and no visible plaque or IMT
< 50%	< 125cm/s with visible plaque or IMT
50-69%	125 – 230 cm/s with visible plaque
> 70% to near occlusion	> 230cm/s with visible plaque and lumen narrowing
100%	No detectable patent lumen and flow is seen

Table 1. Grading of internal carotid artery stenosis upon Doppler velocities and B-mode

6. Flow mediated dilation

Endothelial function is linked to cardiovascular risk factors and provides prognostic information for cardiovascular diseases [61]. Endothelial dysfunction is regarded as the initial step of atherosclerosis and therefore as the earliest detectable manifestation of vascular end-organ

http://dx.doi.org/10.5772/56171

damage. It can be assessed using several methods, with flow-mediated dilation (FMD) being currently the gold-standard in non-invasive evaluation of endothelial dysfunction. In this ultrasound-based method brachial artery diameter is measured before and after an increase in shear stress that is induced by reactive hyperemia. When a sphygmomanometer cuff placed on the forearm or upper-arm and is inflated at 50 mm/Hg above systolic pressure, arterial inflow is occluded causing a local ischemia and dilation of downstream arteries. Cuff deflation induces a high-flow state through the brachial artery (reactive hyperemia) to accommodate the dilated resistance vessels. The increased shear stress leads to endothelium dependent dilation of the brachial artery. FMD occurs predominantly as a result of local endothelial release of nitric oxide. Figure 1 shows the B-mode and Doppler flow images of the brachial artery of a patient with hypertension at baseline and after deflation of the cuff (hyperemia). The FMD was calculated by the equation: FMD = (diameter hyperemia – diameter baseline) * 100 / diameter baseline. A value of 8.1% suggesting a near normal value (>8%) was found.

By using invasive and non-invasive methods impaired endothelial function has been found in uncomplicated hypertensive patients [62, 63]. In one prospective trial a reduction of blood pressure in response to antihypertensive treatment leads to improvement of the FMD suggesting a beneficial effect of antihypertensive treatment on endothelial function [64]. Several other large trials have found relationships between endothelial dysfunction assessed by FMD and prognostic markers of cardiovascular disease and atherosclerosis [65, 66]. Although the FMD test has opened a new field in the clinical research of conduit artery endothelial biology, some practical challenges of this technique have prevented its broad use in daily clinical practice so far. The most important of these are the need for highly trained operators, the time-consuming analysis of results and the care required to minimize environmental or physiological influences such as eating, caffeine ingestion and variations of temperature [67].

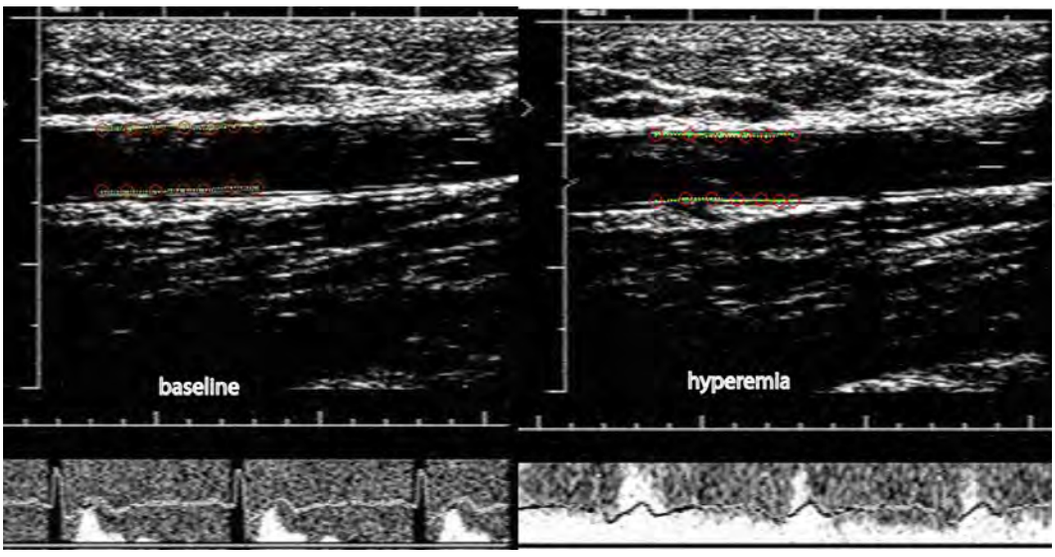

Figure 1. Ultrasound images during testing of the flow mediated dilation. A slightly increase of the brachial diameter from 5.44mm at baseline to 5.88mm under hyperemia was recorded. The Doppler flow shows an increase of the blood flow after deflation of the cuff (hyperemia).

7. Conclusions

In summary, sonography is essential in the workup of a hypertensive patient. Abdominal sonography should be performed in the evaluation of hypertension. The last European guidelines have emphasized that treatment-induced changes of organ damage affect the incidence of cardiovascular events, thereby recommending performance of organ damage examinations including sonography during treatment. When a search for secondary hypertension is indicated, abdominal sonography and Doppler ultrasound of the renal arteries are also recommended. Table 2 summarizes the use of ultrasound in the evaluation of hypertension.

Ultrasound examination	Use in diagnostic workup of hypertension
Abdominal ultrasound	Identification of subclinical and end-organ damage (recommended) • Aortosclerosis • Aortic aneurysm • Nephrosclerosis Screening for secondary causes of hypertension • Renal parenchymal disease • Renal vascular disease • Adrenal adenomas • Phaeochromocytoma
Echocardiography	Identification of subclinical and end organ damage (recommended) • Left ventricular hypertrophy (LVH) • Systolic and diastolic dysfunction • Left atrium dimension and geomertry
Doppler ultrasound of the renal arteries	Screening for secondary causes of hypertension • Renovascular hypertension
Ultrasound of the carotid arteries	Identification of subclinical and end-organ damage (recommended) • Intima – media thickness (IMT) • Carotid plaques • Carotid artery stenosis
Assessment of flow-mediated dilation of brachial artery	Identification of subclinical organ damage (not in clinical use) • Endothelial dysfunction

Table 2. Ultrasound examinations in hypertension

In summary, sonography is essential in the workup of a hypertensive patient. Abdominal sonography should be performed in every newly diagnosed case of hypertension. Performance of further ultrasound techniques depends on age, concomitant diseases, symptoms, and overall cardiovascular risk. Table 2 summarizes the use of ultrasound in the evaluation of hypertension.

Author details

References

[1] Campos C SJ, Rodicio JL. Campos C, Segura J, Rodicio JL.. Investigations in secondary hypertension: renal disease. Hypertension. 2001:119-26.

[2] Hodis HN, Mack WJ, LaBree L, Selzer RH, Liu CR, Liu CH et al. The role of carotid arterial intima-media thickness in predicting clinical coronary events. Ann Intern Med. 1998;128(4):262-9.

[3] Rezneck RH. AP. Imaging in endocrinology. The adrenal glands.. Clin Endocrinol (Oxf). 1994;40(5):561-76.

[4] Reisch N, Peczkowska M, Januszewicz A and Neumann HP. Pheochromocytoma: presentation, diagnosis and treatment. Journal of hypertension. 2006;24(12):2331-9.

[5] Burton S. RP. Adrenal Glands. Magnetic Resonanc Imaging. 1999.

[6] Goldstein RE ONJ, Jr., Holcomb GW. Clinical experience over 48 years with pheochromocytoma. Ann Surg. 1999;229(6):755-64.

[7] Schwerk WB, Gorg C, Gorg K and Restrepo IK. Adrenal pheochromocytomas: a broad spectrum of sonographic presentation. Journal of ultrasound in medicine: official journal of the American Institute of Ultrasound in Medicine. 1994;13(7):517-21.

[8] Lloyd-Jones DM, Larson MG, Leip EP, Beiser A, D'Agostino RB, Kannel WB et al. Lifetime risk for developing congestive heart failure: the Framingham Heart Study. Circulation. 2002;106(24):3068-72.

[9] Reichek N and Devereux RB. Left ventricular hypertrophy: relationship of anatomic, echocardiographic and electrocardiographic findings. Circulation. 1981;63(6):1391-8.

[10] Mancia G, De Backer G, Dominiczak A, Cifkova R, Fagard R, Germano G et al. [ESH/ESC 2007 Guidelines for the management of arterial hypertension]. Rev Esp Cardiol. 2007;60(9):968 e1-94.

[11] Devereux RB, Wachtell K, Gerdts E, Boman K, Nieminen MS, Papademetriou V et al. Prognostic significance of left ventricular mass change during treatment of hypertension. Jama. 2004;292(19):2350-6.

[12] Devereux RB, Alonso DR, Lutas EM, Gottlieb GJ, Campo E, Sachs I et al. Echocardiographic assessment of left ventricular hypertrophy: comparison to necropsy findings. Am J Cardiol. 1986;57(6):450-8.

[13] Muiesan ML, Salvetti M, Monteduro C, Bonzi B, Paini A, Viola S et al. Left ventricular concentric geometry during treatment adversely affects cardiovascular prognosis in hypertensive patients. Hypertension. 2004;43(4):731-8.

[14] Milani RV, Lavie CJ, Mehra MR, Ventura HO, Kurtz JD and Messerli FH. Left ventricular geometry and survival in patients with normal left ventricular ejection fraction. Am J Cardiol. 2006;97(7):959-63.

[15] Tsioufis C, Vezali E, Tsiachris D, Dimitriadis K, Taxiarchou E, Chatzis D et al. Left ventricular hypertrophy versus chronic kidney disease as predictors of cardiovascular events in hypertension: a Greek 6-year-follow-up study. J Hypertens. 2009;27(4): 744-52.

[16] Gerdts E, Wachtell K, Omvik P, Otterstad JE, Oikarinen L, Boman K et al. Left atrial size and risk of major cardiovascular events during antihypertensive treatment: losartan intervention for endpoint reduction in hypertension trial. Hypertension. 2007;49(2):311-6.

[17] Gerdts E, Cramariuc D, de Simone G, Wachtell K, Dahlof B and Devereux RB. Impact of left ventricular geometry on prognosis in hypertensive patients with left ventricular hypertrophy (the LIFE study). Eur J Echocardiogr. 2008;9(6):809-15.

[18] Aeschbacher BC, Hutter D, Fuhrer J, Weidmann P, Delacretaz E and Allemann Y. Diastolic dysfunction precedes myocardial hypertrophy in the development of hypertension. Am J Hypertens. 2001;14(2):106-13.

[19] Gotsman I, Zwas D, Lotan C and Keren A. Heart failure and preserved left ventricular function: long term clinical outcome. PLoS One. 2012;7(7):e41022.

[20] Paulus WJ, Tschope C, Sanderson JE, Rusconi C, Flachskampf FA, Rademakers FE et al. How to diagnose diastolic heart failure: a consensus statement on the diagnosis of heart failure with normal left ventricular ejection fraction by the Heart Failure and Echocardiography Associations of the European Society of Cardiology. Eur Heart J. 2007;28(20):2539-50.

[21] Moller JE, Sondergaard E, Poulsen SH and Egstrup K. Pseudonormal and restrictive filling patterns predict left ventricular dilation and cardiac death after a first myocardial infarction: a serial color M-mode Doppler echocardiographic study. J Am Coll Cardiol. 2000;36(6):1841-6.

[22] Galderisi M, Caso P, Severino S, Petrocelli A, De Simone L, Izzo A et al. Myocardial diastolic impairment caused by left ventricular hypertrophy involves basal septum more than other walls: analysis by pulsed Doppler tissue imaging. J Hypertens. 1999;17(5):685-93.

[23] Kasner M, Westermann D, Steendijk P, Gaub R, Wilkenshoff U, Weitmann K et al. Utility of Doppler echocardiography and tissue Doppler imaging in the estimation of diastolic function in heart failure with normal ejection fraction: a comparative Doppler-conductance catheterization study. Circulation. 2007;116(6):637-47.

[24] Melenovsky V, Borlaug BA, Rosen B, Hay I, Ferruci L, Morell CH et al. Cardiovascular features of heart failure with preserved ejection fraction versus nonfailing hypertensive left ventricular hypertrophy in the urban Baltimore community: the role of atrial remodeling/dysfunction. J Am Coll Cardiol. 2007;49(2):198-207.

[25] Lang RM, Bierig M, Devereux RB, Flachskampf FA, Foster E, Pellikka PA et al. Recommendations for chamber quantification. Eur J Echocardiogr. 2006;7(2):79-108.

[26] Lang RM, Bierig M, Devereux RB, Flachskampf FA, Foster E, Pellikka PA et al. Recommendations for chamber quantification: a report from the American Society of Echocardiography's Guidelines and Standards Committee and the Chamber Quantification Writing Group, developed in conjunction with the European Association of Echocardiography, a branch of the European Society of Cardiology. J Am Soc Echocardiogr. 2005;18(12):1440-63.

[27] Gopal AS, Schnellbaecher MJ, Shen Z, Boxt LM, Katz J and King DL. Freehand three-dimensional echocardiography for determination of left ventricular volume and mass in patients with abnormal ventricles: comparison with magnetic resonance imaging. J Am Soc Echocardiogr. 1997;10(8):853-61.

[28] Buck T, Hunold P, Wentz KU, Tkalec W, Nesser HJ and Erbel R. Tomographic three-dimensional echocardiographic determination of chamber size and systolic function in patients with left ventricular aneurysm: comparison to magnetic resonance imaging, cineventriculography, and two-dimensional echocardiography. Circulation. 1997;96(12):4286-97.

[29] Cuspidi C, Ambrosioni E, Mancia G, Pessina AC, Trimarco B and Zanchetti A. Role of echocardiography and carotid ultrasonography in stratifying risk in patients with essential hypertension: the Assessment of Prognostic Risk Observational Survey. J Hypertens. 2002;20(7):1307-14.

[30] Schillaci G, De Simone G, Reboldi G, Porcellati C, Devereux RB and Verdecchia P. Change in cardiovascular risk profile by echocardiography in low- or medium-risk hypertension. J Hypertens. 2002;20(8):1519-25.

[31] Elliott W. Secondary hypertension: renovascular hypertension. Hypertension: a Companion to Braunwald's Heart Disease. 2007:93-105.

[32] Radermacher J, Chavan A, Schaffer J, Stoess B, Vitzthum A, Kliem V et al. Detection of significant renal artery stenosis with color Doppler sonography: combining extrarenal and intrarenal approaches to minimize technical failure. Clinical nephrology. 2000;53(5):333-43.

[33] Simoni C, Balestra G, Bandini A and Rusticali F. [Doppler ultrasound in the diagnosis of renal artery stenosis in hypertensive patients: a prospective study]. Giornale italiano di cardiologia. 1991;21(3):249-55.

[34] Safian RD and Textor SC. Renal-artery stenosis. N Engl J Med. 2001;344(6):431-42.

[35] Radermacher J and Brunkhorst R. Diagnosis and treatment of renovascular stenosis--a cost-benefit analysis. Nephrology, dialysis, transplantation: official publication of the European Dialysis and Transplant Association - European Renal Association. 1998;13(11):2761-7.

[36] Schwerk WB, Restrepo IK, Stellwaag M, Klose KJ and Schade-Brittinger C. Renal artery stenosis: grading with image-directed Doppler US evaluation of renal resistive index. Radiology. 1994;190(3):785-90.

[37] Krumme B. Renal Doppler sonography--update in clinical nephrology. Nephron. Clinical practice. 2006;103(2):c24-8.

[38] Pearce JD, Edwards MS, Craven TE, English WP, Mondi MM, Reavis SW et al. Renal duplex parameters, blood pressure, and renal function in elderly people. American journal of kidney diseases: the official journal of the National Kidney Foundation. 2005;45(5):842-50.

[39] Radermacher J, Chavan A, Bleck J, Vitzthum A, Stoess B, Gebel MJ et al. Use of Doppler ultrasonography to predict the outcome of therapy for renal-artery stenosis. N Engl J Med. 2001;344(6):410-7.

[40] Zanchetti A, Bond MG, Hennig M, Neiss A, Mancia G, Dal Palu C et al. Calcium antagonist lacidipine slows down progression of asymptomatic carotid atherosclerosis: principal results of the European Lacidipine Study on Atherosclerosis (ELSA), a randomized, double-blind, long-term trial. Circulation. 2002;106(19):2422-7.

[41] Bots ML, Hoes AW, Koudstaal PJ, Hofman A and Grobbee DE. Common carotid intima-media thickness and risk of stroke and myocardial infarction: the Rotterdam Study. Circulation. 1997;96(5):1432-7.

[42] Lorenz MW, Markus HS, Bots ML, Rosvall M and Sitzer M. Prediction of clinical cardiovascular events with carotid intima-media thickness: a systematic review and meta-analysis. Circulation. 2007;115(4):459-67.

[43] Mansia G, De Backer G, Dominiczak A, Cifkova R, Fagard R, Germano G et al. 2007 ESH-ESC Guidelines for the management of arterial hypertension: the task force for the management of arterial hypertension of the European Society of Hypertension (ESH) and of the European Society of Cardiology (ESC). Blood Press. 2007;16(3):135-232.

[44] Stein JH, Korcarz CE, Hurst RT, Lonn E, Kendall CB, Mohler ER et al. Use of carotid ultrasound to identify subclinical vascular disease and evaluate cardiovascular disease risk: a consensus statement from the American Society of Echocardiography

Carotid Intima-Media Thickness Task Force. Endorsed by the Society for Vascular Medicine. J Am Soc Echocardiogr. 2008;21(2):93-111; quiz 89-90.

[45] Wong M, Edelstein J, Wollman J and Bond MG. Ultrasonic-pathological comparison of the human arterial wall. Verification of intima-media thickness. Arterioscler Thromb. 1993;13(4):482-6.

[46] Touboul PJ, Hennerici MG, Meairs S, Adams H, Amarenco P, Bornstein N et al. Mannheim carotid intima-media thickness consensus (2004-2006). An update on behalf of the Advisory Board of the 3rd and 4th Watching the Risk Symposium, 13th and 15th European Stroke Conferences, Mannheim, Germany, 2004, and Brussels, Belgium, 2006. Cerebrovasc Dis. 2007;23(1):75-80.

[47] Paini A, Boutouyrie P, Calvet D, Zidi M, Agabiti-Rosei E and Laurent S. Multiaxial mechanical characteristics of carotid plaque: analysis by multiarray echotracking system. Stroke. 2007;38(1):117-23.

[48] EA Rosei MM. Assessment of preclinical target organ damage in hypertension: carotid intima-media thickness and plaque. European Society of Hypertension Schientific Newsletter. 2011pp. 19-20.

[49] Zanchetti A, Hennig M, Hollweck R, Bond G, Tang R, Cuspidi C et al. Baseline values but not treatment-induced changes in carotid intima-media thickness predict incident cardiovascular events in treated hypertensive patients: findings in the European Lacidipine Study on Atherosclerosis (ELSA). Circulation. 2009;120(12): 1084-90.

[50] Sehestedt T, Jeppesen J, Hansen TW, Rasmussen S, Wachtell K, Ibsen H et al. Which markers of subclinical organ damage to measure in individuals with high normal blood pressure? J Hypertens. 2009;27(6):1165-71.

[51] Salonen JT and Salonen R. Ultrasonographically assessed carotid morphology and the risk of coronary heart disease. Arterioscler Thromb. 1991;11(5):1245-9.

[52] Werner GS, Fritzenwanger M, Prochnau D, Schwarz G, Ferrari M, Aarnoudse W et al. Determinants of coronary steal in chronic total coronary occlusions donor artery, collateral, and microvascular resistance. J Am Coll Cardiol. 2006;48(1):51-8.

[53] Zanchetti A, Crepaldi G, Bond MG, Gallus G, Veglia F, Mancia G et al. Different effects of antihypertensive regimens based on fosinopril or hydrochlorothiazide with or without lipid lowering by pravastatin on progression of asymptomatic carotid atherosclerosis: principal results of PHYLLIS--a randomized double-blind trial. Stroke. 2004;35(12):2807-12.

[54] Chalmers J, Todd A, Chapman N, Beilin L, Davis S, Donnan G et al. International Society of Hypertension (ISH): statement on blood pressure lowering and stroke prevention. J Hypertens. 2003;21(4):651-63.

[55] Collins R, Peto R, MacMahon S, Hebert P, Fiebach NH, Eberlein KA et al. Blood pressure, stroke, and coronary heart disease. Part 2, Short-term reductions in blood pres-

sure: overview of randomised drug trials in their epidemiological context. Lancet. 1990;335(8693):827-38.

[56] Rodgers A, MacMahon S, Gamble G, Slattery J, Sandercock P and Warlow C. Blood pressure and risk of stroke in patients with cerebrovascular disease. The United Kingdom Transient Ischaemic Attack Collaborative Group. Bmj. 1996;313(7050):147.

[57] Wardlaw JM, Chappell FM, Best JJ, Wartolowska K and Berry E. Non-invasive imaging compared with intra-arterial angiography in the diagnosis of symptomatic carotid stenosis: a meta-analysis. Lancet. 2006;367(9521):1503-12.

[58] Guidelines for management of ischaemic stroke and transient ischaemic attack 2008. Cerebrovasc Dis. 2008;25(5):457-507.

[59] Grant EG, Duerinckx AJ, El Saden SM, Melany ML, Hathout GM, Zimmerman PT et al. Ability to use duplex US to quantify internal carotid arterial stenoses: fact or fiction? Radiology. 2000;214(1):247-52.

[60] Brott TG, Halperin JL, Abbara S, Bacharach JM, Barr JD, Bush RL et al. 2011 ASA/ACCF/AHA/AANN/AANS/ACR/ASNR/CNS/SAIP/SCAI/SIR/SNIS/SVM/SVS guideline on the management of patients with extracranial carotid and vertebral artery disease: executive summary. J Neurointerv Surg.3(2):100-30.

[61] Celermajer DS, Sorensen KE, Gooch VM, Spiegelhalter DJ, Miller OI, Sullivan ID et al. Non-invasive detection of endothelial dysfunction in children and adults at risk of atherosclerosis. Lancet. 1992;340(8828):1111-5.

[62] Iiyama K, Nagano M, Yo Y, Nagano N, Kamide K, Higaki J et al. Impaired endothelial function with essential hypertension assessed by ultrasonography. Am Heart J. 1996;132(4):779-82.

[63] Panza JA, Quyyumi AA, Brush JE, Jr. and Epstein SE. Abnormal endothelium-dependent vascular relaxation in patients with essential hypertension. N Engl J Med. 1990;323(1):22-7.

[64] Muiesan ML, Salvetti M, Monteduro C, Rizzoni D, Zulli R, Corbellini C et al. Effect of treatment on flow-dependent vasodilation of the brachial artery in essential hypertension. Hypertension. 1999;33(1 Pt 2):575-80.

[65] Kathiresan S, Gona P, Larson MG, Vita JA, Mitchell GF, Tofler GH et al. Cross-sectional relations of multiple biomarkers from distinct biological pathways to brachial artery endothelial function. Circulation. 2006;113(7):938-45.

[66] Juonala M, Viikari JS, Alfthan G, Marniemi J, Kahonen M, Taittonen L et al. Brachial artery flow-mediated dilation and asymmetrical dimethylarginine in the cardiovascular risk in young Finns study. Circulation. 2007;116(12):1367-73.

[67] Corretti MC, Anderson TJ, Benjamin EJ, Celermajer D, Charbonneau F, Creager MA et al. Guidelines for the ultrasound assessment of endothelial-dependent flow-medi-

http://dx.doi.org/10.5772/56171

ated vasodilation of the brachial artery: a report of the International Brachial Artery Reactivity Task Force. J Am Coll Cardiol. 2002;39(2):257-65.

IntechOpen

IntechOpen

12

Application of Orbital Sonography in Neurology

Michael Ertl[1], Maria-Andreea Gamulescu[2] and Felix Schlachetzki[1]
[1]*Department of Neurology, University of Regensburg, Bezirksklinikum Regensburg*
[2]*Department of Ophthalmology, Regensburg University Medical Center*
Germany

1. Introduction

Color-coded duplex sonography is a well established non-invasive method for vascular and parenchymal examination in a wide range of neurological disorders including stroke, cerebral venous thrombosis and degenerative diseases, amongst others. Considering development, cell types and vascular structures as well as pathology and pathophysiology, high similarities and interactions exist between the central nervous system (CNS) and the eye.

When applied to the eye and the orbit, high-resolution color-coded duplex sonography (OCCS) may depict a variety of pathologic alterations such as papilledema or central retinal artery occlusion, that represent manifestation of CNS disorders (i.e. raised intracranial pressure) or systemic diseases (i.e. atherothrombotic/ thrombembolic occlusions), respectively. Although easily accessible, OCCS has not yet gained widespread use in daily neurological practice despite the fact that most modern ultrasound systems are capable of performing such an endeavor. However, this technique may be a very helpful, fast and powerful diagnostic procedure in addition to the diagnostic battery needed for unraveling specific CNS or systemic diseases.

In this book chapter article we highlight different aspects of OCCS and concentrate on methods and diseases relevant for neurologists. The differential diagnosis of orbital tumors (e.g. lymphoma, optic sheath meningeoma, pseudotumor orbitae, myositis, and others) or vascular abnormalities (e.g. varicosis, superior orbital venous dilatation in arterio-venous-fistula) will not be discussed. The first part introduces the reader to the technical requirements, restraints and safety for performing sonography of the eye. Normal relevant anatomy as well as normal values will be given. The second part focuses on common vascular pathologies such as central retinal artery occlusion in the context of suspected giant cell arteritis as well as swelling of the optic nerve and papilledema linked to raised intracranial pressure. Being a fairly young technique, few studies employing OCCS exist, yet a large variety of interesting pathology and variations may be found as exemplified in the third and final part of the chapter.

Ocular color-coded duplex sonography is a fascinating technique with high potential for neurologists in differential diagnosis and therapy of an expanding variety of acute and chronic CNS disease.

2. Technique and safety considerations

Orbital sonography can be easily performed using most color duplex ultrasound systems equipped with high frequency linear array transducers. Since the optic lens as well as the vitreous do not absorb significant ultrasound energy and make near field artifacts virtually impossible, commonly used transmit frequencies in neurology from 7 to 15 MHz may be used. According to the physics of wave propagation in tissue and the resulting axial and lateral resolutions, the general aim is to apply high frequencies up to 14 MHz or more. The acoustic output of the ultrasound systems needs to be adjusted to the requirements of orbital sonography according to the ALARA principle (‚as low as reasonable achievable') in order to avoid damage to the lens and retina (Toms 2006). The main biological effects would be cavitation and temperature increase, the latter being dependent from the insonation time. In animal experiments harmful effects of ultrasound acoustic power to ocular structures (esp. lens and choroid) could be demonstrated (Lizzi et al. 1978). Therefore, current guidelines released by the FDA limit the acoustic output to temporal average intensities of up to 50mW/cm^2 and a mechanical index (MI) of up to 0.23 (Food and Drug Administration 2008). An on-screen indicator of ultrasonic output, the MI is a measure of the likelihood that a clinically important non-thermal biological effect may occur during a diagnostic examination (American Institute of Ultrasound in Medicine 2000). However, most examinations last less than 5 minutes for each eye, hereby limiting the possibility of thermal damage. In order to prevent cavitation effects, the settings for orbital sonography may be as follows:

- B-mode – transmit frequency 14 MHz, mechanical index (MI) = 0.23, single focal zone at 2.5 cm, bandwidth 74 dB;
- C-mode – transmit frequency 10 MHz, MI = 0.23, color scale optimized for low velocities, no wall filter;
- pw-Mode – transmit frequency 2 MHz, MI = <0.23 (<0.44*) (Tab. 1).

	B-mode	C-mode	pw-mode
transmit frequency	14MHz	10MHz	2MHz
mechanical index (MI)	<0.23	<0.23	0.23 (<0.44*)
single focal zone	2.5cm		
bandwidth	74dB		
Special recommendations		color scale optimized for low velocities no wall filter	

Table 1. Machine parameters in B-mode, C-mode and pw-mode, *often the lowest output value

It needs to be kept in mind that most color-duplex machines require reduction of the acoustic output in each mode, that is the B-mode, color-mode and spectral Doppler-mode (the latter might not display values below 0.44).

During the examination the patient lies in supine position with the eyes closed (Fig. 1a). A layer of acoustic gel is applied to the closed lids, the transducer is placed on the upper and

slightly lateral eye-lids with the examiner's hand resting on the orbital margin to minimize pressure on the globe (Fig. 1b/c). To optimize the display of anatomical stuctures, esp. the optic nerve, the transducer is positioned a little on the temporal side and the patient is asked to try to look straight even with the eyes closed. Pressure on the globe should be as low as possible as this might result in a decrease in blood flow velocity of retro-orbital vessels (Tranquart et al. 2003). The optic nerve presents as a hypoechogenic structure beyond the globe in this horizontal scanning plane and the optic disc and provides an anatomical landmark for the ultrasound examination (Fig. 2).

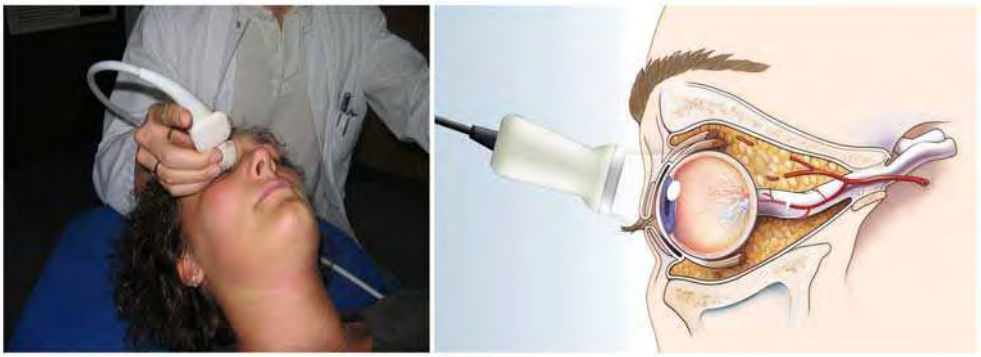

(a) (b)

Fig. 1. Standard examination parameters. (a) Patient lies in supine position with the eyes closed. (b) The transducer is placed on the upper eye-lids (slightly lateral) with the examiner's hand resting on the orbital margin. (c) Illustration of correct transducer positioning and anatomical overview. Copyright ® M.Ertl, with permission

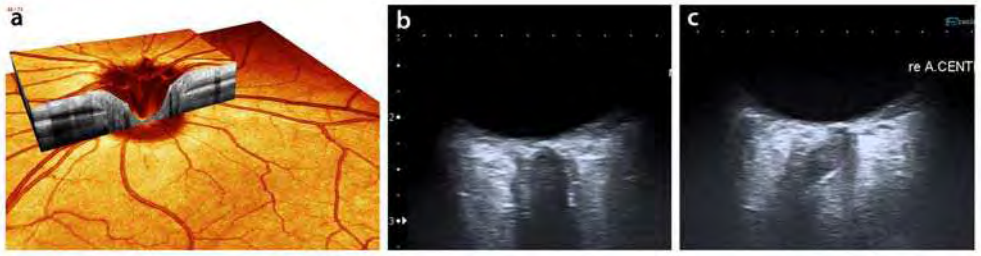

Fig. 2. Anatomical landmarks for ultrasound examination (a) Ocular coherence tomography (Spectralis ®, Heidelberg Engineering, Germany) excellently demonstrating the retinal vasculature and layers of the retina. However, inlay demonstrates limited penetration beyond the level of the retina. (b) High resolution B-mode sonography in the horizontal and lateral scanning plane presenting the optic nerve as a hypoechogenic structure beyond the retina surrounded by the hyperechoic subarachnoid space and the hypoechoic dura mater. The optic nerve provides an anatomical landmark for the ultrasound examination. For anatomical correlates see Figure 3. (c) In a strictly axial horizontal image plane, the optic nerve appears curved limiting the diagnostic accuracy of optic nerve diameter measurements

In order to enable side-to-side comparison, the left side on the monitor pictures the nasal orbit.

3. Vascular diagnostics

The central retinal artery (CRA), a distal branch of the ophthalmic artery, enters the optic nerve approximately 1-1,5 cm distal from the globe coming from the dorsolateral direction (Fig. 3). It supplies the retina and can be identified together with its parallel running central retinal vein (CRV) using the color-mode.

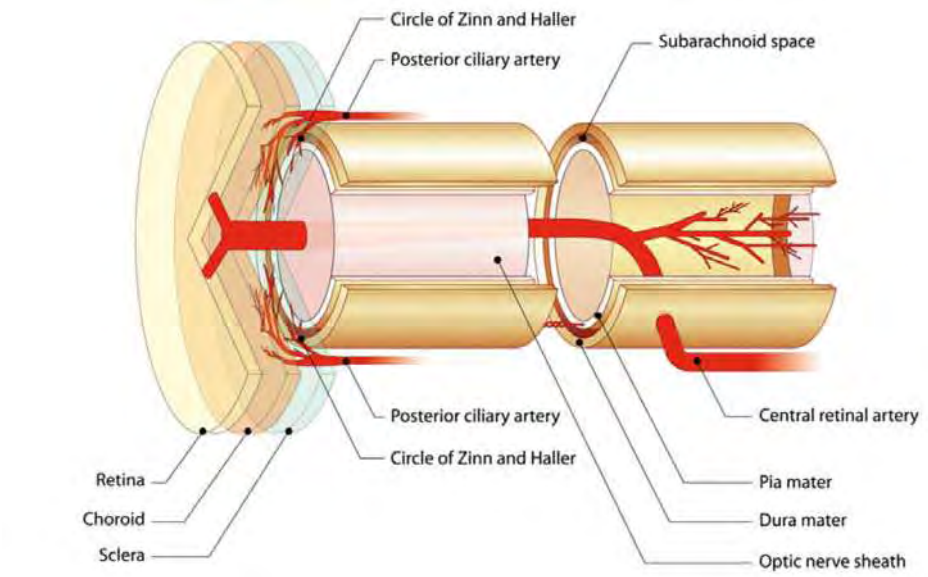

Fig. 3. Anatomy of retrobulbar structures: vascular supply of the retina and the optic nerve and sorrounding structures. Copyright ® M.Ertl, with permission

Normal values were first established by Lieb et al. 1991 and are summarized in Table 2 (Lieb et al. 1991). For best visualization, the probe should be positioned as described above with a good view of the optic nerve in the axial plane. The focus zone should be set in at the level of the optic disc. In color-mode the pulse-repetition-frequency should be adjusted to register low-flow signals of the central retinal artery and the central retinal vein. Color gain has to be adapted according to the flow velocities as well as to reduce background noise and color signals generated by minimal eye movements (movement artifacts) (Fig. 4).

Orbital vessel	Mean ± SD Blood Flow, cm/s (Range)
Central retinal artery	10.3 ± 2.1 (6.4-17.2)
Central retinal vein	2.9 ± 0.73 (1.9-5.4)
Ophthalmic artery	31.4 ± 4.2 (23.5-39.8)
Posterior ciliary artery	12.4 ± 4.8 (1.4-22.7)

Table 2. Maximum systolic blood flow velocities in orbital vessels

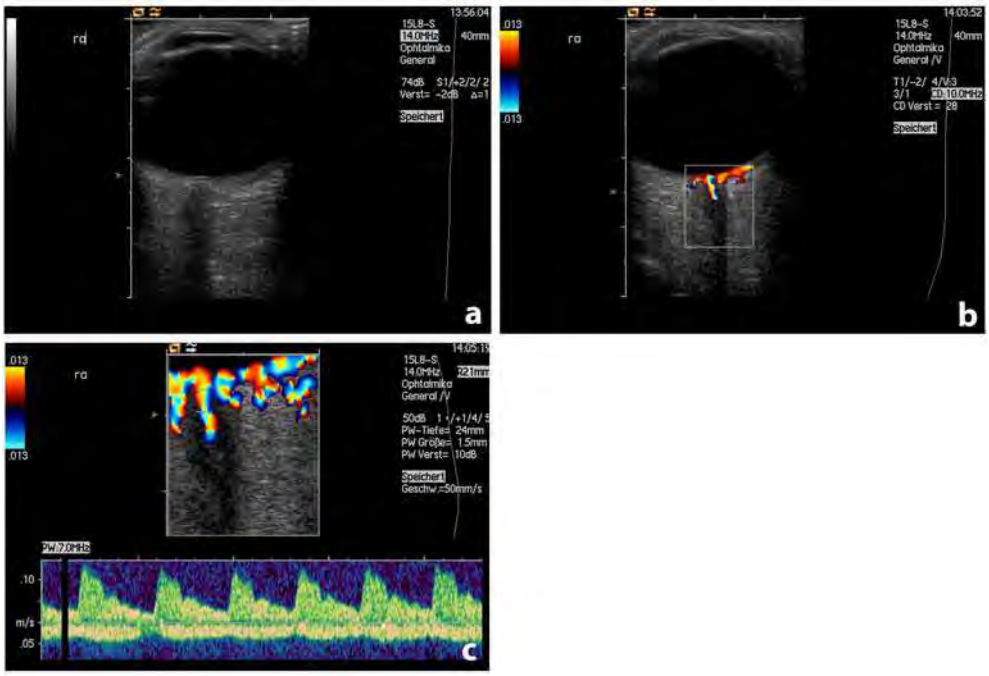

Fig. 4. Normal retrobulbar findings using high-resolution ultrasound in B-mode, Color-mode and spectral Doppler: B-mode: (a) The optic nerve presents as a hypoechogenic structure beyond the retina and the optic disc (b) Color-coded Duplex mode: central retinal artery (CRA) accompanying the optic nerve; section of retinal vessels from the posterior ciliary artery and the Circle of Zinn and Haller (c) Spectral-Doppler with Duplex-mode: normal spectrum of the CRA with peak-systolic velocity of 10.3 ± 2.1 cm/s and the underlying central retinal vein with peak-systolic velocity of 2.9 ± 0.73 cm/s (see also Table 2)

Alterations of flow in the CRA can occur in a variety of circumstances causing decreased visual acuity. In elderly patients this is mainly due to hypoperfusion or occlusion of the CRA caused by thrombo-embolic events (Brown and Magargal 1982; Gold 1977) or as CRA involvement in temporal arteritis (TA) (McFadzean 1998). In case of a central retinal artery occlusion (CRAO) a hyperechoic structure might be depicted in the optic nerve head, representing a fresh cholesterol embolus (Pfaffenbach and Hollenhorst 1972), which was termed "spot sign" by Schlachetzki and colleagues (Schlachetzki et al. 2010) (Fig. 5a). This finding is accompanied by absent flow in the CRA, whereas flow in the CRV is still detectable (Fig. 5b). The incidence of this phenomenon was first investigated by Foroozan et al. (Foroozan et al. 2002). In their retrospective study a "spot sign" occurred in 31% of cases of sudden ocular blindness. However, in an ongoing prospective study we found an incidence of up to 90% in patients with CRAO (Ertl et al., submitted).

In patients with TA, either reduced (Fig. 6a) or absent flow in CRA (Fig. 6c) was evident. The diagnosis of TA can by firmly supported by hypoechoic vasculitic vessel wall changes in the temporal arteries (so called "halo"-sign) (Arida et al. 2010), but the negative predictive

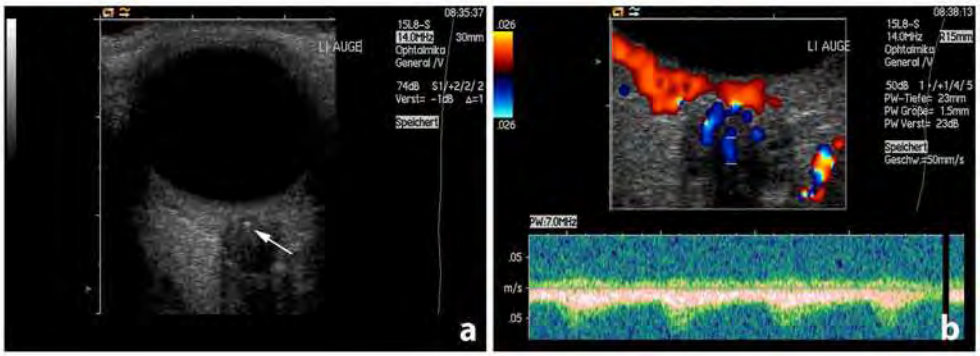

Fig. 5. Ultrasound findings in a patient with embolic central retinal artery occlusion. (a) B-mode: Hyperechogenic „spot sign" in the optic nerve head (arrow), representing an embolus in the distal CRA. (b) Color-Duplex- and spectral Doppler-mode: absent flow in the CRA with persistant perfusion of the central retinal vein

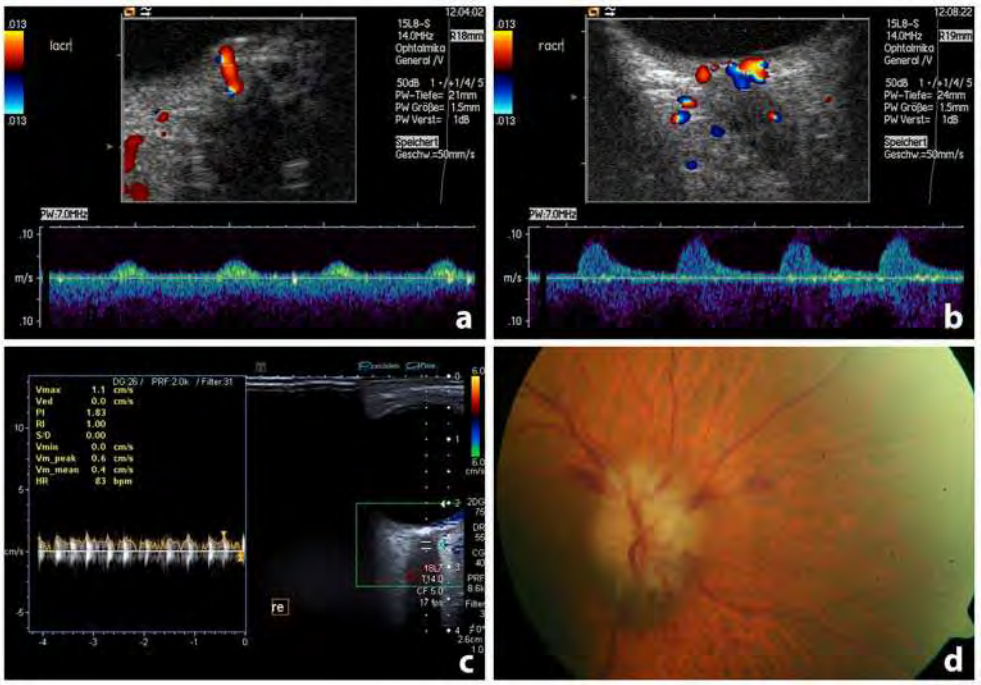

Fig. 6. Ultrasound and funduscopic findings in patients with central retinal artery occlusion due to temporal arteritis. (a) Patient 1: Color-Duplex- and spectral Doppler-mode: Pseudovenous flow in the affected CRA. (b) Patient 1: Color-Duplex- and spectral Doppler-mode: normal flow in the unaffected contralateral CRA. (c) Patient 2: Color-Duplex- and spectral Doppler-mode: zero-flow in the affected CRA. (d) Patient 2: fundoscopy: blurred rim of optic disc, optic disc edema and hyperemia, small splinter hemorrhage

value is only 68% and thus far not sufficient to rule out that disease. In patients with sudden retinal blindness and borderline symptoms for TA (only 2-3 positive ACR-criteria), a visible "spot sign" could be very helpful to rule out vasculitis, as could be demonstrated in the above-mentioned prospective study (Ertl et al., submitted).

Quick and sound differentiation of both etiologies is important for the initiation of specific treatments: thrombo-embolic occlusions need to be treated with platelet-inhibitors and high doses of cholesterol-lowering drugs, among control of additional cerebrovascular risk factors, whereas TA requires a sufficient and long-lasting steroid therapy to prevent secondary blindness of the unaffected eye.

Absent or reduced flow in the central retinal artery should lead to detailed workup looking for sources of cardiac emboli (ECG, cardiac echo, long term ECG, holter monitoring) and artherosclerosis (IMT using carotid ultrasound, presence of hemodynamically relevant carotid stenoses, etc.). Muller et al. found that in the majority of patients with ocular syndromes and ICA-stenosis greater than 50% (according to the NASCET-classification (Arning et al. 2010)), the ICA-stenosis was located on the ipsilateral side (Muller et al. 1993). Reversely, other studies could show a significant flow reduction in the ophthalmic artery and the central retinal artery in patients with ICA-stenosis of 70% or more (NASCET-classification) (Paivansalo et al. 1999). Consequently peak systolic velocity in the CRA and the posterior ciliary artery improved after carotid endarterectomy (Mawn et al. 1997).

A major advantage of OCCS is the visualization of structures lying behind the retina. Indirect fundoscopy and photodocumentation, common tools for ophthalmic investigations, are excellent methods to display pathologies up to the level of the retina or the choroid. Unfortunately, these techniques lack sensitivity or depth penetration beyond the choroid, and thus cannot elicitate the underlying cause of CRAO. Conventional A- and B-mode ultrasound systems for visualization of the globe and orbit used in opthmalmology have transmit frequencies between 10 to 20MHz. The last mentioned very high frequency has difficulties to penetrate beyond the choroid, and often these equipment lack Doppler or color-coded Doppler capabilities.

4. Assessment of intracranial pressure

Elevation of intracranial pressure (ICP) is a common phenomenon caused by a variety of neurological disorders as brain tumors, intracranial bleedings, or head trauma. Elevated ICP can be associated with life threatening conditions, e. g. brainstem herniation. Therefore these critically ill patients need to be monitored regularly to an extend of several times a day. Neuroimaging techniques as computed tomography (CT) and magnet resonance imaging (MRI) can help to assess raised ICP but have their diagnostic limitations as well (Hiler et al. 2006; Winkler et al. 2002) and require a potentially harmful patient transport. The gold standard for ICP measurement remain to be invasive intracranial devices: in addition to the need for neurosurgical operation and contraindications (e.g. thrombocytopenia) these methods are associated with certain complications as hemmorhage, infections and shunt malfunction (Brain Trauma Foundation 2000).

OCCS might be an interesting bedside alternative for follow-up examination of these critically ill patients. Several studies investigated the utility of measurements of the optic

nerve sheath diameter (ONSD) as an indicator for ICP measurement and management (Antonelli et al. 2009; Galetta et al. 1989; Hansen and Helmke 1997). The optic nerve as part of the central nervous system (CNS) is surrounded by cerebrospinal fluid (CSF), and thus communicates with the inner and outer subarachnoid space. Therefore, elevation of ICP can be assessed by measuring the ONSD, but also the intraocular prominence of the papilla.

The transducer is positioned as described in the technical segment, the beam is focused on the area behind the papilla and the optic nerve should be depicted in the axial plane. The optic nerve sheath is demonstrated as a thin bilateral hyperechogenic line surrounding the hypoechogenic optic nerve (Fig. 7). Due to trabecular structures in this compartment the optic nerve sheat (ONS) reflects a high fraction of ultrasonic energy, while the optic nerve runs in line with the ultrasound beam without reflection. The ONSD is measured 3 mm behind the optic disc by measuring the distance between the hyperechogenic borders of the ONS (Fig. 7). Most authors suggest normal values < 5,0 mm for patients > 1 year (Ballantyne et al. 2002; Blaivas et al. 2003; Girisgin et al. 2007; Helmke and Hansen 1996; Newman et al. 2002; Tayal et al. 2007; Tsung et al. 2005). A reliable cut-off value to predict an ICP > 20cmH_2O seems to be 5,7-6,0 mm with a sensitivity of 87-95% and a specificity of 79-100% (Geeraerts et al. 2007; Geeraerts et al. 2008; Soldatos et al. 2008; Watanabe et al. 2008). A meta-analysis of six studies having compared the reliability ONSD-measurements with classical invasive ICP monitoring in patients with intracranial hemorrhage and traumatic

Fig. 7. Measurement of optic nerve sheath diameter using ultrasound: the optic nerve sheath is demonstrated as a thin bilateral hyperechogenic line surrounding the hypoechogenic optic nerve. The diameter is calculated by the distance of the two cursors named "2". Normal values range from 5,7-6,0 mm with a definitely pathologic diameter in this patient

brain injury also showed a good accuracy of the ultrasound technique. The pooled sensitivity for the detection of raised ICP was 90% (Dubourg et al. 2011). In the hands of experienced sonographers and standardized examination procedures several studies demonstrated a high intra- and interoberserver reliability (Ballantyne et al. 2002; Helmke and Hansen 1996).

Apart from the above mentioned symptomatic causes of raised ICP in idiopathic intracranial hypertension (IIH), also often referred to as pseudotumor cerebri, the mechanism of ICP increase are still not well understood. Classically patients, often obese women during childbearing age, present with headache and loss of visual acuity or visual field deficits (Degnan and Levy 2011). Though not being a life threatening condition it is still associated with permanent, and partly severe, visual deficits (Friedman 2001; Lueck and McIlwaine 2002; Rowe and Sarkies 1998; Wall 2010). Visual symptoms are thought to be due to transient or permanent ischemic damage to the optic nerve caused by pressure (Jaggi et al. 2010; Wall 2010). Regular ophthalmologic follow-up examinations with visual acuity tests and fundoscopy are recommended, and patients often need to reduce weight and need to be treated with diuretic drugs (esp. acetazolamide), regular lumbar punctures or even operative shunt techniques.

Bäuerle et al. performed a prospective study to evaluate the immediate correlation of optic nerve diameter (OND), ONSD and papilledema with CSF-pressure reduction caused by therapeutic lumbar puncture in patients with IIH. Patients with IIH showed a significantly enlarged ONSD (6.4 ± 0.6 mm bilaterally) compared with healthy individuals (5.4 ± 0.5 mm) and a significant decrease in ONSD (right ONSD 5.8 ± 0.7 mm, $p < 0.004$; left ONSD 5.9 ± 0.7 mm, $p < 0.043$) 24 hours after lumbar puncture (Bauerle and Nedelmann 2011). In some patients with IIH, though, the ONSD did not change at all after lumbar puncture. This could be an effect of a postulated optic nerve compartment syndrome, an idea which first came up with persistent papilledema and visual disturbance in IIH-patients despite a functioning lumbo-peritoneal shunt (Kelman et al. 1991). Pathologic changes in trabecular structures of the ONS might interfere with the physiologic bidirectional flow of the CSF to the basal cisterns leading to persistent optic disc swelling (Killer et al. 2007). Years ago, Ossoinig suggested the use of the stretch-test (originally called the "30 degrees-test"): in widened optic nerve patterns due to fluid around the optic nerve parenchyma, a decreased optic nerve thickness was observed after performing the stretch-test (positive test result), whereas in solid lesions of the optic nerve no change of optic nerve thickness was found (negative test result) (Haritoglou et al. 2002). In patients with increased ICP due to any cause, either ophthalmoscopic evaluation or bilateral retrobulbar ultrasound is mandatory, as asymmetric and unilateral papilledemae in patients with IIH are well described (Seggia and De Menezes 1993). In addition, Bäuerle et al. did not find any correlation of papilledema and OND with CSF reduction in the short-term follow-up. Due to anatomic reasons the anterior segment of the ONSD responds quickly to changes of CSF pressure. This is a particular advantage of retrobulbar ultrasound compared to funduscopic re-evaluations, as changes behind the level of the optic disc cannot be visualized by the latter technique.

Although papilledema does not quickly respond to changes in CSF-pressure it is a manifestation of chronic ICP-increase (Villa et al. 1997) and other diseases as optic neuritis (Ashurst et al. 2010) for example.

To find a proper scanning plane, the probe is set as described above, with a good view on the optic nerve in the axial plane. The plane with the maximum disc elevation or excavation is selected, the measurements are performed in the "freeze" mode: disc elevation is quantified by putting the first caliper on the uppermost part of the swollen disc, the second caliper is positioned on the strongly reflecting line representing the lamina cribrosa (Fig. 8).

Fig. 8. Measurement of papilledema using ultrasound: disc elevation is quantified by putting the first caliper on the uppermost part of the swollen disc, the second caliper is positioned on the strongly reflecting line representing the lamina cribrosa

In patients with IIH the severity of disc swelling seems to have prognostic implications as well: in a combined retrospective and prospective study Wall et al. found a significant correlation of the severity of papilledema in patients with asymmetric papilledema and IIH, and their visual deficits (Wall and White 1998). This underlies the importance of regular follow-up quantification of optic disc swelling in these patients. Quantification of optic disc swelling is a reliable and reproducible technique, which was demonstrated by Tamburelli et al (Tamburrelli et al. 2000). In their study, data from patients with IIH taken by a confocal scanning laser ophthalmoscope were compared to ultrasound measurements demonstrating a good correlation. The mean depth measurements ranged from 0.68 to 2.01 mm (1.17 +/- 0.38 mm) and were comparable to those quantified by a confocal scanning laser ophthalmoscope (0.45 to 1.23 mm (0.93 +/- 0.24 mm)) (Tamburrelli et al. 2000).

Retrobulbar sonography is an inexpensive, quick, safe and reliable tool to monitor ICP changes. It is relatively easy to learn compared to transcranial duplex sonography, which improves inter-observer reliability. Still, in critically ill patients, invasive ICP measurement

techniques remain the gold standard but can be complemented by using orbital ultrasound. In IIH ONSD measurements are a suitable alternative to funduscopy for non-ophthalmologists in the long-term follow up.

5. Miscellaneous

In clinical practice the neurologist is sometimes faced with the problem to discriminate between papilledema and pseudopapilledema. Papilledema is a correlate for raised ICP. A complete diagnostic workup to find the underlying cause is mandatory.

A common cause for pseudopapilledema are optic disc drusen. They can be an incidental finding in routine ophthalmologic exams. Most optic disc drusen remain asymptomatic (Davis and Jay 2003), but upon thorough investigation visual field defects can be detected in up to 90% (Gaynes and Towle 1967; Savino et al. 1979). The funduscopic discrimination between papilledema and pseudopapilledema is not trivial, as the term "pseudopapilledema" already indicates. Typical signs of true papilledema in funduscopy are cotton wool spots, multiple hemorrhages around the disc, hyperemia, venous congestion, and exudates.

Drusen consist of calcific dispositions in the optic nerve head and can be depicted as high-reflectance spots in the anterior optic nerve, especially after lowering the gain. Therefore retrobulbar b-mode-sonography can help to confirm the diagnosis of optic disc drusen if the fundoscopy is not decisive (Fig. 9).

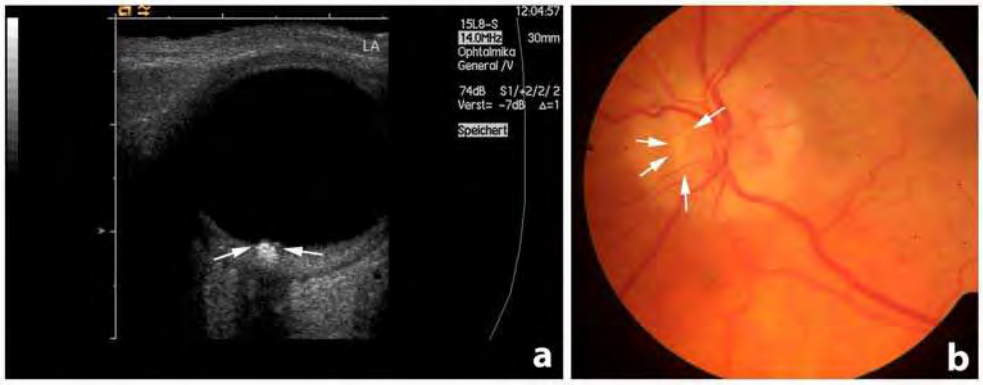

Fig. 9. Optic disc drusen seen in funduscopy and high-resolution ultrasound: (a) B-mode sonography: calcific dispositions in the optic nerve head representing optic disc drusen. (b) Fundoscopy: nasally located superficial drusen, blurred rim of optic disc, optic disc edema and hyperemia

6. References

American Institute of Ultrasound in Medicine (2000). "Section 7--discussion of the mechanical index and other exposure parameters. American Institute of Ultrasound in Medicine." *J Ultrasound Med* 19(2): 143-148, 154-168.

Antonelli, M., E. Azoulay, M. Bonten, J. Chastre, G. Citerio, G. Conti, D. De Backer, F. Lemaire, H. Gerlach, J. Groeneveld, G. Hedenstierna, D. Macrae, J. Mancebo, S. M. Maggiore, A. Mebazaa, P. Metnitz, J. Pugin, J. Wernerman and H. Zhang (2009). "Year in review in Intensive Care Medicine, 2008: I. Brain injury and neurology, renal failure and endocrinology, metabolism and nutrition, sepsis, infections and pneumonia." *Intensive Care Med* 35(1): 30-44.

Arida, A., M. Kyprianou, M. Kanakis and P. P. Sfikakis (2010). "The diagnostic value of ultrasonography-derived edema of the temporal artery wall in giant cell arteritis: a second meta-analysis." *BMC Musculoskelet Disord* 11: 44.

Arning, C., B. Widder, G. M. von Reutern, H. Stiegler and M. Gortler (2010). "[Revision of DEGUM ultrasound criteria for grading internal carotid artery stenoses and transfer to NASCET measurement]." *Ultraschall Med* 31(3): 251-257.

Ashurst, J., J. Schofer and P. Sierzenski (2010). "Unilateral papilledema: a case of optic neuritis diagnosed with bedside ocular sonography." *Del Med J* 82(4): 137-139.

Ballantyne, S. A., G. O'Neill, R. Hamilton and A. S. Hollman (2002). "Observer variation in the sonographic measurement of optic nerve sheath diameter in normal adults." *Eur J Ultrasound* 15(3): 145-149.

Bauerle, J. and M. Nedelmann (2011). "Sonographic assessment of the optic nerve sheath in idiopathic intracranial hypertension." *J Neurol*.

Blaivas, M., D. Theodoro and P. R. Sierzenski (2003). "Elevated intracranial pressure detected by bedside emergency ultrasonography of the optic nerve sheath." *Acad Emerg Med* 10(4): 376-381.

Brain Trauma Foundation (2000). "The Brain Trauma Foundation. The American Association of Neurological Surgeons. The Joint Section on Neurotrauma and Critical Care. Recommendations for intracranial pressure monitoring technology." *J Neurotrauma* 17(6-7): 497-506.

Brown, G. C. and L. E. Magargal (1982). "Central retinal artery obstruction and visual acuity." *Ophthalmology* 89(1): 14-19.

Davis, P. L. and W. M. Jay (2003). "Optic nerve head drusen." *Semin Ophthalmol* 18(4): 222-242.

Degnan, A. J. and L. M. Levy (2011). "Pseudotumor Cerebri: Brief Review of Clinical Syndrome and Imaging Findings." *AJNR Am J Neuroradiol*.

Dubourg, J., E. Javouhey, T. Geeraerts, M. Messerer and B. Kassai (2011). "Ultrasonography of optic nerve sheath diameter for detection of raised intracranial pressure: a systematic review and meta-analysis." *Intensive Care Med*.

Food and Drug Administration (2008). "Food and Drug Administration: Information for Manufacturers Seeking Clearance of Diagnostic Ultrasound Systems and Transducers."

Foroozan, R., P. J. Savino and R. C. Sergott (2002). "Embolic central retinal artery occlusion detected by orbital color Doppler imaging." *Ophthalmology* 109(4): 744-747; discussion 747-748.

Friedman, D. I. (2001). "Papilledema and pseudotumor cerebri." *Ophthalmol Clin North Am* 14(1): 129-147, ix.

Galetta, S., S. F. Byrne and J. L. Smith (1989). "Echographic correlation of optic nerve sheath size and cerebrospinal fluid pressure." *J Clin Neuroophthalmol* 9(2): 79-82.

Gaynes, P. M. and P. A. Towle (1967). "Hemorrhage in hyaline bodies (drusen) of the optic disc during an attack of migraine." *Am J Ophthalmol* 63(6): 1693-1696.

Geeraerts, T., Y. Launey, L. Martin, J. Pottecher, B. Vigue, J. Duranteau and D. Benhamou (2007). "Ultrasonography of the optic nerve sheath may be useful for detecting raised intracranial pressure after severe brain injury." *Intensive Care Med* 33(10): 1704-1711.

Geeraerts, T., S. Merceron, D. Benhamou, B. Vigue and J. Duranteau (2008). "Non-invasive assessment of intracranial pressure using ocular sonography in neurocritical care patients." *Intensive Care Med* 34(11): 2062-2067.

Girisgin, A. S., E. Kalkan, S. Kocak, B. Cander, M. Gul and M. Semiz (2007). "The role of optic nerve ultrasonography in the diagnosis of elevated intracranial pressure." *Emerg Med J* 24(4): 251-254.

Gold, D. (1977). "Retinal arterial occlusion." *Trans Sect Ophthalmol Am Acad Ophthalmol Otolaryngol* 83(3 Pt 1): OP392-408.

Hansen, H. C. and K. Helmke (1997). "Validation of the optic nerve sheath response to changing cerebrospinal fluid pressure: ultrasound findings during intrathecal infusion tests." *J Neurosurg* 87(1): 34-40.

Haritoglou, C., H. Herzum, O. Ehrt, K. C. Ossoinig and A. Kampik (2002). "[Echographic differential diagnosis of optic nerve widening]." *Ophthalmologe* 99(7): 559-565.

Helmke, K. and H. C. Hansen (1996). "Fundamentals of transorbital sonographic evaluation of optic nerve sheath expansion under intracranial hypertension II. Patient study." *Pediatr Radiol* 26(10): 706-710.

Hiler, M., M. Czosnyka, P. Hutchinson, M. Balestreri, P. Smielewski, B. Matta and J. D. Pickard (2006). "Predictive value of initial computerized tomography scan, intracranial pressure, and state of autoregulation in patients with traumatic brain injury." *J Neurosurg* 104(5): 731-737.

Jaggi, G. P., M. Harlev, U. Ziegler, S. Dotan, N. R. Miller and H. E. Killer (2010). "Cerebrospinal fluid segregation optic neuropathy: an experimental model and a hypothesis." *Br J Ophthalmol* 94(8): 1088-1093.

Kelman, S. E., R. C. Sergott, G. A. Cioffi, P. J. Savino, T. M. Bosley and M. J. Elman (1991). "Modified optic nerve decompression in patients with functioning lumboperitoneal shunts and progressive visual loss." *Ophthalmology* 98(9): 1449-1453.

Killer, H. E., G. P. Jaggi, J. Flammer, N. R. Miller, A. R. Huber and A. Mironov (2007). "Cerebrospinal fluid dynamics between the intracranial and the subarachnoid space of the optic nerve. Is it always bidirectional?" *Brain* 130(Pt 2): 514-520.

Lieb, W. E., S. M. Cohen, D. A. Merton, J. A. Shields, D. G. Mitchell and B. B. Goldberg (1991). "Color Doppler imaging of the eye and orbit. Technique and normal vascular anatomy." *Arch Ophthalmol* 109(4): 527-531.

Lizzi, F. L., A. J. Packer and D. J. Coleman (1978). "Experimental cataract production by high frequency ultrasound." *Ann Ophthalmol* 10(7): 934-942.

Lueck, C. and G. McIlwaine (2002). "Interventions for idiopathic intracranial hypertension." *Cochrane Database Syst Rev*(3): CD003434.

Mawn, L. A., T. R. Hedges, 3rd, W. Rand and P. A. Heggerick (1997). "Orbital color Doppler imaging in carotid occlusive disease." *Arch Ophthalmol* 115(4): 492-496.

McFadzean, R. M. (1998). "Ischemic optic neuropathy and giant cell arteritis." *Curr Opin Ophthalmol* 9(6): 10-17.

Muller, M., K. Wessel, E. Mehdorn, D. Kompf and C. M. Kessler (1993). "Carotid artery disease in vascular ocular syndromes." *J Clin Neuroophthalmol* 13(3): 175-180.

Newman, W. D., A. S. Hollman, G. N. Dutton and R. Carachi (2002). "Measurement of optic nerve sheath diameter by ultrasound: a means of detecting acute raised intracranial pressure in hydrocephalus." *Br J Ophthalmol* 86(10): 1109-1113.

Paivansalo, M., K. Riihelainen, T. Rissanen, I. Suramo and L. Laatikainen (1999). "Effect of an internal carotid stenosis on orbital blood velocity." *Acta Radiol* 40(3): 270-275.

Pfaffenbach, D. D. and R. W. Hollenhorst (1972). "Morbidity and survivorship of patients with embolic cholesterol crystals in the ocular fundus." *Trans Am Ophthalmol Soc* 70: 337-349.

Rowe, F. J. and N. J. Sarkies (1998). "Assessment of visual function in idiopathic intracranial hypertension: a prospective study." *Eye (Lond)* 12 (Pt 1): 111-118.

Savino, P. J., J. S. Glaser and M. A. Rosenberg (1979). "A clinical analysis of pseudopapilledema. II. Visual field defects." *Arch Ophthalmol* 97(1): 71-75.

Schlachetzki, F., S. Boy, U. Bogdahn, H. Helbig and M. A. Gamulescu (2010). "The Retrobulbar "Spot Sign" - Ocular Sonography for the Differential Diagnosis of Temporal Arteritis and Sudden Blindness." *Ultraschall Med*.

Seggia, J. C. and M. L. De Menezes (1993). "[Pseudotumor cerebri without optic papilledema]." *Arq Neuropsiquiatr* 51(4): 511-518.

Soldatos, T., D. Karakitsos, K. Chatzimichail, M. Papathanasiou, A. Gouliamos and A. Karabinis (2008). "Optic nerve sonography in the diagnostic evaluation of adult brain injury." *Crit Care* 12(3): R67.

Tamburrelli, C., T. Salgarello, C. G. Caputo, A. Giudiceandrea and L. Scullica (2000). "Ultrasonographic evaluation of optic disc swelling: comparison with CSLO in idiopathic intracranial hypertension." *Invest Ophthalmol Vis Sci* 41(10): 2960-2966.

Tayal, V. S., M. Neulander, H. J. Norton, T. Foster, T. Saunders and M. Blaivas (2007). "Emergency department sonographic measurement of optic nerve sheath diameter to detect findings of increased intracranial pressure in adult head injury patients." *Ann Emerg Med* 49(4): 508-514.

Toms, D. A. (2006). "The mechanical index, ultrasound practices, and the ALARA principle." *J Ultrasound Med* 25(4): 560-561; author reply 561-562.

Tranquart, F. O., O. Bergès, P. Koskas, S. Arsene, C. Rossazza, P.-J. Pisella and L. a. Pourcelot (2003). "Color doppler imaging of orbital vessels: Personal experience and literature review." *Journal of Clinical Ultrasound* 31(5): 258-273.

Tsung, J. W., M. Blaivas, A. Cooper and N. R. Levick (2005). "A rapid noninvasive method of detecting elevated intracranial pressure using bedside ocular ultrasound: application to 3 cases of head trauma in the pediatric emergency department." *Pediatr Emerg Care* 21(2): 94-98.

Villa, A. M., S. F. Anderson and R. E. Abundo (1997). "Bilateral disc edema in retinitis pigmentosa." *Optom Vis Sci* 74(3): 132-137.

Wall, M. (2010). "Idiopathic intracranial hypertension." *Neurol Clin* 28(3): 593-617.

Wall, M. and W. N. White, 2nd (1998). "Asymmetric papilledema in idiopathic intracranial hypertension: prospective interocular comparison of sensory visual function." *Invest Ophthalmol Vis Sci* 39(1): 134-142.

Watanabe, A., H. Kinouchi, T. Horikoshi, M. Uchida and K. Ishigame (2008). "Effect of intracranial pressure on the diameter of the optic nerve sheath." *J Neurosurg* 109(2): 255-258.

Winkler, F., S. Kastenbauer, T. A. Yousry, U. Maerz and H. W. Pfister (2002). "Discrepancies between brain CT imaging and severely raised intracranial pressure proven by ventriculostomy in adults with pneumococcal meningitis." *J Neurol* 249(9): 1292-1297.

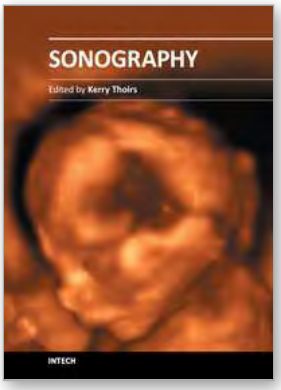

Sonography

Edited by Dr. Kerry Thoirs

ISBN 978-953-307-947-9
Hard cover, 346 pages
Publisher InTech
Published online 03, February, 2012
Published in print edition February, 2012

Medical sonography is a medical imaging modality used across many medical disciplines. Its use is growing, probably due to its relative low cost and easy accessibility. There are now many high quality ultrasound imaging systems available that are easily transportable, making it a diagnostic tool amenable for bedside and office scanning. This book includes applications of sonography that can be used across a number of medical disciplines including radiology, thoracic medicine, urology, rheumatology, obstetrics and fetal medicine and neurology. The book revisits established applications in medical sonography such as biliary, testicular and breast sonography and sonography in early pregnancy, and also outlines some interesting new and advanced applications of sonography.

InTech Europe
University Campus STeP Ri
Slavka Krautzeka 83/A
51000 Rijeka, Croatia
Phone: +385 (51) 770 447
Fax: +385 (51) 686 166
www.intechopen.com

InTech China
Unit 405, Office Block, Hotel Equatorial Shanghai
No.65, Yan An Road (West), Shanghai, 200040, China
中国上海市延安西路65号上海国际贵都大饭店办公楼405单元
Phone: +86-21-62489820
Fax: +86-21-62489821

5

Assessment of Endothelial Function Using Ultrasound

Lee Stoner and Manning J. Sabatier
[1]*Massey University,*
[2]*Clayton State University,*
[1]*New Zealand*
[2]*USA*

1. Introduction

The pathological complications of atherosclerosis, namely heart attacks and strokes, remain the leading cause of mortality in the Western world (Lloyd-Jones & Adams *et al.* 2010). Preceding atherosclerosis is endothelial dysfunction (Ross 1993; Cohn 1999; Quyyumi 2003). The endothelium comprises a continuous monolayer of cells which separate the vascular wall from the circulation (Lerman & Zeiher 2005). Disruption of this essential monolayer is thought to occur early in the pathogenesis of cardiovascular disease (CVD). There is, therefore, interest in the application of non-invasive clinical tools to assess the function and health of this essential monolayer.

The flow-mediated dilation (FMD) test is the standard tool used to assess endothelial function (Celermajer & Sorensen *et al.* 1992). Reduced FMD is an early marker of atherosclerosis (Celermajer & Sorensen *et al.* 1992), has been noted for its capacity to predict future CVD events (Schroeder & Enderle *et al.* 1999; Neunteufl & Heher *et al.* 2000; Heitzer & Schlinzig *et al.* 2001; Murakami & Arai 2001; Yoshida & Kawano *et al.* 2006; Inaba & Chen *et al.* 2010), and an impaired vascular response has also been demonstrated in children as young as 7 years old with familial hypercholesterolemia (Sorensen & Celermajer *et al.* 1994). This review discusses the measurement of endothelial function, with a focus on the FMD technique.

2. The vascular endothelium

From the lumen to the outer wall all arteries are composed of an intima, media, and adventitia (see Fig. 1). The adventitia is the outer most layer, and is mainly composed of connective tissue that maintains vessel shape and limits distention. The media is comprised mainly of vascular smooth muscle cells that regulate blood flow by vasoconstriction or vasodilation. The intima is the inner most lining of the vessel, and consists of the endothelium and underlying connective tissue.

Vascular endothelial cells essentially have the same characteristics as all the cells of the human body: cytoplasm and organelles surrounding a nucleus and contained by the cellular membrane. Endothelial cells form a continuous flat mono-layer that cover the vascular lumina throughout the arterial tree. The endothelium is mechanically and metabolically

strategically located, separating the vascular wall from the circulation and the blood components (Lerman & Zeiher 2005).

The vascular endothelium utilizes autocrine, paracrine, and classical endocrine signaling to promote vascular homeostasis (Luscher & Barton 1997). These cells are capable of producing a variety of agonistic and antagonistic molecules, including vasodilators and vasoconstrictors, pro-coagulants and anti-coagulants, inflammatory and anti-inflammatory, fibrinolytics and anti-fibrinolytics, oxidizing and anti-oxidizing, and many others (Luscher & Barton 1997).

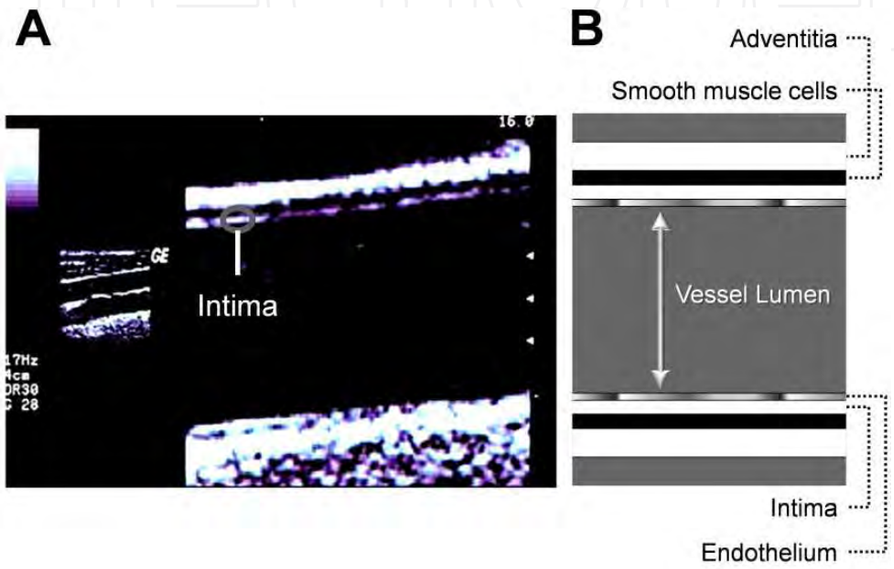

Fig. 1. *Anatomy of the arterial wall.* (A) A conduit artery imaged in the longitudinal plane using ultrasound. (B) The layers comprising the wall of an artery. Endothelial cells form a continuous layer lining the intima throughout the arterial tree.

2.1 Endothelial dysfunction and atherosclerosis

Upsetting the delicate balance of functions performed by the endothelium initiates a number of events that promote atherosclerosis, the precursor to CVD. Although atherosclerosis is commonly described as the presence of plaques that obstruct the lumen of the conduit arteries, endothelial dysfunction precedes plaque formation (Gibbons & Dzau 1994; Ross 1999; Nissen & Yock 2001). Reduced endothelial responses can be observed early in the course of atherogenesis, preceding angiographic or ultrasonic evidence of atherosclerotic plaque (Luscher & Barton 1997).

Disruption of the functional integrity of the vascular endothelium plays an integral role in all stages of atherogenesis, ranging from lesion initiation to plaque rupture. Endothelial dysfunction leads to increased permeability to lipoproteins, foam cell formation, T-cell activation, and smooth muscle migration into the arterial wall (Ross 1999). The first step in the formation of the plaque occurs when the inflammatory response is incited and fatty streaks appear. If these conditions persist, fatty streaks progress and the plaques become vulnerable to rupture.

Parameter	Recommendations
Subject preparation	Fast overnight prior to testing, and avoid exercise during the preceding 24 hrs. Refrain from taking drugs with known vascular effects. Rest supine for 20 mins in a quiet, temperature controlled room at 21 °C. Test conducted with subjects in the supine position. Artery segment of interest must remain at or below heart level. Women should be tested during the early follicular phase of the ovarian cycle (i.e., day 7-14 of the ovarian cycle). For successive tests, subjects should report at the same time of day to reduce error associated with circadian variation.
Probe selection	A higher frequency probe (12MHz) should be used for superficial arteries (e.g., brachial, radial or posterior tibialis). A lower frequency probe (7.5MHz) should be used for deeper arteries (e.g., common femoral). The same transducer should be used for all subjects in a given study.
Probe placement	Mark anatomical placement for studies with repeated measurements. Use a probe holding device to maintain image focus.
Ultrasound Settings	Standardize ultrasound global (acoustic output, gain, dynamic range, gamma, rejection) and probe-dependent (zoom factor, edge enhancement, frame averaging, target frame rate) settings.
Artery	Artery selection should be made based on the population of interest, e.g., lower limb arteries should be measured in patients with SCI.
Diameters (general)	Extend across the entire imaging plane to minimize skewing prior to focusing. Use automated or semi-automated image analysis software. Use mean or end-diastolic diameters.
Baseline diameters	Collect prior to cuff inflation. Subject should hold breath during measurement. Collect and average 3 * 10 sec measurements.
Peak diameters	Capture diameters continuously to ensure true peak diameter.
Blood velocity	The beam-vessel angle must be $\leq$60°. Measure continuously. Time-averaged maximum velocities are more accurate and reproducible than time-averaged mean velocities.
Shear Stimulus	Shear rate is a suitable substitute for shear stress. Diameters and velocities must be captured continuously to estimate shear. Shear rates should be presented as an integral, we recommend 40 secs post-ischemia. Attention should be paid to secondary flow phenomena, e.g., turbulence and velocity acceleration.
Analysis	Present FMD in absolute (mm) and relative (%) terms. The shear rate stimuli should be presented for each research setting. Do not normalize FMD to shear rate as ratio or using ANCOVA. HLM can be used to statistically account for shear rate in the evaluation of FMD.

Table 1. *Recommendations for FMD Testing*

2.2 Stimuli regulating endothelial function

The haemodynamic conditions inside blood vessels lead to the development of superficial stress near the vessel walls which can be divided into two categories: 1) circumferential stress due to pulse pressure variation inside the vessel, and 2) shear stress (Nerem 1992; Papaioannou & Stefanadis 2005; Papaioannou & Karatzis *et al.* 2006). Circumferential stress acts perpendicular to the vessel wall, whereas shear stress acts at a tangent to the wall to create a frictional force at the surface of the endothelium. Circumferential stress applies stress to all layers of the vessel wall (intima, media and adventia), while shear stress is applied principally at the endothelial surface. Shear stress is considered to be the primary stimulus regulating endothelial cell function.

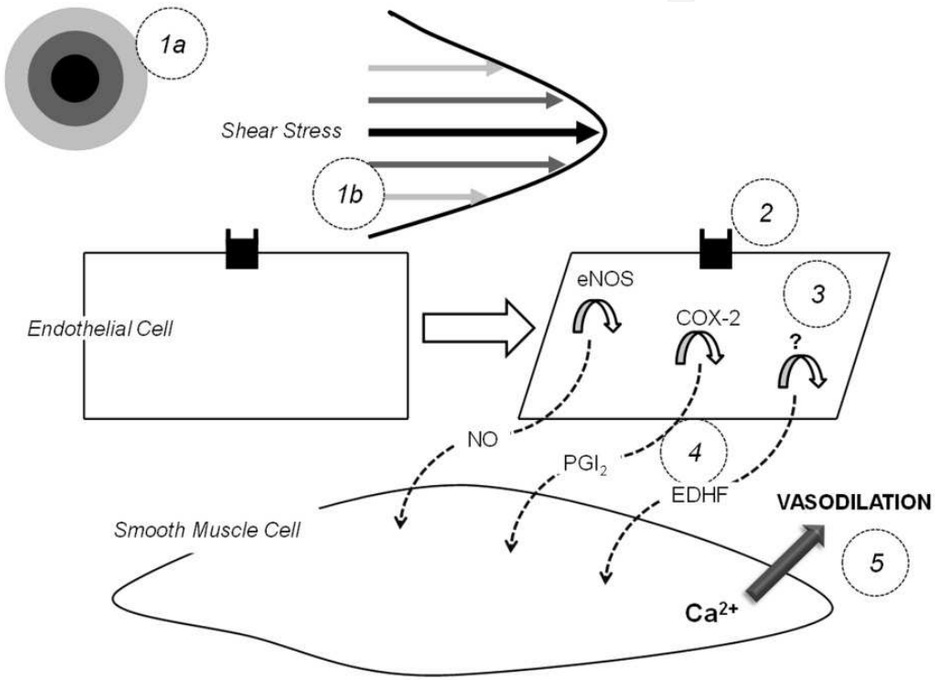

Fig. 2. *Endothelium-dependent dilation.* (1) Blood flowing through an artery creates a shearing stress at the endothelial surface. A composite of superimposed concentric circles is shown in 1a (i.e., transverse plane) to correspond with the gradient of increasing RBC velocity from the periphery to the center of the lumen. RBC velocity is represented as a parabola (i.e., longitudinal plane) in 1b using the same color coding as in 1a. The magnitude of the parabola (left to right) corresponds with the gradient of increasing RBC velocity from the periphery to the center of the lumen. (2) Shear stress-induced deformation of the endothelial cells is detected by mechanoreceptors on the cell membrane. (3) In response to mechanotransduced shear stress, a signaling cascade results in the production of NO, PGI_2 and EDHF . (4) The vasodilators diffuse cross the interstitial space and enter the vascular smooth muscle cells. (5) A signaling cascade is initiated which lowers Ca^{2+} concentration and results in smooth muscle cell relaxation (i.e., vasodilation). Ca^{2+} = calcium; eNOS = endothelial NO synthase; COX-2 = cyclooxygenase; EDHF = endothelial-derived hyperpolarizing factor; NO = nitric oxide; PGI_2 = prostaglandins; RBC = red blood cell.

Shear stress is primarily related to movement of red blood cells close to the endothelial layer (represented by bottom and top-most arrows in Fig. 2.1b). As fluid particles "travel" parallel to the vessel wall, their average velocity increases from a minimum at the wall to a maximum value at some distance from the wall, resulting in a gradient of velocities that form concentric circles in the lumen of the vessel (Fig. 2.1a). This shearing stress therefore acts at a tangent to the wall to create a frictional force at the surface of the endothelium. Although shear stress has a very small magnitude in comparison to circumferential stress, the endothelial cells are equipped with numerous mechanosensors to detect this stress (Olesen & Clapham *et al.* 1988; Davies 1995; Barakat & Leaver *et al.* 1999; Shyy & Chien 2002; Fleming & Busse 2003; Labrador & Chen *et al.* 2003). To maintain physiological levels of vessel wall shear stress, vascular tissues respond to changes in shear stress with acute adjustments in vascular tone (through vasodilation) (Langille & O'Donnell 1986). Vasodilation reflects alterations in the rate of production of endothelial-derived mediators, including nitric oxide (NO), prostacyclin (PGI_2) and endothelium derived hyperpolarizing factor (EHRF), which act locally to modulate vascular smooth muscle tone (see Fig. 2).

3. Flow-mediated dilation testing

In 1970, Rodbard (Rodbard 1970) proposed that the endothelium may sense and respond to shear stress generated by flowing blood. In 1980, Furchgott and Zawadski (Furchgott & Zawadzki 1980) discovered that agonist-mediated vasodilation requires participation by the endothelium. The dependence of FMD on an intact endothelium was subsequently shown to occur in large-conduit arteries as well as in resistance-sized vessels (Rubanyi & Romero *et al.* 1986). More recent studies have demonstrated that vasodilation is directly proportional to increases in shear stress (Koller & Sun *et al.* 1993; Moncada & Higgs 1993).

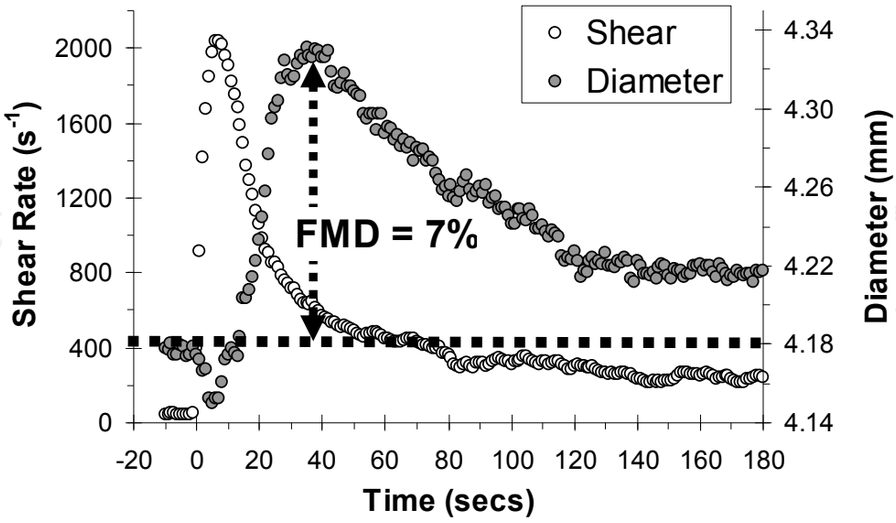

Fig. 3. *Shear rate and diameter responses to 5 minutes ischemia.* The horizontal line represents resting diameter. Flow-mediated dilation (FMD) is typically represented as the peak percentage increase in diameter above rest. Note that the peak diameter occurs ~40 sec whereas the bulk of the hyperemic (shear) response occurs within the initial 20 sec.

Endothelium-dependent agonists, such as acetylcholine, can be used to induce a dilatory response (Furchgott & Zawadzki 1980). However, such practice is invasive and often unpractical, especially for use within clinical settings. Alternatively, the FMD test is a *non-invasive* method (Fig. 3). Typically, a pneumatic tourniquet will be placed around the forearm approximately 5cm below the olecranon process and inflated to a super-systolic blood pressure for 5 minutes. Rapid deflation of the tourniquet instigates increased blood flow (reactive hyperemia) to the oxygen starved forearm muscles, with a subsequent increase in flow through the upstream brachial artery. The flow-induced increase in shear stress results in vasodilation. FMD is typically expressed as the percentage increase in the artery diameter above baseline. Table 1 provides a list of recommendations to consider when conducting this test.

4. Ultrasound

Arndt (Arndt & Klauske *et al.* 1968), in 1968, was the first to apply ultrasound to [carotid] arterial measurements. Since then, the advancement of ultrasound technology has had a profound impact on the capacity of researchers and clinicians alike to non-invasively assess endothelial function and health. Most commercial ultrasound machines now provide duplex Doppler functionality; that is, they can simultaneously image and measure blood velocity in conduit arteries in real-time. Duplex Doppler functionality offers immense potential for tracking vascular mechanical and functional changes.

4.1 Arterial diameter measurements

Conventionally, two-dimensional brightness mode (B-mode) is used to visualize, in real-time, the ultrasound echo amplitude distribution in a tomographic plane. The arteries of interest, except for the aorta, are typically within a depth range of 30 mm; a high carrier frequency (typically 7–13 MHz) is used to provide detailed images of peripheral arteries, in both longitudinal and cross-sectional views (Hoeks & Brands *et al.* 1999). Ultrasound wave reflections will only have a prominent amplitude if they originate from acoustic interfaces with a substantial change in acoustic impedance and, are oriented perpendicular (i.e., at a 90 degree angle) to the ultrasound beam direction. Therefore, in the cross-sectional view the lateral segments of the artery wall are blurred, with relatively low amplitude for the anterior and posterior lumen-wall transitions. In the longitudinal view, both walls will show up distinctly over a certain range, provided that the arterial segment considered is straight and without branches (Fig. 1). The transition of the inner layer of the wall, the intima to the lumen, induces a weak signal while the outer layer, the adventitia, results in reflections with high amplitude. The layer in between, the media, has a relatively low reflectivity and appears as a hypo-echoic band in images obtained with ultrasound systems with sufficient resolution.

A number of laboratories, using commercial or custom edge-detection software, are now able to make semi-automated diameter measurements (Woodman & Playford *et al.* 2001; Craiem & Chironi *et al.* 2007; Peretz & Leotta *et al.* 2007; Padilla & Johnson *et al.* 2008; Pyke & Jazuli 2011; Thijssen & Tinken *et al.* 2011). The authors of this chapter, using custom edge-detection software, are able to make thirty diameter measurements per second. A video capture device is used to make recordings at a rate of 30 frames / second. These video files are broken down and converted into JPEG (Joint Photographic Experts Group) images, which provides

comparable accuracy for ultrasound image measurements compared to the DICOM (Digital Image and Communications in Medicine) standard (Hangiandreou & James *et al.* 2002). The images are analyzed offline using semi-automated edge-detection software (Fig. 4) custom written to interface with National Instruments LabVIEW software (National Instruments, Austin, TX, USA) (Sabatier & Stoner *et al.* 2006; Stoner & Sabatier *et al.* 2006). Custom-written Visual Basic Code is used to fit peaks and troughs to diameter waveforms in order to calculate diastolic, systolic, and mean diameters. The authors use mean diameters for analysis. Traditionally, end-diastolic diameters were used to calculate FMD, owing to: 1) FMD measurements that incorporate non-end-diastolic diameters may introduce measurement errors due to fixed vessel structural issues, and 2) prior to the advent of automated image analysis software, mean diameter measurements were beyond the technical capabilities of most research units. A recent study indicates that calculating FMD based on mean diameters yields comparable results to calculations based on end-diastolic diameters (Kizhakekuttu & Gutterman *et al.* 2010). The within-session $SEM_{3,1}$ for the described set-up is 0.046 mm; between-day coefficients of variation are 2.4-2.7% (Stoner & Sabatier *et al.* 2004).

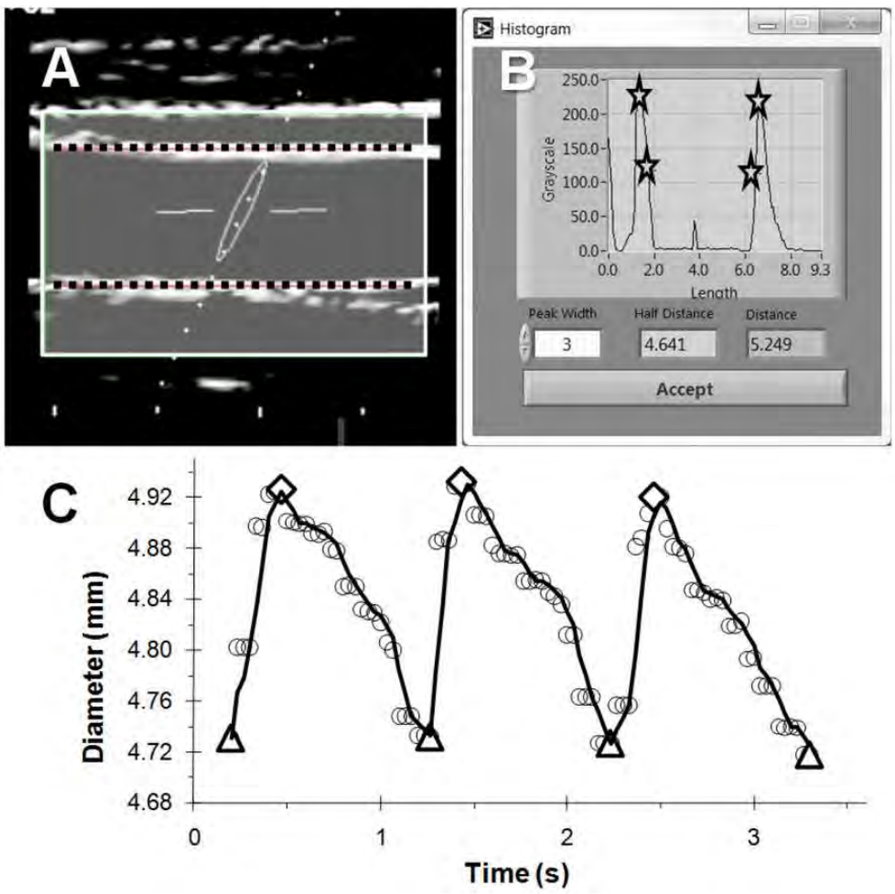

Fig. 4. *Semi-automated diameter analysis.* (A) B-mode image of the brachial artery with a region of interest (ROI) denoted by a selection box. The histogram (B) corresponds with the average pixel brightness of rows in the ROI in (A). The peaks (stars) correspond with the vessel walls. (C) Diameter waveforms from three cardiac cycles. Triangles represent diastole and diamonds represent systole.")

4.1.1 Measurement protocol

When imaging a vessel care should be taken to ensure that the vessel clearly extends across the entire [un-zoomed] plane to minimize likelihood of skewing the vessel walls. The ultrasound transducer should then be adjusted until the vessel walls appear thickest. Ultrasound global (acoustic output, gain, dynamic range, gamma, rejection) and probe-dependent (zoom factor, edge enhancement, frame averaging, target frame rate) settings should be standardized, especially for a given study. Alterations to probe selection and optimization settings – particularly probe selection – can have a significant impact on measurement precision (Stoner, in press). Figure 5 shows two diameter waveforms, both measured on the same subject within 10 minutes, albeit with different probes (11MHz and 6.6MHz); despite all other global and probe-dependent settings being equal, the 6.6mhz resulted in bias for smaller diameters. To ensure image focus is maintained and that diameter waveforms are stable, the ultrasound probe needs to be fixed in place using a probe holding device. The stability of diameter waveforms is also affected by rhythmic breathing patterns; to ensure optimal quality of diameter waveforms, the subject should ideally hold their breath during image acquisition.

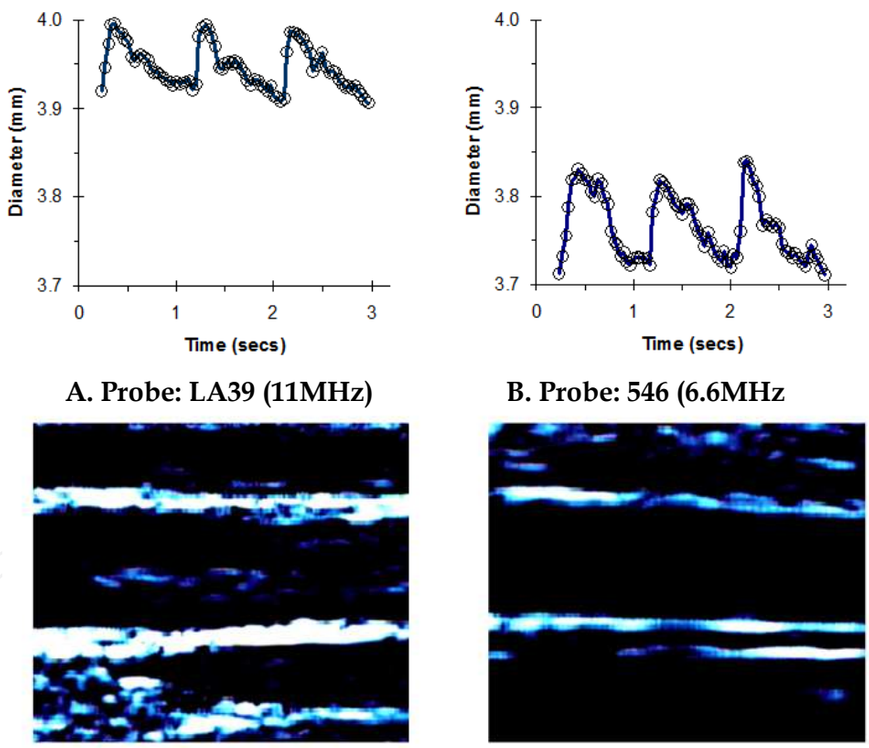

Fig. 5. *Brachial artery diameter waveforms using a GE 11MHz (A) and 6.6MHz (B) probe.* Measurements were taken from the same subjects within 10 minutes of one another. Note the bias towards smaller diameters using the 6.6Mhz probe.

4.1.2 Probe selection

Selection of the appropriate ultrasound probe is dependent on the vessel being imaged. The higher the probe frequency the greater the axial resolution, but this comes at the cost of

tissue penetration (Roelandt & van Dorp *et al.* 1976; Lieu 2010). The operator should use the highest frequency that has adequate tissue penetration to clearly resolve the structure of interest. For superficial arteries, e.g., brachial, radial and posterior tibialis, a 12Mhz probe will allow adequate penetration and will provide optimal axial resolution. When imaging deeper arteries, e.g., common femoral, a 12MHz probe will not provide sufficient penetration, and a lower frequency probe (e.g., 7.5MHz) is recommended. However, the use of a lower frequency probe will yield a lower axial resolution, and will limit the capacity to discern small changes in vessel diameter. The same transducer should be used across subjects for a given study to maximize statistical power (see Fig. 5).

4.2 Blood velocity measurements

Ultrasound assessments of blood velocity have been favorably compared to magnetic resonance imaging, which is capable of higher resolution but is much more costly (Nesbitt & Schmidt-Trucksass *et al.* 2000). With ultrasound, blood velocity is calculated by measuring the Doppler shift, which results from a change in the frequency of a wave due to the motion of the wave source or receiver, or in the case of a reflected wave, motion of the reflector. The Doppler shift is dependent on the insonating frequency, the velocity of moving blood, and the angle between the sound beam and direction of moving blood, as expressed in the Doppler equation:

$$Df = \frac{2 \cdot f \cdot v \cdot \cos q}{c} \tag{1}$$

where: Df is the Doppler shift frequency (the difference between transmitted and received frequencies), f is the transmitted frequency, v is the blood velocity, q is the angle between the sound beam and the direction of moving blood, and c is the speed of sound. The equation can be rearranged to solve for blood velocity, and this is the value calculated by the ultrasound machine:

$$v^{\circ} = \frac{Df \cdot c}{2 \cdot f \cdot \cos q} \tag{2}$$

Since red blood cells travel at different speeds, even for a small measuring volume, there will be a range of blood velocities for a given unit of time. Per cardiac cycle, Doppler ultrasound systems measure minimum, maximum, and mean blood velocities. The maximum velocities represent the fastest moving blood cells flowing through the center of the vessel, whereas mean-velocities represent the average speed of blood cells from across the vessel. Mean velocities tend to be limited by incomplete sampling of Doppler shifts across the full width of the artery (Thrush & Hartshorne 2004). Time-averaged maximum velocities are more accurate and reproducible, even though they may lead to overestimations of blood flow by approximately 40% (Olive & Slade *et al.* 2003).

4.2.1 Measurement protocol

Most commercial ultrasound units come equipped with software to automatically calculate blood velocities. These automated calculations are typically limited to each heart beat. When making simultaneous diameter and blood velocity measurements, a compromise has to be

made. An optimal B-Mode image is obtained when the ultrasound probe is perpendicular (90 degrees) to the imaged vessel, whereas an optimal velocity signal is obtained with a beam-vessel angel $\leq$60°. Error associated with incorrect estimation of insonation angle increases exponentially with angles $\geq$60° (Thrush & Hartshorne 2004). For further discussion on this topic see Thijssen et al. 2011 (Thijssen & Black *et al.* 2011).

4.3 Measurement location

For two decades brachial artery FMD has been widely used as a global endothelial health index (Celermajer & Sorensen *et al.* 1992). However, the brachial artery may not adequately characterize global endothelial health for all populations. For instance, given the incidence of CVD following spinal cord injury (SCI), it may be surprising that normal brachial artery FMD has been reported (De Groot & Poelkens *et al.* 2004). The current authors previously reported decreased FMD in the legs (posterior tibialis) compared to the arms (radial) for patients with SCI (Stoner & Sabatier *et al.* 2006). The retention of upper-extremity function likely explains the lack of deterioration for SCI radial arteries. Patients with paraplegia mostly rely on upper-body function for performing daily activities. Since individuals with SCI actively use their upper extremities, blood flow patterns may be such that the blood vessels retain their functional status due to normal shear stressor activity (Zarins & Zatina *et al.* 1987; Gnasso & Carallo *et al.* 1996). Notably, we subsequently found that 18 weeks of self-administered neuromuscular electrical stimulation-induced resistance exercise therapy significantly increased FMD and arterial range of the posterior tibial artery in male patients with chronic, complete SCI (Stoner & Sabatier *et al.* 2007).

5. Limitations of the FMD test

Despite its potential, validity of the FMD test has been questioned due to lack of normalization to the primary stimulus (Mitchell & Parise *et al.* 2004; Pyke & Tschakovsky 2005; Stoner & McCully 2011). Despite the term *flow*-mediated dilatation, shear stress is the established stimulus for FMD (Koller & Sun *et al.* 1993). The magnitude of the shear stimulus created with reactive hyperemia is influenced by several factors; subsequently, the shear stimulus may differ significantly between individuals. Therefore, in order to efficaciously compare groups of individuals the shear stimulus should be considered (see below for further discussion). For instance, Mitchell *et al.* (Mitchell & Parise *et al.* 2004) demonstrated that reduced FMD may be attributable not only to impaired endothelial release of dilatory molecules, but also as a result of a lesser shear stimulus. Fortunately, the ultrasound technology used to conduct the FMD test can also provide estimates of shear stress.

6. Shear stress estimation

Clinical studies in humans, including FMD studies, typically estimate shear stress by employing a simplified mathematical model based on Poiseuille's law. More sophisticated approaches are available, but are beyond the reach of most clinical studies since such approaches are not readily available, too expensive, technically challenging and time-consuming (Oyre & Pedersen *et al.* 1997; Gatehouse & Keegan *et al.* 2005; Reneman & Arts *et*

al. 2006). Based on Poiseuille's law shear stress is calculated as the product of *shear rate* and blood viscosity, where shear rate equals:

$$\text{Shear rate } (\gamma) = \frac{2(2+n)v}{d} \tag{3}$$

where d is the internal arterial diameter, v is the time-averaged mean blood velocity, and n represents the shape of the velocity profile. For a fully developed parabolic profile, n is 2; this is the normal assumption when estimating shear rate.

Poiseuille's law assumes that: 1) the fluid (blood) is Newtonian, 2) blood flows through a rigid tube, 3) whole blood viscosity represents viscosity at the vessel wall and is linearly proportional to shear rate, 4) the velocity profile is parabolic, and 5) mean blood velocity adequately defines the shear stimulus. First, although blood is a non-Newtonian fluid at low shear rates (smaller than approx 100 reciprocal seconds (s^{-1})) (Chien & Usami *et al.* 1966) *in vivo*, shear rates in large arteries, particularly at the endothelial surface, are generally considerably larger than this threshold value so that the effect of the non-Newtonian behavior does not appear to be pronounced. Second, blood vessels are distensible, meaning that increases in arterial cross-section occur during the cardiac cycle. Wall shear rate may be ~ 30% less in a distensible artery as compared to a rigid tube (Duncan & Bargeron *et al.* 1990).

Third, to estimate shear stress from shear rate, invasive measures of blood viscosity are required. This potentially adds an additional source of error (Tangelder & Teirlinck *et al.* 1985). Human *in vivo* studies are usually limited to whole blood measurements of viscosity. These measurements overestimate the viscosity at the wall of the vessel. Less red blood cells travel along the artery wall, where, in addition to a thin layer of plasma, blood platelets are traveling (Tangelder & Teirlinck *et al.* 1985). Red blood cells tend to stream in the center of the vessel. The result is higher viscosity in the center of the vessel, thereby reducing the shear stress gradients at the vessel wall. It is worth noting that shear stress assessments do not seem to result in conclusions different from shear rate assessments alone (Padilla & Johnson *et al.* 2008). This may be explained by two factors: 1) sources of error from whole blood viscosity estimates, and 2) for a given population, viscosity changes little. Shear rate can therefore be used as an adequate surrogate measure (Gnasso & Carallo *et al.* 1996; Joannides & Bakkali el *et al.* 1997; Betik & Luckham *et al.* 2004; Pyke & Dwyer *et al.* 2004; Padilla & Johnson *et al.* 2008).

Fourth, in arteries, the velocity profile will not form a well-defined parabola as a consequence of flow unsteadiness and short vessel entrance lengths. In both arteries and arterioles, the velocity profiles are actually flattened parabolas (Reneman & Arts et al. 2006). In the common carotid artery, mean wall shear stress is underestimated by a factor of two when assuming a parabolic velocity profile since the velocity difference is smaller between the innermost column of flow and the outermost circumferential layer (Dammers & Stifft *et al.* 2003). However, in the brachial artery - at least under baseline conditions - the underestimation is less pronounced - likely due to a more parabolic velocity profile in this artery (Dammers & Stifft *et al.* 2003).

Despite the aforementioned limitations, shear rate assessments can be reliably made using ultrasound (Samijo & Willigers *et al.* 1997). However, little attention has been given to the most appropriate blood velocity parameter(s) for calculating shear rate (see below).

6.1 Peak or integrated shear rates?

Recently, we conducted a study to determine which shear rate expression explained the most variation in FMD. Seven shear rate expressions were calculated: peak, change (peak hyperemia minus baseline), integrated over 10, 20, 30, and 40 seconds after tourniquet deflation, and integrated to peak diameter time (Stoner & McCully). Shear rates integrated for 40 seconds after tourniquet deflation (i.e., post-ischemia) explained the greatest portion of variation for change in diameter. However, the addition of *peak* shear rate to *time-integrated* shear rate was significant. This suggests that peak shear rate may be an additional important independent predictor of FMD. It is worth noting that while peak shear positively correlated with peak diameter when regressed independently, the addition of 40 seconds integrated shear rate led to a negative relationship between peak shear rate and peak diameter. A greater peak shear rate for a given integrated shear rate is indicative of a more transitory hyperemic response. A less sustained increase in shear rate may result in a lower stimulus mechanotransduced to the endothelial cells. This study was conducted on young, healthy males. Therefore, further study is warranted to confirm these findings on other cohorts.

6.2 Importance of the velocity profile

The earliest studies investigating the implications of shear stress on endothelial function did so by assessing endothelial cell responses to high versus low shear stress. This was until Davies et al. (Davies & Remuzzi *et al.* 1986), in 1986, provided evidence that the time-averaged shear stress alone could not explain the pathological behavior of endothelial cells exposed to complex flow patterns. Subsequent studies (Helmlinger & Geiger *et al.* 1991; Waters & Chang *et al.* 1997; Lum & Wiley *et al.* 2000; McAllister & Du *et al.* 2000; Peng & Recchia *et al.* 2000; Apodaca 2002; Blackman & Garcia-Cardena *et al.* 2002; Cullen & Sayeed *et al.* 2002; Barakat & Lieu 2003) have shown that vascular endothelial cells respond not only to the time-averaged shear stress, but respond differently to different patterns of flow.

The cyclic nature of the beating heart creates pulsatile flow conditions in all arteries. The heart ejects blood during systole, and fills during diastole. These cyclic conditions create relatively simple *mono-phasic* flow pulses in the upper region of the aorta (Wootton & Ku 1999). However, pressure and flow characteristics are substantially altered as blood circulates through the arterial tree. Figure 6 shows an example of a typical brachial artery blood velocity profile. The normal brachial arterial signal is *tri-phasic*, corresponding to 1) rapid blood flow during systole, 2) initial reversal of blood flow in diastole, and 3) gradual return of forward flow during late diastole.

The blood flow profile in the aorta is predominately governed by the force of blood ejected from the heart (Wang & Parker 2004). However, in the periphery the blood flow profile becomes more complex as a result of the energy transfer between the heart and arteries. The heart generates forward-traveling wave energy that propagates through the arteries to maintain tissue and organ perfusion for metabolic homeostasis. An individual forward-

traveling waveform, generated by the heart at the beginning of systole, initiates flow and increases pressure in the arteries. Although most of the wave energy in this initial compression wave travels distally into smaller arteries, some is reflected back towards the heart at sites of impedance mismatch. Interactions between forward- and backward-traveling waves result in complex blood flow patterns. Wave reflections result from arterial geometry, arterial wall compliance, and downstream resistance created by resistance arteries (Perktold & Rappitsch 1995; Barakat & Lieu 2003).

Complex flow characteristics have a profound impact on the shear stress distribution to which vascular endothelial cells are exposed. While human *in vivo* studies typically describe shear stress as a mean construct, numerous secondary phenomena associated with flow, including pulsatile flow, reversing flow, and flow turbulence, can influence the regulation of endothelial cells.

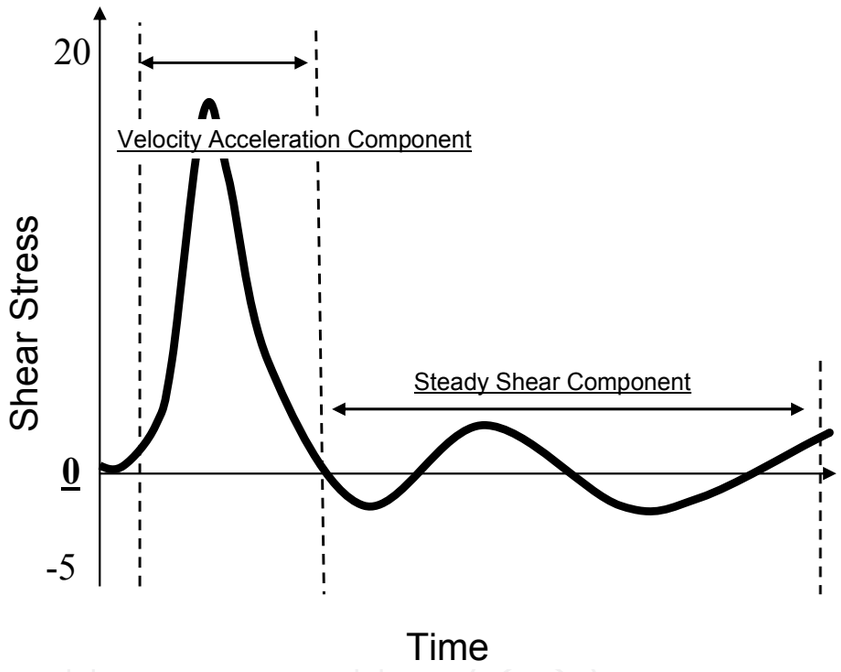

Fig. 6. *Acceleration and steady shear components*. The normal brachial arterial signal is *tri-phasic*, corresponding to the: 1) rapid blood flow during systole, resulting in velocity acceleration, 2) initial reversal of blood flow in diastole, and 3) gradual return of forward flow during late diastole, resulting in steady shear component.

6.2.1 Velocity acceleration and endothelial function

The pulsatile nature of blood flow exposes the endothelial cells to two distinct shear stimuli during the cardiac cycle: a large rate of change in shear at the onset of flow (velocity acceleration), followed by a steady shear component (Fig. 6). *In vitro* studies suggest that these two distinct fluid stimuli (velocity acceleration vs. steady shear) regulate short- and long-term endothelial function via independent biomechanical pathways (Ojha 1994; Bao & Lu et al. 1999; White & Haidekker et al. 2001; Hsiai & Cho et al. 2002 DePaola, 1992). Studies have shown that the rate of velocity acceleration can affect the progression of atherosclerosis

(Ojha 1994; Bao & Lu *et al.* 1999; Hsiai & Cho *et al.* 2001), endothelial cell function (White & Haidekker *et al.* 2001 ; Hsiai & Cho *et al.* 2002), mechanotransduction (Hsieh & Li *et al.* 1993; Bao & Clark *et al.* 2000), calcium kinetics (Helmlinger & Berk *et al.* 1995; Blackman & Barbee *et al.* 2000), and vascular tone (Frangos & Eskin *et al.* 1985; Noris & Morigi *et al.* 1995). Conditions which affect velocity acceleration include ventricular ischemia (Sabbah & Przybylski *et al.* 1987), acute myocardial infarction (Kezdi & Stanley *et al.* 1969), stenosis (Bassini & Gatti *et al.* 1982), hypertension (Sainz & Cabau *et al.* 1995), and hyperthyroidism (Chemla & Levenson *et al.* 1990). Velocity acceleration is also influenced by aging (Sainz & Cabau *et al.* 1995) and physical activity (Bonetti & Barsness *et al.* 2003; Shechter & Matetzky *et al.* 2003).

Recently, we studied the effect of velocity acceleration on FMD in a group of 14 healthy, young, male subjects (Stoner & McCully). FMD was measured prior to, and following, increases in velocity acceleration. Velocity acceleration (see Fig. 6) was increased by inflating a tourniquet around the forearm to 40 mmHg. We found that a 14% increase in velocity acceleration attenuated FMD by 11%. This finding suggests that mean blood velocity alone may not adequately characterize the shear stimulus. Attention to secondary flow phenomena may be particularly important when comparing groups with known secondary flow abnormalities.

6.3 Statistical analysis

Studies using the FMD test (i.e., using 5 minutes ischemia) should *consider* both time integrated- and peak-shear parameters, particularly when attempting to detect differences between experimental groups. Emphasis is placed on *consider* since the FMD test should not be normalized to shear rate using conventional approaches. A number of studies have attempted to account for the effect of shear stimulus on FMD by evaluating the quotient of FMD and shear, rather than FMD alone, or by using an analysis of covariance (ANCOVA), with shear stimulus as the cofactor (De Groot & Poelkens *et al.* 2004; Parker & Ridout *et al.* 2006; Padilla & Johnson *et al.* 2008; Atkinson & Batterham *et al.* 2009; Thijssen & Bullens *et al.* 2009; Pyke & Jazuli 2011). The techniques described above require use of the General Linear Model (GLM) for determining statistical probabilities associated with the differences found between groups or experimental treatments. However, when using a GLM the following assumptions must hold true: 1) there must be at least a moderate correlation between the two variables (i.e., shear and FMD), 2) the relationship between shear and diameter must be linear, 3) the intercept for the regression slope must be zero, 4) variance must be similar between groups, and 5) data must be normally distributed (Allison & Paultre *et al.* 1995; Atkinson & Batterham *et al.* 2009). A recent study found that all assumptions for reliable use of shear-diameter ratios were violated (Atkinson & Batterham *et al.* 2009).

Another alternative is to normalize the FMD response (i.e., change in diameter) to shear using hierarchical linear modeling (HLM) (Raudenbush & Bryk 2001). HLM is a more advanced form of multiple linear regression that accounts for hierarchical (i.e., successive inter-related levels) effects on the outcome variable. This is accomplished in HLM by including a complex random subject effect which can appropriately account for correlations among the data. This approach models different patterns in the data by allowing for the intercepts (initial diameter) and slopes (shear rate-diameter) to randomly vary. A third level

may also be specified; this may be the specification of groups (e.g., to delineate differences in endothelial function), an intervention or a modifiable risk factor such as smoking. This approach has been used to compare upper vs. lower extremity arterial health in persons with spinal cord injury (SCI) (Stoner & Sabatier *et al.* 2006), to assess improvements in arterial health following electrical stimulation-evoked resistance exercise therapy in persons with SCI (Stoner & Sabatier *et al.* 2007), and to assess the effects of occasional cigarette smoking on arterial health (Stoner & Sabatier *et al.* 2008). The disadvantage of this approach is that multiple stimuli (preferably ranging from minimal to maximal shear stimuli) are required to generate a reliable shear-diameter relationship.

7. Improving reliability of the FMD test

The within-subject variability of FMD has been reported to be as low as approximately 50% (De Roos & Bots *et al.* 2003), which helps to explain why FMD is related to low but not medium or high CVD risk (Witte & Westerink *et al.* 2005). Within any given study, FMD tests can consistently demonstrate a smaller degree of dilation in subjects with atherosclerotic/risk factors versus controls. However, subtle changes in FMD are more difficult to detect. Patients with only one CVD risk factor report FMD values of approximately 7% (Accini & Sotomayor *et al.*). For a typical brachial artery with a 4 mm diameter at baseline, this translates to a 0.28 mm increase in diameter. The pixel resolution of a typical ultrasound unit is 0.04 * 0.04 mm. Measurements of 0.28 mm are within the standard error of measurement. To compound the issue maximal diameters in response to reactive hyperemia are short lived and, therefore, hard to capture. Aside from standardizing measurement protocols, measurement reproducibility can be improved by considering the following suggestions.

7.1 Automate diameter measurements

Studies using edge detection software to automate diameter measurement when calculating FMD have reported intersession coefficients of variation of approximately 14-18% (Hijmering & Stroes *et al.* 2001; Woodman & Playford *et al.* 2001).

7.2 Use ANCOVA to account for measurable covariates

FMD can be calculated as: 1) post-only score, 2) change score, 3) fraction, or 4) co-varied for resting diameter. A simulation study found the greatest statistical power for the ANCOVA approach out of the four methods listed above, with fraction scores resulting in the lowest power (Vickers 2001). Expressing FMD as a percentage effectively squares the variation due to resting diameter, and may result in a non-normally distributed statistic from normally distributed data. Using resting diameters as a covariate is most likely to adjust for the bias due to baseline values (Vickers 2001; Twisk & Proper 2004; Tu & Blance et al. 2005)

7.3 Normalize to the stimulus

While FMD is certainly attenuated in a number of disease states, FMD may also be "attenuated" if the magnitude of hyperemia (Mitchell & Parise *et al.* 2004) or the blood velocity profile is altered, including the rate of velocity acceleration (Stoner & McCully).

Further study is required to comprehensively quantify the appropriate expression of the shear stimulus. At present, shear rate can be calculated as described above and used to normalize to FMD through HLM, but not by using ANCOVA or presenting as a ratio.

7.4 Use multiple FMD measurements when possible

The peak diameter in response to reactive hyperemia is short lived and, therefore, hard to capture (see Fig. 3). Variance in peak diameter measurements may be attributable to differences in the stimulus (i.e., shear stress) or to measurement error (see see Fig. 7). Variance due to change in the stimulus can be accounted for by normalizing FMD to shear stress. To account for measurement error, according to laws governing regression to the mean (Shephard 2003), the FMD test would need to be repeated multiple times in order to obtain a "true" response. Alternatively, a more accurate assessment of endothelial function can be achieved by estimating shear rate-diameter dose-response curves (see Fig. 8).

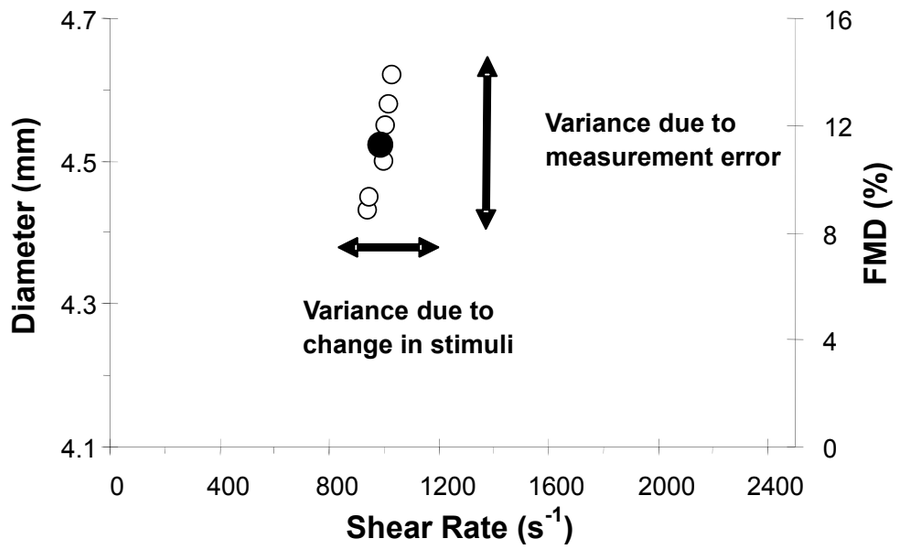

Fig. 7. *Flow-mediated dilation (FMD) measurement variance.* Open circles represent multiple FMD measurements. The closed circle represents mean FMD. Variance due to change in stimuli (shear rate) can be accounted for by normalizing to shear rate. Variance due to measurement error can be minimized by multiple FMD measurements (or by calculating a shear rate : diameter dose response curve).

7.5 Shear rate: Diameter dose response curves

Capturing shear rate-diameter dose-response curves (Stoner & Sabatier *et al.* 2004; Stoner & Sabatier *et al.* 2006; Stoner & Sabatier *et al.* 2007; Stoner & Sabatier *et al.* 2008) will decrease the likelihood of making erroneous conclusions. A standard dose-response curve (Fig. 8) is defined by three parameters: the baseline response (Bottom), the maximum response (Top), and the slope. The slope (i.e., change in diameter per one unit change in shear rate) would most accurately reflect endothelial function. The maximum response reflects the degree of arterial stiffness (Harris & Faggioli *et al.* 1995; Black & Vickerson *et al.* 2003; Sabatier & Stoner *et al.* 2006; Stoner & Sabatier *et al.* 2006).

There are a number of advantages to this approach, namely: 1) the stimulus (shear) is directly accounted for in a manner that does not violate statistical assumptions, 2) improved sensitivity, i.e., the slope (endothelial function) can be clearly identified (with the standard FMD test it cannot be ascertained at which point on the slope endothelial function is being estimated), 3) improved reliability, i.e., the dose-response slope is more resistant to measurement error when compared to a single measurement (Shephard 2003), and 4) more information is provided, i.e., the slope isolates endothelial function whereas the maximum response more likely reflects the degree of arterial stiffness (Harris & Faggioli *et al.* 1995; Black & Vickerson *et al.* 2003; Sabatier & Stoner *et al.* 2006; Stoner & Sabatier *et al.* 2006).

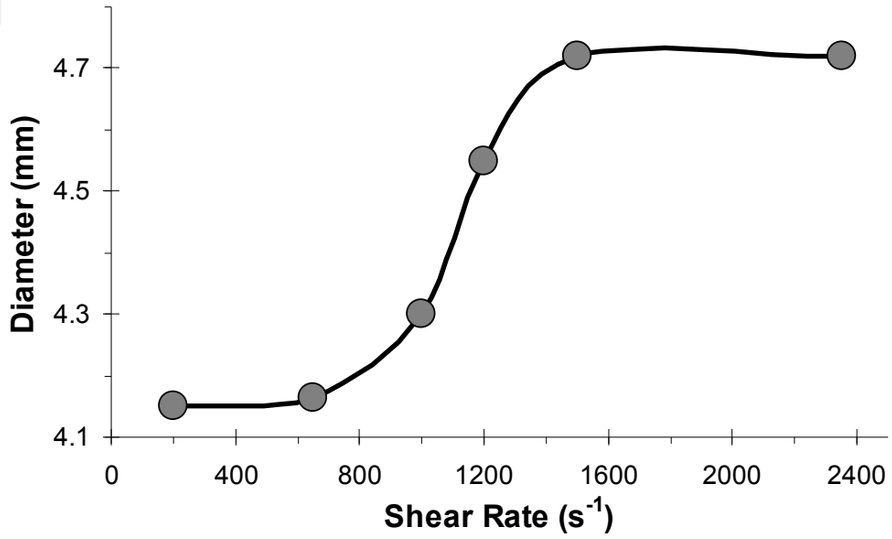

Fig. 8. *Theoretical shear rate-diameter dose-response curve.* Six data points are shown: baseline, and the responses to 5 durations of ischemia.

7.6 Transient versus steady-state shear stress

To overcome the short lived reactive hyperemia response, and hence short lived change in diameter, endothelial function can be evaluated by using sustained increases in shear stress, e.g., through local hand warming and low-intensity handgrip exercise (Mullen & Kharbanda *et al.* 2001; Joannides & Costentin *et al.* 2002; Pyke & Dwyer *et al.* 2004; Stoner & Sabatier *et al.* 2004). This approach would also allow for more accurate assessment of shear rate since the assumptions of Poiseuille's law are less likely to be violated (full description provided above).

Recently, we found that the relationship between shear rate and vasodilatation is comparable when shear rate is increased transiently (ischemia-induced) or in a sustained manner (local hand warming- and handgrip exercise-induced) (Stoner & McCully). This is consistent with a recent study by Pyke et al. (Pyke & Jazuli 2011), who similarly found a significant relationship between ischemia-induced FMD and handgrip exercise-induced FMD when the FMD responses were normalized to shear rate. Consideration has to be given to the mechanism(s) inducing FMD; the mechanisms regulating vascular tone may be dependent on the duration of the shear stimulus (Frangos & Eskin *et al.* 1985; Macarthur &

Hecker *et al.* 1993; Kuchan & Jo *et al.* 1994; Frangos & Huang *et al.* 1996; Mullen & Kharbanda *et al.* 2001), with FMD in response to sustained shear rate likely being less NO-dependent (Doshi & Naka *et al.* 2001). Nonetheless, the endothelium is still thought to primarily govern vasodilation under steady-state shear rate conditions. For instance, studies have shown that hand warming has no effect on brachial artery diameter when flow is not allowed to rise (Joannides & Bakkali el *et al.* 1997; Mullen & Kharbanda *et al.* 2001; Pyke & Dwyer *et al.* 2004). Furthermore, pharmacological blockade of the autonomic nervous system has no effect on radial artery FMD in response to hand warming (Mullen & Kharbanda *et al.* 2001), consistent with animal studies showing that FMD is preserved after surgical or pharmacological denervation (Hilton 1959; Lie & Sejersted *et al.* 1970).

A recent meta-analysis by Inaba et al. (Inaba & Chen *et al.* 2010), which was subsequently re-analyzed by Green et al. (Green & Jones *et al.* 2011), assessed the CVD prognostic strength of FMD by conducting a meta-analysis of observational studies which examined the association between brachial artery FMD and future cardiovascular events. Green et al. found that FMD resulting from more intense and prolonged shear stimuli using proximal cuff placement, which has been demonstrated to be less NO-dependent (Doshi & Naka *et al.* 2001), provides a better prognosis for CVD risk. Further study is needed to confirm these findings and determine whether FMD in response to sustained increases in shear rate provides greater prognostic strength for detecting future CVD events.

8. Conclusions

Assessments of endothelial function offer the potential to predict and track individuals at risk for CVD complications. However, despite the obvious potential, the reliability of this test has been questioned. Recently, a range of practices has been adopted to improve test reliability, including consideration of the shear stimulus and automated diameter measurements. However, the standard approach for inducing the shear stimuli, i.e., reactive hyperemia following ischemia, has inherent limitations, namely: 1) the peak diameter in response to reactive hyperemia is short lived and, therefore, hard to capture, and, 2) there is no consensus on the appropriate calculation of shear stress/rate. These limitations can be overcome with the following strategies: 1) repeat the FMD test multiple times to obtain a more reliable estimate of the "true" response, 2) calculate the shear rate-diameter dose-response to decrease the likelihood of erroneous conclusions, and, 3) use sustained increases in shear stress. Further study is required to determine: 1) whether shear-rate diameter dose-response curves offer greater statistical power, 2) whether FMD in response to sustained increases in shear rate provides greater prognostic strength, and, 3) the importance of secondary flow phenomena to estimations of shear rate.

9. References

Accini, J.L.; Sotomayor, A.; Trujillo, F.; Barrera, J.G.; Bautista, L. & Lopez-Jaramillo, P. (2001). Colombian study to assess the use of noninvasive determination of endothelium-mediated vasodilatation (CANDEV). Normal values and factors associated, *Endothelium,* Vol.8, No.2, pp.157-166

Allison, D.B.; Paultre, F.; Goran, M.I.; Poehlman, E.T. & Heymsfield, S.B. (1995). Statistical considerations regarding the use of ratios to adjust data, *Int J Obes Relat Metab Disord,* Vol.19, No.9, pp.644-652

Apodaca, G. (2002). Modulation of membrane traffic by mechanical stimuli, *Am J Physiol Renal Physiol,* Vol.282, No.2, pp.F179-190

Arndt, J.O.; Klauske, J. & Mersch, F. (1968). The diameter of the intact carotid artery in man and its change with pulse pressure, *Pflugers Arch Gesamte Physiol Menschen Tiere,* Vol.301, No.3, pp.230-240

Atkinson, G.; Batterham, A.M.; Black, M.A.; Cable, N.T.; Hopkins, N.D.; Dawson, E.A.; Thijssen, D.H.; Jones, H.; Tinken, T.M. & Green, D.J. (2009). Is the ratio of flow-mediated dilation and shear rate a statistically sound approach to normalization in cross-sectional studies on endothelial function?, *J Appl Physiol,* Vol.107, No.6, pp.1893-1899

Bao, X.; Clark, C.B. & Frangos, J.A. (2000). Temporal gradient in shear-induced signaling pathway: Involvement of MAP kinase, c-fos, and connexin 43, *Am J Physiol Heart Circ Physiol,* Vol.278, No.5, pp.H1598-1605

Bao, X.; Lu, C. & Frangos, J.A. (1999). Temporal gradient in shear but not steady shear stress induces PDGF-A and MCP-1 expression in endothelial eells : Role of NO, NF{kappa}B, and egr-1, *Arterioscler Thromb Vasc Biol,* Vol.19, No.4, pp.996-1003

Barakat, A. & Lieu, D. (2003). Differential responsiveness of vascular endothelial cells to different types of fluid mechanical shear stress, *Cell Biochem Biophys,* Vol.38, No.3, pp.323-343

Barakat, A.I.; Leaver, E.V.; Pappone, P.A. & Davies, P.F. (1999). A flow-activated chloride-selective membrane current in vascular endothelial cells, *Circ Res,* Vol.85, No.9, pp.820-828

Bassini, M.; Gatti, E.; Longo, T.; Martinis, G.; Pignoli, P. & Pizzolati, P.L. (1982). In vivo recording of blood velocity profiles and studies in vitro of profile alterations induced by known stenoses, *Tex Heart Inst J,* Vol.9, No.2, pp.185-194

Betik, A.C.; Luckham, V.B. & Hughson, R.L. (2004). Flow-mediated dilation in human brachial artery after different circulatory occlusion conditions, *Am J Physiol Heart Circ Physiol,* Vol.286, No.1, pp.H442-448

Black, C.D.; Vickerson, B. & McCully, K.K. (2003). Noninvasive assessment of vascular function in the posterior tibial artery of healthy humans, *Dyn Med,* Vol.2, No.1, pp.1

Blackman, B.R.; Barbee, K.A. & Thibault, L.E. (2000). In vitro cell shearing device to investigate the dynamic response of cells in a controlled hydrodynamic environment, *Ann Biomed Eng,* Vol.28, No.4, pp.363-372

Blackman, B.R.; Garcia-Cardena, G. & Gimbrone, M.A., Jr. (2002). A new in vitro model to evaluate differential responses of endothelial cells to simulated arterial shear stress waveforms, *J Biomech Eng,* Vol.124, No.4, pp.397-407

Bonetti, P.O.; Barsness, G.W.; Keelan, P.C.; Schnell, T.I.; Pumper, G.M.; Kuvin, J.T.; Schnall, R.P.; Holmes, D.R.; Higano, S.T. & Lerman, A. (2003). Enhanced external counterpulsation improves endothelial function in patients with symptomatic coronary artery disease, *J Am Coll Cardiol,* Vol.41, No.10, pp.1761-1768

Celermajer, D.S.; Sorensen, K.E.; Gooch, V.M.; Spiegelhalter, D.J.; Miller, O.I.; Sullivan, I.D.; Lloyd, J.K. & Deanfield, J.E. (1992). Non-invasive detection of endothelial dysfunction in children and adults at risk of atherosclerosis, *Lancet,* Vol.340, No.8828, pp.1111-1115

Chemla, D.; Levenson, J.; Valensi, P.; LeCarpentier, Y.; Pourny, J.C.; Pithois-Merli, I. & Simon, A. (1990). Effect of beta adrenoceptors and thyroid hormones on velocity and acceleration of peripheral arterial flow in hyperthyroidism, *Am J Cardiol,* Vol.65, No.7, pp.494-500

Chien, S.; Usami, S.; Taylor, H.M.; Lundberg, J.L. & Gregersen, M.I. (1966). Effects of hematocrit and plasma proteins on human blood rheology at low shear rates, *J Appl Physiol.,* Vol.21, No.1, pp.81-87

Cohn, J. (1999). Vascular wall function as a risk marker for cardiovascular disease, *Journal of Hypertension,* Vol.17, pp.S41-S44

Craiem, D.; Chironi, G.; Gariepy, J.; Miranda-Lacet, J.; Levenson, J. & Simon, A. (2007). New monitoring software for larger clinical application of brachial artery flow-mediated vasodilatation measurements, *J Hypertens,* Vol.25, No.1, pp.133-140

Cullen, J.P.; Sayeed, S.; Sawai, R.S.; Theodorakis, N.G.; Cahill, P.A.; Sitzmann, J.V. & Redmond, E.M. (2002). Pulsatile Flow-Induced Angiogenesis: Role of Gi Subunits, *Arteriosclerosis, Thrombosis, and Vascular Biology,* Vol.22, No.10, pp.1610-1616

Dammers, R.; Stifft, F.; Tordoir, J.H.; Hameleers, J.M.; Hoeks, A.P. & Kitslaar, P.J. (2003). Shear stress depends on vascular territory: comparison between common carotid and brachial artery, *J Appl Physiol,* Vol.94, No.2, pp.485-489

Davies, P.F. (1995). Flow-mediated endothelial mechanotransduction, *Physiol Rev,* Vol.75, No.3, pp.519-560

Davies, P.F.; Remuzzi, A.; Gordon, E.J.; Dewey, C.F. & Gimbrone, M.A. (1986). Turbulent Fluid Shear Stress Induces Vascular Endothelial Cell Turnover in vitro, *PNAS,* Vol.83, No.7, pp.2114-2117

De Groot, P.C.; Poelkens, F.; Kooijman, M. & Hopman, M.T. (2004). Preserved Flow Mediated Dilation in the inactive legs of spinal cord-injured individuals, *Am J Physiol Heart Circ Physiol,* Vol.287, No.1, pp.H374-380

De Roos, N.M.; Bots, M.L.; Schouten, E.G. & Katan, M.B. (2003). Within-subject variability of flow-mediated vasodilation of the brachial artery in healthy men and women: implications for experimental studies, *Ultrasound Med Biol,* Vol.29, No.3, pp.401-406

Doshi, S.N.; Naka, K.K.; Payne, N.; Jones, C.J.; Ashton, M.; Lewis, M.J. & Goodfellow, J. (2001). Flow-mediated dilatation following wrist and upper arm occlusion in humans: the contribution of nitric oxide, *Clin Sci (Lond),* Vol.101, No.6, pp.629-635.

Duncan, D.D.; Bargeron, C.B.; Borchardt, S.E.; Deters, O.J.; Gearhart, S.A.; Mark, F.F. & Friedman, M.H. (1990). The effect of compliance on wall shear in casts of a human aortic bifurcation, *J Biomech Eng,* Vol.112, No.2, pp.183-188

Fleming, I. & Busse, R. (2003). Molecular mechanisms involved in the regulation of the endothelial nitric oxide synthase, *Am J Physiol Regul Integr Comp Physiol,* Vol.284, No.1, pp.R1-12

Frangos, J.A.; Eskin, S.G.; McIntire, L.V. & Ives, C.L. (1985). Flow effects on prostacyclin production by cultured human endothelial cells., *Science,* Vol.227, No.4693, pp.1477-1479

Frangos, J.A.; Huang, T.Y. & Clark, C.B. (1996). Steady shear and step changes in shear stimulate endothelium via independent mechanisms--superposition of transient and sustained nitric oxide production, *Biochem Biophys Res Commun,* Vol.224, No.3, pp.660-665

Furchgott, R.F. & Zawadzki, J.V. (1980). The obligatory role of endothelial cells in the relaxation of arterial smooth muscle by acetylcholine., *Nature,* Vol.299, pp.373-376

Gatehouse, P.D.; Keegan, J.; Crowe, L.A.; Masood, S.; Mohiaddin, R.H.; Kreitner, K.F. & Firmin, D.N. (2005). Applications of phase-contrast flow and velocity imaging in cardiovascular MRI, *Eur Radiol,* Vol.15, No.10, pp.2172-2184

Gibbons, G.H. & Dzau, V.J. (1994). The emerging concept of vascular remodeling, *N Engl J Med,* Vol.330, No.20, pp.1431-1438.

Gnasso, A.; Carallo, C.; Irace, C.; Spagnuolo, V.; De Novara, G.; Mattioli, P.L. & Pujia, A. (1996). Association between intima-media thickness and wall shear stress in common carotid arteries in healthy male subjects, *Circulation,* Vol.94, No.12, pp.3257-3262

Green, D.J.; Jones, H.; Thijssen, D.; Cable, N.T. & Atkinson, G. (2011). Flow-mediated dilation and cardiovascular event prediction: does nitric oxide matter?, *Hypertension,* Vol.57, No.3, pp.363-369

Hangiandreou, N.J.; James, E.M.; McBane, R.D.; Tradup, D.J. & Persons, K.R. (2002). The effects of irreversible JPEG compression on an automated algorithm for measuring carotid artery intima-media thickness from ultrasound images, *J Digit Imaging,* Vol.15, No.Suppl 1, pp.258-260

Harris, L.M.; Faggioli, G.L.; Shah, R.; Koerner, N.; Lillis, L.; Dandona, P.; Izzo, J.L.; Snyder, B. & Ricotta, J.J. (1995). Vascular reactivity in patients with peripheral vascular disease, *Am J Cardiol,* Vol.76, No.3, pp.207-212

Heitzer, T.; Schlinzig, T.; Krohn, K.; Meinertz, T. & Munzel, T. (2001). Endothelial dysfunction, oxidative stress, and risk of cardiovascular events in patients with coronary artery disease, *Circulation,* Vol.104, No.22, pp.2673-2678

Helmlinger, G.; Berk, B.C. & Nerem, R.M. (1995). Calcium responses of endothelial cell monolayers subjected to pulsatile and steady laminar flow differ, *Am J Physiol,* Vol.269, No.2 Pt 1, pp.C367-375

Helmlinger, G.; Geiger, R.V.; Schreck, S. & Nerem, R.M. (1991). Effects of pulsatile flow on cultured vascular endothelial cell morphology, *J Biomech Eng,* Vol.113, No.2, pp.123-131

Hijmering, M.L.; Stroes, E.S.; Pasterkamp, G.; Sierevogel, M.; Banga, J.D. & Rabelink, T.J. (2001). Variability of flow mediated dilation: consequences for clinical application, *Atherosclerosis,* Vol.157, No.2, pp.369-373

Hilton, S.M. (1959). A peripheral arterial conducting mechanism underlying dilatation of the femoral artery and concerned in functional vasodilatation in skeletal muscle, *J Physiol,* Vol.149, pp.93-111

Hoeks, A.P.; Brands, P.J.; Willigers, J.M. & Reneman, R.S. (1999). Non-invasive measurement of mechanical properties of arteries in health and disease, *Proc Inst Mech Eng [H],* Vol.213, No.3, pp.195-202.

Hsiai, T.K.; Cho, S.K.; Honda, H.M.; Hama, S.; Navab, M.; Demer, L.L. & Ho, C.M. (2002). Endothelial cell dynamics under pulsating flows: Significance of high versus low shear stress slew rates (d(tau)/dt), *Ann Biomed Eng,* Vol.30, No.5, pp.646-656

Hsiai, T.K.; Cho, S.K.; Reddy, S.; Hama, S.; Navab, M.; Demer, L.L.; Honda, H.M. & Ho, C.M. (2001). Pulsatile flow regulates monocyte adhesion to oxidized lipid-induced endothelial cells, *Arteriosclerosis, Thrombosis, and Vascular Biology,* Vol.21, No.11, pp.1770-1776

Hsieh, H.J.; Li, N.Q. & Frangos, J.A. (1993). Pulsatile and steady flow induces c-fos expression in human endothelial cells, *J Cell Physiol,* Vol.154, No.1, pp.143-151

Inaba, Y.; Chen, J.A. & Bergmann, S.R. (2010). Prediction of future cardiovascular outcomes by flow-mediated vasodilatation of brachial artery: a meta-analysis, *Int J Cardiovasc Imaging,* Vol.26, No.6, pp.631-640

Joannides, R.; Bakkali el, H.; Richard, V.; Benoist, A.; Moore, N. & Thuillez, C. (1997). Evaluation of the determinants of flow-mediated radial artery vasodilatation in humans, *Clin Exp Hypertens,* Vol.19, No.5-6, pp.813-826

Joannides, R.; Costentin, A.; Iacob, M.; Compagnon, P.; Lahary, A. & Thuillez, C. (2002). Influence of vascular dimension on gender difference in flow-dependent dilatation of peripheral conduit arteries, *Am J Physiol Heart Circ Physiol,* Vol.282, No.4, pp.H1262-1269

Kezdi, P.; Stanley, E.L.; Marshall, W.J., Jr. & Kordenat, R.K. (1969). Aortic flow velocity and acceleration as an index of ventricular performance during myocardial infarction, *Am J Med Sci,* Vol.257, No.1, pp.61-71

Kizhakekuttu, T.J.; Gutterman, D.D.; Phillips, S.A.; Jurva, J.W.; Arthur, E.I.; Das, E. & Widlansky, M.E. (2010). Measuring FMD in the brachial artery: how important is QRS gating?, *J Appl Physiol,* Vol.109, No.4, pp.959-965

Koller, A.; Sun, D. & Kaley, G. (1993). Role of shear stress and endothelial prostaglandins in flow- and viscosity-induced dilation of arterioles in vitro, *Circ Res,* Vol.72, No.6, pp.1276-1284

Kuchan, M.J.; Jo, H. & Frangos, J.A. (1994). Role of G proteins in shear stress-mediated nitric oxide production by endothelial cells, *Am J Physiol,* Vol.267, No.3, pp.C753-758

Labrador, V.; Chen, K.D.; Li, Y.S.; Muller, S.; Stoltz, J.F. & Chien, S. (2003). Interactions of mechanotransduction pathways, *Biorheology,* Vol.40, No.1-3, pp.47-52

Langille, B.L. & O'Donnell, F. (1986). Reductions in arterial diameter produced by chronic decreases in blood flow are endothelium-dependent, *Science,* Vol.231, No.4736, pp.405-407

Lerman, A. & Zeiher, A.M. (2005). Endothelial function: cardiac events, *Circulation,* Vol.111, No.3, pp.363-368

Lie, M.; Sejersted, O.M. & Kiil, F. (1970). Local regulation of vascular cross section during changes in femoral arterial blood flow in dogs, *Circ Res,* Vol.27, No.5, pp.727-737

Lieu, D. (2010). Ultrasound physics and instrumentation for pathologists, *Arch Pathol Lab Med,* Vol.134, No.10, pp.1541-1556

Lloyd-Jones, D.; Adams, R.J.; Brown, T.M.; Carnethon, M.; Dai, S.; De Simone, G.; Ferguson, T.B.; Ford, E.; Furie, K.; Gillespie, C.; Go, A.; Greenlund, K.; Haase, N.; Hailpern, S.; Ho, P.M.; Howard, V.; Kissela, B.; Kittner, S.; Lackland, D.; Lisabeth, L.; Marelli, A.; McDermott, M.M.; Meigs, J.; Mozaffarian, D.; Mussolino, M.; Nichol, G.; Roger, V.L.; Rosamond, W.; Sacco, R.; Sorlie, P.; Stafford, R.; Thom, T.; Wasserthiel-Smoller, S.; Wong, N.D.; Wylie-Rosett, J.; Committee, o.b.o.t.A.H.A.S. & Stroke Statistics Subcommittee (2010). Heart disease and stroke statistics--2010 update: a report from the American Heart Association, *Circulation,* Vol.121, No.7, pp.e46-215

Lum, R.M.; Wiley, L.M. & Barakat, A.I. (2000). Influence of different forms of fluid shear stress on vascular endothelial TGF-beta1 mRNA expression, *Int J Mol Med,* Vol.5, No.6, pp.635-641

Luscher, T.F. & Barton, M. (1997). Biology of the endothelium, *Clin Cardiol,* Vol.20, pp.3-10

Macarthur, H.; Hecker, M.; Busse, R. & Vane, J.R. (1993). Selective inhibition of agonist-induced but not shear stress-dependent release of endothelial autacoids by thapsigargin, *Br J Pharmacol,* Vol.108, No.1, pp.100-105

McAllister, T.N.; Du, T. & Frangos, J.A. (2000). Fluid shear stress stimulates prostaglandin and nitric oxide release in bone marrow-derived preosteoclast-like cells, *Biochem Biophys Res Commun,* Vol.270, No.2, pp.643-648

Mitchell, G.F.; Parise, H.; Vita, J.A.; Larson, M.G.; Warner, E.; Keaney, J.F., Jr.; Keyes, M.J.; Levy, D.; Vasan, R.S. & Benjamin, E.J. (2004). Local shear stress and brachial artery flow-mediated dilation: the Framingham Heart Study, *Hypertension,* Vol.44, No.2, pp.134-139

Moncada, S. & Higgs, A. (1993). The L-arginine-nitric oxide pathway, *N Engl J Med,*No.329, pp.2002-2012

Mullen, M.J.; Kharbanda, R.K.; Cross, J.; Donald, A.E.; Taylor, M.; Vallance, P.; Deanfield, J.E. & MacAllister, R.J. (2001). Heterogenous nature of flow-mediated dilatation in human conduit arteries in vivo: relevance to endothelial dysfunction in hypercholesterolemia, *Circ Res,* Vol.88, No.2, pp.145-151

Murakami, T. & Arai, Y. (2001). Relationship between non-invasively evaluated endothelial dysfunction and future cardiovascular events., *ACC Conference,* Vol.Session 1263,

Nerem, R.M. (1992). Vascular fluid mechanics, the arterial wall, and atherosclerosis, *J Biomech Eng,* Vol.114, No.3, pp.274-282

Nesbitt, E.; Schmidt-Trucksass, A.; Il'yasov, K.A.; Weber, H.; Huonker, M.; Laubenberger, J.; Keul, J.; Hennig, J. & Langer, M. (2000). Assessment of arterial blood flow characteristics in normal and atherosclerotic vessels with the fast Fourier flow method, *Magma,* Vol.10, No.1, pp.27-34.

Neunteufl, T.; Heher, S.; Katzenschlager, R.; Wolfl, G.; Kostner, K.; Maurer, G. & Weidinger, F. (2000). Late prognostic value of flow-mediated dilation in the brachial artery of patients with chest pain, *Am J Cardiol,* Vol.86, No.2, pp.207-210

Nissen, S.E. & Yock, P. (2001). Intravascular Ultrasound : Novel Pathophysiological Insights and Current Clinical Applications, *Circulation,* Vol.103, No.4, pp.604-616

Noris, M.; Morigi, M.; Donadelli, R.; Aiello, S.; Foppolo, M.; Todeschini, M.; Orisio, S.; Remuzzi, G. & Remuzzi, A. (1995). Nitric oxide synthesis by cultured endothelial cells is modulated by flow conditions, *Circ Res,* Vol.76, No.4, pp.536-543

Ojha, M. (1994). Wall shear stress temporal gradient and anastomotic intimal hyperplasia, *Circ Res,* Vol.74, No.6, pp.1227-1231

Olesen, S.P.; Clapham, D.E. & Davies, P.F. (1988). Haemodynamic shear stress activates a K+ current in vascular endothelial cells, *Nature,* Vol.331, No.6152, pp.168-170

Olive, J.L.; Slade, J.M.; Dudley, G.A. & McCully, K.K. (2003). Blood flow and muscle fatigue in SCI individuals during electrical stimulation, *J Appl Physiol,* Vol.94, No.2, pp.701-708

Oyre, S.; Pedersen, E.M.; Ringgaard, S.; Boesiger, P. & Paaske, W.P. (1997). In vivo wall shear stress measured by magnetic resonance velocity mapping in the normal human abdominal aorta, *Eur J Vasc Endovasc Surg,* Vol.13, No.3, pp.263-271

Padilla, J.; Johnson, B.D.; Newcomer, S.C.; Wilhite, D.P.; Mickleborough, T.D.; Fly, A.D.; Mather, K.J. & Wallace, J.P. (2008). Normalization of flow-mediated dilation to shear stress area under the curve eliminates the impact of variable hyperemic stimulus, *Cardiovasc Ultrasound,* Vol.6, pp.44

Papaioannou, T.G.; Karatzis, E.N.; Vavuranakis, M.; Lekakis, J.P. & Stefanadis, C. (2006). Assessment of vascular wall shear stress and implications for atherosclerotic disease, *Int J Cardiol,*

Papaioannou, T.G. & Stefanadis, C. (2005). Vascular wall shear stress: basic principles and methods, *Hellenic J Cardiol,* Vol.46, No.1, pp.9-15

Parker, B.A.; Ridout, S.J. & Proctor, D.N. (2006). Age and flow-mediated dilation: a comparison of dilatory responsiveness in the brachial and popliteal arteries, *Am J Physiol Heart Circ Physiol,* Vol.291, No.6, pp.H3043-3049

Peng, X.; Recchia, F.A.; Byrne, B.J.; Wittstein, I.S.; Ziegelstein, R.C. & Kass, D.A. (2000). In vitro system to study realistic pulsatile flow and stretch signaling in cultured vascular cells, *Am J Physiol Cell Physiol,* Vol.279, No.3, pp.C797-805

Peretz, A.; Leotta, D.F.; Sullivan, J.H.; Trenga, C.A.; Sands, F.N.; Aulet, M.R.; Paun, M.; Gill, E.A. & Kaufman, J.D. (2007). Flow mediated dilation of the brachial artery: an investigation of methods requiring further standardization, *BMC Cardiovasc Disord,* Vol.7, pp.11

Perktold, K. & Rappitsch, G. (1995). Mathematical modeling of arterial blood flow and correlation to atherosclerosis, *Technol Health Care,* Vol.3, No.3, pp.139-151

Pyke, K.E.; Dwyer, E.M. & Tschakovsky, M.E. (2004). Impact of controlling shear rate on flow-mediated dilation responses in the brachial artery of humans, *J Appl Physiol,* Vol.97, No.2, pp.499-508

Pyke, K.E. & Jazuli, F. (2011). Impact of repeated increases in shear stress via reactive hyperemia and handgrip exercise: no evidence of systematic changes in brachial artery FMD, *Am J Physiol Heart Circ Physiol,* Vol.300, No.3, pp.H1078-1089

Pyke, K.E. & Tschakovsky, M.E. (2005). The relationship between shear stress and flow-mediated dilatation: implications for the assessment of endothelial function, *J Physiol,* Vol.568, No.Pt 2, pp.357-369

Quyyumi, A.A. (2003). Prognostic value of endothelial function, *Am J Cardiol,* Vol.91, No.12A, pp.19H-24H.

Raudenbush, S.W. & Bryk, A.S. (2001). *Hierarchical Linear Models: Applications and Data Analysis Methods (Advanced Quantitative Techniques in the Social Sciences)*. SAGE Publications, Thousand Oaks, CA

Reneman, R.S.; Arts, T. & Hoeks, A.P.G. (2006). Wall Shear Stress -- an Important Determinant of Endothelial Cell Function and Structure -- in the Arterial System in vivo, *Journal of Vascular Research,* Vol.43, No.3, pp.251-269

Rodbard, S. (1970). Negative feedback mechanisms in the architecture and function of the connective and cardiovascular tissues, *Perspect Biol Med,* Vol.13, No.4, pp.507-527

Roelandt, J.; van Dorp, W.G.; Bom, N.; Laird, J.D. & Hugenholtz, P.G. (1976). Resolution problems in echocardiology: a source of interpretation errors, *Am J Cardiol,* Vol.37, No.2, pp.256-262

Ross, R. (1993). The pathogenesis of atherosclerosis: A perspective for the 1990s, *Nature,* Vol.362, No.6423, pp.801-809

Ross, R. (1999). Atherosclerosis -- An Inflammatory Disease, *N Engl J Med,* Vol.340, No.2, pp.115-126

Rubanyi, G.M.; Romero, J.C. & Vanhoutte, P.M. (1986). Flow-induced release of endothelium-derived relaxing factor, *Am J Physiol,* Vol.250, No.6 Pt 2, pp.H1145-1149

Sabatier, M.J.; Stoner, L.; Reifenberger, M. & McCully, K. (2006). Doppler ultrasound assessment of posterior tibial artery size in humans, *J Clin Ultrasound,* Vol.34, No.5, pp.223-230

Sabbah, H.N.; Przybylski, J.; Albert, D.E. & Stein, P.D. (1987). Peak aortic blood acceleration reflects the extent of left ventricular ischemic mass at risk, *Am Heart J,* Vol.113, No.4, pp.885-890

Sainz, A.; Cabau, J. & Roberts, V.C. (1995). Deceleration vs. acceleration: a haemodynamic parameter in the assessment of vascular reactivity. A preliminary study, *Med Eng Phys,* Vol.17, No.2, pp.91-95

Samijo, S.K.; Willigers, J.M.; Brands, P.J.; Barkhuysen, R.; Reneman, R.S.; Kitslaar, P.J. & Hoeks, A.P. (1997). Reproducibility of shear rate and shear stress assessment by means of ultrasound in the common carotid artery of young human males and females, *Ultrasound Med Biol,* Vol.23, No.4, pp.583-590

Schroeder, S.; Enderle, M.D.; Ossen, R.; Meisner, C.; Baumbach, A.; Pfohl, M.; Herdeg, C.; Oberhoff, M.; Haering, H.U. & Karsch, K.R. (1999). Noninvasive determination of endothelium-mediated vasodilation as a screening test for coronary artery disease: pilot study to assess the predictive value in comparison with angina pectoris, exercise electrocardiography, and myocardial perfusion imaging., *Am Heart J,* Vol.138, No.4, pp.731-739

Shechter, M.; Matetzky, S.; Feinberg, M.S.; Chouraqui, P.; Rotstein, Z. & Hod, H. (2003). External counterpulsation therapy improves endothelial function in patients with refractory angina pectoris, *J Am Coll Cardiol,* Vol.42, No.12, pp.2090-2095

Shephard, R.J. (2003). Regression to the mean. A threat to exercise science?, *Sports Med,* Vol.33, No.8, pp.575-584

Shyy, J.Y.J. & Chien, S. (2002). Role of Integrins in Endothelial Mechanosensing of Shear Stress, *Circ Res,* Vol.91, No.9, pp.769-775

Sorensen, K.E.; Celermajer, D.S.; Georgakopoulos, D.; Hatcher, G.; Betteridge, D.J. & Deanfield, J.E. (1994). Impairment of endothelium-dependent dilation is an early event in children with familial hypercholesterolemia and is related to the lipoprotein(a) level, *J Clin Invest,* Vol.93, No.1, pp.50-55

Stoner, L. & McCully, K. (2011). *Blood Velocity Parameters that Contibute to Flow-Mediated Dilation*. LAP LAMBERT Academic Publishing, Saarbrücken, Germany

Stoner, L. & McCully, K. Peak- and time integrated-shear rates independently predict flow-mediated dilation. J Clin Ultrasound, In Press

Stoner, L. & McCully, K. Velocity acceleration as a determinant of flow-mediated dilation. *Ultrasound in Med Biol,* In Press

Stoner, L.; Sabatier, M.; Edge, K. & McCully, K. (2004). Relationship between blood velocity and conduit artery diameter and the effects of smoking on vascular responsiveness, *J Appl Physiol,* Vol.96, No.6, pp.2139-2145

Stoner, L.; Sabatier, M.; VanhHiel, L.; Groves, D.; Ripley, D.; Palardy, G. & McCully, K. (2006). Upper vs lower extremity arterial function after spinal cord injury, *J Spinal Cord Med,* Vol.29, No.2, pp.138-146

Stoner, L.; Sabatier, M.J.; Black, C.D. & McCully, K.K. (2008). Occasional cigarette smoking chronically affects arterial function, *Ultrasound Med Biol,* Vol.34, No.12, pp.1885-1892

Stoner, L.; Sabatier, M.J.; Mahoney, E.T.; Dudley, G.A. & McCully, K.K. (2007). Electrical stimulation-evoked resistance exercise therapy improves arterial health after chronic spinal cord injury, *Spinal Cord,* Vol.45, No.1, pp.49-56

Stoner, L., West, C., Cates, D & Young, J. Optimization of ultrasound assessments of arterial function. *Open Journal of Clinical Diagnostics;* In Press

Tangelder, G.J.; Teirlinck, H.C.; Slaaf, D.W. & Reneman, R.S. (1985). Distribution of blood platelets flowing in arterioles, *Am J Physiol Heart Circ Physiol,* Vol.248, No.3, pp.H318-323

Thijssen, D.H.; Black, M.A.; Pyke, K.E.; Padilla, J.; Atkinson, G.; Harris, R.A.; Parker, B.; Widlansky, M.E.; Tschakovsky, M.E. & Green, D.J. (2011). Assessment of flow-mediated dilation in humans: a methodological and physiological guideline, *Am J Physiol Heart Circ Physiol,* Vol.300, No.1, pp.H2-12

Thijssen, D.H.; Bullens, L.M.; van Bemmel, M.M.; Dawson, E.A.; Hopkins, N.; Tinken, T.M.; Black, M.A.; Hopman, M.T.; Cable, N.T. & Green, D.J. (2009). Does arterial shear explain the magnitude of flow-mediated dilation?: a comparison between young and older humans, *Am J Physiol Heart Circ Physiol,* Vol.296, No.1, pp.H57-64

Thijssen, D.H.; Tinken, T.M.; Hopkins, N.; Dawson, E.A.; Cable, N.T. & Green, D.J. (2011). The impact of exercise training on the diameter dilator response to forearm ischaemia in healthy men, *Acta Physiol (Oxf),* Vol.201, No.4, pp.427-434

Thrush, A. & Hartshorne, T. (2004). *Peripheral Vascular Ultrasound. How, Why and When*. Churchill Livingstone, New York

Tu, Y.K.; Blance, A.; Clerehugh, V. & Gilthorpe, M.S. (2005). Statistical power for analyses of changes in randomized controlled trials, *J Dent Res,* Vol.84, No.3, pp.283-287.

Twisk, J. & Proper, K. (2004). Evaluation of the results of a randomized controlled trial: how to define changes between baseline and follow-up, *J Clin Epidemiol,* Vol.57, No.3, pp.223-228.

Vickers, A.J. (2001). The use of percentage change from baseline as an outcome in a controlled trial is statistically inefficient: a simulation study, *BMC Med Res Methodol,* Vol.1, pp.6

Wang, J.J. & Parker, K.H. (2004). Wave propagation in a model of the arterial circulation, *J Biomech,* Vol.37, No.4, pp.457-470

Waters, C.M.; Chang, J.Y.; Glucksberg, M.R.; DePaola, N. & Grotberg, J.B. (1997). Mechanical forces alter growth factor release by pleural mesothelial cells, *Am J Physiol,* Vol.272, No.3 Pt 1, pp.L552-557

White, C.R.; Haidekker, M.; Bao, X. & Frangos, J.A. (2001). Temporal gradients in shear, but not spatial gradients, stimulate endothelial cell proliferation, *Circulation,* Vol.103, No.20, pp.2508-2513

Witte, D.R.; Westerink, J.; de Koning, E.J.; van der Graaf, Y.; Grobbee, D.E. & Bots, M.L. (2005). Is the association between flow-mediated dilation and cardiovascular risk limited to low-risk populations?, *J Am Coll Cardiol,* Vol.45, No.12, pp.1987-1993

Woodman, R.J.; Playford, D.A.; Watts, G.F.; Cheetham, C.; Reed, C.; Taylor, R.R.; Puddey, I.B.; Beilin, L.J.; Burke, V.; Mori, T.A. & Green, D. (2001). Improved analysis of brachial artery ultrasound using a novel edge-detection software system, *J Appl Physiol,* Vol.91, No.2, pp.929-937

Wootton, D.M. & Ku, D.N. (1999). Fluid mechanics of vascular systems, diseases, and thrombosis, *Annu Rev Biomed Eng,* Vol.1, pp.299-329

Yoshida, T.; Kawano, H.; Miyamoto, S.; Motoyama, T.; Fukushima, H.; Hirai, N. & Ogawa, H. (2006). Prognostic value of flow-mediated dilation of the brachial artery in patients with cardiovascular disease, *Intern Med,* Vol.45, No.9, pp.575-579

Zarins, C.K.; Zatina, M.A.; Giddens, D.P.; Ku, D.N. & Glagov, S. (1987). Shear stress regulation of artery lumen diameter in experimental atherogenesis, *J Vasc Surg,* Vol.5, No.3, pp.413-420

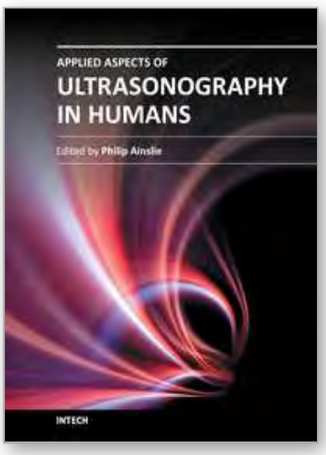

Applied Aspects of Ultrasonography in Humans
Edited by Prof. Philip Ainslie

ISBN 978-953-51-0522-0
Hard cover, 190 pages
Publisher InTech
Published online 25, April, 2012
Published in print edition April, 2012

Written by international experts, this publication provides the reader with the present knowledge and future research directions of diagnostic and therapeutic ultrasound and spectroscopy. Focused topics include Duplex ultrasound, transcranial color Duplex, MRA guided Doppler ultrasonography and near-infrared spectroscopy. New directions in the use and application of transcranial and color Duplex ultrasound are provided, as well as the use of ultrasound and arterial stiffness for measuring human vascular health and circulatory control. Novel use of ultrasound for the detection of intra-cardiac and intra-pulmonary shunts is also described along with its utility for the assessment of gastric regulation and emptying.

INTECH
open science | open minds

InTech Europe
University Campus STeP Ri
Slavka Krautzeka 83/A
51000 Rijeka, Croatia
Phone: +385 (51) 770 447
Fax: +385 (51) 686 166
www.intechopen.com

InTech China
Unit 405, Office Block, Hotel Equatorial Shanghai
No.65, Yan An Road (West), Shanghai, 200040, China
中国上海市延安西路65号上海国际贵都大饭店办公楼405单元
Phone: +86-21-62489820
Fax: +86-21-62489821

IntechOpen

6

Ultrasonography and Tonometry for the Assessment of Human Arterial Stiffness

Graeme J. Koelwyn[1], Katharine D. Currie[2],
Maureen J. MacDonald[2] and Neil D. Eves[1]
[1]*School of Health and Exercise Sciences, University of British Columbia*
[2]*Department of Kinesiology, McMaster University*
Canada

1. Introduction

The structure and function of the human vasculature is integral to the efficacy of the cardiovascular system. In particular, arteries function as both a reservoir to dampen oscillations from the pumping heart, as well as a conduit to transport blood to the periphery. With age and disease, alterations in the composition of the arterial wall can occur. This can result in arteries becoming more resistant to wall deformation, referred to as arterial stiffness, which can have significant implications for the development of cardiovascular disease. Due to the emergence of arterial stiffness as a measure of cardiovascular disease risk, a number of non-invasive techniques have been developed, which include the use of ultrasonic assessment. These techniques are highly effective, reliable, and well validated, and consider stiffness both locally (most commonly measured at the carotid artery) as well as regionally (most commonly measured through the aorta) in the arterial tree. The assessment of arterial stiffness is critical to our understanding of the overall vascular health, and is the focus of this chapter.

2. Anatomy and physiology of the blood vessel

2.1 Anatomy of the artery

The human artery is comprised of a lumen surrounded by a series of concentric layers, which work together cohesively to assist in propagating blood from the heart to the periphery. The arterial wall itself is divided into 3 major regions: the tunica intima, media, and adventitia (Figure 1). The intima is comprised in part by the vascular endothelium, which lines the interface with the lumen. The vascular endothelium is a single layer of simple squamous epithelial cells that play a critical role in the regulation of smooth muscle tone through the release of several vasoactive substances. Adjacent to the endothelium lies a thin layer of elastin and collagen fibers, which attach to the internal elastic lamina, an elastic tissue that forms the outermost layer of the intima region. The tunica media is a more complex structure, and contains smooth muscle amidst a structure of elastin and collagen, which together act as a homogenous unit (Dobrin, 1999). A surrounding structure of thicker elastin bands wraps circumferentially with finer bands of elastin connecting them, and

collagen dispersed in the intervening spaces with some inherent slack. The collagen also attaches to the smooth muscle, which lies internal to the surrounding structure. This latticework provides a flexible "safety net" for the blood vessels to prevent damage to the wall of the artery, especially at high transmural pressures. Finally the outermost region, the tunica adventitia, is separated from the tunica media by the outer elastic lamina, and is a layer of elastin and collagen that merges with the surrounding tissues.

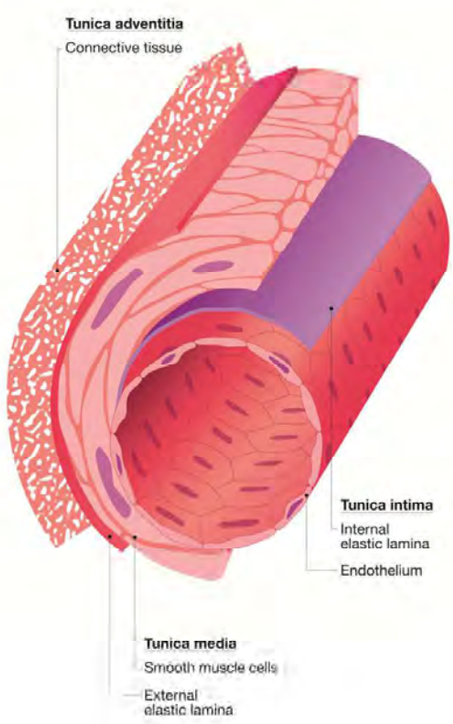

Fig. 1. Anatomy of a blood vessel

2.2 Functions of the arterial system

Arteries act as a conduit system to transport blood through the body, and dampen oscillations from the pulsatile ejection of blood to provide steady flow throughout the arterial tree. There are 3 separate anatomical arterial regions addressing these functions (Nichols & O'Rourke, 2005). First, large elastic arteries such as the aorta provide the predominant cushioning reservoir for blood flow. Second, large muscular arteries act as the conduit for blood to the periphery and actively modify wave propagation through smooth muscle tone regulation. Finally, arterioles function to alter peripheral artery resistance, and subsequently aid in the maintenance of mean arterial pressure and delivery of a continual flow to required systems and subsequent capillary beds.

Several models have been proposed for the functioning of the arterial system, with the propagative/distensible tube model considered superior (Laurent et al., 2006; O'Rourke et al., 2002). The propagative/distensible tube model consists of a single distensible tube with one end representing peripheral resistance, and the other receiving blood in pulses from the left ventricle (Nichols & O'Rourke, 2005). The pressure wave generated from the heart

travels down the tube and is propagated and dampened by the viscoelastic wall of the vessel. When applying this theory to the entire arterial tree several phenomena need to be considered. As the pulse travels down the arterial tree it becomes amplified. This amplification is caused by the progressive increase in stiffness of the arteries distally from the heart (Learoyd & Taylor, 1966) and the branching, bifurcations, and non-linearity in the vascular tree that produce sites where the pressure wave can be reflected. These reflections return in the opposite direction and amplify the pressure signal. Reflection sites are closer to the pulse wave in the periphery (greater branching) than in the central arteries, and amplification is therefore greater (known as the 'amplification phenomena') (Laurent et al., 2006). Thus, the pressure wave at any given location is the result of the summation of the incident and reflected wave (Figure 2) (Davies & Struthers, 2003; O'Rourke et al., 2002), and depending on the elasticity of the vasculature, can create various pressure waveforms.

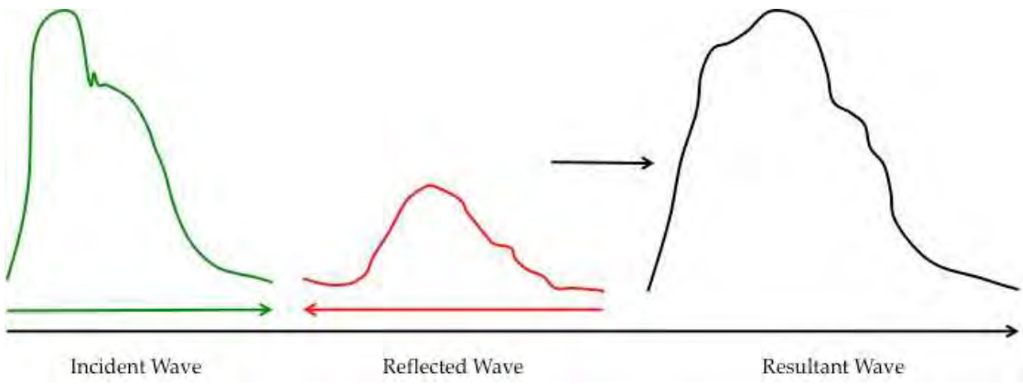

Fig. 2. The pressure waveform is a result of the summation (right) of the incident wave (left) travelling toward the periphery and combining with the reflected wave (middle) returning from the periphery.

The composition of the arterial wall, in particular the elastin and collagen content, changes from central to peripheral arteries. Starting in the proximal aorta, elastin is the dominant component. At the abdominal aorta the content of collagen and elastin appears similar, and by the periphery collagen becomes dominant (Harkness et al., 1957). As collagen is 300 times stiffer than elastin (elastic modulus 1000 x 10^6 dyne/cm^2 vs. 5 x 10^6) (Armentano et al., 1991), the altering arterial wall composition causes an increasing 'stiffness gradient' down the arterial tree. For example, in the central arteries, up to 50% of the stroke volume ejected from the heart is momentarily stored in the aorta and large elastic arteries. Approximately 10% of the energy produced by the heart is used to distend the arteries during systole. The elastic walls of the artery store the energy, and subsequently use it to recoil the vessel wall during diastole (London & Pannier, 2010), thus ensuring continuous flow to the stiffer, more collagen based, peripheral arteries. For this dampening in the central arteries to be most efficient, the energy needed to distend the wall needs to be as low as possible (London & Pannier, 2010), which not only depends on elasticity (and high elastin content), but also the geometry of the vessel walls.

Elastin and collagen cause the pressure–diameter relationship at any specific area on the arterial tree to be non linear (Figure 3) (Armentano et al., 1991). At low distensions, pressure

is mainly governed by elastin fibers, which are quite compliant and the resulting curve is more linear, where at higher tensions it is governed by the supporting latticework of collagen content, which is much stiffer, resulting in a steeper slope (a greater required pressure for a given diameter change) (Lanne et al., 1992).

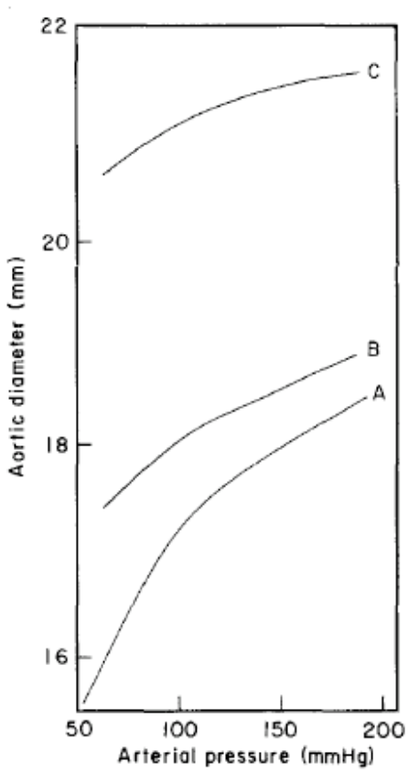

Fig. 3. Pressure-diameter relationship of the abdominal aorta in (A) young (mean 25 yrs), (B) middle aged (mean 51 yrs) and (C) elderly (mean 70 yrs) humans. Reprinted with permission (Lanne et al., 1992)

3. Arterial stiffness

3.1 Development of arterial stiffness

Considerable research supports the measurement of arterial stiffness as a highly relevant tool in the assessment of vascular structure. Degenerative stiffness of the arterial wall is considered arteriosclerosis, and is distinguishable from atherosclerosis, which is the occlusive result of endovascular inflammatory disease, lipid oxidation and plaque formation (Cavalcante et al., 2011). Even in healthy, young individuals, arterial stiffness is heterogeneous throughout the arterial tree, as amplification and the natural stiffness gradient result in more elastic central and stiffer peripheral arteries (London & Pannier, 2010). Arteries in humans, however, also stiffen with healthy ageing and disease (discussed later in the chapter), affecting predominately the aorta and proximal elastic arteries, and to a lesser degree the peripheral arteries (O'Rourke et al., 2002), and can even result in a minimization or reversing of the stiffness gradient (Benetos et al., 1993; Boutouyrie et al., 1992; Laurent et al., 2006). This regional age associated stiffening has been attributed to

longstanding pulsation that induces greater cycles of stress in the central arteries (Adji et al., 2011; Lee & Oh, 2010).

With age and disease, degeneration of the media in the central arteries appears to be the primary structural change associated with chronic increases in arterial stiffness. Fatigue and fracture of elastin and collagen fibers occur. These structural changes to the elastin and collagen functional unit are determined by the extent of circumferential strain, which is greater centrally, and length of strain exposure (number of cardiac cycles) (McEniery et al., 2010). The orderly arrangement of elastic lamellae disappears, and is replaced by thinning, fragmented elastin, greater foundations of collagen (Laurent & Boutouyrie, 2007; Najjar et al., 2005; Zieman et al., 2005) and medial calcification (elastocalcinosis) (Atkinson, 2008). Other age and disease associated changes in the arterial wall include specific changes in the smooth muscle cell connections (Laurent et al., 2005), and inflammation in the form of acute systemic (Vlachopoulos et al., 2005) and chronic (Roman et al., 2005) inflammatory disease.

A stiffer artery propagates a pulse wave faster than a more compliant vessel. This leads to earlier return of the reflected wave, which amplifies systolic pressure and decreases diastolic pressure (Figure 4). Increased systolic pressure places a greater stress (distending pressure) on the wall of the vessel, which over time can accelerate the stiffening and remodeling process. A decrease in diastolic pressure can reduce coronary perfusion pressure, reducing coronary blood flow reserve, which may be a possible link to increase cardiac event risk in

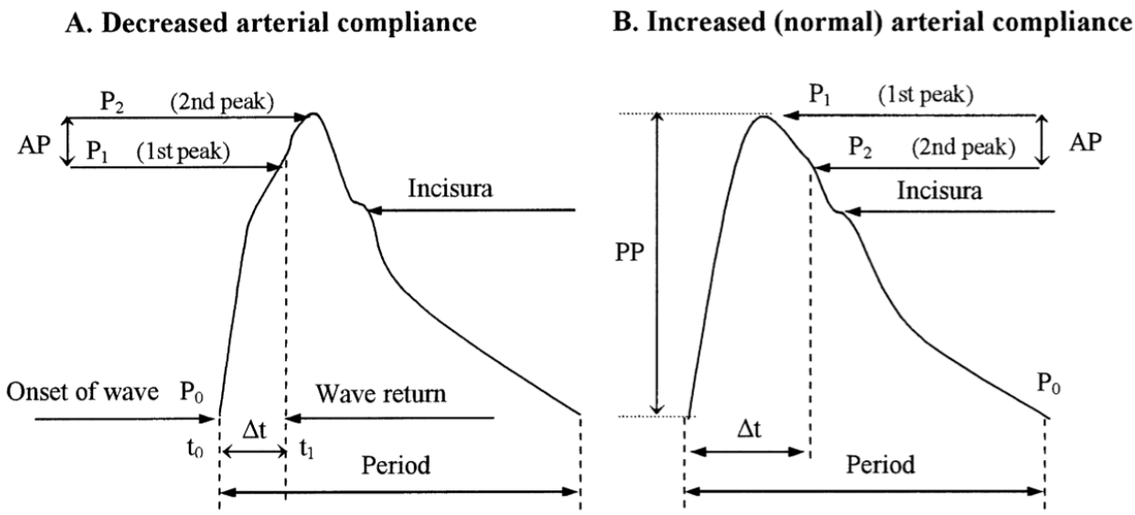

Fig. 4. Effect of decreased (A) and normal (B) arterial compliance on the pulse waveform. P_0: end-diastolic pressure; P_1: early systolic peak; P_2: late systolic peak (from reflected wave); $\triangle t$: time from onset of pressure wave (t_0) to return of reflected wave (t_1); PP: pulse pressure. Reprinted and modified with permission AP: augmentation of systolic aortic pressure (Papaioannou et al., 2004)

subjects with elevated arterial stiffness (Saito et al., 2008). Increased arterial stiffness also results in failure to suppress the pulse oscillations downstream from the central arteries. Decreased pulse suppression potentially increases the risk for damage to micro vascular beds in highly perfused organs such as the brain and kidneys (O'Rourke & Safar, 2005), and has important implications for risk of stroke and renal failure.

Increased arterial stiffness with age and disease is partially compensated for by remodeling of the arteries, through luminal enlargement (Boutouyrie et al., 1992) and wall thickening (Cheng et al., 2002; Zieman et al., 2005). It appears that endothelial dysfunction, which can occur from a decrease in nitric oxide (NO) release, increase in oxidative stress, and/or a decrease in antioxidant capacity with age or disease, is the earliest change in the vasculature that can lead to advancing vascular disease (Taddei et al., 2001; Widlansky et al., 2003). Decreased NO leads to increasing vascular tone of the small arteries responsible for major changes in total peripheral resistance (arterioles). Increasing vascular tone leads to structural and functional changes upstream in the larger arteries, resulting in stiffening and remodeling, increasing blood pressure (in particular pulse pressure), as well as atherosclerotic plaque development and additional functional abnormalities (Folkow, 1995). However, this temporal sequence in the manifestation of arterial disease is not always present, as structural changes can present without obvious functional changes, and these structural changes are not always homogenous across the vascular tree (Naghavi, 2009).

Arterial stiffness is emerging as one of the most important determinants of increased systolic blood pressure and pulse pressure in ageing and disease. It is the root cause of a number of cardiovascular complications including left ventricular hypertrophy, left ventricular failure, aneurism formation and rupture, and is a major contributor to atherosclerotic and small vessel disease, which can lead to stroke, myocardial infarction and renal failure (Nichols & O'Rourke, 2005). Central artery stiffening, in particular aortic stiffening, is strongly related to cardiovascular events, independent of age, arterial pressure, and conventional risk factors for cardiovascular disease (Adji et al., 2011), as well as future hypertension risk after correcting for systolic blood pressure, age, sex, body mass index, heart rate, total cholesterol, diabetes, smoking, alcohol and physical activity (Dernellis & Panaretou, 2005). In fact, stiffening of the aorta rather than left ventricular myocardial abnormalities appears to be the predominant cause of cardiac failure with age (Levy & Brink, 2005) as it produces higher systolic pressures in the aorta and left ventricle. These elevated systolic pressures present a high load on the ventricle, predisposing it to increased systolic wall stress and remodeling, which can progress to dysfunction and failure (Adji et al., 2011).

A variety of techniques for measuring arterial stiffness have been developed. In particular, with the use of ultrasonography, two techniques have been utilized extensively and have been validated for measuring central arterial stiffness non-invasively. In the measurement of regional arterial stiffness, pulse wave velocity has emerged as the gold standard (Laurent et al., 2006) for the noninvasive assessment of arterial stiffness, while local arterial stiffness measures, specifically at the carotid artery, have emerged as an important tool for the mechanistic study of vascular structure and function. Although researchers and clinicians extensively use arterial stiffness measures, a number of potential limitations to these techniques have been identified (Laurent et al., 2006; O'Rourke et al., 2002). Assumption of a homogenous vascular wall when it is heterogeneous in nature, the use of different locations for measures of pressure and arterial diameter, and failing to account for the altering effects

of heart rate (which affects the rate that pulse pressure amplifies) (Wilkinson et al., 2002) and cardiac contractility (O'Rourke et al., 2002) are common oversights in measurement. Furthermore, nervous system activity, fluctuations in autonomic control, vasoactive substances such as nitric oxide, and hormones influence vascular smooth muscle, which can also influence arterial stiffness. Muscular arteries, particularly smaller arteries (O'Rourke et al., 2002), are also subject to spontaneous vasomotor changes that affect both diameter and stiffness (Hayoz et al., 1993). Despite these limitations, measures of arterial stiffness are considered an integral tool in the noninvasive assessment of vascular structure and function, and are an important determinant for cardiovascular risk.

3.2 Local arterial stiffness and measurement

3.2.1 Viscoelastic properties of the arterial wall

The arterial wall is considered to be viscoelastic, as it contains both elastic and viscous properties (Nichols & O'Rourke, 2005). When a stress is applied (a force that produces deformation) to a perfectly elastic material, it will regain its original form when the stress is removed. In an artery, however, wall viscosity is present, which leads to the wall retaining part of the deformation (London & Pannier, 2010). This is partially responsible for hysteresis seen in the pressure-diameter loop (Figure 5). Unfortunately the viscosity of the wall is difficult to measure in humans, and therefore the elasticity component of the arterial wall is what has been extensively evaluated.

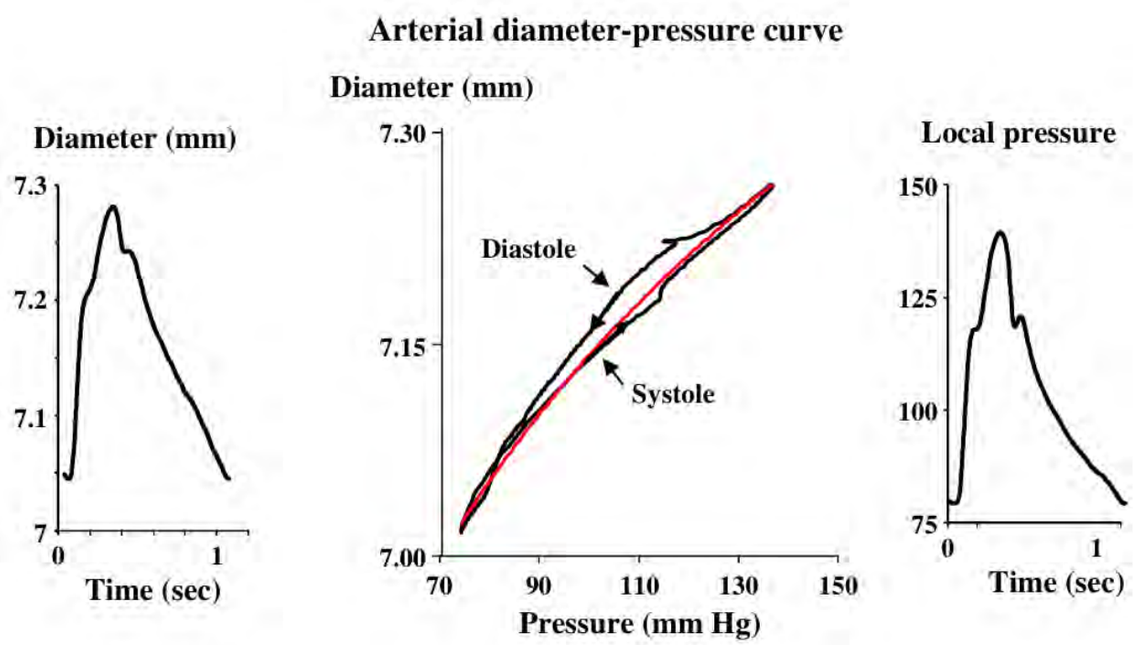

Fig. 5. Diameter-pressure curve (middle) derived from the diameter (left) and local pressure (right) of the common carotid artery. Differences in systole and diastole represent the energy dissipation due to viscous properties of the arterial wall. The red line is the averaged pressure-diameter curve. Reprinted and modified with permission (London & Pannier, 2010)

3.2.2 Calculations of local arterial stiffness

The elasticity of the arterial wall can be gauged by understanding the stress/strain relationship. While stress is the force producing deformation, strain is the resulting deformation incurred as a percentage change in length (Cavalcante et al., 2011). Strain therefore is dimensionless, and the stress/strain ratio is known as the elastic modulus, or Young's modulus (O'Rourke et al., 2002). In an artery, assuming the segment is a cylindrical tube with a circular luminal cross-section (Pannier et al., 2002; Reneman et al., 2005), compliance is considered the absolute change in volume (strain) due to a change in pressure (stress). Distensibility takes into account the initial dimensions of the artery, and is considered the relative change in volume for a given pressure. The equations are as follows:

$$\text{Compliance} = \frac{\Delta CSA}{PP} = \frac{\Pi r^2 - \Pi r^2}{PP} = \frac{\Pi\left(\frac{d\,max}{2}\right)^2 - \Pi\left(\frac{d\,min}{2}\right)^2}{PP} \quad (1)$$

$$\text{Distensibility} = \frac{\Pi\left(\frac{d\,max}{2}\right)^2 - \Pi\left(\frac{d\,min}{2}\right)^2}{\Pi\left(\frac{d\,min}{2}\right)^2 \times PP} \quad (2)$$

where dmax is the maximum systolic diameter, dmin is the minimum diastolic diameter, and PP is the carotid pulse pressure. Compliance and distensibility can both be estimated as a change in radius, diameter, flow, or cross sectional area for a given change in pulse pressure, measured at the same site (Nichols & O'Rourke, 2005). The resistance to deformation is known as stiffness, which in turn is the reciprocal of compliance.

Local arterial stiffness of the central arteries is directly determined, as denoted from a change in pressure producing a given change in volume (Laurent et al., 2006) (Figure 6). In the large elastic arteries (i.e. the carotid artery or aorta) the relationship between lumen cross sectional area and change in pressure is linear (Meinders & Hoeks, 2004) and the error from this assumption is quite small (Reneman et al., 2005). In stiffer peripheral muscular arteries this error can be large (Reneman et al., 2005), therefore direct measures done at the carotid artery and aorta for determining local stiffness have been extensively explored.

Young's modulus, or the incremental elastic modulus (E_{inc}), outlined in equation [3], has been used extensively (Nichols & O'Rourke, 2005). It estimates the elastic properties of the arterial wall by taking into account it's thickness. Current measuring techniques unfortunately cannot differentiate the load bearing section of the wall (media/adventitia) from the non-load bearing portion (intima). Intima-media thickness (IMT) is used as a surrogate for wall thickness, as the adventitia is indistinguishable from surrounding structures with ultrasound imaging techniques. The assumptions are that the IMT is load bearing, and that the arterial wall is homogeneous (Adji et al., 2011; O'Rourke et al., 2002). Thus caution should be exercised in using Young's modulus as current measurements can be imprecise and unrealistic (O'Rourke et al., 2002).

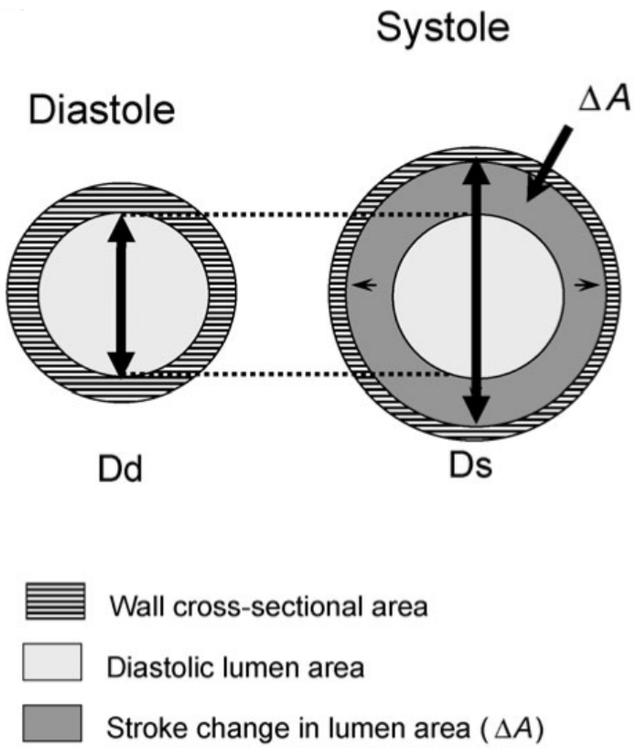

Fig. 6. Measurement of local arterial stiffness: change in luminal cross sectional area (△A) for a given change in pressure (diastole to systole). Reprinted and modified with permission (Laurent et al., 2006)

$$E_{inc} = \frac{3\left(\frac{1+\Pi\left(\frac{d\,min}{2}\right)^2}{\Pi\left(\frac{de}{2}\right)^2-\Pi\left(\frac{di}{2}\right)^2}\right)}{\frac{CSA}{\Pi\left(\frac{d\,min}{2}\right)^2\times PP}} \quad (3)$$

where de is the external diameter and di is the internal diameter, measured in diastole.

Peterson's elastic modulus (Peterson et al., 1960), outlined in equation [4], is different from Young's elastic modulus. It assumes a linear stress strain relationship, is inversely related to arterial distensibility, and needs to be specified at a given blood pressure (Cheng et al., 2002). In turn, an equation that provides an index of arterial compliance independent of distending pressure is the β stiffness index (Hirai et al., 1989), outlined in equation [5], where SBP is systolic blood pressure, and DBP is diastolic blood pressure.

$$\text{Peterson} = \frac{\Pi\left(\frac{d\,\min}{2}\right)^2 \times PP}{\Pi\left(\frac{d\,\max}{2}\right)^2 - \Pi\left(\frac{d\,\min}{2}\right)^2} \tag{4}$$

$$\beta = \frac{\ln\left(\frac{SBP}{DBP}\right)}{\left(\frac{d\,\max - d\,\min}{d\,\min}\right)} \tag{5}$$

3.2.3 Measurement of local arterial stiffness with ultrasound and tonometry

Ultrasound is a common tool used in the non-invasive assessment of the elastic properties of the arterial wall. Many devices have been developed to determine vascular diameters and IMT. These include echo tracking software (Hoeks et al., 1990; Tardy et al., 1991), which use radiofrequency signals to obtain a high precision image, as well as B-mode ultrasound equipped with a high-resolution linear array transducer (Currie et al., 2010; Nualnim et al., 2011; Redheuil et al., 2010; Tanaka et al., 2000) in combination with various edge detection and image analysis software. Both methods have been shown to have high agreement for assessing vessel diameter (A. S. Kelly et al., 2004). Measurement of IMT using non-invasive ultrasound systems is also an important tool and is used as a surrogate measure for wall thickness in measures of elasticity of the arterial wall such as Young's modulus. IMT is also often used as an indicator for cardiovascular disease (O'Leary et al., 1999) and has been employed in clinical studies (Molinari et al., 2010; Simon et al., 2002).

Most commonly, B-mode ultrasound images are collected at a minimum of 10 frames/sec with a 7.5-11 MHz linear array transducer positioned longitudinally to the common carotid artery with collection ~1-2 cm below the bifurcation of the external and internal carotid arteries. Analysis of time points associated with the maximal diameter in systole and the minimum diameter in diastole are selected and diameters are determined by measurement of the far wall from the interface of the lumen and intima to the near wall interface of the adventitia and media (Tanaka et al., 2000). Imaging of media-adventitia interface of the near wall is used, as the intima-lumen interface can be difficult to obtain. Determination of arterial diameters can be made manually using calipers, or with edge-detection software. Most edge-detection software determines the arterial diameter by identifying the arterial wall within a selected region of interest, based on the contrasting intensity of brightness between the arterial wall boundary and the lumen (Currie et al., 2010; Peters et al., 2011). Measurements are made at numerous points within the region of interest (typically ≥100 points), thereby increasing the precision of the measurement. Other software uses the radiofrequency signals generated from the tissue echo reflections to detect boundaries in tissue density. The radiofrequency detection has the added advantage of not being

dependent on the post-processing of the B-mode images but is less commonly available (Woodman et al., 2001).

Local arterial measures also require measurement of local blood pressure. Applanation tonometry has been shown to produce near-identical pulse waveforms as those performed invasively (R. Kelly et al., 1989). Applanation tonometry uses a probe that incorporates a high fidelity strain gauge transducer which records continuous pressure waveforms in an artery. It is placed over the greatest area of pulsation, and requires support from solid structures (bone, bone plus ligaments) to flatten the artery slightly to produce a consistent and reproducible signal (R. Kelly et al., 1989). Based on the assumption that diastolic and mean blood pressure are constant through the arterial tree (Nichols & O'Rourke, 2005), Kelly and Fitchett developed a system of approximation of local arterial pressure using a tonometer (R. Kelly & Fitchett, 1992), which has been shown to provide the highest accuracy compared to invasive methods (Van Bortel et al., 2001). As baseline levels acquired by the tonometer are subject to hold down pressure, diastolic and mean blood pressures are equated to brachial blood pressures. Local systolic blood pressure is then determined by the extrapolation of the maximal tonometer signal and calibrated pressures, due to the amplification in systolic blood pressure (Nichols & O'Rourke, 2005). An example of this is provided in Figure 7. Ideally carotid artery pressures should be calibrated to concurrent brachial blood pressures measured continuously using various automated oscillometric blood pressure devices (Ex. Finometer (Finapres Medical Systems B.V.; Amsterdam, The Netherlands), Nexfin (BMEYE; Amsterdam, The Netherlands), CMB-700 (Colin Medical Instruments; San Antonio, TX, USA)), which correct to brachial blood pressure from either finger or radial artery waveforms. When this is not possible, carotid artery pressures can

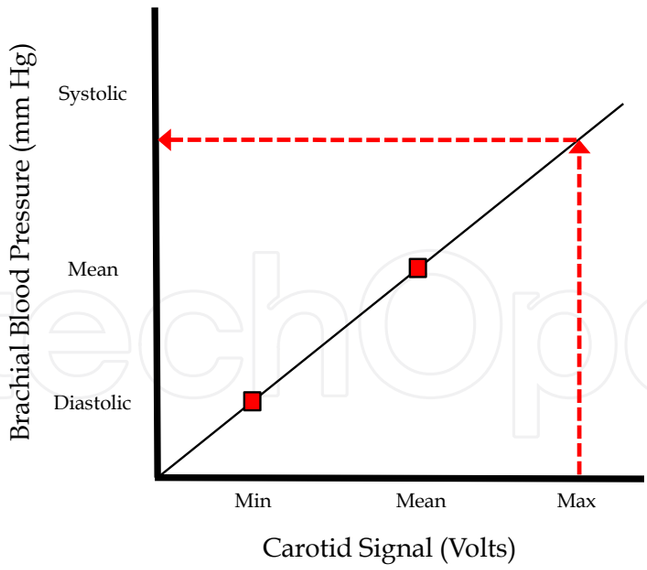

Fig. 7. Approximation of carotid systolic pressure. Minimum and mean carotid artery tonometry values are equated to the diastolic and mean brachial artery blood pressures (red squares), and the equation of the line connecting the points is generated. The pressure (y-axis) at which the maximum carotid artery tonometry value intersects with this line is identified as the predicted carotid artery systolic blood pressure.

also be calibrated to discrete brachial blood pressures collected using a manual sphygmomanometer or an automated oscillometric device. It should be mentioned that previous investigations (Barenbrock et al., 2002; Dijk et al., 2005; Tsivgoulis et al., 2006) have used brachial pulse pressures in the calculation of arterial stiffness measurements when the collection of localized pulse pressure is not available; however, this is not recommended.

Common carotid artery diameter and simultaneous carotid artery blood pressures are collected for 10 cardiac cycles (Currie et al., 2010) in the supine position following at least 10 minutes of quiet rest. Assessments should be performed in a temperature-controlled room, at the same time of day (for repeated measures), and individuals should abstain from caffeine, food consumption, and smoking for at least 3 hours, and alcohol consumption for at least 10 hours prior to testing (Laurent et al., 2006). Section 4 will discuss the association between local measures of carotid artery stiffness and disease; however; it has been suggested that local measures of arterial stiffness be used in mechanistic studies in pathophysiology, pharmacology, and therapeutics, rather than epidemiological studies moving forward (Laurent et al., 2006).

3.2.4 Validity, reliability, and reproducibility of local arterial measurements

Carotid measurements have been validated in clinical studies (Boutouyrie et al., 1999), as both ultrasound imaging for detection of lumen diameter and IMT (Gamble et al., 1994; Hoeks et al., 1990; Hoeks et al., 1997; A. S. Kelly et al., 2004) and use of applanation tonometry (R. Kelly et al., 1989) has been shown to be accurate and reproducible. Between visit coefficient of variation for distensibility measures using B-mode ultrasound imaging techniques is approximately 10% (Kanters et al., 1998; Liang et al., 1998), whereas IMT measures have a coefficient of variation of 2.6-2.8% (Currie et al., 2010; Liang et al., 1998).

3.2.5 Limitations of local arterial measurements

There are several limitations when measuring local arterial stiffness. Applanation of an artery requires a firm background surface to flatten the artery and low levels of subcutaneous fat to avoid dampening of the pulse (Reneman et al., 2005), therefore acquiring a pulse can be an issue in obese individuals. Local stiffness measures using ultrasound are also less sensitive than MRI measures of age-related ascending aortic stiffness in individuals free of cardiovascular disease (Redheuil et al., 2010). However, ultrasound is still a highly accessible clinical tool, and its use for determination of stiffness in the carotid artery is an accepted technique in the assessment of central artery stiffening. Finally, the predictive capacity of carotid stiffness measures for vascular events in patients with manifest arterial disease has been shown to be limited (Dijk et al., 2005). Although, brachial pressures were used in this study as a surrogate of local carotid pressure, therefore caution should be used when considering this result (see Figure 7).

3.3 Regional arterial stiffness and measurement

Regional arterial stiffness can be assessed using pulse wave velocity (PWV), which is commonly defined as the speed of the arterial pulse wave throughout the vasculature (O'Rourke et al., 2002). As previously described, ventricular ejection produces an incident pressure wave, which moves away from the heart and towards the peripheral vasculature at

a finite speed. The assessment of how fast the incident wave travels, or its PWV, can provide information about the stiffness of different arterial segments. The faster the PWV, the stiffer the artery, which is addressed by the Moens-Korteweg equation (O'Rourke, 2006):

$$PWV = \sqrt{\frac{Eh}{2Rp}} \tag{6}$$

where E represents the intrinsic elastic properties of the vessel (Young's modulus in the circumferential direction), p is the blood density, and (h/2R) is the ratio of arterial wall thickness to vessel diameter. However, PWV can be determined practically and non-invasively using a variety of pulse detection tools including continuous wave or pulsed wave Doppler ultrasound.

3.3.1 Measurement of regional arterial stiffness

The assessment of PWV involves recording pulse waves at two different arterial sites, for a minimum of 10-15 seconds, to ensure measurement across at least one respiratory cycle (Van Bortel et al., 2002). Traditionally PWV is separated into central and peripheral measurements to account for differences in vascular composition of different portions of the vascular tree. Central PWV, also referred to as aortic PWV, provides an index of stiffness of the large elastic arteries, and is commonly measured as the PWV between the carotid and femoral arterial sites. Peripheral pulse wave velocity provides an index of stiffness of the medium sized muscular arteries, and can be separated into upper limb and lower limb measures. Upper limb assessments typically involve pulse detection at the carotid and brachial or radial arterial sites, where as lower limb PWV can be measured from the femoral artery to either the dorsalis pedis or posterior tibial arterial sites. Doppler ultrasound can be used to collect blood velocity signals at any of the sites listed above. However, aortic PWV can also be determined by collecting blood velocity signals at the suprasternal notch (root of the left subclavian artery), and the umbilicus (near the bifurcation of the abdominal aorta) (Lehmann et al., 1998).

3.3.2 Calculations of regional arterial stiffness

PWV is calculated using the following equation:

$$PWV = \frac{D}{\Delta t} \tag{7}$$

where D is the distance between measurement sites, and Δt is the pulse transit time.

Distance is measured along the surface of the body with anthropometric measuring tape, using specific anatomical landmarks. Central PWV measurements can be made using one of the following pathways: 1) total distance between carotid (carotid artery site to sternal notch) and femoral (sternal notch to inferior border of the umbilicus + inferior border of the umbilicus to the femoral artery site) arterial sites, 2) subtracting the distance of the carotid artery site from the total distance, or 3) subtracting the distance of the carotid artery site

from the femoral artery site, which has recently been shown to have the best agreement with invasive measures (Weber et al., 2009). When standardization between distance measurement pathways is needed, central distance values can be converted to the total distance between carotid and femoral arterial sites (The Reference Values for Arterial Stiffness' Collaboration, 2010). PWV can then be multiplied by 0.8 to correct for the overestimation (The Reference Values for Arterial Stiffness' Collaboration, 2010). For upper limb PWV, the distance between the carotid artery site to the sternal notch is subtracted from the distance between the sternal notch and the upper limb site (brachial or radial artery site), which is measured when the arm is abducted 90 degrees. Lower limb measurements are made from the femoral artery site along the leg to either the dorsalis pedis or posterior tibial artery site.

The pulse transit time is determined as the time delay between the arrival of the pulse wave at the two arterial sites, and is calculated using the following equation:

$$\Delta t = T_2 - T_1 \tag{8}$$

where T_2 is the pulse arrival time at the distal site, and T_1 is the pulse arrival time at the proximal site. Time at each site can be determined online or offline. Online analysis uses the ECG trace and manual calipers to determine the time at the R-spike and at the arrival of the blood velocity waveform, which is commonly identified as the foot of the waveform. By subtracting the two values, you can determine time for that arterial site (either T_1 or T_2). To perform offline analysis, the raw audio signal from the color wave or pulsed wave Doppler ultrasound is outsourced to an external data collection system. The most reliable techniques include identifying, 1) the intersecting point between the tangent to the initial systolic upstroke of the blood velocity signal, and the horizontal line through the minimum point, and 2) the second derivative of the blood velocity signal, where the arrival of the waveform is identified as the maximum value (Figure 8) (Chiu et al., 1991). However, identification of the arrival of the pulse wave using derivatives has been criticized, since the shape of the waveform changes with heart rate fluctuations (Nichols & O'Rourke, 2005), altering where the peak of the derivative identifies. The arrival of the waveform can also be identified based on the phase velocity theory, which suggests the foot of the waveform is primarily composed of frequencies between 5 and 30 Hz, near the 30 Hz value (McDonald, 1968; Munakata et al., 2003). By filtering out the lower and higher frequencies from the signal using a band-pass filter (<5Hz, >30Hz), the foot of the waveform can be identified as the minimum value of the filtered signal. Unlike the derivative method, fluctuations in heart rate do not influence analysis since the frequencies are unaffected (Nichols & O'Rourke, 2005). When blood velocity signals are collected simultaneously using more than one Doppler probe, time at each site can easily be identified using the maximum or minimum value. When signals are collected sequentially, time at each site is determined using an ECG trace, similar to the online analysis.

3.3.3 Additional devices for the assessment of regional arterial stiffness

The assessment of PWV using Doppler ultrasound has been shown to be valid and reliable (Jiang et al., 2008; Sutton-Tyrrell et al., 2001). However, there are several other techniques available for the detection of the pulse wave in the determination of PWV including

applanation tonometry (as previously described), photoplethysmographic sensors, and magnetic resonance imaging (MRI). Photoplethysmographic sensors contain an infrared emitting diode (peak wavelength 880nm), and a phototransistor detector. The infrared light is either absorbed by the blood and vascular tissue, scattered by other tissues, or reflected back to the detector. The arterial waveform in generated based on how much infrared light is reflected back to the detector (Loukogeorgakis et al., 2002). Flow measurements can also be made using MRI. This technique is capable of providing accurate PWV assessments since distance can be measured along the anatomical segment (Mohiaddin et al., 1993).

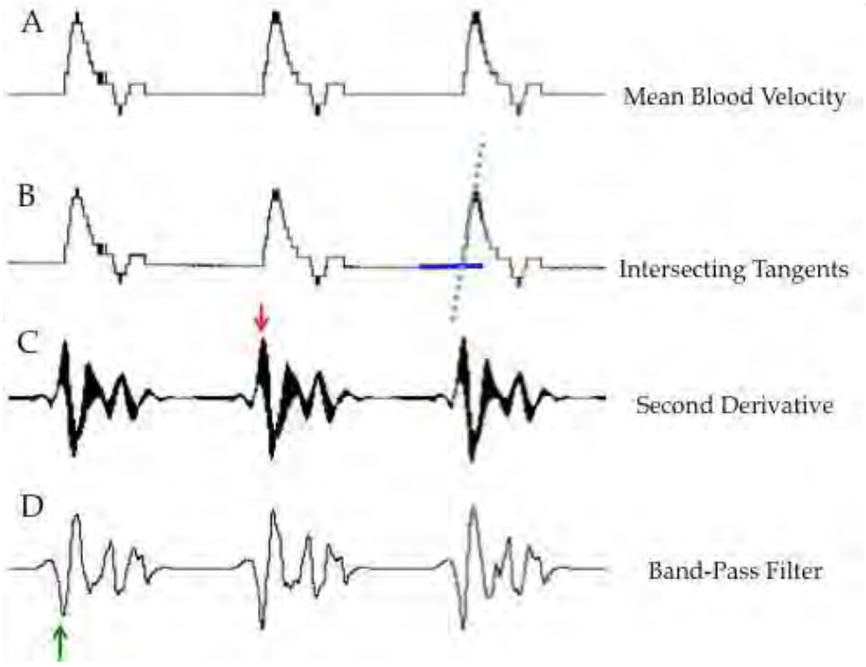

Fig. 8. Various analysis methods for identifying pulse transit time. The arrival of the mean blood velocity waveform (A) is identified with a red arrow. The intersecting tangent (B) analysis locates the point of intersection between the tangent to the initial systolic upstroke of the signal (dotted line), and the horizontal line through the minimum point (closed line). Pulse arrival can also be identified as the maximum value of the second derivative (C), or the minimum value of the band-pass filter (D).

3.3.4 Limitations of regional arterial stiffness measurements

PWV does have its limitations. The measurement of distance along the surface of the body is not a true anatomical representative of the arterial segment and therefore can introduce error into the PWV calculation. Pulse wave measurements at the two arterial sites should be collected simultaneously; however, equipment limitations may not permit this. While the collection of sequential measurements is sufficient, caution should be exercised when interpreting results. While MRI assessments of PWV are not subjective to these limitations, the technique is not that widely used given the lack of available equipment and high cost per use.

3.3.5 Local versus regional assessment of arterial stiffness

Aortic stiffness measures (via carotid-femoral PWV) and local carotid measures of distensibility have been compared (Paini et al., 2006). Strong correlations exist between the two measures in healthy subjects, but decrease with an increasing number of comorbidities (hypertension; hypertension and type 2 diabetes), as the aorta stiffens disproportionately to the carotid artery with age and other cardiovascular risk factors (Paini et al., 2006). Stiffness measures at the carotid artery, therefore, seem to provide a strong estimation for aortic stiffness in less diseased individuals, but aortic and carotid stiffness measures should not be used synonymously in higher risk populations.

4. Arterial stiffness in health and disease

Indices of arterial stiffness provide a non-invasive assessment of the health of the vasculature, and can provide relevant information about an individual's future risk of morbidity and mortality. While arterial stiffening is primarily attributed to modifications to the intrinsic structure of the vessel, several lifestyle factors can transiently augment or attenuate arterial stiffness. Caffeine consumption (Mahmud & Feely, 2001), smoking (Mahmud & Feely, 2003), and resistance exercise (DeVan et al., 2005) have been shown to temporarily increase arterial stiffness, whereas alcohol consumption (Mahmud & Feely, 2002), food consumption (Ahuja et al., 2009), and aerobic exercise (Kingwell et al., 1997) transiently decrease arterial stiffness. Chronic exposure to these factors, however, can lead to more permanent changes in arterial stiffness. Elevated resting arterial stiffness is observed in habitual smokers and individuals who consume excess caffeine and alcohol. Conversely, individuals who are habitually active, or who undergo an exercise training program are capable of attenuating or reversing age associated increases in arterial stiffness (Tanaka et al., 2000). Resting arterial stiffness is also affected by time of day, with larger arterial diameters and lower blood pressures reported at night (Kool et al., 1992).

Arterial stiffness increases naturally with age (O'Rourke & Hashimoto, 2007), and the rate of arterial stiffening is often associated with lifestyle factors (discussed above) and disease. Arterial stiffness is present in individuals with congenital diseases such as Marfan syndrome (Hirata et al., 1991), congenital heart diseases including coarctation of the aorta (de Divitiis et al., 2001) and tetralogy of Fallot (Cheung et al., 2006), as well as non-congenital conditions including but not limited to Kawasaki disease (Senzaki et al., 2005) and end-stage renal disease (Blacher et al., 1999). Traditional risk factors for cardiovascular disease are associated with increased arterial stiffening in adults, including obesity (Danias et al., 2003), type 2 diabetes (Henry et al., 2003), hypertension (Ting et al., 1986), and hypercholesterolemia (Wilkinson et al., 2002). Additionally, the presence of atherosclerosis is associated with arterial stiffening at various sites within the vascular tree (van Popele et al., 2001; van Popele et al., 2006). Not surprisingly, elevated arterial stiffness is present in individuals with cardiovascular diseases including coronary artery disease (Weber et al., 2004), heart failure (Kawaguchi et al., 2003), and stroke (Mattace-Raso et al., 2006).

Adolescents and children with cardiovascular disease risk factors including familial hypercholesterolemia (Aggoun et al., 2000), obesity (Tounian et al., 2001), and type 1 diabetes (Heilman et al., 2009) demonstrate greater arterial stiffness than their age and

gender matched peers. While these studies are cross-sectional in design, and provide no information about their future outcomes, the research suggests children and adolescents with impaired arterial compliance are at a greater risk for disease development in adulthood.

Several investigations have examined the association between indices of arterial stiffness and future risk of cardiovascular morbidity and mortality and all-cause mortality. Aortic (carotid to femoral) PWV is considered the non-invasive gold standard measure of arterial stiffness. In apparently healthy men and women, higher aortic PWV (≥ 11.8 m/s) is associated with a 48% increased risk of first major cardiovascular disease event including myocardial infarction, unstable angina, heart failure and/or stroke (Mitchell et al., 2010). According to a meta-analysis on aortic PWV, an increase of 1 m/s corresponds to an age, gender, and risk factor adjusted risk increase of 15% for cardiovascular and all-cause mortality (Vlachopoulos et al., 2010). This systematic review included a variety of populations and measurement techniques and therefore provides a comprehensive examination of the risk associated with elevated aortic stiffness. However, there are numerous other studies demonstrating increased risk of mortality in clinical populations with elevated aortic PWV including but not limited to end-stage renal disease (Blacher et al., 1999), hypertension (Laurent et al., 2001), and type 2 diabetes (Cruickshank et al., 2002).

The literature on the relationship between other indices of arterial stiffness and future risk of morbidity and mortality is not as well defined. Some investigations demonstrate no association between decreased carotid artery compliance and distensibility and future risk (Leone et al., 2008; van Dijk et al., 2001), whereas other studies demonstrate elevated risk in individuals with carotid artery stiffness (Barenbrock et al., 2002; Tsivgoulis et al., 2006). Additionally, not all of these investigations used local carotid pulse pressure in the calculation of arterial stiffness; therefore the findings should be interpreted with caution.

5. Future directions and conclusions

Efforts have recently been made to establish reference values of arterial stiffness for carotid-femoral PWV (The Reference Values for Arterial Stiffness' Collaboration, 2010). This is an important first step in understanding the baseline changes that occur with arterial stiffness in the healthy person as they age. Furthering these attempts will continue to elucidate the role of stiffness in aging, and will significantly contribute to understanding the role of stiffness in disease. Furthermore, even though stiffness measures have been shown to be strong prognostic indicators for the occurrence of cardiovascular events, work has yet to be done to show if the reduction or attenuation of arterial stiffness is associated with a reduction of cardiovascular events, independent of other risk factors (Laurent & Boutouyrie, 2007). Indeed, more immediate changes such as reductions in blood pressure, hyperglycemia, and lipids do show reductions in cardiovascular risk scores. However, improvements in the wall of the vessel (stiffness) may in fact suggest more long lasting reductions in cardiovascular risk, but this remains to be seen (Laurent & Boutouyrie, 2007).

Despite these future considerations, measurement of arterial stiffness is critical in understanding changes in the vascular tree, as its indices can be transiently and chronically altered by aging, disease, and lifestyle factors. Aortic PWV is considered the gold standard for non-invasive assessments of arterial stiffness, and can provide the most relevant

information about an individual's future risk of cardiovascular morbidity and mortality, and all-cause mortality. Measurement of local arterial stiffness, while requiring more expertise and time, has also emerged as an important tool for the mechanistic study of vascular structure and function, especially in less diseased populations. In combination, these ultrasonic techniques provide a simple, comprehensive, and non-invasive approach to understand arterial structure and function. They should therefore be considered in the study of overall vascular health.

6. References

Adji, A., O'Rourke, M. F., & Namasivayam, M. (2011). Arterial stiffness, its assessment, prognostic value, and implications for treatment. *American Journal of Hypertension*, Vol. 24, No. 1 (Jan 2011), pp. 5-17. 1941-7225

Aggoun, Y., Bonnet, D., Sidi, D., Girardet, J. P., Brucker, E., Polak, M., Safar, M. E., & Levy, B. I. (2000). Arterial mechanical changes in children with familial hypercholesterolemia. *Arteriosclerosis, Thrombosis, and Vascular Biology*, Vol. 20, No. 9 (Sept 2000), pp. 2070-2075. 1524-4636

Ahuja, K. D., Robertson, I. K., & Ball, M. J. (2009). Acute effects of food on postprandial blood pressure and measures of arterial stiffness in healthy humans. *The American Journal of Clinical Nutrition*, Vol. 90, No. 2 (Aug 2009), pp. 298-303. 1938-3207

Armentano, R. L., Levenson, J., Barra, J. G., Fischer, E. I., Breitbart, G. J., Pichel, R. H., & Simon, A. (1991). Assessment of elastin and collagen contribution to aortic elasticity in conscious dogs. *American Journal of Physiology*, Vol. 260, No. 6 (Jun 1991), pp. H1870-1877. 0002-9513

Atkinson, J. (2008). Age-related medial elastocalcinosis in arteries: mechanisms, animal models, and physiological consequences. *Journal of Applied Physiology*, Vol. 105, No. 5 (Nov 2008), pp. 1643-1651. 8750-7587

Barenbrock, M., Kosch, M., Joster, E., Kisters, K., Rahn, K. H., & Hausberg, M. (2002). Reduced arterial distensibility is a predictor of cardiovascular disease in patients after renal transplantation. *Journal of Hypertension*, Vol. 20, No. 1 (Jan 2002), pp. 79-84. 0263-6352

Benetos, A., Laurent, S., Hoeks, A. P., Boutouyrie, P. H., & Safar, M. E. (1993). Arterial alterations with aging and high blood pressure. A noninvasive study of carotid and femoral arteries. *Arteriosclerosis, Thrombosis, and Vascular Biology*, Vol. 13, No. 1 (Jan 1993), pp. 90-97. 1049-8834

Blacher, J., Guerin, A. P., Pannier, B., Marchais, S. J., Safar, M. E., & London, G. M. (1999). Impact of aortic stiffness on survival in end-stage renal disease. *Circulation*, Vol. 99, No. 18 (May 1999), pp. 2434-2439. 1524-4539

Boutouyrie, P., Bussy, C., Lacolley, P., Girerd, X., Laloux, B., & Laurent, S. (1999). Association between local pulse pressure, mean blood pressure, and large-artery remodeling. *Circulation*, Vol. 100, No. 13 (Sept 1999), pp. 1387-1393. 1524-4539

Boutouyrie, P., Laurent, S., Benetos, A., Girerd, X. J., Hoeks, A. P., & Safar, M. E. (1992). Opposing effects of ageing on distal and proximal large arteries in hypertensives. *Journal of Hypertension Supplement*, Vol. 10, No. 6 (Aug 1992), pp. S87-91. 0952-1178

Cavalcante, J. L., Lima, J. A., Redheuil, A., & Al-Mallah, M. H. (2011). Aortic stiffness: current understanding and future directions. *Journal of the American College of Cardiology*, Vol. 57, No. 14 (Apr 2011), pp. 1511-1522. 1558-3597

Cheng, K. S., Baker, C. R., Hamilton, G., Hoeks, A. P., & Seifalian, A. M. (2002). Arterial elastic properties and cardiovascular risk/event. *European Journal of Vascular and Endovascular Surgery*, Vol. 24, No. 5 (Nov 2002), pp. 383-397. 1078-5884

Cheung, Y. F., Ou, X., & Wong, S. J. (2006). Central and peripheral arterial stiffness in patients after surgical repair of tetralogy of Fallot: implications for aortic root dilatation. *Heart*, Vol. 92, No. 12 (Dec 2006), pp. 1827-1830. 1468-201X

Chiu, Y. C., Arand, P. W., Shroff, S. G., Feldman, T., & Carroll, J. D. (1991). Determination of pulse wave velocities with computerized algorithms. *American Heart Journal*, Vol. 121, No. 5 (May 1991), pp. 1460-1470. 0002-8703

Cruickshank, K., Riste, L., Anderson, S. G., Wright, J. S., Dunn, G., & Gosling, R. G. (2002). Aortic pulse-wave velocity and its relationship to mortality in diabetes and glucose intolerance: an integrated index of vascular function? *Circulation*, Vol. 106, No. 16 (Oct 2002), pp. 2085-2090. 1524-4539

Currie, K. D., Proudfoot, N. A., Timmons, B. W., & MacDonald, M. J. (2010). Noninvasive measures of vascular health are reliable in preschool-aged children. *Applied Physiology, Nutrition, and Metabolism*, Vol. 35, No. 4 (Aug 2010), pp. 512-517. 1715-5312

Danias, P. G., Tritos, N. A., Stuber, M., Botnar, R. M., Kissinger, K. V., & Manning, W. J. (2003). Comparison of aortic elasticity determined by cardiovascular magnetic resonance imaging in obese versus lean adults. *American Journal of Cardiology*, Vol. 91, No. 2 (Jan 2003), pp. 195-199. 0002-9149

Davies, J. I., & Struthers, A. D. (2003). Pulse wave analysis and pulse wave velocity: a critical review of their strengths and weaknesses. *Journal of Hypertension*, Vol. 21, No. 3 (Mar 2003), pp. 463-472. 0263-6352

de Divitiis, M., Pilla, C., Kattenhorn, M., Zadinello, M., Donald, A., Leeson, P., Wallace, S., Redington, A., & Deanfield, J. E. (2001). Vascular dysfunction after repair of coarctation of the aorta: impact of early surgery. *Circulation*, Vol. 104, No. 12 (Sep 2001), pp. I165-170. 1524-4539

Dernellis, J., & Panaretou, M. (2005). Aortic stiffness is an independent predictor of progression to hypertension in nonhypertensive subjects. *Hypertension*, Vol. 45, No. 3 (Mar 2005), pp. 426-431. 1524-4563

DeVan, A. E., Anton, M. M., Cook, J. N., Neidre, D. B., Cortez-Cooper, M. Y., & Tanaka, H. (2005). Acute effects of resistance exercise on arterial compliance. *Journal of Applied Physiology*, Vol. 98, No. 6 (Jun 2005), pp. 2287-2291. 8750-7587

Dijk, J. M., Algra, A., van der Graaf, Y., Grobbee, D. E., & Bots, M. L. (2005). Carotid stiffness and the risk of new vascular events in patients with manifest cardiovascular disease. The SMART study. *European Heart Journal*, Vol. 26, No. 12 (Jun 2005), pp. 1213-1220. 0195-668X

Dobrin, P. B. (1999). Distribution of lamellar deformations: implications for properties of the arterial media. *Hypertension*, Vol. 33, No. 3 (Mar 1999), pp. 806-810. 0194-911X

Folkow, B. (1995). Hypertensive structural changes in systemic precapillary resistance vessels: how important are they for in vivo haemodynamics? *Journal of Hypertension*, Vol. 13, No. 12 (Dec 1995), pp. 1546-1559. 0263-6352

Gamble, G., Zorn, J., Sanders, G., MacMahon, S., & Sharpe, N. (1994). Estimation of arterial stiffness, compliance, and distensibility from M-mode ultrasound measurements of the common carotid artery. *Stroke*, Vol. 25, No. 1 (Jan 1994), pp. 11-16. 0039-2499

Harkness, M. L., Harkness, R. D., & McDonald, D. A. (1957). The collagen and elastin content of the arterial wall in the dog. *Proceedings of the Royal Society of London, Series B. Containing papers of a Biological character*, Vol. 146, No. 925 (Jun 1957), pp. 541-551. 0080-4649

Hayoz, D., Tardy, Y., Rutschmann, B., Mignot, J. P., Achakri, H., Feihl, F., Meister, J. J., Waeber, B., & Brunner, H. R. (1993). Spontaneous diameter oscillations of the radial artery in humans. *American Journal of Physiology*, Vol. 264, No. 6 (Jun 1993), pp. H2080-2084. 0002-9513

Heilman, K., Zilmer, M., Zilmer, K., Lintrop, M., Kampus, P., Kals, J., & Tillmann, V. (2009). Arterial stiffness, carotid artery intima-media thickness and plasma myeloperoxidase level in children with type 1 diabetes. *Diabetes Research and Clinical Practice*, Vol. 84, No. 2 (May 2009), pp. 168-173. 1872-8227

Henry, R. M., Kostense, P. J., Spijkerman, A. M., Dekker, J. M., Nijpels, G., Heine, R. J., Kamp, O., Westerhof, N., Bouter, L. M., & Stehouwer, C. D. (2003). Arterial stiffness increases with deteriorating glucose tolerance status: the Hoorn Study. *Circulation*, Vol. 107, No. 16 (Apr 2003), pp. 2089-2095. 1524-4539

Hirai, T., Sasayama, S., Kawasaki, T., & Yagi, S. (1989). Stiffness of systemic arteries in patients with myocardial infarction. A noninvasive method to predict severity of coronary atherosclerosis. *Circulation*, Vol. 80, No. 1 (Jul 1989), pp. 78-86. 0009-7322

Hirata, K., Triposkiadis, F., Sparks, E., Bowen, J., Wooley, C. F., & Boudoulas, H. (1991). The Marfan syndrome: abnormal aortic elastic properties. *Journal of the American College of Cardiology*, Vol. 18, No. 1 (Jul 1991), pp. 57-63. 0735-1097

Hoeks, A. P., Brands, P. J., Smeets, F. A., & Reneman, R. S. (1990). Assessment of the distensibility of superficial arteries. *Ultrasound in Medicine & Biology*, Vol. 16, No. 2 1990), pp. 121-128. 0301-5629

Hoeks, A. P., Willekes, C., Boutouyrie, P., Brands, P. J., Willigers, J. M., & Reneman, R. S. (1997). Automated detection of local artery wall thickness based on M-line signal processing. *Ultrasound in Medicine & Biology*, Vol. 23, No. 7 (1997), pp. 1017-1023. 0301-5629

Jiang, B., Liu, B., McNeill, K. L., & Chowienczyk, P. J. (2008). Measurement of pulse wave velocity using pulse wave Doppler ultrasound: comparison with arterial tonometry. *Ultrasound in Medicine & Biology*, Vol. 34, No. 3 (Mar 2008), pp. 509-512. 0301-5629

Kanters, S. D., Elgersma, O. E., Banga, J. D., van Leeuwen, M. S., & Algra, A. (1998). Reproducibility of measurements of intima-media thickness and distensibility in the common carotid artery. *European Journal of Vascular & Endovascular Surgery*, Vol. 16, No. 1 (Jul 1998), pp. 28-35. 1078-5884

Kawaguchi, M., Hay, I., Fetics, B., & Kass, D. A. (2003). Combined ventricular systolic and arterial stiffening in patients with heart failure and preserved ejection fraction: implications for systolic and diastolic reserve limitations. *Circulation*, Vol. 107, No. 5 (Feb 2003), pp. 714-720. 1524-4539

Kelly, A. S., Kaiser, D. R., Dengel, D. R., & Bank, A. J. (2004). Comparison of B-mode and echo tracking methods of assessing flow-mediated dilation. *Ultrasound in Medicine & Biology*, Vol. 30, No. 11 (Nov 2004), pp. 1447-1449. 0301-5629

Kelly, R., & Fitchett, D. (1992). Noninvasive determination of aortic input impedance and external left ventricular power output: a validation and repeatability study of a

new technique. *Journal of the American College of Cardiology*, Vol. 20, No. 4 (Oct 1992), pp. 952-963. 0735-1097

Kelly, R., Hayward, C., Avolio, A., & O'Rourke, M. (1989). Noninvasive determination of age-related changes in the human arterial pulse. *Circulation*, Vol. 80, No. 6 (Dec 1989), pp. 1652-1659. 0009-7322

Kingwell, B. A., Berry, K. L., Cameron, J. D., Jennings, G. L., & Dart, A. M. (1997). Arterial compliance increases after moderate-intensity cycling. *Am J Physiol*, Vol. 273, No. 5 (Nov 1997), pp. H2186-2191. 0002-9513

Kool, M. J., Struijker-Boudier, H. A., Wijnen, J. A., Hoeks, A. P., & van Bortel, L. M. (1992). Effects of diurnal variability and exercise training on properties of large arteries. *Journal of Hypertension Supplement*, Vol. 10, No. 6 (Aug 1992), pp. S49-52. 0952-1178

Lanne, T., Sonesson, B., Bergqvist, D., Bengtsson, H., & Gustafsson, D. (1992). Diameter and compliance in the male human abdominal aorta: influence of age and aortic aneurysm. *European Journal of Vascular Surgery*, Vol. 6, No. 2 (Mar 1992), pp. 178-184. 0950-821X

Laurent, S., & Boutouyrie, P. (2007). Recent advances in arterial stiffness and wave reflection in human hypertension. *Hypertension*, Vol. 49, No. 6 (Jun 2007), pp. 1202-1206. 1524-4563

Laurent, S., Boutouyrie, P., Asmar, R., Gautier, I., Laloux, B., Guize, L., Ducimetiere, P., & Benetos, A. (2001). Aortic stiffness is an independent predictor of all-cause and cardiovascular mortality in hypertensive patients. *Hypertension*, Vol. 37, No. 5 (May 2001), pp. 1236-1241. 1524-4563

Laurent, S., Boutouyrie, P., & Lacolley, P. (2005). Structural and genetic bases of arterial stiffness. *Hypertension*, Vol. 45, No. 6 (Jun 2005), pp. 1050-1055. 1524-4563

Laurent, S., Cockcroft, J., Van Bortel, L., Boutouyrie, P., Giannattasio, C., Hayoz, D., Pannier, B., Vlachopoulos, C., Wilkinson, I., & Struijker-Boudier, H. (2006). Expert consensus document on arterial stiffness: methodological issues and clinical applications. *European Heart Journal*, Vol. 27, No. 21 (Nov 2006), pp. 2588-2605. 0195-668X

Learoyd, B. M., & Taylor, M. G. (1966). Alterations with age in the viscoelastic properties of human arterial walls. *Circulation Research*, Vol. 18, No. 3 (Mar 1966), pp. 278-292. 0009-7330

Lee, H. Y., & Oh, B. H. (2010). Aging and arterial stiffness. *Circulation Journal*, Vol. 74, No. 11 (Nov 2010), pp. 2257-2262. 1347-4820

Lehmann, E. D., Hopkins, K. D., Rawesh, A., Joseph, R. C., Kongola, K., Coppack, S. W., & Gosling, R. G. (1998). Relation between number of cardiovascular risk factors/events and noninvasive Doppler ultrasound assessments of aortic compliance. *Hypertension*, Vol. 32, No. 3 (Sept 1998), pp. 565-569. 0194-911X

Leone, N., Ducimetiere, P., Gariepy, J., Courbon, D., Tzourio, C., Dartigues, J. F., Ritchie, K., Alperovitch, A., Amouyel, P., Safar, M. E., & Zureik, M. (2008). Distension of the carotid artery and risk of coronary events: the three-city study. *Arteriosclerosis, Thrombosis, and Vascular Biology,* Vol. 28, No. 7 (Jul 2008), pp. 1392-1397. 1524-4636

Levy, D., & Brink, S. (2005). *A Change of Heart: How the People of Framingham, Massachusetts, Helped Unravel the Mysteries of Cardiovascular Disease* (1st edition), Knopf, 0375412751, New York

Liang, Y. L., Teede, H., Kotsopoulos, D., Shiel, L., Cameron, J. D., Dart, A. M., & McGrath, B. P. (1998). Non-invasive measurements of arterial structure and function:

repeatability, interrelationships and trial sample size. *Clinical Science (London)*, Vol. 95, No. 6 (Dec 1998), pp. 669-679. 0143-5221

London, G. M., & Pannier, B. (2010). Arterial functions: how to interpret the complex physiology. *Nephrology, Dialysis, Transplantation*, Vol. 25, No. 12 (Dec 2010), pp. 3815-3823. 1460-2385

Loukogeorgakis, S., Dawson, R., Phillips, N., Martyn, C. N., & Greenwald, S. E. (2002). Validation of a device to measure arterial pulse wave velocity by a photoplethysmographic method. *Physiological Measurements*, Vol. 23, No. 3 (Aug 2002), pp. 581-596. 0967-3334

Mahmud, A., & Feely, J. (2001). Acute effect of caffeine on arterial stiffness and aortic pressure waveform. *Hypertension*, Vol. 38, No. 2 (Aug 2001), pp. 227-231. 1524-4563

Mahmud, A., & Feely, J. (2002). Divergent effect of acute and chronic alcohol on arterial stiffness. *American Journal of Hypertension*, Vol. 15, No. 3 (Mar 2002), pp. 240-243. 0895-7061

Mahmud, A., & Feely, J. (2003). Effect of smoking on arterial stiffness and pulse pressure amplification. *Hypertension*, Vol. 41, No. 1 (Jan 2003), pp. 183-187. 1524-4563

Mattace-Raso, F. U., van der Cammen, T. J., Hofman, A., van Popele, N. M., Bos, M. L., Schalekamp, M. A., Asmar, R., Reneman, R. S., Hoeks, A. P., Breteler, M. M., & Witteman, J. C. (2006). Arterial stiffness and risk of coronary heart disease and stroke: the Rotterdam Study. *Circulation*, Vol. 113, No. 5 (Feb 2006), pp. 657-663. 1524-4539

McDonald, D. A. (1968). Regional pulse-wave velocity in the arterial tree. *Journal of Applied Physiology*, Vol. 24, No. 1 (Jan 1968), pp. 73-78. 0021-8987

McEniery, C. M., Spratt, M., Munnery, M., Yarnell, J., Lowe, G. D., Rumley, A., Gallacher, J., Ben-Shlomo, Y., Cockcroft, J. R., & Wilkinson, I. B. (2010). An analysis of prospective risk factors for aortic stiffness in men: 20-year follow-up from the Caerphilly prospective study. *Hypertension*, Vol. 56, No. 1 (Jul 2010), pp. 36-43. 1524-4563

Meinders, J. M., & Hoeks, A. P. (2004). Simultaneous assessment of diameter and pressure waveforms in the carotid artery. *Ultrasound in Medicine & Biology*, Vol. 30, No. 2 (Feb 2004), pp. 147-154. 0301-5629

Mitchell, G. F., Hwang, S. J., Vasan, R. S., Larson, M. G., Pencina, M. J., Hamburg, N. M., Vita, J. A., Levy, D., & Benjamin, E. J. (2010). Arterial stiffness and cardiovascular events: the Framingham Heart Study. *Circulation*, Vol. 121, No. 4 (Feb 2010), pp. 505-511. 1524-4539

Mohiaddin, R. H., Firmin, D. N., & Longmore, D. B. (1993). Age-related changes of human aortic flow wave velocity measured noninvasively by magnetic resonance imaging. *Journal of Applied Physiology*, Vol. 74, No. 1 (Jan 1993), pp. 492-497. 8750-7587

Molinari, F., Zeng, G., & Suri, J. S. (2010). A state of the art review on intima-media thickness (IMT) measurement and wall segmentation techniques for carotid ultrasound. *Computer Methods and Programs in Biomedicine*, Vol. 100, No. 3 (Dec 2010), pp. 201-221. 1872-7565

Munakata, M., Ito, N., Nunokawa, T., & Yoshinaga, K. (2003). Utility of automated brachial ankle pulse wave velocity measurements in hypertensive patients. *American Journal of Hypertension*, Vol. 16, No. 8 (Aug 2003), pp. 653-657. 0895-7061

Naghavi, M. (2009). *Asymptomatic Atherosclerosis* (1st edition), Humana Press, 9781603271783, New York

Naidu, M. U., Reddy, B. M., Yashmaina, S., Patnaik, A. N., & Rani, P. U. (2005). Validity and reproducibility of arterial pulse wave velocity measurement using new device with oscillometric technique: a pilot study. *Biomedical Engineering Online*, Vol. 4, No. (2005), pp. 49. 1475-925X

Najjar, S. S., Scuteri, A., & Lakatta, E. G. (2005). Arterial aging: is it an immutable cardiovascular risk factor? *Hypertension*, Vol. 46, No. 3 (Sept 2005), pp. 454-462. 1524-4563

Nichols, W. W., & O'Rourke, M. F. (2005). *McDonald's Blood Flow in Arteries: Theoretical, Experimental and Clinical Principles* (5th edition), Hodder Arnold, 0340809418, London

Nualnim, N., Barnes, J. N., Tarumi, T., Renzi, C. P., & Tanaka, H. (2011). Comparison of central artery elasticity in swimmers, runners, and the sedentary. *American Journal of Cardiology*, Vol. 107, No. 5 (Mar 2011), pp. 783-787. 1879-1913

O'Leary, D. H., Polak, J. F., Kronmal, R. A., Manolio, T. A., Burke, G. L., & Wolfson, S. K., Jr. (1999). Carotid-artery intima and media thickness as a risk factor for myocardial infarction and stroke in older adults. Cardiovascular Health Study Collaborative Research Group. *New England Journal of Medicine*, Vol. 340, No. 1 (Jan 1999), pp. 14-22. 0028-4793

O'Rourke, M. F. (2006). Principles and definitions of arterial stiffness, wave reflections and pulse pressure amplification, In: *Arterial Stiffness in Hypertension*, Safar, M. E. & O'Rourke, M. F., pp. 3-20, Elsevier, Amsterdam

O'Rourke, M. F., & Hashimoto, J. (2007). Mechanical factors in arterial aging: a clinical perspective. *Journal of the American College of Cardiology*, Vol. 50, No. 1 (Jul 2007), pp. 1-13. 1558-3597

O'Rourke, M. F., & Safar, M. E. (2005). Relationship between aortic stiffening and microvascular disease in brain and kidney: cause and logic of therapy. *Hypertension*, Vol. 46, No. 1 (Jul 2005), pp. 200-204. 1524-4563

O'Rourke, M. F., Staessen, J. A., Vlachopoulos, C., Duprez, D., & Plante, G. E. (2002). Clinical applications of arterial stiffness; definitions and reference values. *American Journal of Hypertension*, Vol. 15, No. 5 (May 2002), pp. 426-444. 0895-7061

Paini, A., Boutouyrie, P., Calvet, D., Tropeano, A. I., Laloux, B., & Laurent, S. (2006). Carotid and aortic stiffness: determinants of discrepancies. *Hypertension*, Vol. 47, No. 3 (Mar 2006), pp. 371-376. 1524-4563

Pannier, B. M., Avolio, A. P., Hoeks, A., Mancia, G., & Takazawa, K. (2002). Methods and devices for measuring arterial compliance in humans. *American Journal of Hypertension*, Vol. 15, No. 8 (Aug 2002), pp. 743-753. 0895-7061

Papaioannou, T. G., Stamatelopoulos, K. S., Gialafos, E., Vlachopoulos, C., Karatzis, E., Nanas, J., & Lekakis, J. (2004). Monitoring of arterial stiffness indices by applanation tonometry and pulse wave analysis: reproducibility at low blood pressures. *Journal of Clinical Monitoring and Computing*, Vol. 18, No. 2 (Apr 2004), pp. 137-144. 1387-1307

Peters, S. A., den Ruijter, H. M., Palmer, M. K., Grobbee, D. E., Crouse, J. R., 3rd, O'Leary, D. H., Evans, G. W., Raichlen, J. S., Lind, L., & Bots, M. L. (2011). Manual or semi-automated edge detection of the maximal far wall common carotid intima-media

thickness: a direct comparison. *Journal of Internal Medicine*, Vol. No. (Jul 2011), pp. 1365-2796

Peterson, L. H., Jensen, R. E., & Parnell, J. (1960). Mechanical Properties of Arteries in Vivo. *Circulation Research*, Vol. 8, No. 3 (May 1960), pp. 622-639.

Redheuil, A., Yu, W. C., Wu, C. O., Mousseaux, E., de Cesare, A., Yan, R., Kachenoura, N., Bluemke, D., & Lima, J. A. (2010). Reduced ascending aortic strain and distensibility: earliest manifestations of vascular aging in humans. *Hypertension*, Vol. 55, No. 2 (Feb 2010), pp. 319-326. 1524-4563

Reneman, R. S., Meinders, J. M., & Hoeks, A. P. (2005). Non-invasive ultrasound in arterial wall dynamics in humans: what have we learned and what remains to be solved. *European Heart Journal*, Vol. 26, No. 10 (May 2005), pp. 960-966. 0195-668X

Roman, M. J., Devereux, R. B., Schwartz, J. E., Lockshin, M. D., Paget, S. A., Davis, A., Crow, M. K., Sammaritano, L., Levine, D. M., Shankar, B. A., Moeller, E., & Salmon, J. E. (2005). Arterial stiffness in chronic inflammatory diseases. *Hypertension*, Vol. 46, No. 1 (Jul 2005), pp. 194-199. 1524-4563

Saito, M., Okayama, H., Nishimura, K., Ogimoto, A., Ohtsuka, T., Inoue, K., Hiasa, G., Sumimoto, T., & Higaki, J. (2008). Possible link between large artery stiffness and coronary flow velocity reserve. *Heart*, Vol. 94, No. 6 (Jun 2008), pp. e20. 1468-201X

Senzaki, H., Chen, C. H., Ishido, H., Masutani, S., Matsunaga, T., Taketazu, M., Kobayashi, T., Sasaki, N., Kyo, S., & Yokote, Y. (2005). Arterial hemodynamics in patients after Kawasaki disease. *Circulation*, Vol. 111, No. 16 (Apr 2005), pp. 2119-2125. 1524-4539

Simon, A., Gariepy, J., Chironi, G., Megnien, J. L., & Levenson, J. (2002). Intima-media thickness: a new tool for diagnosis and treatment of cardiovascular risk. *Journal of Hypertension*, Vol. 20, No. 2 (Feb 2002), pp. 159-169. 0263-6352

Sutton-Tyrrell, K., Mackey, R. H., Holubkov, R., Vaitkevicius, P. V., Spurgeon, H. A., & Lakatta, E. G. (2001). Measurement variation of aortic pulse wave velocity in the elderly. *American Journal of Hypertension*, Vol. 14, No. 5 (May 2001), pp. 463-468. 0895-7061

Taddei, S., Virdis, A., Ghiadoni, L., Salvetti, G., Bernini, G., Magagna, A., & Salvetti, A. (2001). Age-related reduction of NO availability and oxidative stress in humans. *Hypertension*, Vol. 38, No. 2 (Aug 2001), pp. 274-279. 1524-4563

Tanaka, H., Dinenno, F. A., Monahan, K. D., Clevenger, C. M., DeSouza, C. A., & Seals, D. R. (2000). Aging, habitual exercise, and dynamic arterial compliance. *Circulation*, Vol. 102, No. 11 (Sept 2000), pp. 1270-1275. 1524-4539

Tardy, Y., Meister, J. J., Perret, F., Brunner, H. R., & Arditi, M. (1991). Non-invasive estimate of the mechanical properties of peripheral arteries from ultrasonic and photoplethysmographic measurements. *Clinical Physics and Physiological Measurement*, Vol. 12, No. 1 (Feb 1991), pp. 39-54. 0143-0815

The Reference Values for Arterial Stiffness' Collaboration. (2010). Determinants of pulse wave velocity in healthy people and in the presence of cardiovascular risk factors: 'establishing normal and reference values'. *European Heart Journal*, Vol. 31, No. 19 (Oct 2010), pp. 2338-2350. 1522-9645

Ting, C. T., Brin, K. P., Lin, S. J., Wang, S. P., Chang, M. S., Chiang, B. N., & Yin, F. C. (1986). Arterial hemodynamics in human hypertension. *The Journal of Clinical Investigations*, Vol. 78, No. 6 (Dec 1986), pp. 1462-1471. 0021-9738

Tounian, P., Aggoun, Y., Dubern, B., Varille, V., Guy-Grand, B., Sidi, D., Girardet, J. P., & Bonnet, D. (2001). Presence of increased stiffness of the common carotid artery and endothelial dysfunction in severely obese children: a prospective study. *Lancet*, Vol. 358, No. 9291 (Oct 2001), pp. 1400-1404. 0140-6736

Tsivgoulis, G., Vemmos, K., Papamichael, C., Spengos, K., Daffertshofer, M., Cimboneriu, A., Zis, V., Lekakis, J., Zakopoulos, N., & Mavrikakis, M. (2006). Common carotid arterial stiffness and the risk of ischaemic stroke. *European Journal of Neurology*, Vol. 13, No. 5 (May 2006), pp. 475-481. 1351-5101

Van Bortel, L. M., Balkestein, E. J., van der Heijden-Spek, J. J., Vanmolkot, F. H., Staessen, J. A., Kragten, J. A., Vredeveld, J. W., Safar, M. E., Struijker Boudier, H. A., & Hoeks, A. P. (2001). Non-invasive assessment of local arterial pulse pressure: comparison of applanation tonometry and echo-tracking. *Journal of Hypertension*, Vol. 19, No. 6 (Jun 2001), pp. 1037-1044. 0263-6352

Van Bortel, L. M., Duprez, D., Starmans-Kool, M. J., Safar, M. E., Giannattasio, C., Cockcroft, J., Kaiser, D. R., & Thuillez, C. (2002). Clinical applications of arterial stiffness, Task Force III: recommendations for user procedures. *American Journal of Hypertension*, Vol. 15, No. 5 (May 2002), pp. 445-452. 0895-7061

van Dijk, R. A., Dekker, J. M., Nijpels, G., Heine, R. J., Bouter, L. M., & Stehouwer, C. D. (2001). Brachial artery pulse pressure and common carotid artery diameter: mutually independent associations with mortality in subjects with a recent history of impaired glucose tolerance. *European Journal of Clinical Investigations*, Vol. 31, No. 9 (Sept 2001), pp. 756-763. 0014-2972

van Popele, N. M., Grobbee, D. E., Bots, M. L., Asmar, R., Topouchian, J., Reneman, R. S., Hoeks, A. P., van der Kuip, D. A., Hofman, A., & Witteman, J. C. (2001). Association Between Arterial Stiffness and Atherosclerosis: The Rotterdam Study. *Stroke*, Vol. 32, No. 2 (2001), pp. 454-460.

van Popele, N. M., Mattace-Raso, F. U., Vliegenthart, R., Grobbee, D. E., Asmar, R., van der Kuip, D. A., Hofman, A., de Feijter, P. J., Oudkerk, M., & Witteman, J. C. (2006). Aortic stiffness is associated with atherosclerosis of the coronary arteries in older adults: the Rotterdam Study. *Journal of Hypertension*, Vol. 24, No. 12 (2006), pp. 2371-2376.

Vlachopoulos, C., Aznaouridis, K., & Stefanadis, C. (2010). Prediction of cardiovascular events and all-cause mortality with arterial stiffness: a systematic review and meta-analysis. *Journal of the American College of Cardiology*, Vol. 55, No. 13 (Mar 2010), pp. 1318-1327. 1558-3597

Vlachopoulos, C., Dima, I., Aznaouridis, K., Vasiliadou, C., Ioakeimidis, N., Aggeli, C., Toutouza, M., & Stefanadis, C. (2005). Acute systemic inflammation increases arterial stiffness and decreases wave reflections in healthy individuals. *Circulation*, Vol. 112, No. 14 (Oct 2005), pp. 2193-2200. 1524-4539

Weber, T., Ammer, M., Rammer, M., Adji, A., O'Rourke, M. F., Wassertheurer, S., Rosenkranz, S., & Eber, B. (2009). Noninvasive determination of carotid-femoral pulse wave velocity depends critically on assessment of travel distance: a comparison with invasive measurement. *Journal of Hypertension*, Vol. 27, No. 8 (Aug 2009), pp. 1624-1630. 1473-5598

Weber, T., Auer, J., O'Rourke, M. F., Kvas, E., Lassnig, E., Berent, R., & Eber, B. (2004). Arterial stiffness, wave reflections, and the risk of coronary artery disease. *Circulation*, Vol. 109, No. 2 (Jan 2004), pp. 184-189. 1524-4539

Widlansky, M. E., Gokce, N., Keaney, J. F., Jr., & Vita, J. A. (2003). The clinical implications of endothelial dysfunction. *Journal of the American College of Cardiology*, Vol. 42, No. 7 (Oct 2003), pp. 1149-1160. 0735-1097

Wilkinson, I. B., Mohammad, N. H., Tyrrell, S., Hall, I. R., Webb, D. J., Paul, V. E., Levy, T., & Cockcroft, J. R. (2002). Heart rate dependency of pulse pressure amplification and arterial stiffness. *American Journal of Hypertension*, Vol. 15, No. 1 (Jan 2002), pp. 24-30. 0895-7061

Wilkinson, I. B., Prasad, K., Hall, I. R., Thomas, A., MacCallum, H., Webb, D. J., Frenneaux, M. P., & Cockcroft, J. R. (2002). Increased central pulse pressure and augmentation index in subjects with hypercholesterolemia. *Journal of the American College of Cardiology*, Vol. 39, No. 6 (Mar 2002), pp. 1005-1011. 0735-1097

Woodman, R. J., Playford, D. A., Watts, G. F., Cheetham, C., Reed, C., Taylor, R. R., Puddey, I. B., Beilin, L. J., Burke, V., Mori, T. A., & Green, D. (2001). Improved analysis of brachial artery ultrasound using a novel edge-detection software system. *Journal of Applied Physiology*, Vol. 91, No. 2 (Aug 2001), pp. 929-937. 8750-7587

Zieman, S. J., Melenovsky, V., & Kass, D. A. (2005). Mechanisms, pathophysiology, and therapy of arterial stiffness. *Arteriosclerosis, Thrombosis, and Vascular Biology*, Vol. 25, No. 5 (May 2005), pp. 932-943. 1524-4636

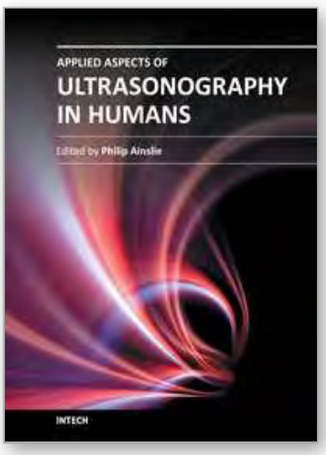

Applied Aspects of Ultrasonography in Humans
Edited by Prof. Philip Ainslie

ISBN 978-953-51-0522-0
Hard cover, 190 pages
Publisher InTech
Published online 25, April, 2012
Published in print edition April, 2012

Written by international experts, this publication provides the reader with the present knowledge and future research directions of diagnostic and therapeutic ultrasound and spectroscopy. Focused topics include Duplex ultrasound, transcranial color Duplex, MRA guided Doppler ultrasonography and near-infrared spectroscopy. New directions in the use and application of transcranial and color Duplex ultrasound are provided, as well as the use of ultrasound and arterial stiffness for measuring human vascular health and circulatory control. Novel use of ultrasound for the detection of intra-cardiac and intra-pulmonary shunts is also described along with its utility for the assessment of gastric regulation and emptying.

How to reference
In order to correctly reference this scholarly work, feel free to copy and paste the following:

Graeme J. Koelwyn, Katharine D. Currie, Maureen J. MacDonald and Neil D. Eves (2012). Ultrasonography and Tonometry for the Assessment of Human Arterial Stiffness, Applied Aspects of Ultrasonography in Humans, Prof. Philip Ainslie (Ed.), ISBN: 978-953-51-0522-0, InTech, Available from: http://www.intechopen.com/books/applied-aspects-of-ultrasonography-in-humans/ultrasonography-and-tonometry-for-the-assessment-of-human-arterial-stiffness

INTECH
open science | open minds

InTech Europe
University Campus STeP Ri
Slavka Krautzeka 83/A
51000 Rijeka, Croatia
Phone: +385 (51) 770 447
Fax: +385 (51) 686 166
www.intechopen.com

InTech China
Unit 405, Office Block, Hotel Equatorial Shanghai
No.65, Yan An Road (West), Shanghai, 200040, China
中国上海市延安西路65号上海国际贵都大饭店办公楼405单元
Phone: +86-21-62489820
Fax: +86-21-62489821

IntechOpen

7

The Role of Ultrasonography in the Assessment of Arterial Baroreflex Function

Yu-Chieh Tzeng
Cardiovascular Systems Laboratory
University of Otago
New Zealand

1. Introduction

Cardiovascular disease is the leading cause of mortality in the developed world [1]. Experimental research indicates that in addition to traditional risk factors such as hypertension and dyslipidemia, dysfunction of the autonomic nervous system is also a powerful independent risk factor for death from cardiovascular disease. Although not yet routinely assessed in clinical practice, depressed baroreflex function increases the risk of death following myocardial infarction [2], in chronic heart failure [3], and recent trials also clearly indicate an increased risk for both ischemic and hemorrhagic stroke [4, 5]. In the context of these morbid epidemiological correlations, it is not difficult to justify the need for a better understanding of the mechanisms and factors involved in normal human baroreflex regulation.

Ultrasonography has played a vital role over the past decades not only in clinical medicine but also in advancing our understanding of fundamental biological processes. This proposition is certainly true for human cardiovascular research, where the non-invasive nature of ultrasonography has enabled physiologists and clinicians to study regulatory mechanisms that could otherwise only be examined in animal models under sedation or anaesthesia. The aim of this chapter is to review the pivotal role that ultrasonography has played in advancing our understanding of human baroreflex function. The chapter will begin with an overview of the human baroreflex in section 2 with particular emphasis on cardio-vagal regulation of the heart, and vascular sympathetic regulation of peripheral vascular resistance. Section 3 will introduce the technical application of ultrasonography in baroreflex research with emphasis on the use of B-mode imaging in the evaluation of the mechanical and neural components of the baroreflex arc. Important practical, analytical, and physiological considerations will be discussed. Finally, the literature will be reviewed in section 4 to illustrate how the practical application of vascular ultrasound imaging has lead to deeper insights into the workings of the human baroreflex not otherwise possible.

2. Physiology of the baroreflex

The arterial baroreflex is critical to both short and long term regulation of blood pressure. The sensory components of this reflex comprise of stretch sensitive nerve endings situated

in vessel walls of some arteries, particularly in the carotid sinus and the aortic arch that respond to changes in vascular distention pressure by altering afferent discharge activity in the carotid sinus nerve (a branch of the glossopharyngeal nerve) and the aortic nerves.

Afferent baroreceptor inputs project to regions of the nucleus tractus solitarius, which extends almost over the entire length of the medulla and is the exclusive first relay station and integration area for afferent baroreceptor information [6]. Numerous inter-connections exist between the nucleus tractus solitarius and other structures important in the baroreflex, including the hypothalamus, amygdala, parabrachial nuclei, subfornical organ, cerebellum, and rostral ventrolateral medulla [7]. However, the precise central interneuronal connections that drive parasympathetic and sympathetic motoneurons, and the locations of vagal-cardiac motoneurons have not been located in humans. In animals they are found in variable locations, including the nucleus ambigus in the cat [8], and dorsal motor nucleus of the vagus in dogs and monkeys [9]. Sympathetic pre-ganglionic motoneurons are located in the intermediolateral column of the spinal cord [10]. Irrespective of the precise central neuronal connections mediating the baroreflex, it is clear that the end effector response to arterial baroreflex stimulation is an increase in efferent vagal activity, and a decrease in efferent sympathetic activity [11].

The efferent limbs of the baroreflex can be functionally considered as consisting of a cardiac component and a vascular component. The cardiac baroreflex refers to the prompt adjustment of heart rate, stroke volume (and therefore cardiac output) in response to changes in blood pressure. These responses are mediated primarily via the vagus nerve because they are markedly attenuated following surgical vagotomy and muscarinic cholinergic [12]. In healthy humans at rest, and during exercise, the cardiac baroreflex can respond rapidly with cardiac period intervals beginning to adjust within 0.5 sec following baroreceptor loading with neck suction [13]. Although maximal responses increase with advancing age, in the young, they generally takes place within 3-4 seconds following baroreceptor loading, and 2-3 sec following baroreceptor unloading respectively in the young [14]. Reflex alterations in heart rate can also arise due to the action of the sympathetic nervous system. Increased sympathetic activity can increase heart rate via the release of noradrenalin in postganglionic nerve terminals, or the release of adrenaline into the systemic circulation from the adrenal medulla. It is important to recognize that whereas the chronotropic response of the heart to baroreflex stimulation is dominated by vagal activity (via the release of acetylcholine), the inotropic responses to baroreflex stimulation responsible for changes in stroke volume are mediated via the sympathetic nervous systems.

In contrast, the vascular baroreflex refers to regulation of peripheral vascular smooth muscle tone. The major site of vascular resistance is thought to reside in the arterioles and capillaries, which in the systemic circulation are densely innervated with post-ganglionic sympathetic fibers. Although sympathetic regulation of venous tone is not a key determinant of peripheral vascular resistance, venous constriction influences blood volume distribution. The reaction times of the vascular sympathetic baroreflex are slower compared to cardiac responses. Even though changes in sympathetic nerve activity can occur with latencies of ~200ms after changes of afferent nervous activity to the central nervous system, the lag times associated with sympathetic neurovascular transduction at the level of the neuromuscular junction are substantially longer such that the first changes

in end organ response are seen only after 2-3 seconds. The maintenance of blood pressure therefore requires the effective regulation and integration of both the cardiac and vascular baroreflex arc.

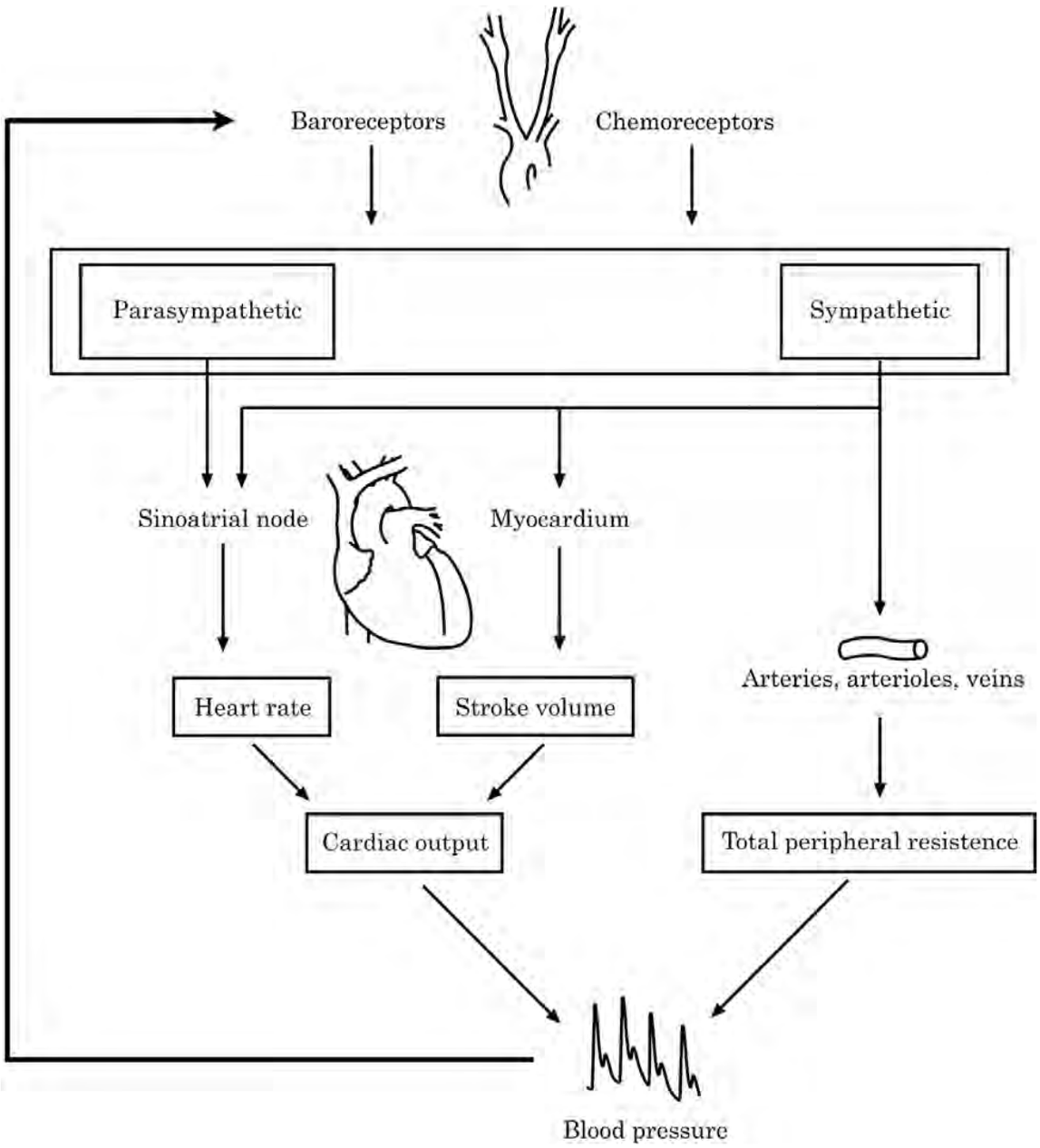

Fig. 1. Schematic showing the major mechanistic pathways involved with short-term systemic blood pressure control. Note that in vivo the baroreflex arc is a closed-loop system.

3. Assessment of the mechanical and neural components of the cardiac baroreflex

3.1 Overview

Baroreflex gain has traditionally been quantified as the relation between changes in arterial blood pressure and cardiac period (R-R intervals), heart rate, or sympathetic nerve activity. This analysis assumes that blood pressure is the input that drives reflex autonomic changes. However, baroreceptors respond to mechanical deformation and not the pressure *per se*. Therefore, the transduction of blood pressure into barosensory stretch, and the consequent transduction of barosensory stretch into efferent parasympathetic and sympathetic neural outflow are critical steps that determine the integrated baroreflex response. The major contribution of vascular ultrasound imaging to baroreflex research has been the enabling of these critical components of the integrated baroreflex arc to be studied separately and non-invasively in humans through the use of B and M-mode imaging processes [15].

In principal, the imaging analysis can be combined with any baroreflex assessment technique provided adequate ultrasound images can be obtained. In practice, however, apart from the modified Oxford method, the approach has only been successfully applied in subjects performing the Valsalva maneuver [16] and under steady state resting conditions using linear transfer function analysis [17]. Therefore, considering the relative novelty of the approach, and the fact that no method can be considered the gold standard, investigators wishing to undertake this form of analysis should choose their approach based on their unique experimental requirements, and an understanding of the analytical and theoretical shortcomings of each method. In this section, methods that are *technically* suitable for this form of analysis from an imaging perspective will be presented in context of some of these considerations. Beyond the scope are methods that do not permit the accurate acquisition of carotid images (e.g. neck suction/pressure, dynamic squat-stand maneuvers) and techniques based on highly controversial physiological assumptions (e.g. spontaneous sequence method, high frequency transfer function gain) [18, 19].

3.2 Carotid ultrasound scanning protocol

The assessment begins with the identification of wall boundaries, which appear as parallel echogenic lines separated by a hypoechonic space in longitudinal B-mode image (figure 2). Although the internal carotid, bulb, and common carotid arteries can all be imaged (figure 3), the latter generally yields the best image quality because the vessel course is parallel to the surface of the skin and is positioned at right angles to the ultrasound beam. The first echo along the far wall corresponds to the lumen-intima interface whilst the second and normally brighter echo corresponds to the media-adventitia interface. The echolucent zone in between corresponds to the media. It is important to recognize that interfaces may be difficult to discern when the near and far walls of the vessels are curvilinear and not at right angels to the ultrasound beam. Therefore, within the carotid bulb where the walls flare and dilate, or along the proximal internal carotid where the walls do not lie in parallel, only short segments of wall may be seen on a single frame. For these reasons, vascular distention waveforms are generally acquired 1-2cm of the bifurcation even though baroreceptor density is greatest at the carotid bulb. Other causes for the loss of wall interface that are unrelated to scanning technique include the presence of atherosclerotic plaques or the presence of fat in the arterial wall.

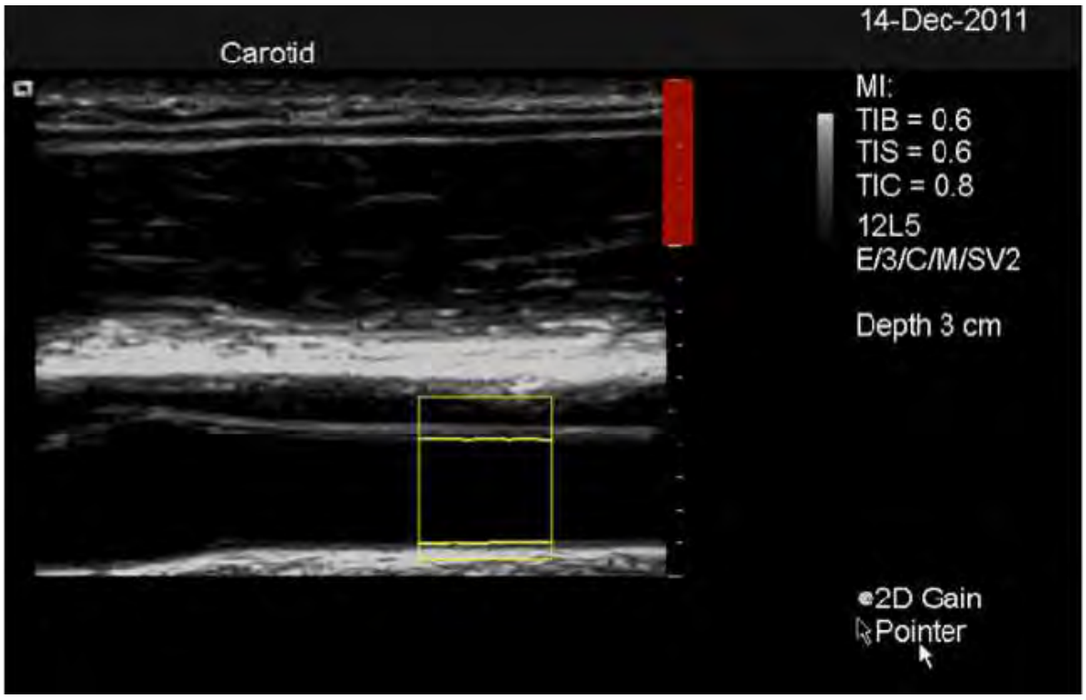

Fig. 2. Sample screen shot showing the custom edge tracking of the carotid luminal diameter.

Studies are conducted using linear array probes (7.5-13 Mhz) with the subjects head tilted ~45^{o} away from the side of the study to capture a longitudinal section of the common carotid artery ~1 cm proximal to the bifurcation. This usually requires an initial cursory scan to orient the sonographer to the subject's carotid anatomy to establish the site of the bifurcation and to differentiate between the internal and the external the external carotid artery. Upon identifying the distance common carotid immediately proximal to the bulb, the probe should be manipulated to optimize the view of the arterial wall such that the lumen-intima and media-adventitia interfaces over a 1-cm length can be clearly displayed. Images should be captured as close to a 45 degrees angle as possible and both the near and far walls should be clearly visible for robust analysis.

The continuous digital video screen shot of the optimized B-mode images are then recorded and saved for offline analysis using custom written edge-tracking software (figure 2). The region of interest is calibrated for length, and using a pixel-density algorithm the vessel walls are tracked and diameter measured at 30 Hz resolution for the entire video that encompassed the Oxford trial. In contrast to methods originally described by Hunt et al., where hardware limitations meant that image sets could only be acquired on approximately every other cardiac cycle, our technique enables the carotid diameter data to be acquired for every cardiac cycle throughout the duration of the baroreflex test (~3 minutes). High resolution tracking of carotid distension waveforms can also be obtained using a number of commercially available systems that employ interlaced M-mode and B-mode imaging, such as the ART.Lab system (Esaote, Maastrict) or the QFM-21 (Haedco, Japan). However, the use of A-mode imaging with the QFM-21 limits the utility of this device given there is no visual feedback in B-mode to guide the accurate placement of the probe relative to the length of the carotid artery.

Method	Strength	Weaknesses
Modified Oxford method	Partial open loop analysis of baroreflex gain Not confounded by differences in respiration rate Enables the assessment of baroreflex hysteresis Evaluate cardiac baroreflex gain as well as the neural arc of the smpathetic baroreflex	Invasive procedure require venous cannulation Potential influence of drugs on vascular transduction Does not permit evaluation of sympathetic neurovascular transduction given the use of vasoactive drugs Subjectivity of analysis
Valsalva manuever	Non-invasive Non-pharmacological Partial open loop analysis of baroreflex gain Enables the assessment of baroreflex hysteresis Evaluate both cardiac and symaptethic baroreflex function	Need for subject compliance Poor consistency across subjects
Spectral methods	Non-invasive Non-pharmacological Does not permit assessment of baroreflex hysteresis Prone to confounding by changes in respiration	Liable to confounding by non-baroreflex mediated fluctuations in vagal outflow (e.g. respiration) Controversial physiological assumptions Closed-loop analysis

Table 1. Comparison of methods for the assessment of baroreflex function

3.3 Overview of techniques and data analysis

The following overview summaries the data analysis that is involved in the quantification of integrated, mechanical and neural baroreflex gains. Only methods involving general linear regression and linear transfer function analysis will be outlined. Higher order mathematical models of baroreflex function fall outside the scope of this chapter.

The modified Oxford method

In 1969 Smyth et al., proposed a method for assessing arterial baroreflex gain that involved regressing reflex cardiac interval responses to systolic blood pressure changes induced with vasoactive drugs [20]. Commonly referred to as the 'Oxford method', this technique has become widely regarded as the gold standard measure of baroreflex function. Although the assessment was originally carried out using bolus injections of angiotensin, the method has undergone many incremental modifications since its introduction. These include, for example, the use of drugs with minimal direct cardiac chronotropic effects, and the administration of vasodilator and vasoconstriction drugs in sequence to enable the complete characterization of both the cardiac and sympathetic baroreflex function (modified 'Oxford method').

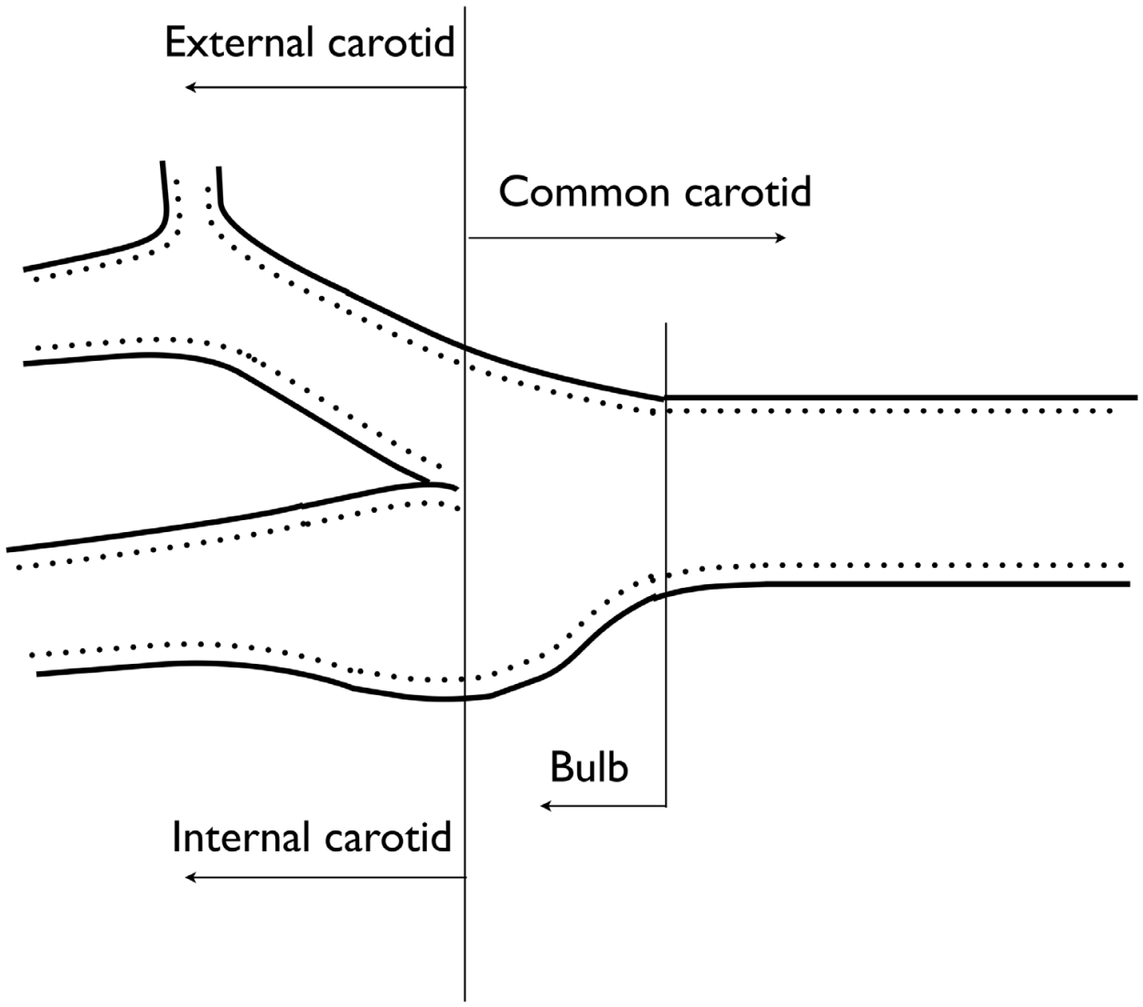

Fig. 3. Schematic showing the common, internal and external carotid arteries. The carotid bulb can be recognized in most subjects as the site where common carotid dilates slightly and the vessel walls flare out such that they're no longer parallel to each other. The elliptically shaped bulb is geometrically complex in the longitudinal view and therefore can be difficult to image in its entirety within a single frame. The external carotid artery lies anterior and medial to the internal carotid in 90% of subjects but is reversed in the remaining 10%. The internal carotid artery is generally larger than the external carotid, and has no braches as it ascends into the skull to supply the brain, whereas the external carotid has branches that supply the neck and face.

A key advantage of the method is that blood pressure can be perturbed across a wide range within a sufficiently short time frame to *clearly* engage the baroreflex. This is a critical consideration given the baroreflex is a closed-loop system (figure 1) and accurate quantification of input-output relations in theory requires the loop to be opened. Whilst the open-loop condition cannot be meet under the majority of human experimental settings, the active perturbation of blood pressure does allow the loop to be partial-opened to yield robust estimates of baroreflex gain [21]. The key objection to the Oxford method relates to the use of vaso-active agents, which may exert unquantifiable effects on baroreceptor transduction, cardiopulmonary afferent activity and sinus node activity. However, the practical significance of these concerns remains unclear. Other strengths and weaknesses of the method are summarized in Table 1.

Technically the modified Oxford method involves sequential intravenous bolus injections sodium nitroprusside (SNP) and phenylephrine hydrochloride (PE). Once recordings of hemodynamic measurements have begun, blood pressure should be carefully monitored and allowed to stabilize, after which the injection of SNP can be administered. This should be followed ~60 seconds later by the injection of PE. Recording can cease when systolic blood pressure began to plateau after the rise after the PE injection. Oxford trials, therefore, typically last 120 to 180 seconds. Doses given for SNP and PE are typically 150 and 200g, respectively, although this should be adjusted on an individual basis if an insufficient blood pressure perturbation is achieved (systolic blood pressure change <15 mm Hg). It is common practice to account for known baroreflex delays, which can be done by matching systolic blood pressure values to either the concurrent heartbeat for R-R intervals >800 ms or a 1 beat delay for shorter heart periods (typically between 500 and 800 ms). Due to baroreflex hysteresis, baroreflex sensitivities should be calculated separately for SNP and PE injections to identify the gain (or sensitivity) against falling and rising blood pressure.

Figure 4 shows a representative tracing of heart rate, carotid artery lumen diameter, and finger blood pressure during a modified Oxford baroreflex test sequence. For the assessment of cardio-vagal BRS, the pressure to R-R interval relation for falling pressures are examined at the onset of the systolic blood pressure decrease, which typically occur ~30 sec after the bolus injection of SNP, and ends when systolic blood pressure reached its nadir. For rising pressures, data selection begins at the nadir in systolic blood pressure and end when pressure peaks after the bolus injection of PE.

It is common for the identification and elimination of the saturation and threshold regions to be done via visual data inspection [22, 23]. However, mathematical modeling procedures can be applied for more objective analysis. For example, a piecewise linear regression can be applied to the raw data points to statistically identify breakpoints that occur at the upper and lower ends of the data set (Figure 5) [24, 25]. Other approaches for the objective identification of cardiac-vagal BRS have been reported in the literature including the use sigmoid [26], logistic [27] and elliptical functions [28].

Typically, an arbitrary threshold for the correlation coefficient of the linear segment is set at 0.6 to justify the use of a linear regression model. It is also conventional to account for respiratory-related fluctuations in R-R interval and systolic blood pressure by averaging R-R

intervals or heart rate across 2 or 3 mm Hg bins. However, although data binning improves the correlation coefficients, neither respiratory rate [23] nor data binning [26] materially influence the magnitude of the gain estimates.

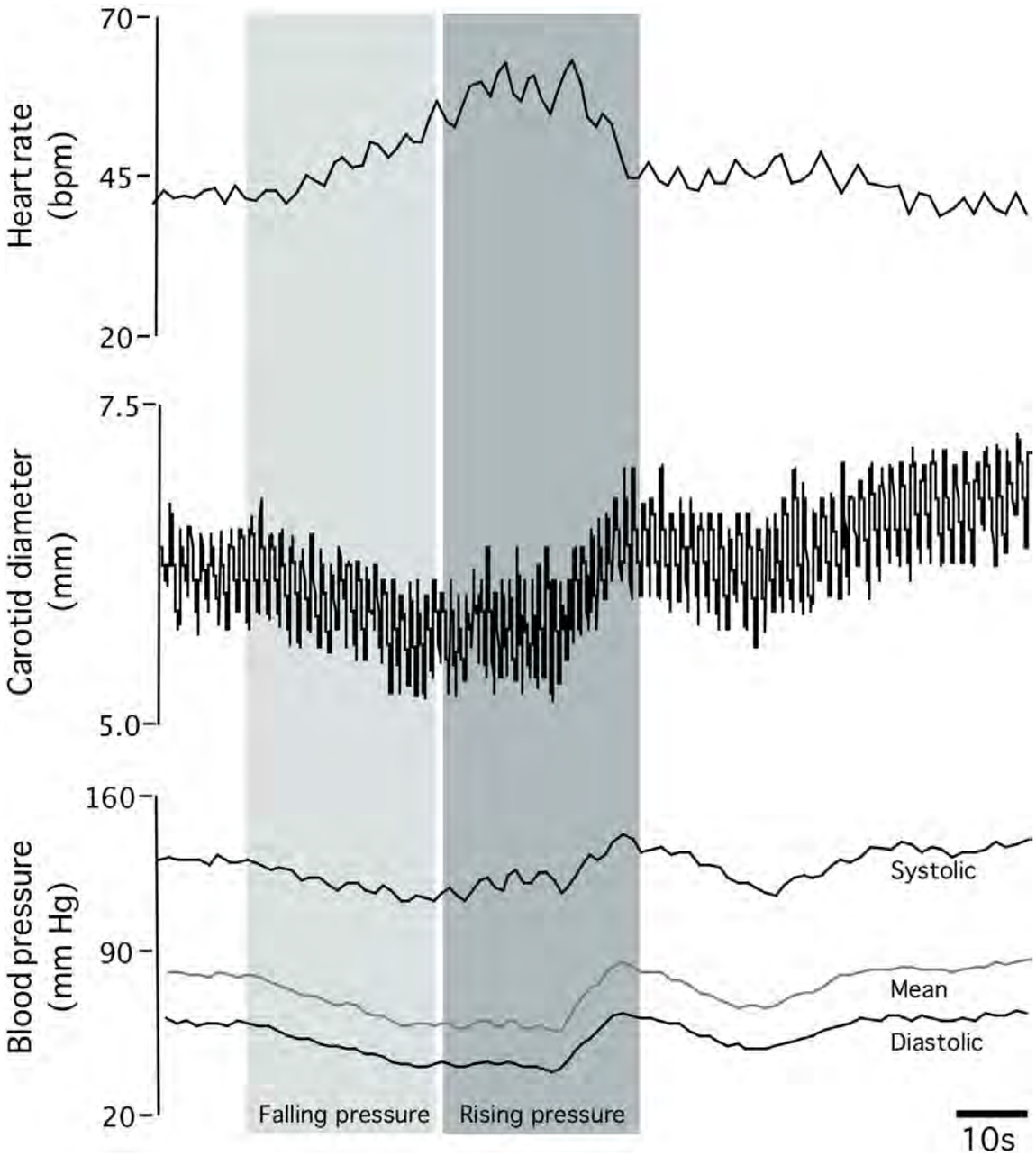

Fig. 4. Representative recording of a modified Oxford baroreflex test sequence. Intravenous bolus injections of sodium nitroprusside were followed ~60 s later by phenylephrine hydrochloride. The grey scale areas indicate the data segments typically taken for the determination of baroreflex gain.

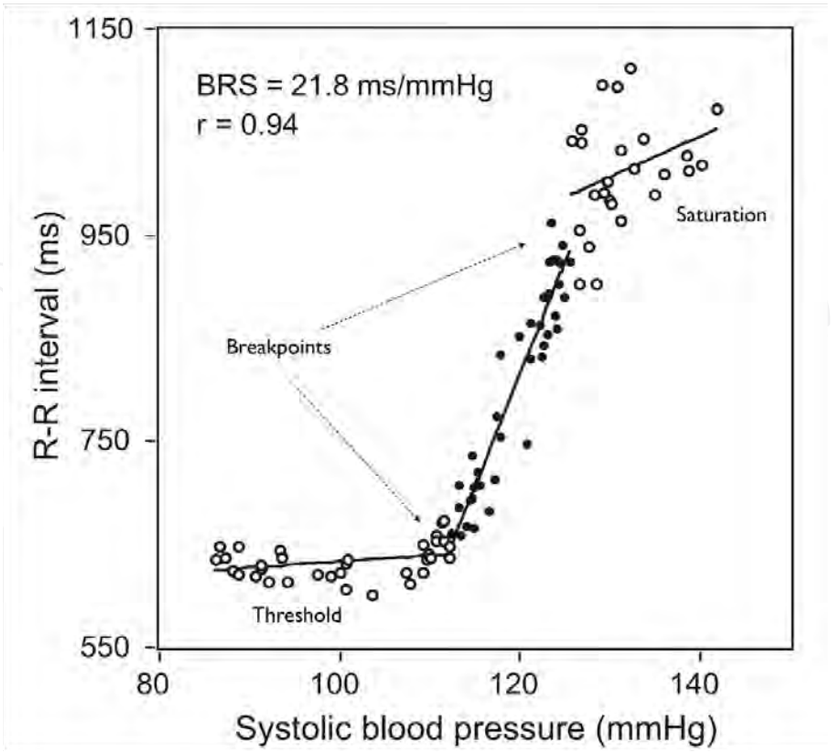

Fig. 5. Piecewise regression model for elimination of threshold and saturation regions of the integrated baroreflex response to rising pressures. Open circles (○) represent the threshold and saturation regions and the closed circles (●) represent the linear portion of the baroreflex gain. Arrows indicate breakpoints that separate the threshold, saturation, and linear region (Adapted from Taylor et al., 2011).

The gain of the mechanical and neural components can be calculated separately for both rising and falling pressures, with exclusion of the threshold and saturation regions as done for the assessment of integrated gain. For the mechanical component, systolic carotid lumen diameter measurements within a cardiac cycle should be plotted against systolic blood pressure, and for the neural component, R-R intervals or heart rate should be plotted against systolic carotid lumen diameter (figure 6).

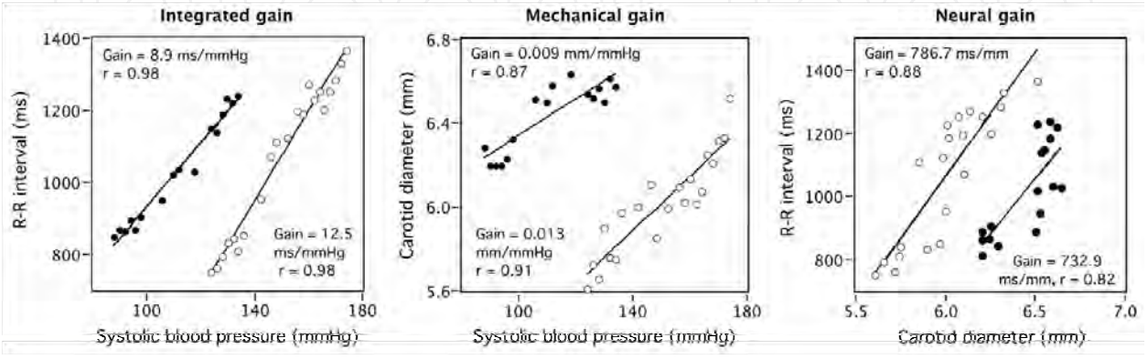

Fig. 6. Integrated, mechanical and neural gains for rising pressures in the morning (●) and afternoon (○) for one subject. (adapted from Taylor et a., 2011).

For assessment of integrated, mechanical, and neural components of the sympathetic baroreflex, simple linear regression procedures are generally applied but with few modifications. First, instead of systolic lumen diameters and systolic pressures, integrated and mechanical gains for the sympathetic arc are derived using diastolic lumen diameters and diastolic blood pressure. This is because diastolic pressure correlates more strongly to sympathetic activity, which in humans are generally recordings of muscle sympathetic nerve activity (MSNA) made in the peroneal nerve [29]. Second, sympathetic activity has a bursting pattern that rarely maintains a 1:1 relation with cardiac cycles even at low blood pressures where baroreflex-mediated sympatho-inhibition is low. Therefore, pharmacological baroreflex testing across a wide range of blood pressures invariably results in an over-representation of cardiac cycles with zero sympathetic activity. To account for this error, cardiac cycles can be weighted according to the presence or absence of observable sympathetic bursts. For example, cardiac cycles with zero's below the lowest pressure associated with a sympathetic burst are assigned a weight of 0 ('false' zero) whereas zeros above the highest pressure associated with a sympathetic burst were assigned a weight of 1 ('true' zero) [30]. Some groups employ data binning (e.g. across 3mmHg blood pressure increments) to reduce the statistical impact of inherent beat-to-beat variability in nerve activity [31], which are generally represented as total integrated sympathetic activity (i.e. the product of burst frequency and average burst area in arbitrary units).

The Valsalva maneuver

The Valsalva maneuver was first described by Antonia Maria Valsalva in the 17th century as a method for testing the patency of the Eustachian tube. However, the maneuver has gained subsequent acceptance as a means of stressing the baroreflex due to its well-characterized effects on cardiac output, venous return, and blood pressure. Essentially the maneuver involves forced expiration against a closed glottis, or a short tube to enhance expiratory resistance. Mouth pressure is measured and maintained at a constant level (e.g. 40 mmHg) for 15 seconds. Figure 7 shows the typical response in blood pressure and heart rate (MSNA not shown), which have been characterized into four phases. Phase one is the initial blood pressure rise and heart rate and MSNA reduction (via the baroreflex) due to a mild rise in stroke volume secondary to elevated intrathoracic pressure forcing blood out of the pulmonary circulation into the left atrium. The sustained elevation in introthoracic pressure

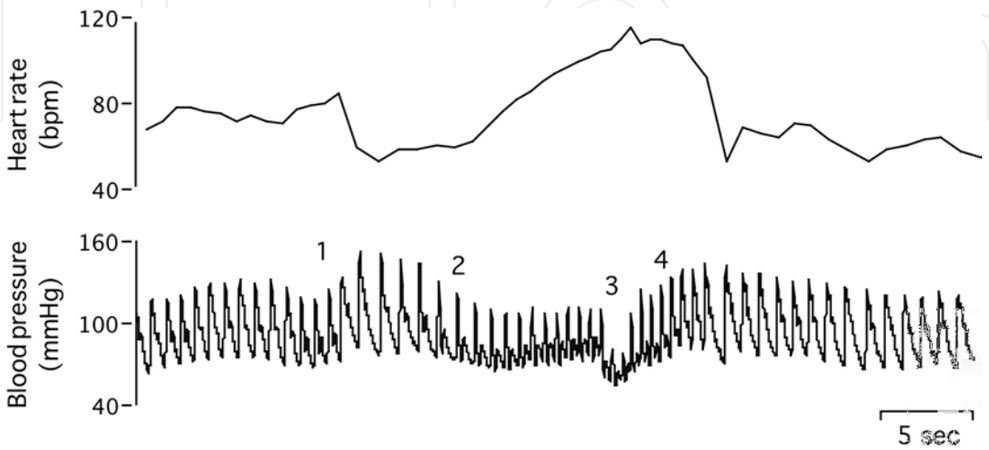

Fig. 7. Blood pressure and heart rate changes during the Valsalva manuver.

during phase two impedes venous return and consequently reduces cardiac output. This phase triggers a baroreflex mediated increase in heart rate and MSNA. Phase three commences with the pressure release and resumption of normal breathing. During this phase blood pressure decreases briefly as the external compression on the aorta is released and heart rate increases. This is followed by phase four as blood pressure starts to rise due to an increased in cardiac output secondary to a rapid increase in venous return, and the background of elevated sympathetic vascular resistance that occurred during phase two. During phase four, heart rate decreases and MSNA falls.

The regression approaches described for the modified Oxford method are also applicable to the Valsalva maneuver. In general, estimates of cardia-vagal baroreflex gain can be determined from both phase two or four of the response. However, satisfactory sympathetic baroreflex slopes may only be obtainable during phase two, given the relative paucity of sympathetic bursts during phase four [32].

Transfer function analysis

Integrated, neural, and mechanical baroreflex gains can be quantified using transfer-function analysis of spontaneously occurring low frequency (0.14-0.15 Hz) blood pressure, carotid lumen diameter, R-R interval, and normalized MSNA fluctuations. The data processing typically begins with interpolation (e.g. linear, spline) and re-sampling (1-4 Hz) of beat-to-beat systolic pressure, carotid lumen diameter, and R-R intervals to provide equidistant time series that are required for Fourier analysis. Due to noise inherent in finite data series, its common to apply the Welch averaging technique to minimize data variance in exchange for reduced frequency resolution. Welch averaging involves the subdivision of the entire data epoch into successive overlapping segments of equal lengths. The data within each window should be de-trended and passed through a Hanning window before spectral analysis. The frequency-domain transforms can be computed with a fast Fourier transformation algorithm. The transfer function H (*f*) between the two signals was calculated as:

$$H(f) = Sxy(f)/Sxx(f)$$

where S_{xx} (*f*) is the autospectrum of input signal and S_{xy} (*f*) is the cross-spectrum between the two signals. The transfer function gain $|H(f)|$ and phase spectrum $|\Phi(f)|$ were obtained from the real part H_R (*f*) and imaginary part H_I (*f*) of the complex transfer function:

$$|H(f)| = \{[HR(f)]2 + [HI(f)]2\}$$

$$\Phi(f) = \tan\text{-}1[HI(f)/HR(f)]$$

The squared coherence function MSC (f) was estimated as:

$$MSC(f) = |Sxy(f)|2/[Sxx(f)Syy(f)],$$

where S_{yy}(*f*) is the autospectrum of changes in output signal. Given that transfer function analysis is a linear methodology that is yields only valid gain estimates if the cross-spectral coherence is sufficiently high. This threshold is conventionally set at 0.5 although lower thresholds have been applied.

According to this approach, the integrated cardiac baroreflex gain corresponds to the average systolic pressure to R-R interval transfer function gain within the low frequency range (0.04-0.15) [33]. The mechanical component is the average transfer function gain between systolic blood pressure and systolic carotid diameter fluctuations whereas the neural gain is the average systolic carotid diameter to R-R interval transfer function gain within the same frequency range. In theory the transduction of carotid diameter fluctuations to changes in MSNA can also be assessed although details of these transfer function characteristics in humans have not yet been reported in the literature.

The major advantage of the spontaneous spectral approach is that the assessment can be made non-invasively without the use of drugs or special provocation maneuvers (the procedure becomes invasive if MSNA recordings are made). However, there are important potential shortcomings with this technique. First, because input and output relationships between the various haemodynamics parameters are assessed under spontaneous conditions, the derived transfer function parameters reflect close-loop relations that may not accurately reflex open-loop gains [34]. Furthermore, the technique is highly liable to confounding from respiratory influences. For example, fluctuations in R-R intervals associated with respiratory activity (respiratory sinus arrhythmia) can merge, accentuate, and confound the magnitude of low frequency fluctuations if breathing rate falls within the low frequency range (i.e.<0.15Hz) [23]. Such respiratory influences need to be carefully controlled for and may be minimized with the use of pace respiration.

4. New insights into baroreflex physiology gain through the application of vascular ultrasound

The technical advances described in section 3 offer the potential for more detailed understanding of mechanisms underlying changes in baroreflex function not previously attainable in health and disease [35]. The following is a summary of new insights into baroreflex physiology that have been gained with the aid of ultrasonography.

4.1 Baroreflex hysteresis

It is well recognised that cardiac baroreflex function exhibits hysteresis; baroreflex responses are greater for rising vs. falling blood pressures. Hysteresis is an intrinsic feature to the cardiac baroreflex, and is observable with both pharmacologically induced changes in blood pressure (Pickering et al. 1972; Bonyhay et al. 1997; Rudas et al. 1999) and direct neck pressure stimulation (Eckberg & Sleight, 1992). This pattern of hysteresis has classically been attributed solely to the visoelastic properties of barosensory vessels such that, for a given blood pressure, vessel diameters are greater if the pressure was on the ascent. However, Studinger et al., showed that hysteresis derives not only from barosensory vessel mechanics, but also from complex interactions with neural resetting which often offset the changes in mechanical gain [24]. These findings further reinforce the concept that the integrated baroreflex gain derives from the combined influences of mechanical transduction of pressure into baroreceptor stretch, and neural transduction of baroreceptor stretch into vagal outflow.

4.2 Baroreflex changes with aerobic exercise

Although baroreflex impairment is a strong predictor of adverse cardiac and cerebrovascular outcomes, very few interventions have been shown to successful ameliorate the decline in baroreflex function associated with aging and cardiovascular disease. Some data suggest that aerobic exercise training may enhance cardiac baroreflex function although the mechanisms underpinning these changes are poorly understood. Using the valsalva technique, Komine et al., showed that in young men who had engaged in regular running exercise for ~80 min/day, 5 days/week for 6-7 years showed increases in arterial baroreflex gain through changes in the neural component of the baroreflex arc and not through alterations in carotid artery compliance [16]. Similarly, Deley showed that among previously sedentary elderly men and women, participation in a regular aerobic training program involving treadmill, elliptical training, and bicycle exercise at 70-80% heart rate reserve for six months enhanced baroreflex gain by 26%. The improvement in baroreflex gain was directly related to the amount of exercise performed and was derived primarily from changes in the neural component [36].

4.3 Effects of posture

Baroreflex function testing is generally conducted in the supine position. However, there are many activities in day-to-day living that produce physiological challenges and that have been associated with changes in baroreflex function, such as the assumption of an upright posture.[37] The risk of vasovagal syncope is greatly increased in the morning,[38] which may be associated with insufficient baroreflex function to maintain adequate blood pressure during orthostatic stress.[39] A number of studies have been performed to investigate the effects of orthostatic stress on integrated baroreflex function. The current consensus is that orthostatic stress augments vascular sympathetic gainand reduces cardio-vagal.[37, 40] Saeed et al., have provided further insight by showing that the differences in observed integrated BRS primarily arise from reduced mechanical transduction. These studies suggest that the propensity to orthostatic intolerance may be greater in those with structural vascular disease that affect the mechanical transduction properties of the integrated baroreflex arc.[41]

4.4 Stress response and baroreceptor function

Greater blood pressor responses to mental stress have been associated with greater risk of cardiovascular events, including the development of hypertension, stroke, coronary artery disease (CAD). Although blunting of baroreceptor function may underpin the exaggerated pressure responses associated with mental stress, the mechanisms underpinning the baroreceptor dysfunction are poorly understood. Deley et al., recently studied the mechanical and neural component of the baroreflex among healthy individuals and patients with documented coronary artery disease during the performance of a mental arithmetic and speaking task [42]. However, whilst patients with CAD showed exaggerated heart rate and blood pressure responses to the tasks, there were no differences in integrated, mechanical or neural baroreflex gains between healthy and CAD patients, which suggests that the augmented pressure response does not result from generalised baroreflex dysfunction.

4.5 Post exercise depression of baroreflex function

A single bout of moderate to high intensity exercise is associated with a period of post-exercise hypotension. Although the underlying cause of the hypotension remains unclear, studies have shown that following exercise in borderline hypertensive and young healthy subjects the integrated cardiac baroreflex gain changes dynamically. This change is characterised by an initial reduction [43] or no change [44] shortly after exercise (10-30 minutes), followed by elevation above baseline levels 40-55 minutes post exercise cessation. However, although these results clearly indicate that cardiac baroreflex function is altered during the post-exercise period, details regarding the sites and mechanisms underlying the changes remain entirely unknown.

Recently we examined for the first time the changes in cardiac baroreflex function before and at 10, 30, and 60 minutes after 40 minutes of cycling at 60% estimated maximal oxygen consumption.[45] We found that following aerobic exercise baroreflex gain is reduced and hysteresis manifests. The reduction in baroreflex gain to falling blood pressure is mediated by decreased mechanical and neural gains, whereas the decreased baroreflex gain to rising blood pressure is mediated by a reduced mechanical gain only. These findings indicate that impaired neural transduction of the cardiac baroreflex plays an important role in transient autonomic dysfunction after exercise that account for the increased propensity for syncope in the period immediately post exercise.

4.6 Diurnal variations in baroreflex function

We applied the technique to further understand the mechanisms underlying circadian variation in blood pressure, which exhibit a characteristic 'morning surge' following waking that has been linked to higher incidence of cardiac and cerebrovascular events [46]. We have shown that 1) the morning rise in blood pressure is related to overall reductions in integrated baroreflex gain, 2) that for falling pressures the lower integrated gain in the morning was caused by reduced neural gain compared with the afternoon, and 3) for rising pressures the lower integrated gain in the morning was caused by reduced mechanical gain compared with the afternoon [25]. These unique findings hold the prospect of guiding the development of future treatment strategies aimed at lowering cardio- and cerebrovascular events that occur more frequently in the morning. For example, given increases in blood pressure such as those that occur in the morning, may predispose to cerebral haemorrhage [47], hypertensive patients may benefit most from clinical interventions that focus augmenting the mechanical component by enhancing vascular properties. Conversely, individuals suffering from orthostatic intolerance, for which the risk is also greatest in the morning [48], may benefit from interventions aimed at enhancing the neural component [49].

5. References

[1] Grundy SM, D'Agostino Sr RB, Mosca L, Burke GL, Wilson PW, Rader DJ, Cleeman JI, Roccella EJ, Cutler JA, Friedman LM. Cardiovascular risk assessment based on us cohort studies: Findings from a national heart, lung, and blood institute workshop. *Circulation*. 2001;104:491-496.

[2] La Rovere MT, Pinna GD, Hohnloser SH, Marcus FI, Mortara A, Nohara R, Bigger JT, Jr., Camm AJ, Schwartz PJ. Baroreflex sensitivity and heart rate variability in the

identification of patients at risk for life-threatening arrhythmias: Implications for clinical trials. *Circulation*. 2001;103:2072-2077.

[3] La Rovere MT, Pinna GD, Maestri R, Robbi E, Caporotondi A, Guazzotti G, Sleight P, Febo O. Prognostic implications of baroreflex sensitivity in heart failure patients in the beta-blocking era. *J Am Coll Cardiol*. 2009;53:193-199.

[4] Sykora M, Diedler J, Rupp A, Turcani P, Rocco A, Steiner T. Impaired baroreflex sensitivity predicts outcome of acute intracerebral hemorrhage. *Crit Care Med*. 2008;36:3074-3079.

[5] Sykora M, Diedler J, Turcani P, Hacke W, Steiner T. Baroreflex: A new therapeutic target in human stroke? *Stroke*. 2009

[6] Jordan D, Spyer KM. Brainstem integration of cardiovascular and pulmonary afferent activity. *Prog Brain Res*. 1986;67:295-314.

[7] Scharf SM, Pinsky MR, Magder S. Heart-lung interactions. In: Scharf sm, pinsky mr, magder s, editors, respiratory-circulatory interactions in health and disease. Marcel dekker, new york, basel. 2001:1-7.

[8] Nosaka S, Yamamoto T, Yasunaga K. Localization of vagal cardioinhibitory preganglionic neurons with rat brain stem. *J Comp Neurol*. 1979;186:79-92.

[9] Gunn CG, Sevelius G, Puiggari J, Myers FK. Vagal cardiomotor mechanisms in the hindbrain of the dog and cat. *Am J Physiol*. 1968;214:258-262.

[10] Calaresu FR, Faiers AA, Mogenson GJ. Central neural regulation of heart and blood vessels in mammals. *Prog Neurobiol*. 1975;5:1-35.

[11] Fritsch JM, Smith ML, Simmons DT, Eckberg DL. Differential baroreflex modulation of human vagal and sympathetic activity. *Am J Physiol*. 1991;260:R635-641.

[12] Casadei B, Meyer TE, Coats AJ, Conway J, Sleight P. Baroreflex control of stroke volume in man: An effect mediated by the vagus. *J Physiol*. 1992;448:539-550.

[13] Eckberg DL, Kifle YT, Roberts VL. Phase relationship between normal human respiration and baroreflex responsiveness. *J Physiol*. 1980;304:489-502.

[14] Fisher JP, Kim A, Young CN, Ogoh S, Raven PB, Secher NH, Fadel PJ. Influence of ageing on carotid baroreflex peak response latency in humans. *J Physiol*. 2009;587:5427-5439.

[15] Hunt BE, Fahy L, Farquhar WB, Taylor JA. Quantification of mechanical and neural components of vagal baroreflex in humans. *Hypertension*. 2001;37:1362-1368.

[16] Komine H, Sugawara J, Hayashi K, Yoshizawa M, Yokoi T. Regular endurance exercise in young men increases arterial baroreflex sensitivity through neural alteration of baroreflex arc. *J Appl Physiol*. 2009;106:1499-1505.

[17] Saeed M, Link MS, Mahapatra S, Mouded M, Tzeng D, Jung V, Contreras R, Swygman C, Homoud M, Estes NA, 3rd, Wang PJ. Analysis of intracardiac electrograms showing monomorphic ventricular tachycardia in patients with implantable cardioverter-defibrillators. *Am J Cardiol*. 2000;85:580-587.

[18] Eckberg DL. Point:Counterpoint: Respiratory sinus arrhythmia is due to a central mechanism vs. Respiratory sinus arrhythmia is due to the baroreflex mechanism. *J Appl Physiol*. 2009;106:1740-1742.

[19] Karemaker JM. Counterpoint: Respiratory sinus arrhythmia is due to the baroreflex mechanism. *J Appl Physiol*. 2009;106:1742-1743.

[20] Smyth HS, Sleight P, Pickering GW. Reflex regulation of arterial pressure during sleep in man. A quantitative method of assessing baroreflex sensitivity. *Circ Res*. 1969;24:109-121.
[21] Diaz T, Taylor JA. Probing the arterial baroreflex: Is there a 'spontaneous' baroreflex? *Clin Auton Res*. 2006;16:256-261.
[22] Lipman RD, Salisbury JK, Taylor JA. Spontaneous indices are inconsistent with arterial baroreflex gain. *Hypertension*. 2003;42:481-487.
[23] Tzeng YC, Sin PY, Lucas SJ, Ainslie PN. Respiratory modulation of cardiovagal baroreflex sensitivity. *J Appl Physiol*. 2009;107:718-724.
[24] Studinger P, Goldstein R, Taylor JA. Mechanical and neural contributions to hysteresis in the cardiac vagal limb of the arterial baroreflex. *J Physiol*. 2007;583:1041-1048.
[25] Taylor CE, Atkinson G, Willie CK, Jones H, Ainslie PN, Tzeng YC. Diurinal variation in the mechanical and neural component of the baroreflex. *Hypertension*. 2011;Under review
[26] Hunt BE, Farquhar WB. Nonlinearities and asymmetries of the human cardiovagal baroreflex. *Am J Physiol Regul Integr Comp Physiol*. 2005;288:R1339-1346.
[27] Leitch JW, Newling R, Nyman E, Cox K, Dear K. Limited utility of the phenylephrine-nitroprusside sigmoid curve method of measuring baroreflex function after myocardial infarction. *J Cardiovasc Risk*. 1997;4:179-184.
[28] Ler AS, Cohen MA, Taylor JA. A planar elliptical model of cardio-vagal hysteresis. *Physiol Meas*. 2010;31:857-873.
[29] Vallbo AB, Hagbarth KE, Torebjork HE, Wallin BG. Somatosensory, proprioceptive, and sympathetic activity in human peripheral nerves. *Physiol Rev*. 1979;59:919-957.
[30] Studinger P, Goldstein R, Taylor JA. Age- and fitness-related alterations in vascular sympathetic control. *J Physiol*. 2009;587:2049-2057.
[31] Hart EC, Joyner MJ, Wallin BG, Karlsson T, Curry TB, Charkoudian N. Baroreflex control of muscle sympathetic nerve activity: A nonpharmacological measure of baroreflex sensitivity. *Am J Physiol Heart Circ Physiol*. 2010;298:H816-822.
[32] Kamiya A, Iwase S, Kitazawa H, Mano T, Vinogradova OL, Kharchenko IB. Baroreflex control of muscle sympathetic nerve activity after 120 days of 6 degrees head-down bed rest. *Am J Physiol Regul Integr Comp Physiol*. 2000;278:R445-452.
[33] Electrophysiology TFotESoCatNASoPa. Heart rate variability: Standards of measurement, physiological interpretation and clinical use. *Circulation*. 1996;93:1043-1065.
[34] Kamiya A, Kawada T, Shimizu S, Sugimachi M. Closed-loop spontaneous baroreflex transfer function is inappropriate for system identification of neural arc but partly accurate for peripheral arc: Predictability analysis. *J Physiol*. 2011;589:1769-1790.
[35] Halliwill JR, Taylor JA, Hartwig TD, Eckberg DL. Augmented baroreflex heart rate gain after moderate-intensity, dynamic exercise. *Am J Physiol*. 1996;270:R420-426.
[36] Deley G, Picard G, Taylor JA. Arterial baroreflex control of cardiac vagal outflow in older individuals can be enhanced by aerobic exercise training. *Hypertension*. 2009;53:826-832.
[37] O'Leary DD, Kimmerly DS, Cechetto AD, Shoemaker JK. Differential effect of head-up tilt on cardiovagal and sympathetic baroreflex sensitivity in humans. *Exp Physiol*. 2003;88:769-774.

[38] Mineda Y, Sumiyoshi M, Tokano T, Yasuda M, Nakazato K, Nakazato Y, Nakata Y, Yamaguchi H. Circadian variation of vasovagal syncope. *J Cardiovasc Electrophysiol*. 2000;11:1078-1080.

[39] Cooper VL, Hainsworth R. Effects of head-up tilting on baroreceptor control in subjects with different tolerances to orthostatic stress. *Clin Sci (Lond)*. 2002;103:221-226.

[40] Taylor JA, Eckberg DL. Fundamental relations between short-term rr interval and arterial pressure oscillations in humans. *Circulation*. 1996;93:1527-1532.

[41] Saeed NP, Reneman RS, Hoeks AP. Contribution of vascular and neural segments to baroreflex sensitivity in response to postural stress. *J Vasc Res*. 2009;46:469-477.

[42] Deley G, Lipman RD, Kannam JP, Bartolini C, Taylor JA. Stress responses and baroreflex function in coronary disease. *J Appl Physiol*. 2009;106:576-581.

[43] Somers VK, Conway J, LeWinter M, Sleight P. The role of baroreflex sensitivity in post-exercise hypotension. *J Hypertens Suppl*. 1985;3:S129-130.

[44] Halliwill JR, Taylor JA, Eckberg DL. Impaired sympathetic vascular regulation in humans after acute dynamic exercise. *J Physiol*. 1996;495 (Pt 1):279-288.

[45] Willie CK, Ainslie PN, Taylor CE, Jones H, Sin PY, Tzeng YC. Neuromechanical features of the cardiac baroreflex after exercise. *Hypertension*. 2011;57:927-933.

[46] Elliott WJ. Circadian variation in the timing of stroke onset: A meta-analysis. *Stroke*. 1998;29:992-996.

[47] Muller JE, Tofler GH, Willich SN, Stone PH. Circadian variation of cardiovascular disease and sympathetic activity. *J Cardiovasc Pharmacol*. 1987;10 Suppl 2:S104-109; discussion S110-101.

[48] Lewis NC, Atkinson G, Lucas SJ, Grant EJ, Jones H, Tzeng YC, Horsman H, Ainslie PN. Diurnal variation in time to presyncope and associated circulatory changes during a controlled orthostatic challenge. *Am J Physiol Regul Integr Comp Physiol*. 2010;299:R55-61.

[49] Thomas KN, Burgess KR, Basnyat R, Lucas SJ, Cotter JD, Fan JL, Peebles KC, Lucas RA, Ainslie PN. Initial orthostatic hypotension at high altitude. *High Alt Med Biol*. 2010;11:163-167.

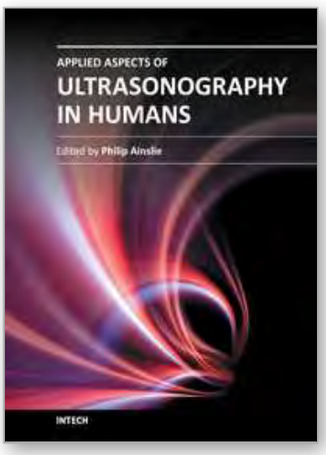

Applied Aspects of Ultrasonography in Humans
Edited by Prof. Philip Ainslie

ISBN 978-953-51-0522-0
Hard cover, 190 pages
Publisher InTech
Published online 25, April, 2012
Published in print edition April, 2012

Written by international experts, this publication provides the reader with the present knowledge and future research directions of diagnostic and therapeutic ultrasound and spectroscopy. Focused topics include Duplex ultrasound, transcranial color Duplex, MRA guided Doppler ultrasonography and near-infrared spectroscopy. New directions in the use and application of transcranial and color Duplex ultrasound are provided, as well as the use of ultrasound and arterial stiffness for measuring human vascular health and circulatory control. Novel use of ultrasound for the detection of intra-cardiac and intra-pulmonary shunts is also described along with its utility for the assessment of gastric regulation and emptying.

InTech Europe
University Campus STeP Ri
Slavka Krautzeka 83/A
51000 Rijeka, Croatia
Phone: +385 (51) 770 447
Fax: +385 (51) 686 166
www.intechopen.com

InTech China
Unit 405, Office Block, Hotel Equatorial Shanghai
No.65, Yan An Road (West), Shanghai, 200040, China
中国上海市延安西路65号上海国际贵都大饭店办公楼405单元
Phone: +86-21-62489820
Fax: +86-21-62489821

IntechOpen